CELLULAR ENTRY PATHWAY OF PANCREATIC-TYPE RIBONUCLEASES

by

Tzu-Yuan Cindy Chao

A dissertation submitted in partial fulfillment

of the requirements for the degree of

Doctor of Philosophy

(Biochemistry)

at the

UNIVERSITY OF WISCONSIN–MADISON

2010

CELLULAR ENTRY PATHWAY OF PANCREATIC-TYPE RIBONUCLEASES

submitted to the Graduate School of the
University of Wisconsin-Madison
in partial fulfillment of the requirements for the
degree of Doctor of Philosophy

By

TZU-YUAN CINDY CHAO

Date of final oral examination: Aug 10, 2010
Month and year degree to be awarded: August 2010

The dissertation is approved by the following members of the Final Oral Committee:

Ronald T. Raines, Professor, Department of Biochemistry and Chemistry
Thomas Martin, Professor, Department of Biochemistry
Ivan Rayment, Professor, Department of Biochemistry
Alessandro Senes, Assistant Professor, Department of Biochemistry
Paul Lambert, Professor, Department of Oncology

CELLULAR ENTRY PATHWAY OF PANCREATIC-TYPE RIBONUCLEASES

Tzu-Yuan Cindy Chao

Under the supervision of Professor Ronald T. Raines

at the University of Wisconsin–Madison

Bovine pancreatic ribonuclease (RNase A) is a remarkably well characterized protein and perhaps the most-studied enzyme of the 20th century. Owing to the relative small size, high stability and availability in large quantities, RNase A has served as a model protein in numerous biochemical, biophysical, and enzymological studies. It is also the prototype of a class of highly conserved vertebrate-specific endoribonucleases.

Members of the RNase A superfamily have been found to participate in a variety of biological activities by catalyzing the hydrolysis of RNA. Notably, Onconase® (ONC), an amphibian homologue of RNase A, exhibits selective toxicity towards cancer cells. This finding led to the surprising discovery that RNase A, initially dismissed as a digestive enzyme, can be engineered into a cytotoxin with therapeutic properties superior to ONC. Altogether, these cytotoxic ribonucleases have opened the door to a novel class of anticancer therapeutics.

The overall mechanism of ribonuclease-mediated cytotoxicity involves multiple steps, including cell-surface binding, endocytosis, endosomal translocation, and ultimately degradation of cellular RNA. Details of the cellular entry route are poorly

understood for many of the cytotoxic ribonucleases currently under clinical development. This thesis aims to explore the internalization properties of ribonucleases by dissecting the cellular entry pathway and developing assays specific for individual steps.

Ribonucleases have been proposed to target cancer cells by interacting with anionic cell-surface moieties up-regulated in cancer cells. To test this hypothesis, the effect of cell-surface anionicity on ribonuclease cell-surface binding, internalization, and cytotoxicity was determined and described in CHAPTER 2. Glycan structures mediating RNase A internalization were identified. In CHAPTER 3, the endocytic mechanism utilized by RNase A was further explored and compared with a class of peptides that enters cells via similar pathways as RNase A. CHAPTER 4 describes the development of a novel assay measuring the endosomal translocation efficiency of ribonucleases. In CHAPTER 5, the competing influences of Coulombic forces acting at the cell surface and in the cytoplasm were examined and discussed for RNase 1, the human homologue of RNase A.

The use of novel latent fluorogenic labels has been indispensable in the study of ribonuclease internalization. While the applications of these novel fluorophores are described throughout this dissertation, the design, synthesis, and initial characterizations are described in CHAPTERS 6–9. CHAPTER 6 describes a rhodamine$_{110}$-based latent fluorophore activatable by esterase activities while CHAPTER 7 describes red and blue fluorogenic substrates for esterases. A series of highly stable acetoxymethyl ester-based fluorogenic substrates are described in CHAPTER 8. In CHAPTER 9, a novel fluorogenic substrate for cytochrome P450 was devised and characterized in living cells.

Finally, several potential future directions of this work are proposed in CHAPTER 10, with the overall goal being to guide and to facilitate the development of ribonuclease-based cancer therapeutics by furthering our understanding of the mechanisms of ribonuclease-mediated cytotoxicity.

Acknowledgements

I would like to express my deepest gratitude towards all the people who have generously provided their support and assistance, in one way or another, during my graduate career. First and foremost, I am grateful for the opportunity that my advisor, Professor Ronald T. Raines, has given me to work in his research group. His enthusiasm and optimism for science, breadth of knowledge, as well as his extraordinary ability with words have been truly inspirational; I thank him for the all the guidance and assistance he has provided.

I am thankful for my science teachers back in Taiwan, who cultivated my early interest in science, as well as those in Canada—Cheri Smith and Trevor Fowler—who gave me the most confidence in pursuing science. I would also like to thank my present mentors—members of my thesis committee, including Paul Lambert, Tom Martin, Ivan Rayment, Alessandro Senes, and Chris Wiese, for their helpful guidance and advice.

Many thanks to staff at the Comprehensive Cancer Center Flow Cytometry Facility, especially Joel Puchalski, for his help with numerous experiments. I am grateful to the Dr. James Chieh-Hsia Mao Wisconsin Distinguished Graduate Fellowship Program and Professor Raines for funding during my graduate training.

I could not have made it thus far without the help from many talented individuals in the Raines Laboratory, past and present, who have been an invaluable source of advice, support, and friendship to me. I am grateful for the advice from Kim Dickson, Steve Fuchs, Kelly Gorres, Jeremy Johnson, Eugene Lee, Brian Miller, Tom Rutkoski, and

Bryan Smith when I first began my research here. I thank my long-term collaborator Luke Lavis for sharing his "bright ideas" and other helpful discussion. I have had the pleasure to work right next to Jeet Kalia and Joelle Lomax, both of whom have been there during my ups and downs. Their patience in listening to my science and life stories is much appreciated. I am grateful to other members of the lab—Joe Binder, Margie Borra, Christine Bradford, Sayani Chattopadhyay, Amit Choudhary, Chelcie Eller, Greg Ellis, Greg Jakubczak, Sean Johnston, Mike Levine, Langdon Martin, Nicky McElfresh, Eddie Myers, Mike Palte, Matt Shoulders, Nadia Sundlass, Annie Tam, Rebecca Turcotte, Rex Watkins—for helpful discussions and contributing to a positive work environment.

I am grateful to many friends outside the lab—Oat, Lingyin Li, Lingling Liu, Yuanyuan Liu, Shihu Sun, Lei Tong, Jielin Xu, Xuan Ye—for their support and cheerful encouragement, and others who I have shared many memorable moments with. Special thanks to Sheng Yang for lending me courage and mental support for the past years.

Lastly, I would like to thank my parents and family for their unconditional support and encouragement, as well as my pets—Ogner, Rona, Emily and Joshua—for being there for me.

Table of Contents

CHAPTER 7

CHAPTER 8

List of Tables

List of Figures

List of Schemes

List of Abbreviations

ε	extinction coefficient
6-FAM	6-carboxyfluorescein
6-TAMRA	6-carboxytetramethylrhodamine
AM	acetoxymethyl
ANG	angiogenin
ATCC	American Type Culture Collection
BCA	bicinchoninic acid
BSA	bovine serum albumin
BS-RNase	bovine seminal ribonuclease
CD	cytochalasin D
CHO	Chinese hamster ovary
CPP	cell-penetrating peptide
CPZ	chlorpromazine
CTB	cholera toxin subunit B
CV	cresyl violet
Da	Dalton
DAPI	4′,6-diamidino-2-phenylindole
DMEM	Dulbecco's modified Eagle's medium
DMF	dimethylformamide
DMSO	dimethylsulfoxide

DNA	deoxyribonucleic acid
DPSB	Dulbecco's phosphate buffered saline
D-*threo*-PPMP	D-*threo*-1-phenyl-2-palmitoylamino-3-morpholino-1-propanol
DRNG RNase A	D38R/R39D/N67R/G88R variant of RNase A
DTNB	5,5′-dithiobis(2-nitrobenzoic acid)
DTT	dithiothreitol
ECP	eosinophilic cationic protein; RNase 3
EDTA	ethylenediaminetetraacetic acid
EIPA	5-(*N*-ethyl-*N*-isopropyl)amiloride
FBS	fetal bovine serum
FDG	fluorescein di-β-D-galactopyranoside
FPLC	fast performance liquid chromatography
FRET	Förster resonance energy transfer
h	hour
HCl	hydrochloric acid
HEPES	2[4-(2-hydroxyethyl)-1-piperazinyl]ethanesulfonic acid
HPLC	high performance (pressure) liquid chromatography
hRI	human ribonuclease inhibitor
HSPG	heparan sulfate proteoglycan
IPTG	isopropyl-1-thio-β-D-galactopyranoside
k_{cat}	first-order enzymatic rate constant

K_d	equilibrium dissociation constant
kDa	kilodalton
K_i	inhibitor dissociation constant
K_M	Michaelis constant
λ_{em}	emission wavelength
λ_{ex}	excitation wavelength
LB	Luria–Bertani medium
MALDI–TOF	matrix-assisted laser desorption/ionization time-of-flight
MβCD	methyl-β-cyclodextrin;
MES	2-(*N*-morpholino)-ethanesulfonic acid
min	minute
mRNA	messenger ribonucleic acid
NaCl	sodium chloride
NaOH	sodium hydroxide
ONC	Onconase®; ranpirnase; P-30; Pannon
OVS	oligo(vinylsulfonic acid)
PBS	phosphate-buffered saline
PDB	protein data bank
PEG	poly(ethylene glycol)
p*I*	isoelectric point
pK_a	log of the acid dissociation constant

PTD	protein transductions domain; cell penetrating peptide
R_9	nonaarginine
RFU	relative fluorescence units
Rh_{110}	rhodamine 110
RI	ribonuclease inhibitor
RNA	ribonucleic acid
RNase A	bovine pancreatic ribonuclease
RNase 1	human pancreatic ribonuclease
rRNA	ribosomal ribonucleic acid
s	second
TAT	residues 47–57 of the HIV-1 trans-activator of transcription.
TB	terrific broth
T_m	temperature at the midpoint of the denaturation curve
TLC	thin-layer chromatography
TML	trimethyl lock
TNB	2-nitro-5-thiobenzoate
Tris	2-amino-2-(hydroxymethyl)-1,3-propanediol
UV	ultraviolet
Z	net molecular charge (Arg + Lys – Asp – Glu)

CHAPTER 1

Introduction:

Mechanism of Ribonuclease-Mediated Cytotoxicity:

Focusing on Cellular Entry

1.1 Abstract

The pancreatic-type ribonucleases constitute a class of highly conserved secretory endoribonucleases that mediate diverse biological actions by catalyzing the cleavage of RNA. Collectively, the pancreatic-type ribonucleases exhibit angiogenic, antibacterial, antiproliferative, cytotoxic, antitumoral, antiviral, aspermatogenic, and embryotoxic activities, many of which require access to cellular RNA substrates in the cytoplasm or nucleus. The processes by which these circulating ribonucleases enter the cytoplasm of their respective target cells have not been fully elucidated, though the cellular entry pathway has been proposed to consist of the following general steps: cell-surface binding, endocytosis, and endosomal escape. A comprehensive understanding of the cellular entry steps is particularly crucial for ribonucleases demonstrating selective toxicity towards cancerous cells—Onconase®, as well as variants of ribonuclease A and human ribonuclease 1. Onconase® was recently granted fast track and orphan drug status as chemotherapeutic agent for treating malignant mesothelioma. Ribonuclease A and ribonuclease 1 are mammalian ribonucleases with immense therapeutic potential owing to their low immunogenicity, favorable tissue distribution, and high therapeutic index. The clinical utility of the above cytotoxic ribonucleases could be greatly enhanced by modulating their cellular entry route. Here, we review the internalization properties of pancreatic-type ribonucleases, and discuss strategies that have been employed to augment toxicity of cytotoxic ribonucleases by altering cellular uptake.

1.2 Introduction

RNA is regarded as the key intermediate in the central dogma of molecular biology, transmitting genetic information from DNA to proteins. With the advent of technologies such as high-throughput sequencing and microarrays, the cellular transcriptome has been painstakingly recorded for numerous cell types in the past decade, greatly expanding our understanding of RNA. Among those, the discovery of noncoding RNAs—siRNA, miRNA, and piRNA—reshaped the traditional view of RNA from being merely transcripts of DNA to molecules with regulatory functions (Blow, 2009). The importance of RNA in diverse biological processes is becoming increasingly evident.

The processing, turnover and degradation of various classes of RNA is tightly regulated by ribonucleases (RNases) (Deutscher, 1988), a diverse group of enzymes that catalyze the cleavage of RNA at phosphodiester bonds. A single cell has been estimated to express as many as 20 distinct RNases with overlapping specificities (Deutscher and Li, 2001). By modulating RNA levels, RNases participate in a broad range of biological activities including cell maturation, host defense, and angiogenesis (Benito *et al.*, 2005). Intriguingly, several types of cancer have been correlated to alterations in RNase activity or patterns of expression, suggesting a potential role for RNases as regulators of tumor development (Kim and Lee, 2009).

Destruction of RNA has only recently become a viable therapeutic strategy for treating cancer and other human diseases (Tafech *et al.*, 2006). One way of targeting RNA involves the use of antisense oligonucleotides to block the expression of specific

oncogenes and disease genes. Many antisense DNA and RNA are currently being tested in clinical trials (Tafech *et al.*, 2006). Another therapeutic approach utilizes ribonucleolytic activities to destroy RNA molecules (Leland and Raines, 2001; Arnold and Ulbrich-Hofmann, 2006; Lee and Raines, 2008). In particular, members of the pancreatic-type ribonuclease family have received much attention due to their anti-cancer properties (Youle and D'Alessio, 1997). The pancreatic-type ribonucleases constitute a class of secretory endoribonucleases with a distinct three-dimensional fold highly conserved across vertebrate species (Beintema *et al.*, 1988). The prototype of this family, bovine pancreatic ribonuclease (RNase A), is a small (13-kDa) cationic protein that catalyzes RNA hydrolysis at a rate approaching the diffusion limit (Park and Raines, 2003). Unlike antisense oligonucleotides, members of the RNase A superfamily do not require delivery vehicles to enter cells (Haigis and Raines, 2003). The pancreatic-type ribonucleases therefore represent an emerging class of anticancer chemotherapeutics combining efficient RNA degradation with unique "cell-penetrating" capabilities.

The antitumoral activity of pancreatic-type ribonucleases was initially observed with Onconase® (ONC), an amphibian homologue of RNase A from the oocytes of *Rana Pipiens* (Youle and D'Alessio, 1997). ONC mediates selective toxicity towards malignant cells both *in vitro* and *in vivo* (Darzynkiewicz *et al.*, 1988; Mikulski *et al.*, 1990). Although degradation of rRNA, tRNA, and siRNA has been associated with ONC treatment (Zhao *et al.*, 2008; Wu *et al.*, 1993; Iordanov *et al.*, 2000a; Saxena *et al.*, 2002), its impact on cell physiology does not appear to be simply a result of inhibiting protein synthesis, as is typically observed with cyclohexamide treatment (Iordanov *et al.*, 2000a).

ONC has been reported to induce cytostatic effects, arresting cells at G_1 phase (Darzynkiewicz *et al.*, 1988), as well as cytotoxic effects, activating caspase-9/caspase-3 and serine proteases, leading to apoptosis (Iordanov *et al.*, 2000b). Additional pancreatic-type ribonucleases that also exhibit innate antitumoral activities include bovine seminal ribonuclease (BS-RNase), and two other frog ribonucleases: *catesbeiana* sialic acid-binding lectin (cSBL), and *japonica* sialic acid-binding lectin (jSBL) (Nitta *et al.*, 1994a; Laccetti *et al.*, 1992). The mechanisms by which these cytotoxic ribonucleases mediate cell death are not well understood.

In contrast to the amphibian homologues, most pancreatic-type ribonucleases of mammalian sources are not natural cytotoxins due to the action of the ribonuclease inhibitor (RI) (Haigis *et al.*, 2003). RI is a 50-kDa cytosolic protein that has evolved to bind mammalian ribonucleases with femtomolar affinities ($K_d = 6.9 \times 10^{-16}$ M for the bovine RI·RNase A complex) (Dickson *et al.*, 2005; Johnson *et al.*, 2007b), while it only interacts with amphibian ribonucleases with K_i values in the micromolar range ($K_i = 1.5 \times 10^{-7}$ M for the human RI for ONC under no salt conditions) (Turcotte and Raines, 2008). The high affinity of RI for mammalian ribonucleases and its ubiquitous expression in all mammalian cells suggest a role for RI as a cellular sentry—protecting cells against rogue ribonucleases (Haigis *et al.*, 2003).

Mammalian ribonucleases can be endowed with cytotoxicity by evasion of RI binding through chemical modifications and site-directed mutagenesis (Rutkoski and Raines, 2008). For example, cytotoxic variants of RNase A have been created by disrupting the shape-complementarity within the RI–RNase A molecular interface

(Rutkoski *et al.*, 2005). In addition, polyethylenimine-, and dendrimer-cationization, multimerization by chemical linkage and mutagenesis, as well as conjugation to other proteins have also resulted in cytotoxic variants of mammalian ribonucleases through RI-evasion (Futami *et al.*, 2005; Piccoli *et al.*, 1999; Suzuki *et al.*, 1999; Rutkoski *et al.*, 2010). Though ONC is currently being evaluated as a chemotherapeutic for the treatment of malignant mesothelioma, its dosage is limited by renal toxicity and immunogenicity (Lee and Raines, 2008). Many of the RI-evasive mammalian ribonucleases have enormous therapeutic potential as they elicit less off-target effects and immunogenic responses in comparison to ONC. Hence, the development of future generations of mammalian ribonuclease-based anticancer agents is underway.

To improve further the efficacy of cytotoxic ribonucleases, factors such as catalytic ability, conformational stability, and cellular uptake must be considered in addition to RI binding (Rutkoski and Raines, 2008). Among these, internalization of ribonucleases has been proven to be highly inefficient, despite their endogenous ability to enter cells. In general, the cellular entry pathway of ribonucleases consists of the following steps: 1) cell-surface binding, 2) endocytosis, and 3) endosomal escape (Leland and Raines, 2001; Arnold, 2008). As depicted in Fig. 1.1, cytotoxic ribonucleases must traverse cellular membranes to reach the cytoplasm, where they can exert toxicity by cleaving cellular RNA substrates. Details of this pathway have yet to be elucidated fully. A thorough understanding of the cellular entry pathways of ribonucleases is not only necessary for the development of cytotoxic ribonuclease-based chemotherapeutics, but this research might also help elucidate biological activities carried out by other members

of the RNase A superfamily. Herein, we review past efforts to understand and enhance each individual step of the internalization process for pancreatic-type ribonucleases with an emphasis on the relationship between ribonuclease internalization and cytotoxicity.

1.3 Cell-Surface Interactions of Pancreatic-Type Ribonucleases

1.3.1 Specificity of amphibian ribonucleases

All of the known pancreatic-type ribonucleases from amphibians are natural cytotoxins, and these include ONC and amphinase (Amph), which were isolated from oocytes of the Northern Leopard frog *Rana pipiens*, as well as the sialic acid-binding lectins cSBL and jSBL, which were isolated from oocytes of the Bull frogs *Rana catebeiana* and *Rana japonica* respectively (Benito *et al.*, 2008). Early studies on the cell-surface interactions and antitumoral properties of these amphibian ribonucleases laid the foundation for subsequent work on their mammalian homologues and led to the blossoming of ribonuclease-based chemotherapeutics.

cSBL and jSBL are two of the few pancreatic-type ribonucleases with well established cell-surface receptors. They initially drew interest based on their ability to agglutinate various transformed cells *in vitro* and *in vivo*, but not nontransformed cells (Kawauchi *et al.*, 1975). Later studies revealed that their preference was due to interaction with clustered sialyl oligosaccharides *O*-linked to glyocoproteins on the surface of transformed cells, hence the name "sialic acid-binding lectins". cSBL binds to a high molecular weight (180-kDa) sialyl glycoprotein found on various tumor cells

(Nitta *et al.*, 1987), while jSBL interacts with a glycoprotein with 25% carbohydrate content, 11% of which are sialic acid (Sakakibara *et al.*, 1979). Sialidase treatment not only resulted in inhibition of tumor cell agglutination and cell-surface binding but also abolished the antiproliferative activities exhibited by cSBL and jSBL (Nitta *et al.*, 1994a). Characterization of a cSBL-resistant mutant cell line further confirmed the requirement for a specific sialylated glycoprotein in cellular entry and cytotoxicity (Nitta *et al.*, 1994b).

By contrast, ONC has no known sialic acid binding activities, though it shares 50% sequence identity with the lectins (Irie *et al.*, 1998). Instead, conflicting results were obtained for the cell-surface interaction of ONC. In a study using ^{125}I labeled ONC, two saturable binding sites with different affinities ($K_d = 6.2 \times 10^{-8}$ M and 2.5×10^{-7} M) were identified on 9L glioma cells (Wu *et al.*, 1993). Another study also supports the notion of a receptor-mediated endocytic mechanism for ONC (Rodriguez *et al.*, 2007); however, no cell-surface receptor has been identified or isolated for ONC thus far. Indeed, fluorescently labeled ONC was found to interact with Hela cells in a nonsaturable manner by flow cytometry (Haigis and Raines, 2003). This apparent discrepancy could be due to differences in the choices of cell lines and techniques. Nonetheless, it is indisputable that ONC is distinct from cSBL and jSBL in that it is internalized by essentially all cell types, suggesting the presence of one or more broadly distributed, possibly nonspecific receptor(s).

RNase A shares 30% sequence identity with ONC and ~20% homology with cSBL. The backbone structure of RNase A and ONC have been compared to the structure

of cSBL in complex with two sialic acids (Fig. 1.2) (Irie *et al.*, 1998). One of the sialic acid residues lies near the active-site cavity, where the three proteins align similarly, whereas another sialic acid residue binds with less affinity lies near the loop formed by residues 57–70, which is clearly in steric clash with RNase A but not ONC. These results hint at the possibility of RNase A and ONC lectin activities and prompted investigations on the interaction between ribonucleases and sialylated cell-surface moieties, which are described in CHAPTER 2.

1.3.2 Specificity of mammalian ribonucleases

The bovine-seminal ribonuclease (BS-RNase) mediates an impressive array of biological actions including immunosuppressive, embryotoxic, aspermatogenic, antimetastatic, as well as antitumoral activities both in *vitro and in vivo* (Benito *et al.*, 2008; Youle and D'Alessio, 1997). The native cytotoxicity displayed by BS-RNase is unique among mammalian ribonucleases, and is often attributed to its natural dimer formation, allowing evasion from RI inhibition (Kim *et al.*, 1995b).

By using ^{125}I-labeled BS-RNase, investigations into the cancer-cell selectivity of BS-RNase led to the identification of saturable binding sites with similar affinities ($K_d \sim 10^{-7}$ M) on the surface of primary mouse fibroblast, Balb C 3T3, and SVT2, a virally transformed cell line, indicating that BS-RNase does not differentiate between cancer and normal cells at the cell surface (Mastronicola *et al.*, 1995). Interestingly, the binding site was further found to be located within the extracellular matrix, and no membrane-bound receptors have been detected. In line with this finding, homologue-scanning mutagenesis

carried out with BS-RNase demonstrated that hybrid and semisynthetic variants of BS-RNase were indistinguishable from the wild-type protein with respect to catalysis and cytotoxicity (Kim *et al.*, 1995b). Altogether, these results strongly repudiate the presence of a specific protein receptor for BS-RNase.

Angiogenin (ANG) belongs to the RNase A superfamily and is the only angiogenic factor possessing ribonucleolytic activity (Riordan, 1997). Although the role of ANG in the induction of neovascularization is not well-understood, it has been demonstrated to activate several signaling pathways involving extracellular signal-related kinase 1/2 (Erk 1/2) (Liu *et al.*, 2001), protein kinase B/Akt (Kim *et al.*, 2007), and cell-surface plasminogen activator in cultured human umbilical vein endothelial cells (Hu *et al.*, 1994). Considering the activation of phospholipase C and A_2 by ANG, and the subsequent rapid generation of second messengers in endothelial cells (production of diacylglycerol in <2.5 min) (Riordan, 1997), identification of a membrane receptor for angiogenin was expected. Yet, no direct evidence for interaction between angiogenin and G protein-coupled receptors has been found.

Several ANG binding proteins on the surface of endothelial cells were recognized, but only one was demonstrated to have functional relevance to the induction of angiogenesis. First, two binding sites on calf pulmonary artery endothelial (CPAE) cells with $K_d = 5 \times 10^{-9}$ M and 0.2×10^{-6} M were identified with ^{125}I-labeled ANG (Badet *et al.*, 1989). A 42-kDa cell-surface dissociable smooth muscle type α-actin corresponding to the high affinity binding site was subsequently isolated from CPAE cells (Hu *et al.*, 1991; Hu *et al.*, 1993). Incubation with actin and anti-actin antibodies both inhibited the

angiogenic activity induced by ANG, indicating that actin binding is essential in angiogenesis (Hu *et al.*, 1993). Furthermore, a high molecular weight heparinase-sensitive proteoglycan (apparent MW >200 kDa) (Soncin *et al.*, 1994) and a membrane protein (170 kDa) were identified as putative ANG receptors (Hu *et al.*, 1997), and isolated from human tumor cells (HT 29) and endothelial cells respectively. In all cases, expression of the putative ANG receptors was reported to be dependent on cell density (Riordan, 1997). Thus, ANG could interact with different receptors under different environmental signals. Finally, similar to other mitogens, such as basic fibroblast growth factor (bFGF) and vascular endothelial growth factor (VEGF), evidence suggests that interaction with cell-surface glycosaminoglycans is important for the mitogenic and proliferative activities by ANG (Soncin *et al.*, 1994).

Serving as a model enzyme, RNase A has played a monumental role in the biochemical and biophysical studies of proteins; however, understanding of its endogenous roles is lacking. Although pancreatic ribonucleases such as RNase A and RNase 1, the human homologue, were initially proposed to be digestive enzymes, recent evidence suggests their possible involvement in host defense mechanisms and regulation of extracellular RNA (Kannemeier *et al.*, 2007; Rosenberg, 2008). Yet, none of the proposed biological roles for pancreatic ribonucleases require internalization and access to intracellular RNA. Consequently, possible existence of a specific membrane-associated protein receptor for RNase A or RNase 1 remains debatable. In addition, fluorescently labeled RNase A has been observed to interact with human cells in a nonsaturable

fashion, providing evidence for nonspecific cell-surface interaction (Haigis and Raines, 2003).

Considering the homology of pancreatic ribonucleases with ANG and BS-RNase (~50% and ~85% sequence identity, respectively) (Rutkoski and Raines, 2008), it is possible that RNase A and RNase 1 also recognize components of the ECM, α-actin, and heparan sulfate-containing proteoglycans. Consistent with this speculation, the heparin binding site found in ANG is completely conserved in RNase 1 and partially conserved in RNase A (Soncin *et al.*, 1997). Any lectin activities by RNase A and RNase 1 need to be further scrutinized; the results could shed light on the endogenous roles of these proteins.

1.3.3 Role of Coulombic force in ribonuclease cell-surface interactions

Coulombic forces are one of the many noncovalent forces governing interactions among macromolecules. Compared to other noncovalent interactions commonly found in biology, such as hydrogen-bonding and van der Waals interactions, Coulombic forces are considered to be a relatively long-range interaction. Hence, Coulombic forces are thought to play a larger role in determining association rates of molecules rather than dissociation rates of complexes (Johnson *et al.*, 2007a).

The pancreatic-type ribonucleases have evolved to be highly cationic proteins, with isoelectric points (p*I*) between 9 and 11 (Vasandani *et al.*, 1996), presumably to facilitate catalysis of RNA, which is a polyanion. In the active site of RNase A, at least four cationic residues participate in Coulombic interactions in substrate binding or catalysis (Raines, 1998). Oligomers of vinylsulfonic acid (OVS), which is a polymer with

sulfate groups, has been shown to be a potent inhibitor of RNase A activity ($K_i = 10^{-11}$ M) through the formation of eight favorable Coulombic interactions (Smith *et al.*, 2003).

The surface of mammalian cells is coated with an extensive network of carbohydrates known as the glycocalyx. Many of the oligosaccharides within this layer contain negatively charged carboxyl or sulfuryl groups, giving rise to the overall negative charge of the cell surface. Glycosaminoglycans (GAGs) such as heparan sulfate or chondroitin sulfate are long, unbranched polymers with regularly spaced anionic functional groups, mimicking RNA molecules. Several of the pancreatic-type ribonucleases, including cSBL, ANG and the eosinophil cationic protein (ECP; RNase 3) have been reported to bind heparin (Fan *et al.*, 2007; Irie *et al.*, 1998; Soncin *et al.*, 1997; Garcia-Mayoral *et al.*, 2010). Both the conformation and cationicity of the active-site cavity of ribonucleases, which are optimized to bind RNA (Fisher *et al.*, 1998), are well-poised to accommodate anionic cell-surface glycan structures. It is therefore conceivable that Coulombic interactions between ribonucleases and cell-surface glycans are the basis for the nonspecific cell-surface interactions observed for ONC and RNase A.

Further enhancing the Coulombic interactions by increasing the cationicity of ribonucleases has been correlated to increased cellular uptake and resulted in higher toxicity (Turcotte *et al.*, 2009; Johnson *et al.*, 2007a). Yet, as the interactions between RI and mammalian ribonucleases are also mediated through Coulombic interactions, higher cationicity implies greater affinity for RI. The optimal positive charge on a ribonuclease must balance the two interactions (Johnson *et al.*, 2007a). Investigations into the dichotomy of electrostatic charge are described in CHAPTER 5.

1.3.4 Contribution of cell-surface moieties to selective toxicity by ribonucleases

A number of ribonucleases demonstrate the ability to attack malignant cells preferentially. BS-RNase and the amphibian ribonucleases dramatically inhibit the growth of carcinomas induced in mice without significant toxic effects on the animals (Youle and D'Alessio, 1997). In addition, variants of RNase A, synthetic RNase 1 dimers, BS-RNase, and ONC have been shown to be much more cytotoxic toward transformed cell lines compared to their respective parent cell lines (Piccoli *et al.*, 1999; Mastronicola *et al.*, 1995; Smith *et al.*, 1999).

The biological basis underlying the selective toxicity exhibited by cytotoxic ribonuclease is not known, though a number of plausible mechanisms have been proposed. For example, cytotoxic ribonucleases have been suggested to target tumor-specific intracellular RNA molecules (Costanzi *et al.*, 2005; Mikulski *et al.*, 1990). Also, factors such as the rates of endocytosis and replication, as well as trafficking of ribonuclease could differ significantly between cancerous and noncancerous cells, resulting in disparate cell susceptibilities.

Importantly, another factor that has been proposed to influence cell susceptibility to cytotoxic ribonucleases is the anionicity of cell surfaces (Benito *et al.*, 2005). Indeed, cancerous cells are known to have more anionic cell surfaces than their wild-type counterparts (Slivinsky *et al.*, 1997), and the increase in negative charge has been attributed to elevated expression of charged cell-surface glycans (Dube and Bertozzi, 2005). In particular, increased display of sialic-acid containing structures such as gangliosides, Lewis x, Lewis y, and polysialic acids have been associated with cancer

(Dube and Bertozzi, 2005). The relocation of phosphotidylserine to the outer plasma membrane is also thought to contribute to increased anionicity of cancer cell surfaces (Ran *et al.*, 2002). Considering the mode of ribonuclease cell-surface association, the enzymes could be more drawn toward cancerous cells due to more favorable Coulombic interactions with cancer cell surfaces.

1.4 Endocytosis and Trafficking of Pancreatic-Type Ribonucleases

1.4.1 The role of endocytosis in the cellular entry of cytotoxins and cationic peptides

One way for eukaryotic cells to interact with the extracellular environment is through endocytosis, the process by which cells internalize extracellular substances from outside the cell by engulfing them with their membrane. Large particles, such as pathogens or cells, are taken up by cells in a form of endocytosis known as phagocytosis ("cell eating"), whereas smaller molecules are internalized by a variety of mechanisms collectively known as pinocytosis ("cell drinking") (Fig. 1.3) (Mukherjee *et al.*, 1997). Phagocytosis is thought to be prevalent only in specialized cell types, such as macrophages and neutrophils, which function to remove pathogens and cell debris (Conner and Schmid, 2003). By contrast, pinocytosis occurs in all mammalian cells. In all cases of endocytosis, extracellular substances are enclosed in vesicles formed by plasma membrane invagination, and go through membrane-bound compartments including endosomes and lysosomes, where sorting, trafficking, and degradation take place.

The pinocytic mechanism utilized by a particular molecule is highly dependent on its interaction with the cell surface. Molecules with high affinity cell-surface receptors are internalized most efficiently by receptor-mediated endocytosis via clathrin-coated pits, where a concentration of receptors, linked to the clathrin coat through adaptor proteins, is often observed (Mukherjee *et al.*, 1997). The assembly of clathrin trimers into a polygonal lattice drives membrane curvature while membrane scission by the GTPase dynamin completes the formation of clathrin-coated vesicles. Diverse cargo molecules are taken up via clathrin-mediated endocytosis; the prototypical markers of this pathway include transferrin and low-density lipoprotein (LDL) (Mukherjee *et al.*, 1997).

A well-characterized pinocytic pathway independent of clathrin is caveolae-mediated endocytosis. Caveolae are flask-shaped membrane invaginations associated with cholesterol- and sphingolipid-rich microdomains of the plasma membrane known as lipid-rafts (Conner and Schmid, 2003). Similar to clathrin-mediated endocytosis, caveolin-mediated endocytosis is dependent on the coat protein caveolin-1 and the GTPase dynamin. Direct interaction between caveolin-1 and cholesterol renders caveolae highly sensitive to cholesterol depletion (Kirkham and Parton, 2005). Caveosomes have been shown to be involved in the uptake of simian virus 40 (SV40) and the B subunit of cholera toxin (CtxB) (Doherty and McMahon, 2009).

In contrast to clathrin- and caveolae-mediated endocytosis, macropinocytosis does not require coat proteins or dynamin (Mayor and Pagano, 2007). Instead, formation of macropinosomes is characterized by membrane ruffling, a strong dependence on actin, and engulfment of large volumes of extracellular material (Jones, 2007). Markers for this

pathway include high molecular weight dextrans and horseradish peroxidase. Additional clathrin- and caveolin-independent pathways are not considered here due to the scope of this thesis.

Endocytosis can also be viewed as a way for substances to gain entry into the cells. Toxins and pathogens, for example, often exploit endocytic pathways to gain access to the cell interior to mediate toxicity. Anthrax toxin, cholera toxin, and ricin interact with cell-surface transmembrane proteins TEM8 and CMG2, ganglioside GM1, and β1-4 linked galactosides, respectively, and enter cells via clathrin-mediated endocytosis (Doherty and McMahon, 2009; Mukherjee *et al.*, 1997). Pathogens such as viruses have evolved to hijack endocytic machineries; as many as eight different pathways were found to be used by viruses (Doherty and McMahon, 2009). Although nearly every endocytic pathway is exploited, clathrin-mediated endocytosis appears to be the major target pathway for toxin and pathogen entry (Mudhakir and Harashima, 2009). Moreover, particles such as CTxB and influenza virus simultaneously utilize multiple endocytic pathways; inhibition of a particular endocytic mechanism is compensated by other pathways (Torgersen *et al.*, 2001; Doherty and McMahon, 2009).

In addition to cell-surface binding and endocytosis, most toxins and pathogens have evolved ways to escape from endocytic compartments either by traversing endosomal membranes or retrograde transport to the *trans*-Golgi network (TGN) to avoid lysosomal degradation. Toxins such as ricin or the *Pseudomonas* exotoxin do not possess translocation capabilities and are mostly degraded in lysosomes, with only 2–5% of being targeted to the TGN (Mukherjee *et al.*, 1997).

Cell-penetrating peptides (CPPs), which constitute a class of peptides containing a high density of basic residues, are also adventitiously internalized by mammalian cells. The "cell-penetrating" phenomenon was initially observed with the HIV-1 TAT protein (Frankel and Pabo, 1988). Subsequently, it was soon recognized that the "protein transduction" function was mediated by an 11-residue segment in the TAT protein, and that the segment was able to induce internalization outside the context of the TAT protein (Vives *et al.*, 1997). The discovery that CPPs can mediate intracellular delivery of a wide range of cargos in *cis* and in *trans* sparked intense interest utilizing CPPs as vehicles in pharmaceutical development (Noguchi and Matsumoto, 2006; Patel *et al.*, 2007).

Unlike most toxins and pathogens, which recognize specific cell-surface moieties with high affinities, CPPs are thought to interact with multiple anionic cell-surface moieties mainly by forming favorable Coulombic interactions (Brooks *et al.*, 2005; Patel *et al.*, 2007). Glycosaminoglycans have been implicated in the cell-surface association of CPPs (Simon *et al.*, 2009; Kosuge *et al.*, 2008; Nakase *et al.*, 2007; Fuchs and Raines, 2004). Arginine residues, which are much more effective than lysine residues in inducing CPP cell transduction (Wadia and Dowdy, 2005), are thought to form bidentate hydrogen bonds with anionic groups on the surface of the cell (Calnan *et al.*, 1991; Fuchs and Raines, 2006).

Consistent with an adsorptive mode of cell-surface association, multiple endocytic pathways mediate the cellular uptake of CPPs. At least four different pathways, including clathrin- and caveolae-mediated endocytosis, clathrin- and caveolin-independent endocytosis, as well as macropinocytosis, have been implicated in the internalization of

CPPs with or without cargos (Patel *et al.*, 2007; Melikov and Chernomordik, 2005). Furthermore, the involvement of a novel nonendocytic mechanism was recently demonstrated for several CPPs at high concentrations (>10 μM) (Duchardt *et al.*, 2007). Therefore, the endocytic mechanism of CPPs not only relies on the size and nature of their cargos, but is also concentration-dependent.

Internalized CPPs are mainly localized to endosomal compartments, the cytoplasm, and the nucleus. The majority of CPPs are degraded in lysosomes (Melikov and Chernomordik, 2005). Their ability to escape from endocytic compartments is highly dependent on their arginine content and their concentration. For example, polyarginine (Arg_9) is more efficiently translocated into the cytoplasm than other CPPs (Duchardt *et al.*, 2007). Cargo molecules also affect the subcellular distribution of CPPs, often changing the localization from a more diffused staining to a punctate, endosomal staining (Maiolo *et al.*, 2005; Tunnemann *et al.*, 2006).

Cytotoxic ribonucleases are similar to CPPs with respect to cationicity and ability to undergo endosomal translocation. In addition, the kinetic profile of RNase 1 uptake was found to be comparable to that of TAT peptides, suggesting shared endocytic mechanisms between the two (Johnson *et al.*, 2007a). Studies on the internalization properties of CPPs may shed light on the cellular entry pathways of ribonucleases.

1.4.2 Endocytic mechanisms of pancreatic-type ribonucleases

Endocytic internalization is a crucial determinant of ribonuclease cytotoxicity (Leich *et al.*, 2007). The cellular uptake of several pancreatic-type ribonucleases, including RNase 1, RNase A, ONC, BS-RNase A, and the human eosinophil cationic

protein (ECP), has been visualized in punctate endocytic compartments (Johnson *et al.*, 2007a; Haigis and Raines, 2003; Rodriguez *et al.*, 2007; Bracale *et al.*, 2002). Still, the endocytic mechanisms mediating the internalization of ribonucleases have not been fully elucidated. Although these ribonucleases share ~30–90% homology, different modes of cellular uptake have been observed for ECP, ONC, and RNase A.

Human RNase 3, also known as ECP, is a member of the RNase A superfamily involved in host defense system with potent bactericidal, helminthotoxic, and antiviral activities (Benito *et al.*, 2008). Being the most cationic pancreatic-type ribonuclease, with an estimated p*I* of 10.8 ($Z = +13$), the bactericidal activity of ECP is mediated by a membrane-lytic mechanism involving both aromatic and cationic residues (Carreras *et al.*, 2003). Nevertheless, ECP was found to enter human bronchial epithelial cell line Beas-2B via heparan sulfate-facilitated, lipid raft-dependent macropinocytosis (Fan *et al.*, 2007). Given the biological roles of ECP, it is unclear whether such findings have any physiological relevance.

The endocytic mechanism of the amphibian ribonuclease, onconase, has been investigated independently by two groups with conflicting results. By using Hela cells overexpressing the K44A dynamin dominant-negative mutant (K44A Dyn), thus excluding all dynamin-dependent endocytic pathways, Haigis *et al.* showed that onconase toxicity was enhanced by two-fold. This observation suggests that ONC internalization is independent of dynamin (Haigis and Raines, 2003). In contrast, Rodriguez *et al.* showed that overexpression of dominant-negative inhibitors of the clathrin/AP2 pathway, including K44A Dyn, Eps15, and intersectin SH3 domain, protected the cells from

onconase toxicity by two-fold (Rodriguez *et al.*, 2007). The intracellular routing of onconase was also shown to coincide with that of transferrin in the latter study, suggesting a clathrin-mediated endocytic mechanism for onconase. The discrepancy between the two studies was ultimately attributed to a slight increase in endosomal pH as a result of K44A dynamin overexpression in Hela cells that potentiated onconase toxicity (Rodriguez *et al.*, 2007). It has been noted, however, that upregulation of other pathways could occur when clathrin-mediated endocytosis is inhibited (Damke *et al.*, 1995). Therefore, the involvement of additional pathways enhancing onconase toxicity in K44A Dyn Hela cells cannot be ruled out.

The endocytic mechanism of RNase A was also determined to be dynamin-independent by using K44A Dyn Hela cells (Haigis and Raines, 2003). In addition to enhanced toxicity, microscopy analysis showed that the cellular uptake was minimally affected by the expression of the K44A Dyn mutant, indicating that dynamin is not required for RNase A internalization by Hela cells. Further characterization of the endocytic mechanism of RNase A is described in CHAPTER 3.

1.4.3 Intracellular routing of pancreatic-type ribonucleases

Following endocytosis, the majority of internalized ribonucleases remain within endocytic compartments with the exception of ANG and BS-RNase, which have been localized to the nucleus and the TGN respectively. ANG has a nuclear localization signal (residues 31–35; RRRGL), and thus it is thought to be actively imported into the nucleus, concentrating in nucleolar regions (Riordan, 1997). BS-RNase was reported to colocalize

with a TGN marker, TGN38, in transformed mouse SVT2 fibroblasts, but not in 3T3 normal fibroblasts (Bracale *et al.*, 2002). The differential routing of BS-RNase in normal and transformed cells was proposed to contribute to the selective toxicity of BS-RNase towards cancerous cells. Interestingly, RNase A contains a lysosomal degradation signal (residues 7–11; KFERQ), yet disrupting this signal sequence has no effect on ribonuclease-mediated cytotoxicity (Haigis *et al.*, 2002).

The intracellular routing of pancreatic-type ribonucleases has been probed with various pharmacological inhibitors in assays measuring their anti-proliferative effects. Deacidification of endosomal compartments with ammonium chloride had no effect on the uptake of ONC and RNase A (Wu *et al.*, 1993; Haigis and Raines, 2003; Rodriguez *et al.*, 2007). Treatment with the polyether ionophore monensin, which may disrupt Golgi trafficking in addition to neutralization of endosomal compartments, had little effect on RNase A but potentiated the toxicity of ONC and BS-RNase by 10- to 100-fold (Wu *et al.*, 1993; Wu *et al.*, 1995; Haigis and Raines, 2003; Rodriguez *et al.*, 2007). Additionally, cytotoxicity of RNase A and ONC was increased by 10-fold in the presence of brefeldin A, which inhibits endoplasmic reticulum (ER) to Golgi transport as well as disassembles Golgi stacks (Haigis and Raines, 2003). Notably, retinoic acid (10 μM), which specifically disrupts the Golgi, was found to significantly potentiate the toxicity of ONC and BS-RNase while endowing ANG and RNase 1 with cytotoxicity (Wu *et al.*, 1995). Because brefeldin A counteracted the effects of retinoic acid, it was concluded that retinoic acid promotes the transport of ribonucleases though the *cis*-Golgi, and possibly to the ER. Altogether, these results suggest that neither acidification of endosomal

compartments, nor trafficking through the Golgi, is required for ribonuclease cytotoxicity.

1.5 Endosomal Translocation by Pancreatic-Type Ribonucleases

1.5.1 Mechanism of translocation

Translocation of macromolecules across biological membranes is not trivial. Elaborate supramolecular complexes, consisting of protein channels, receptors, chaperones, and regulatory accessory proteins, have evolved to translocate endogenous cellular proteins across membrane bound compartments (Agarraberes and Dice, 2001). Intriguingly, many toxins and pathogens that gain entry into host cells via endocytosis traverse endocytic membranes to reach their final subcellular destinations, and translocation is often achieved with single protein domains.

Bacterial toxins of the A/B type contain distinct protein modules responsible for their translocation across endosomal membranes. Diphtheria toxin is one example of the A/B type toxins, where the translocation domain undergoes a conformational change at acidic pH (5–6), exposing hydrophobic α-helices for insertion into endosomal membranes (Wang and London, 2009). *In vitro* assays have shown that such interaction is sufficient to induce liposome leakage and formation of giant pores (50–200 nm diameters), allowing the translocation of macromolecules (Khramtsov *et al.*, 2008). Another mode of translocation adopted by toxins is demonstrated by anthrax toxin, where the translocation peptide, PA, assembles into oligomers to form protein channels in the endosomal

membranes, thereby allowing partially unfolded peptides to cross the membrane barrier (Gruenberg and van der Goot, 2006).

Pathogens such as viruses have also evolved potent membrane-disruptive proteins to facilitate the escape from endosomal compartments. Enveloped viruses typically contain fusion proteins that promote fusion between the viral envelope and the endosomal membranes (White, 1990; Mudhakir and Harashima, 2009). Examples of such proteins include hemagglutinin (HA) (influenza virus), F1 (simian virus 5), and GP2 (ebola virus), all of which form trimers that protrude into the phospholipid bilayer to trigger membrane fusion. By contrast, nonenveloped viral particles translocate across endosomal membranes by two alternative mechanisms: membrane disruption (adenovirus and papillomavirus) and pore formation (reovirus and poliovirus) (Mudhakir and Harashima, 2009). Membrane disruption is generally achieved with cationic peptides, whereas pore formation requires bundles of amphipathic α-helices. Remarkably, much like the protein transduction domains in cell-penetrating proteins, many of the translocation domains function outside the context of the proteins (White, 1990).

Most cell-penetrating peptides (CPPs) also possess the ability to traverse membranes. Transient pore formation in liposomal models has been observed for both amphipathic and cationic peptides (Herce *et al.*, 2009; Lamaziere *et al.*, 2007). Instead of forming protein-lined channels, as is the case for certain bacterial toxins and viral translocation proteins, the strong electrostatic interaction between cationic residues and phosphate head groups is proposed to create large distortions of the phospholipid ordering, inducing saddle-shaped negative Gaussian curvature in the membranes (Herce

and Garcia, 2007; Schmidt *et al.*, 2010). As the local density of the CPPs increases, a gradual decrease in the thickness of the bilayer leads to pore formation and translocation of the peptides (Herce and Garcia, 2007). Both a pH gradient and an electrostatic potential gradient across the membrane are thought to enhance translocation (Terrone *et al.*, 2003; Magzoub *et al.*, 2005); however, it is unclear whether such gradients are essential for CPP translocation across cellular membranes.

1.5.2 Endosomal translocation of pancreatic-type ribonucleases

The mechanism of ribonuclease translocation has not been elucidated, though certain pancreatic-type ribonucleases, including BS-RNase, engineered dimers of RNase 1 and RNase A, have been reported to induce membrane aggregation, increase membrane fluidity, as well as promote membrane fusion in liposomal models (Notomista *et al.*, 2006). In addition, it was found that the ability to induce membrane perturbations correlated with the cationicity of the ribonuclease; monomeric RNases with a net charge less than six had minimal effects on membrane stability (Notomista *et al.*, 2006). Considering the various mechanisms of translocation discussed above, it is likely that pancreatic-type ribonucleases also form transient pores in the membranes in a fashion similar to the CPPs. The translocation efficiency of ribonucleases is expected to be much less compared with the CPPs due to their larger size and smaller charge density.

The relative translocation efficiency of several ribonuclease variants and homologues has been investigated in cell-free systems. First, through immunoblot of subcellular fractionated cell lysates, Leich *et al.* quantified the relative distribution of

endocytosed RNase A and RNase 1 variants in various cellular compartments (Leich *et al.*, 2007). Corroborating *in vitro* liposomal studies, engineered RNase 1 dimers were found to have greater endosomal translocation than monomeric RNase A variants. Higher cationicity was also shown to be advantageous in the cytoplasmic delivery of ribonuclease (Leich *et al.*, 2007). Another study measuring the translocation of ^{125}I-labeled ONC from purified endosomes showed that ONC translocation is energy dependent, and that it occurs more efficiently at neutral pH (Rodriguez *et al.*, 2007). The requirement for ATP hydrolysis suggests potential involvement of cellular proteins in ONC translocation while neutral pH was proposed to facilitate translocation of ONC by preventing its dissociation from an unknown cell-surface receptor.

The translocation of pancreatic-type ribonucleases has not been investigated in live cells due to the lack of a sensitive detection method for monitoring such events. As the majority of endocytosed ribonucleases are entrapped in endocytic compartments, it is difficult to track the rare translocation events over the inordinate background from endosomes and lysosomes. As an initial attempt in characterizing endosomal translocation *in cellulo*, we have devised a novel fluorescent-based assay for monitoring the cytoplasmic entry of ribonucleases. This work is further discussed in CHAPTER 4.

1.6 Redirecting Internalization as a Strategy for Enhancing Ribonuclease-Mediated Cytotoxicity

Internalization is a prime determinant of ribonuclease-mediated cytotoxicity (Leich *et al.*, 2007), yet this process has not been optimized for pancreatic-type ribonucleases. The inefficiency of ribonuclease internalization is demonstrated in a study where extracellularly administered RNase A was found to be harmless to frog oocytes at high concentrations while direct microinjection of RNase A into the cytoplasm of oocytes made it a potent cytotoxin (Rybak *et al.*, 1991). The hurdles that ribonucleases have to overcome to reach the cytoplasm are manifold: each step along the ribonuclease internalization pathway has an impact on the eventual cytoplasmic concentration of ribonucleases, which is closely associated with the cytotoxic capabilities exhibited by ribonucleases.

Different approaches have been used to improve the internalization efficiency of cytotoxic ribonucleases with the overall goal of achieving better efficacy and a higher therapeutic index for these potential chemotherapeutics. For example, cationization through site-directed mutagenesis or chemical conjugation has long been recognized as a way to increase overall internalization of ribonucleases (Futami and Yamada, 2008; Johnson *et al.*, 2007a; Futami *et al.*, 2001). 100 and 1000 fold augmentation of cytotoxicity were observed for RNase A when the net charge was increased from +4 to +20 and +46 respectively (Futami *et al.*, 2001; Futami *et al.*, 2005). Increased cytotoxicity was also observed for transferrin and anti-CD22 single chain antibody

conjugates of RNase A and ONC (Rybak, 2008). Targeting ribonucleases for a specific receptor-mediated endocytosis pathway enhanced both the specificity and internalization efficiencies. Furthermore, insertion of a nuclear localization signal redirected intracellular routing of RNase 1 to the nucleus and endowed it with cytotoxic capabilities even though it is sensitive to RI inhibition (Bosch *et al.*, 2004; Tubert *et al.*, 2010). Finally, a weak-base amphipathic peptide known as the Endo-porter drastically increased the toxicity of a cationic RNase A variant, presumably by facilitating the endosomal translocation of the variant (Futami and Yamada, 2008). Altogether, these results indicate that ribonuclease-mediated toxicity can be modulated by altering the internalization properties of pancreatic-type ribonucleases.

Among the major determinants of ribonuclease-mediated cytotoxicity—conformational stability, catalytic ability, internalization, and interaction with RI—internalization is the only property that has not been actively optimized for pharmaceutical purposes. A thorough understanding of the cellular entry pathway of pancreatic-type ribonucleases is imperative for the further development of ribonuclease-based chemotherapeutics. This thesis describes the characterization of internalization properties of RNase A (CHAPTER 2, CHAPTER 3), ONC (CHAPTER 2), and RNase 1 (CHAPTER 5), as well as the development of novel assays specifically measuring the endocytosis (CHAPTER 6) and cytoplasmic delivery of ribonucleases (CHAPTER 4). The design and synthesis of novel latent fluorogenic labels have been indispensable to the study of ribonuclease internalization, and these are described in CHAPTERS 6–9.

Figure 1.1 Putative mechanism of ribonuclease cytotoxicity.

(A) Ribonucleases, represented by the bean-like shapes, interact with the cell surface, (B) and enter cells by endocytosis. (C) Upon internalization, a fraction of internalized ribonucleases translocate from endocytic compartments into the cytoplasm, (D) where they can either be (E) bound by RI, denoted by the horseshoe-like shape, or (F) evade RI inhibition, leading to apoptosis (Rutkoski and Raines, 2008).

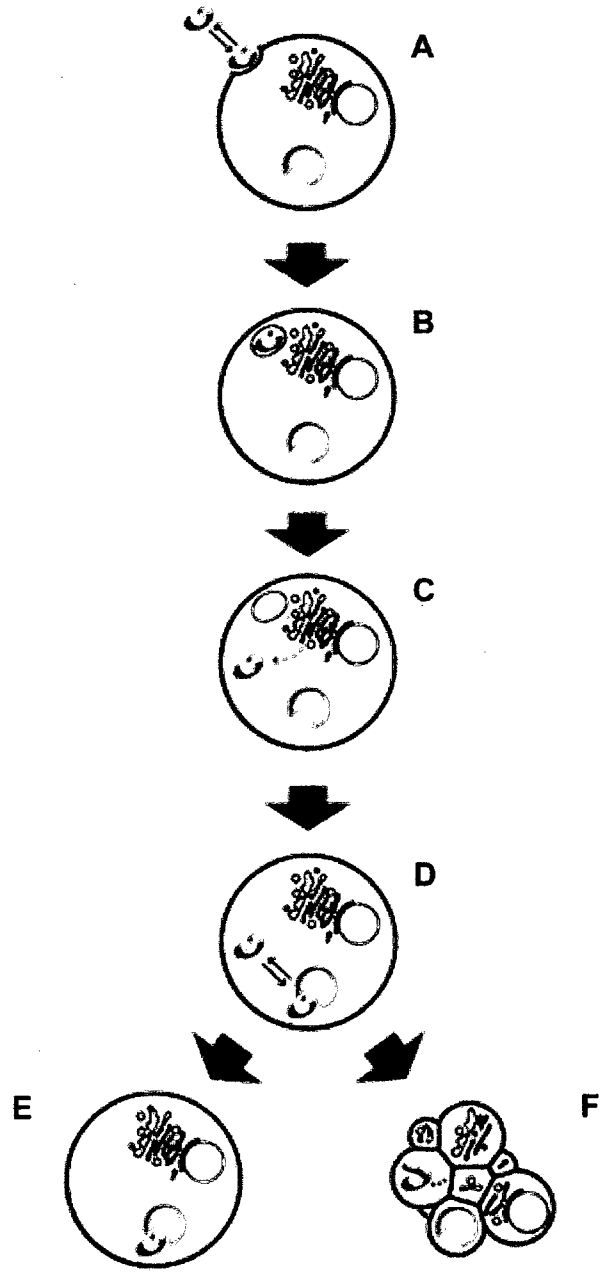
A
B
C
D
E
F

Figure 1.2 Comparison of the crystalline structures of ribonuclease homologues. (A) Superposition of the backbone structures of ONC (thin lines; PDB entry 10NC) vs cSBL-sialic acid complex (thick lines). (B) Superposition of the backbone structures of RNase A (thin lines; PDB entry IRPG) vs cSBL-sialic acid complex (thick lines). Sialic binding sites are indicated as (I) higher affinity site, and (II) lower affinity site. Numbers represent the residue numbers of RNase A (Irie *et al.*, 1998).

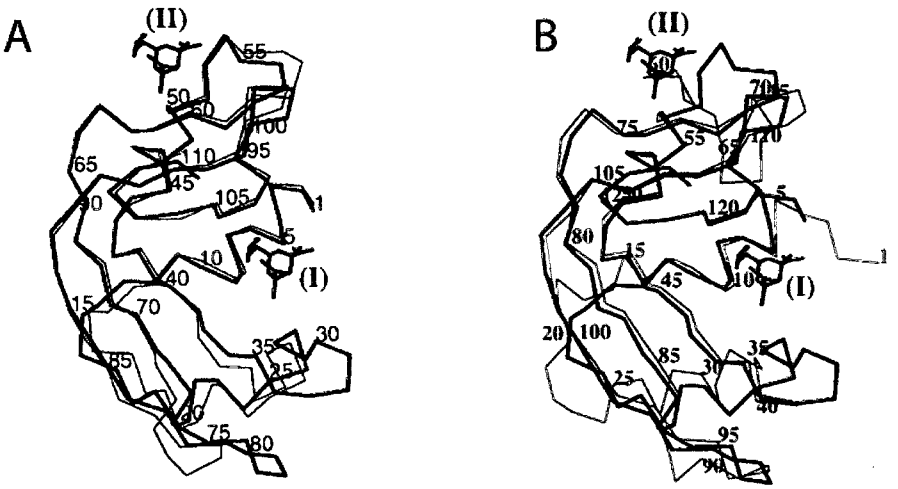
A
(II)
55
50
60
100
65
110
95
45
105
1
90
5
10
(I)
40
15
70
30
35
85
80
75
B
(II)
60
70
75
55
65
120
105
5
120
80
15
45
(I)
20
100
85
35
25
40
95

Figure 1.3 Overview of endocytic mechanisms of mammalian cells. Phagocytosis and macropinocytosis rely heavily on actin, which is represented by short grey line segments. Clathrin, which is drawn in red, assembles into a basket-like structure that coats the cytoplasmic site of the vesicles, whereas Caveolin-1 assembles into spiral structures coating the flask shaped membrane invagination. Dynamin forms a ring around the neck of vesicles (Conner and Schmid, 2003).

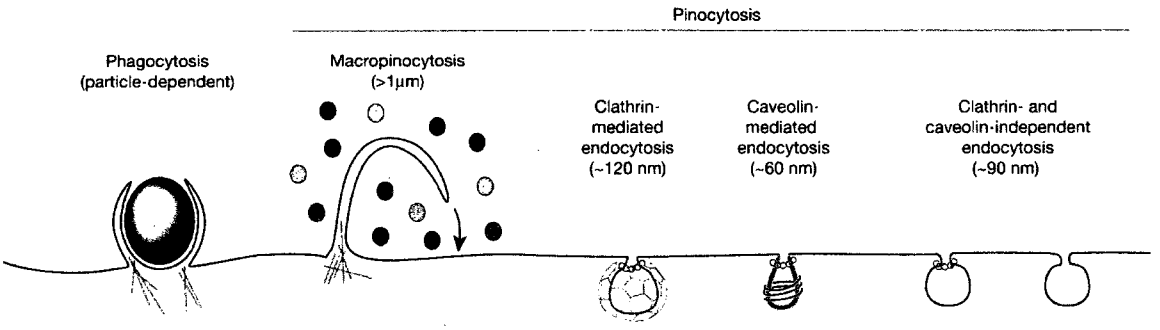
Pinocytosis
Phagocytosis
(particle-dependent)
Macropinocytosis
(>1μm)
Clathrin-
mediated
endocytosis
(~120 nm)
Caveolin-
mediated
endocytosis
(~60 nm)
Clathrin- and
caveolin-independent
endocytosis
(~90 nm)

CHAPTER 2

Contribution of Anionic Glycans

to the Cellular Uptake of Ribonucleases

Contribution: I performed all of the research described in this chapter, except for the synthesis of latent fluorophore (L.D. Lavis) and glycan array analysis (Consortium for Functional Glycomics).

Prepared for submission as:
Chao, T.-Y., Lavis, L.D., Raines, R.T. (2010)
Contribution of anionic glycans to the cellular uptake of ribonucleases

2.1 Abstract

Cationic proteins can enter human cells. Here, we report on the biochemical basis for the cellular uptake of two such proteins. One, Onconase® (ONC), is an amphibian cytotoxin of demonstrated clinical utility as an anticancer agent. The other, bovine pancreatic ribonuclease (RNase A), is a well-known mammalian homologue of ONC. We find that neither RNase A nor ONC has high affinity for any particular cell-surface glycan in a comprehensive array. The uptake of RNase A, but not ONC, does correlate directly with cell anionicity. Analyses *in vitro* and *in cellulo* indicate that RNase A targets abundant cell-surface proteoglycans and sialic acid-containing glycoproteins, whereas ONC binds to glycoproteins that do not necessarily lead to productive internalization. RNase A achieves a steady-state cellular level within a few hours; ONC internalization is much slower. We conclude that mammalian but not amphibian ribonucleases target the anionic cell-surface moieties that are especially abundant on tumor cells.

2.2 Introduction

Cancer has been the second leading cause of death in the U.S. since 1935. As a consequence, tremendous efforts have been devoted to the development of anticancer agents with a high efficacy and therapeutic index. Traditional cancer chemotherapy is based on small molecules that target DNA synthesis and transcription (Dan *et al.*, 2002). Newer small-molecule and monoclonal antibody-based anticancer drugs interfere with the function of a wider variety of proteins (Onyango, 2004). The use of oligonucleotides or derivatives to target RNA is another strategy, but one that now suffers from inefficient delivery (Alvarez-Salas, 2008). The pancreatic-type ribonucleases represent a novel class of cancer chemotherapeutic agent that interrupts the flow of genetic information at the RNA level. One such ribonuclease, Onconase® (ONC (Lee and Raines, 2008)), is on the verge of approval as a chemotherapeutic agent for malignant mesothelioma, and has orphan-drug and fast-track status.

Isolated from oocytes of the Northern leopard frog *Rana pipiens*, ONC exhibits cytostatic and cytotoxic activity that is selective for cancer cells (Darzynkiewicz *et al.*, 1988). Cells treated with sub-micromolar concentrations of ONC exhibit significant inhibition of protein synthesis and arrest at G_1 phase within 24–48 h of incubation (Wu *et al.*, 1993; Darzynkiewicz *et al.*, 1988). ONC cleaves various RNAs, including rRNA, tRNA, and siRNA (Iordanov *et al.*, 2000a; Wu *et al.*, 1993; Zhao *et al.*, 2008); RNA degradation can activate caspase-9/caspase-3 and serine proteases, leading to apoptosis (Iordanov *et al.*, 2000b; Mei *et al.*, 2010).

Surprisingly, bovine pancreatic ribonuclease (RNase A (Raines, 1998); EC 3.1.27.5) is not cytotoxic, despite being homologous to ONC. Unlike ONC, RNase A interacts tightly with the cytosolic ribonuclease inhibitor (RI) (Vicentini *et al.*, 1990). Variants of RNase A that evade RI are cytotoxic (Leland *et al.*, 1998). One such variant, D38R/R39D/N67R/G88R RNase A (DRNG RNase A), contains four amino-acid substitutions that disrupt shape complementarity within the RI–RNase A interface, resulting in a 2×10^6-fold increase in the K_d value of the RI·RNase A complex and a concomitant gain in cytotoxicity (Rutkoski *et al.*, 2005). *In vitro* studies have shown that DRNG RNase A has greater cancer-cell selectivity than ONC (Rutkoski *et al.*, 2005). Thus, cytotoxic mammalian ribonucleases such as DRNG RNase A are promising chemotherapeutic agents with the possibility of fewer off-target effects and less immunogenicity.

The accepted pathway by which ribonucleases mediate cytotoxicity consists of cell-surface binding/association, internalization, endosomal escape, and cleavage of cytosolic RNA (Leland and Raines, 2001; Rutkoski and Raines, 2008). Efficient cellular uptake is a prime determinant of ribonuclease cytotoxicity (Leich *et al.*, 2007). As both DRNG RNase A and ONC are highly cationic proteins, adsorptive endocytosis rather than receptor-mediated endocytosis has been proposed as the mechanism of internalization (Benito *et al.*, 2005).

Several lines of evidence suggest that Coulombic interaction plays a role in the initial association of ribonucleases with the anionic cell surface. Condensing carboxyl groups with ethylenediamine increases the net charge of RNase A as well as its

cytotoxicity (Futami *et al.*, 2005; Futami and Yamada, 2008). Similarly, cationization of ONC, its homologue cSBL, and RNase A by site-directed mutagenesis enhances internalization and cytotoxicity (Turcotte *et al.*, 2009; Fuchs *et al.*, 2007; Ogawa *et al.*, 2002). In addition, ONC and RNase A bind to the cell surface in a nonsaturable manner (Haigis and Raines, 2003).

The toxicity of certain ribonucleases is highly specific for cancer cells *in vivo* and *in vitro* (Arnold and Ulbrich-Hofmann, 2006), but the underlying mechanism for this preference is unclear. The specificity has been attributed to unusual intracellular trafficking patterns, a high metabolic state, and the activation of pro-apoptotic pathways that are present in malignant cells but not normal cells (Bracale *et al.*, 2002; Smith *et al.*, 1999; Iordanov *et al.*, 2000b). There is another hypothesis. Cancer cells are known to have altered cell-surface molecules and lipid-bilayer composition. Elevated levels of carboxyl- and sulfuryl-containing carbohydrates are frequently observed on cancer-cell surfaces (Dube and Bertozzi, 2005), along with increased phosphatidylserine content in the outer leaflet of the plasma membrane (Ran *et al.*, 2002). As a result, the surface of cancer cells is often more anionic than that of normal cells (Slivinsky *et al.*, 1997).

We sought to determine if cell-surface charge plays a role in ribonuclease cytotoxicity. We did so by analyzing cell-surface binding of DRNG RNase A and ONC using cells with varying degrees of cell-surface charge. Additionally, through measuring the internalization of the ribonucleases into mutant cells with cell-surface carbohydrate deficiencies, we discovered which cell-surface molecules mediate uptake. Although these ribonucleases share a similar structure and net charge, we observed marked and

unexpected differences regarding their cellular uptake. These results shed new light on the biochemical basis for ribonuclease cytotoxicity.

2.3 Experimental Procedures

2.3.1 Materials

Escherichia coli strains BL21 (DE3) was from Novagen (Madison, WI). [*methyl*-^{3}H]Thymidine (6.7 Ci/mmol) was from Perkin–Elmer (Boston, MA). *Clostridium perfringens* neuraminidase was from New England Biolabs (Ipswich, MA). *Staphylococcus aureus* strain V8 protease was from Sigma–Aldrich (St. Louis, MO). Rabbit IgG raised against RNase A was from Biodesign International (Kennebunk, ME). Chicken antiserum raised against ONC was a generous gift from Alfacell Corporation (Bloomfield, NJ). D-*threo*-1-Phenyl-2- palmitoylamino-3-morpholino-1-propanol–HCl (D-*threo*-PPMP) was from Matreya (Pleasant Gap, PA). All other chemicals and reagents were of commercial reagent grade or better, and were used without further purification.

2.3.2 Mammalian cell lines

CHO-K1, CHO-677 (pgsD-677), CHO-745 (pgsA-745), Pro 5, Lec 2 cells were obtained from the American Type Culture Collection (Manassas, VA). CHO cell lines were grown in F12 medium. Pro 5 cells were grown in α-MEM with ribonucleosides and deoxyribonucleosides. Lec 2 cells were grown in α-MEM. All medium for mammalian cell culture contained FBS (10% v/v), penicillin (100 units/mL), and streptomycin (100

μg/mL). Cell-culture medium and supplements were from Invitrogen (Carlsbad, CA). Cells were cultured at 37 °C in a humidified incubator containing CO_2(g) (5% v/v).

2.3.3 Instrumentation

Molecular mass was measured by MALDI–TOF mass spectrometry using sinapinic acid as a matrix with a Voyager-DE-PRO Biospectrometry Workstation (Applied Biosystems, Foster City, CA) in the campus Biophysics Instrumentation Facility. Radioactivity was quantified by scintillation counting using a Microbeta TriLux liquid scintillation counter (Perkin–Elmer, Boston, MA). Flow cytometry data were collected in the University of Wisconsin Paul P. Carbone Comprehensive Cancer Center with a FACSCalibur flow cytometer equipped with a 488-nm argon-ion laser (Becton Dickinson, Franklin Lakes, NJ). Microscopy images were obtained with a Nikon C1 laser scanning confocal microscope with a 60× oil immersion objective with NA 1.4. The zeta potential of cells was measured with a Malvern Zetasizer 3000HS dynamic light scattering instrument (Malvern, Worcestershire, UK).

2.3.4 Purification of ribonucleases

Unlabeled variants of RNase A and ONC were produced in *E. coli* strain BL21(DE3) and purified as described previously (Leland *et al.*, 1998). Following purification, protein solutions were dialyzed against PBS and filtered (0.2-μm pore size) prior to use. Protein concentrations were determined by UV spectroscopy using

extinction coefficients of $\varepsilon_{280} = 0.87$ $(mg \cdot mL^{-1})^{-1}cm^{-1}$ for ONC and $\varepsilon_{278} = 0.72$ $(mg \cdot mL^{-1})^{-1} \cdot cm^{-1}$ for RNase A.

2.3.5 *Fluorophore labeling of ribonucleases*

DRNG A19C RNase A and S61C ONC contain free cysteine residues for site-specific conjugation. During their purification, the free thiol groups were protected by reaction with 5,5′-dithio-bis(2-nitrobenzoic acid) (DTNB). Immediately prior to latent-fluorophore attachment, TNB-protected ribonucleases were deprotected with a four-fold excess of dithiothreitol and desalted by chromatography on a PD-10 column (GE Biosciences, Piscataway, NJ). A maleimido-containing latent fluorophore (**1**) was synthesized as described previously (Lavis *et al.*, 2006a). Deprotected ribonucleases were reacted for 6 h at 25 °C with a ten-fold molar excess of latent fluorophore **1** (Fig. 2.2A) (Lavis *et al.*, 2006a). Conjugates were purified by chromatography using a HiTrap SP HP cation-exchange column (GE Biosciences, Piscataway, NJ). The molecular masses of RNase A, its variants, and conjugates were confirmed by MALDI–TOF mass spectrometry. Protein concentration was determined by using a bicinchoninic acid (BCA) assay kit (Pierce, Rockford, IL) with wild-type RNase A as a standard.

2.3.6 *Glycan array screening*

A glycan array was screened for ribonuclease ligands by the standard procedure of Core H of the Consortium for Functional Glycomics (Blixt *et al.*, 2004). The array (version 2.0) comprises 264 synthetic and natural biologically relevant amine-

functionalized glycoconjugates that are immobilized to *N*-hydroxysuccinimide-activated glass slides (Blixt *et al.*, 2004). Briefly, stock solutions of wild-type ONC and RNase A were diluted to a concentration of 200 μg/mL with binding buffer (20 mM Tris–HCl, pH 7.4, containing 150 mM sodium chloride, 2 mM calcium chloride, 2 mM magnesium chloride, 0.05% v/v Tween 20, and 1% w/v BSA). Binding of ribonucleases was detected by incubating with primary antibodies and secondary antibodies labeled with Alexa Fluor® 594 (Invitrogen, Carlsbad, CA), which is a xanthene dye (Panchuk-Voloshina *et al.*, 1999). Primary antibody against RNase A was used at a concentration of 1 μg/mL; antiserum against ONC was used at a 1:100 dilution. To correct for antibody binding, the antibodies were screened against the array independently and fluorescence values obtained with antibodies were subtracted from the wild-type proteins.

2.3.7 Heparin-affinity chromatography

The affinity of ribonuclease for heparin was assessed *in vitro*. DRNG RNase A and ONC were mixed in a 1:1 ratio (1.0 mg each) in PBS at pH 7.2. This mixture was loaded onto a 1.0-mL HiTrap Heparin HP column (GE Healthcare, Piscataway, NJ). The column was washed with PBS, and ribonucleases were eluted with a linear gradient of NaCl (0.00–0.45 M) in PBS. Elution was monitored by absorbance at 280 nm, and eluted proteins were identified by mass spectrometry.

2.3.8 Flow cytometry

The cellular internalization of ribonucleases was followed by monitoring the unmasking of a pendant latent fluorophore by intracellular esterases. CHO cells from near confluent flasks were detached with a non-enzymic cell-dissociation solution (Sigma–Aldrich, St. Louis, MO), collected by centrifugation, and resuspended at a density of 1×10^6 cells/mL in fresh F12 media containing FBS (10% v/v). Labeled or unlabeled ribonucleases (10 μM) were added to 250 μL of F12/FBS containing 1×10^6 cells/mL of CHO cells. Samples were then allowed to incubate with ribonucleases at 37 °C for varying times. To quench internalization, CHO cells were collected by centrifugation at 1,000 rpm for 5 min at 4 °C, washed once with ice-cold PBS, and resuspended with 250 μL of PBS. Samples remained on ice until analyzed by flow cytometry.

Fluorescence was detected through a 530/30-nm band-pass filter. Cell viability was determined by staining with propidium iodide, which was detected through a 660-nm long-pass filter. The mean channel fluorescence intensity of 20,000 viable cells was determined for each sample with CellQuest software and used for subsequent analyses. To determine the steady-state rate constant for ribonuclease internalization, fluorescence intensity data were fitted to eq 2.1, in

$$F = F_{\max}(1 - e^{-k_i t}) \tag{2.1}$$

which F_{max} is the fluorescence intensity upon reaching the steady-state and k_I is the first-order rate constant for ribonuclease internalization into CHO cells.

2.3.9 Zeta potential measurements

The zeta potential (ζ) of cells, which is a measure of their net charge, was determined by assessing their electrophoretic mobility in a fixed electric field (19 V/cm). This electrophoretic mobility is related to zeta potential by eq 2.2, in which μ is electrophoretic mobility, and ε and η

$$\mu = \frac{\varepsilon\zeta}{4\pi\eta} \tag{2.2}$$

are the dielectric constant and viscosity of the solution, respectively. CHO cells in a near-confluent culture were detached from flasks by using a non-enzymatic cell-dissociation solution. The cells were collected by centrifugation at 1,000 rpm for 5 min, washed once with PBS (pH 7.0), and resuspended at a density of 3×10^4 cells/mL. Cells were then passed through a 40-μm nylon cell strainer immediately prior to use. The instrument was calibrated with a Zeta Potential Transfer Standard solution ($\zeta = -50 \pm 5$ mV). Electrophoretic mobility was determined by measurements for 15 min at 25 °C with 3 mL of cell suspension. Values of ζ are the mean (±SE) from at least three independent experiments with at least five measurements each.

2.3.10 Immunofluorescence microscopy

The binding of ribonucleases to cells was visualized by immunofluorescence microscopy. CHO cells were plated on coverslips placed in six-well plates 18–24 h before the experiment at a density of 5×10^5 cells/well. The next day, cells were washed twice with ice-cold medium, resuspended in 800 μL of medium containing FBS (10% v/v), followed by addition of a ribonuclease to 10 μM. The plate was then incubated on ice for 30 min. Samples were washed three times with medium containing FBS (10% v/v) and fixed with paraformaldehyde (4% v/v) for 20 min at 4 °C to prevent endocytosis. Following fixation, cells were washed five times with PBS containing Ca^{2+}/Mg^{2+} (1 mM each) and Tween 20 (0.1% v/v). Cell-surface associated ribonucleases were detected with a primary antibody (1 μg/mL), and fluorophore-labeled secondary antibody (1:1000 dilution). Coverslips were mounted on microscopy slides with MOWIOL 4-88 (Calbiochem, Gibbstown, NJ) and stored at 4 °C until analysis by confocal microscopy.

2.3.11 Cytotoxicity assays

The effect of a ribonuclease on the proliferation of CHO cells was assayed as described previously (Leland *et al.*, 1998; Rutkoski *et al.*, 2005). After a 44-h incubation with DRNG RNase A or ONC, cells were treated with [*methyl*-^{3}H]thymidine for 4 h, and the incorporation of radioactive thymidine into cellular DNA was quantitated by liquid scintillation counting. The results are reported as the percentage of [*methyl*-^{3}H]thymidine incorporated relative to control cells. Data are the average of three measurements for each

concentration, and the entire experiment was repeated in triplicate. Values of IC_{50}, which is the concentration of ribonucleases that decreases cell proliferation to 50%, were calculated by fitting the data using nonlinear regression to a sigmoidal dose–response curve, eq 2.3, in which y is the DNA synthesis following the [*methyl*-^{3}H]thymidine pulse and h is the slope of the curve.

$$y = \frac{100\%}{1+10^{(\log(IC_{50})-\log[\text{ribonuclease}])h}} \tag{2.3}$$

2.4 Results

2.4.1 Glycan array screening

Eukaryotic cells are covered by a glycocalyx—an extensive network of polysaccharides (Varki *et al.*, 2008). The glycocalyx serves as a rich source of binding sites for receptors and ligands, as well as pathogens and toxins. The mammalian glycome is estimated to consist of a few hundred unique glycan structures on glycoproteins and glycolipids (Drickamer and Taylor, 2002). To identify the oligosaccharides recognized by RNase A and ONC, we screened these ribonucleases against a library of 264 glycans.

Initially, we assessed binding to glycans by using ribonucleases labeled directly with Alexa Fluor® 488 (Panchuk-Voloshina *et al.*, 1999). The resulting binding profile, however, showed no significant signals from ONC, and those from RNase A were of low intensity and high standard error. To increase the signal-to-noise ratio, we assessed binding by using polyclonal antibodies against RNase A and ONC, and a fluorophore-

labeled secondary antibody. As mammalian serum can contain anti-carbohydrate antibodies, we screened the antibodies against the array independently and subtracted the resulting fluorescence values from those in the presence of RNase A. The results are shown in Fig. 2.1.

RNase A bound to a few glycan structures with moderate affinity (Fig. 2.1A). These structures fall into two categories: glycoproteins and unbranched glycans. The glycoproteins bound by RNase A are serum proteins with complex glycan modifications. Human α1-acid glycoprotein (AGP, glycan **1–3**) contains various forms of di-, tri- and tetraantennary sialylated carbohydrate chains; transferrin (glycan **6**) contains two disialylated biantennary glycans; and ceruloplasmin (glycan **4**) possesses bi- and triantennary *N*-glycosidic glycans (Nakano *et al.*, 2004; Charlwood *et al.*, 1998; Endo *et al.*, 1982). All forms of these glycoproteins are anionic (p*I* 2.7–5.5). Thus, the high fluorescence from RNase A binding could have arisen through nonspecific electrostatic interaction with the proteins.

Also recognized by RNase A were several tetrasaccharides and hexasaccharides. The hexasaccharides Fucα1-2Galβ1-3GalNAcβ1- 3Galα1-4Galβ1-4Glcα-Sp9 (glycan **56**) and Neu5Acaα2-3Galβ1-3GalNAcβ1-3Galα1-4Galβ1-4Glcβ-Sp0 (glycan **223**) belong to the globo-series of glycosphingolipids. Glycan **56**, also known as the Globo-H antigen, is found on a variety of cells and is the basis for an anti-cancer vaccine in a clinical trial (Warren *et al.*, 2007). Glycan **223** represents the Stage Specific Embryonic Antigen 4, which is expressed briefly during early stages of development and in certain teratocarcinoma cells (Kannagi *et al.*, 1983; Venable *et al.*, 2005). Surprisingly, RNase A

bound only weakly to the pentasaccharide precursor to these molecules, Galβ1-3GalNAcβ1-3Galα1-4Galβ1-4Glc (glycan **127**), but interacted tightly with a similar structure, GalNAcβ1-3Galα1-4Galβ1-4GlcNAcβ-Sp0 (glycan **90**). Together, these results suggest that RNase A recognizes the core tetrasaccharide GalNAcβ1-3Galα1-4Galβ1-4Glc that constitutes all globo-series glycosphingolipids. Still, the relative fluorescence indicates that RNase A had somewhat higher affinity for the glycoproteins than the globo-series glycans.

In marked contrast to RNase A, ONC did not recognize specific glycoconjugates in the array. Instead, ONC interacted with a broad range of structures (Fig. 2.1B). The mean fluorescence was 13890 relative fluorescence units (RFUs), and 92% of the glycans fell within twofold of the mean value. Additionally, ONC had similar affinity for glycans that terminated in sulfated galactose (glycan **26–47**), fructose (glycan **55–78**), *N*-acetyl galactosamine (glycan **79–93**), galactose (glycan **94–155**), mannose (glycan **189–200**), and sialic acid (glycan **53**, **54**, **201–264**). These data indicate that ONC does not have a preference for a specific monosaccharide structure, nor does it have a preference for an anionic terminal residue. The promiscuity of ONC binding was unexpected, as close homologues of ONC (cSBL and jSBL) are known to recognize cell-surface sialoglyconjugates (Irie *et al.*, 1998). Still, two of the five glycan structures that displayed the highest fluorescence (glycans **94**, **114**, **145**, **203**, and **235**) terminate in sialic acid. Glycan **203**, in particular, contains four consecutive sialic-acid residues linked through α-2,8 linkages, mimicking polysialic acid.

2.4.2 *Interaction with glycosaminoglycans*

One major class of glycans that is not represented in the glycan array is the glycosaminoglycans (GAGs), which are long unbranched polysaccharides consisting of repeating disaccharide units (Laremore *et al.*, 2009). As cell-surface GAGs are highly heterogeneous, we first sought to determine if RNase A and ONC interact with heparin, which is a relatively homogeneous mimic of the GAGs on the surface of a mammalian cell (Fuchs and Raines, 2004; Varki *et al.*, 2008). To minimize the effect of non-specific Coulombic interactions, we employed the cytotoxic DRNG variant of RNase A, which has the same the net charge ($Z = +6$) as wild-type ONC. We were surprised to find that, despite having an identical charge, ONC had markedly less affinity for heparin than did DRNG RNase A (Fig. 2.2A). Interestingly, the affinity of ONC for oligonucleotides is <1% that of RNase A (Lee and Raines, 2003), suggesting that ONC has a general deficiency relative to RNase A in its ability to interact with anionic biopolymers.

Next, we sought to discover whether this difference in the mammalian and amphibian ribonucleases is replicated on the cell surface. To do so, we employed CHO-745 cells, which have defects in xylosyltransferase and are thus deficient in both heparan sulfate and chondroitin sulfate on the cell surface (Esko *et al.*, 1985). The internalization of ribonucleases into wild-type and mutant cells was assessed by conjugation to latent fluorophore **2.1**, which become fluorescent upon hydrolysis by cellular esterases (Fig. 2.2B); the obfuscating extracellular fluorescence from cell-surface associated ribonucleases that would appear with typical fluorophores is absent (Lavis *et al.*, 2006a; Johnson *et al.*, 2007a).

First, internalization was visualized by live-cell confocal microscopy. RNase A was internalized to a much higher level by wild-type (CHO-K1) cells (Fig. 2.2C, panel i) than by mutant (CHO-745) cells (panel ii), suggesting the glycaosaminoglycans play a role in RNase A uptake. By contrast, the level of ONC uptake is similar in CHO-K1 (panel iii) and CHO-745 cells (panel iv), and is much lower than that of RNase A.

Next, we examined the kinetics of internalization by using flow cytometry. The cellular uptake of DRNG RNase A was linear for the first 2 h and then approached a steady-state level (Fig. 2.2D). The fluorescence intensity in the steady-state was dependent on the dose of DRNG RNase A up to 10 μM (data not shown), indicating that cell-surface binding sites are not saturable. The ribonuclease-binding sites can, however, be depleted after hours of continuous internalization, and this depletion apparently leads to a steady state. The decrease in uptake rate was specific for RNase A, as the rate of uptake for endocytic markers such as transferrin was constant for 6 h (data not shown). Finally, CHO cells did not show signs of apoptosis or enhanced propidium iodide staining after 6 h of incubation. Wild-type RNase A, which is not cytotoxic, exhibited the same pattern as the cytotoxic variant DRNG RNase A, but at a lower steady-state level (data not shown).

The uptake of DRNG RNase A by CHO cells can be analyzed quantitatively. Fitting the data in Fig. 2.2D to eq 2.1 gives an uptake $t_{1/2} = \ln 2/k_1 = 100$ and 120 min for CHO-K1 and CHO-745 cells, respectively, values comparable to those for the uptake of RNase 1 by K562 cells (20). The initial rate of DRNG RNase A uptake by CHO-K1 cells (220 ± 30 RFU h^{-1} at 10 μM) is ~4-fold greater than that by CHO-745 cells (60 ± 20 RFU

h^{-1}). Similarly, the steady-state level attained by CHO-K1 cells is ~4-fold greater than by CHO-745 cells. As the fluid-phase endocytic rate is comparable for these cell lines (data not shown), these results imply that heparan sulfate and chondroitin sulfate play key roles in mediating RNase A uptake.

In contrast to DRNG RNase A, the internalization rate of ONC is similar in CHO-K1 and CHO-745 cells (Fig. 2.2E), suggesting that these GAGs are not involved in ONC uptake. Moreover, the initial rate of ONC uptake by CHO-K1 cells (4.1 ± 0.2 RFU h^{-1} at 10 μM) is ~50-fold less than that of DRNG RNase A uptake, and only slightly above the rate of fluid-phase uptake as measured with dextran. These data are in gratifying agreement with the biochemical analyses of heparin-binding by DRNG RNase A and ONC (Fig. 2.2A). The disparate rates and modes of RNase A and ONC uptake also indicate that these homologous proteins bind distinctly to the cell surface and could avail distinct internalization mechanisms.

2.4.3 Cellular binding and cell-surface charge

Most GAGs are polyanionic. Heparan sulfate, in particular, contains a high density of sulfuryl groups and carries 4 negative charges per disaccharide unit (Laremore *et al.*, 2009). Together with sialic acid (Chen and Varki, 2010), these anionic carbohydrate moieties constitute the majority of cell-surface charge. To characterize further the relationship between cell-surface charge and ribonuclease binding, we employed other mutant cells with GAG deficiencies. CHO-677 cells lack heparan sulfate and produce 3-fold more chondroitin sulfate than do CHO-K1 cells (Lidholt *et al.*, 1992;

Norgard-Sumnicht *et al.*, 2000). We estimated the relative cell-surface charges of the wild-type and mutant CHO cells from their electrophoretic mobility (μ). By eq 2.4, the value of μ is related directly to the zeta potential (ζ), which in turn correlates with the surface charge density (σ) by a form of the Gouy–Chapman equation (Mehrishi, 1972):

$$\sigma = 13{,}410\left[1+(1-\alpha)^{1/2}\right]\sinh(\zeta/51.3) \tag{2.4}$$

where α refers to the fraction of the surface that is unavailable to counterions. As listed in Table 2.1, CHO-K1 cells, which have the most complete complement of GAGs, have the largest μ values, followed by CHO-677 cells, and then CHO-745 cells. Likewise, as shown in Fig. 2.3A–C, the amount of RNase A bound to the cell surface decreases in the order: CHO-K1 > CHO-677 > CHO-745. Unlike with RNase A, ONC binding is similar to each of the three CHO cell lines (Fig. 2.3D–F). This result corroborates the glycan array data, which likewise indicated no preference for charged carbohydrates by ONC.

2.4.4 Uptake by Pro 5 and Lec 2 cells

Sialic acid is a common terminal residue of glycolipids, and *N*- and *O*-linked glycans (Chen and Varki, 2010). Elevated levels of sialic acid on the cell surface have been associated with numerous types of tumors as a result of increased activities of *N*-acetylglycosaminyltransferase V and upregulation of sialyltransferases (Dube and Bertozzi, 2005). To determine if cell-surface sialic acid mediates the internalization of

ribonucleases, we compared DRNG RNase A and ONC uptake by sialic acid-deficient cells. Lacking the ability to translocate CMP-sialic acid across Golgi membranes, Lec 2 cells have a 90% reduction in the sialylation of glycoproteins and gangliosides compared with Pro 5 cells (Stanley *et al.*, 1980; Deutscher *et al.*, 1984). The kinetic profiles of ribonuclease uptake by these cell lines are shown in Fig. 2.4. Similar to the CHO cells, internalization of DRNG RNase A into Pro 5 and Lec 2 cells approach steady-state levels. The uptake by Pro 5 and Lec 2 cells has $t_{1/2}$ = 131 and 102 min, respectively, with Pro 5 cells reaching a higher steady-state level than Lec 2 cells. These $t_{1/2}$ values are comparable to those of CHO cells, which is consistent with a similar uptake mechanism by these cell lines. Notably, however, the difference in steady-state levels is smaller than expected—by 6 h, Pro 5 cells are only 1.8-fold more fluorescent than are Lec 2 cells, even though the difference in cell-surface sialic acid content is 10-fold. This dichotomy suggests that only a small fraction of cell-surface sialic acid is involved in RNase A internalization; most of the sialic acids are either not bound by RNase A or do not lead to efficient uptake. ONC uptake, on the other hand, does not depend on sialic acids since the initial rates are the same in Pro 5 and Lec 2 cells (Fig. 2.4B). Again, the rate and magnitude of ONC uptake is in drastic contrast to that of DRNG RNase A.

2.4.5 Uptake by treated cells

Using the paired cell lines, we have shown that multiple cell-surface moieties can mediate the uptake of RNase A. To investigate further the relative contribution of cell-surface molecules to ribonuclease uptake, we monitored internalization of DRNG

RNase A and ONC into cells that had been treated chemically or enzymatically to remove or modify certain classes of cell-surface molecules. First, cell-surface gangliosides were depleted by treating cells with D-*threo*-PPMP, a specific inhibitor of glucosylceramide synthase, which catalyzes the first glucosylation step in the synthesis of all glucosylceramide-based glycosphingolipids (Li *et al.*, 2000; Zurita *et al.*, 2001). As shown in Fig. 2.5, treatment with D-*threo*-PPMP (1 μM) for 7 days did not have an effect on the uptake of DRNG RNase A or ONC by CHO-K1 cells. (High levels of D-*threo*-PPMP (≤10 μM) were not notably cytotoxic; data not shown.) As CHO-K1 cells display predominantly the ganglioside GM3 (Crespo *et al.*, 2004), this finding indicates that GM3 is not a mediator of ribonuclease uptake. Second, protease-treated CHO-K1 cells exhibited an 80 and 60% reduction in DRNG RNase A and ONC uptake, respectively. Based on the data with glycan arrays and mutant CHO cells, the proteins that mediate DRNG RNase A uptake are likely to be anionic cell-surface proteins, including proteoglycans containing GAGs, such as heparan sulfate and chondroitin sulfate. Although ONC uptake was also decreased significantly after protease treatment, cell-surface proteins that mediate ONC internalization are likely to differ from those that mediate the uptake of DRNG RNase A. The glycan array data indicate that ONC binds to glycoproteins and glycan structures with similar affinities, irrespective of charge or structure. Hence, ONC could be interacting nonspecifically with a broad spectrum of cell-surface proteins, some of which lead to internalization and account for the majority of ONC uptake by CHO-K1 cells. Finally, neuraminidase treatment resulted in a 30 and 10% reduction in DRNG RNase A and ONC uptake, respectively. Sequential protease

and neuraminidase treatment gave similar results, as did protease treatment alone (data not shown). Apparently, the sialic acids bound by ribonucleases are components of glycoproteins rather than glycolipids, corroborating the results from D-*threo*-PPMP treatment. In conclusion, cell-surface proteoglycans and glycoproteins mediate ribonuclease uptake, whereas glycolipids do not.

2.4.6 Cytotoxicity of ribonucleases

To evaluate the toxicity of DRNG RNase A and ONC, we measured the proliferation of the CHO, Pro 5, and Lec 2 cells in the presence of ribonucleases. The results are listed as IC_{50} values in Table 2.2. For DRNG RNase A, the IC_{50} value for CHO-745 cells is 1.5-fold that for CHO-K1 cells; likewise, the IC_{50} value for Lec 2 cells is 1.5-fold that for Pro 5 cells. Although the differences in cytotoxicity do not correlate directly with the steady-state levels attended by DRNG RNase A, a trend was observed—cell lines that internalized more ribonuclease were more vulnerable to their cytotoxic activity. KDRNG RNase A is another cytotoxic variant that contains an additional, K7A, substitution, and has biochemical attributes similar to DRNG RNase A but one less charge at neutral pH. As listed in Table 2.2, the IC_{50} values of KDRNG RNase A also correlated with internalization. On the contrary, ONC displayed strikingly low IC_{50} values that range from $^1/_8$ to $^1/_{45}$ those of DRNG RNase A, even though its uptake was much less than that of DRNG RNase A. Apparently, internalized ONC is a more efficient cytotoxin than is internalized DRNG RNase A.

2.5 Discussion

DRNG RNase A and ONC are homologous cytotoxic ribonucleases. We have characterized the relevant binding repertoire of these ribonucleases *in vitro* by using a glycan array (Fig. 2.1) and heparin-affinity chromatography, as well as *in cellulo* by monitoring binding and internalization (Fig. 2.2–2.5). The use of mutant cell lines permitted us to assess the relationship between cell-surface charge and ribonuclease binding and internalization. The resulting data revealed insights into a potential tumor targeting mechanism for mammalian ribonucleases, as well as differences in the interaction of the amphibian and mammalian ribonuclease with human cells.

By quantifying the internalization of DRNG RNase A and ONC into a panel of cell lines, we find that DRNG RNase A is taken up by cells much more rapidly than is ONC. The kinetic profile of DRNG RNase A uptake is non-linear, and approaches a steady-state level after 3 h of incubation (Fig. 2.2D). For human pancreatic ribonuclease (RNase 1), the establishment of a steady-state level had been thought to be due to lysosomal degradation of ribonucleases (Johnson *et al.*, 2007a). Yet, RNase A variants are now known to resist proteolysis for up to 54 h in K562 cells (Leich *et al.*, 2007). We also found that little or no loss of fluorescence occurred if RNase A conjugates were removed from the medium during the last 3 h of incubation (data not shown). Hence, lysosomal degradation cannot account for the decrease in the rate of internalization. Instead, the rapid uptake depletes cell-surface binding sites and subsequent internalization, resulting in a gradual diminution of the rate constant over the time course.

In contrast, the depletion of binding sites for ONC is insignificant, and ONC maintains a constant uptake rate (Fig. 2.2E).

Endocytosis is a complex, multi-step process requiring the precise coordination of numerous molecules. When endocytosis is dissected into a series of kinetic events, the dynamics of cell-surface association and the mechanism of uptake are often reflected in measured kinetic parameters. In the present study, the internalization of DRNG RNase A at 10 μM can be approximated by a first-order kinetics model (eq 2.1) with rate constants of $k_I = 0.41 \pm 0.07$ h^{-1} and 0.32 ± 0.05 h^{-1} for CHO-K1 and Pro 5 cells, respectively. Kinetic analyses of RNase A uptake at additional concentrations (2 and 5 μM; data not shown) yielded a similar rate constant, as expected from this model. Similar to RNase A, the internalization of cell-penetrating peptides such as Tat has also been described by first-order kinetics (Zorko and Langel, 2005), consistent with a common uptake mechanism. From reported time-course data (Jones *et al.*, 2005), we estimate the rate constant for Tat uptake by CHO-K1 cells to be 1.2 h^{-1}. Although Tat and RNase A both interact with GAGs (Kosuge *et al.*, 2008), the uptake rate of Tat into CHO-K1 cells is 3-fold higher than that of DRNG RNase A. The greater uptake rate exhibited by Tat could be due to a higher positive charge-to-weight ratio, which leads to more favorable interaction with the anionic cell surface and thus faster uptake.

In contrast to DRNG RNase A, ONC is internalized at a constant rate for up to 10 h. Uptake of ONC (10 μM) by CHO-K1 and Pro 5 cells proceeded with initial rates of 4.1 ± 0.2 and 4.5 ± 0.2 RFU h^{-1}, respectively. A comparison of the uptakes rates of DRNG RNase A and ONC indicates that DRNG RNase A has a much more efficient

internalization mechanism, either due to higher affinity for the cell-surface or interaction with fast turnover cell-surface molecules. Although DRNG RNase A and ONC carry the same charge at physiological pH, DRNG RNase A has more arginine and lysine residues on its concave side, which could make favorable contacts with anionic cell-surface moieties. This hypothesis is consistent with the recent finding that the location of cationic residues is key to ONC internalization (Turcotte *et al.*, 2009). Our data with CHO cells suggest that ONC interacts minimally with cell-surface GAGs and sialic acids (Fig. 2.2E and 2.4B). Yet, ONC does bind to the cell surface (Fig. 2.3D–F). Protease treatment eliminated 56% of ONC uptake by CHO-K1 cells (Fig. 2.5), indicting glycoproteins as a major mediator of ONC uptake. Hence, whereas RNase A targets abundant cell-surface proteoglycans and sialic acid-containing glycoproteins, ONC binds to glycoproteins that might not mediate productive internalization.

The cytotoxicity of ribonucleases is determined by the interplay of a number of factors, including conformational stability, catalytic ability, internalization, and affinity for mammalian RI (4). With the exception of some residual affinity for human RI, DRNG RNase A is superior to ONC as a cytotoxin in all biochemical attributes. It is therefore surprising to find that ONC has lower IC_{50} values than does DRNG RNase A. Steps downstream from internalization must account for the toxicity demonstrated by ONC. For example, while RNase A resides in acidic late endosomal/lysosomal compartments (Haigis and Raines, 2003), ONC is in recycling endosomes, where the near neutral pH could facilitate ONC translocation (Rodriguez *et al.*, 2007). Ribonucleases must traverse the phospholipid bilayer to the cytosol to exert their ribonucleolytic activity, and ONC

could be translocated more efficiently than RNase A. Once in the cytosol, the cleavage of certain RNA molecules could be especially detrimental to cells. ONC degrades a broad range of RNA substrates (6-8). RNase A could be more limited in its substrates and hence less effective in triggering apoptosis. Further studies are necessary to determine the contribution of additional factors to ribonuclease cytotoxicity.

The toxicity exhibited by mammalian ribonucleases is specific for tumor cells (Rutkoski *et al.*, 2005). The basis for this specificity is unknown. As cancer cells frequently have more anionic surfaces than do their wild-type counterparts (Slivinsky *et al.*, 1997), the anionicity of the cell surface could be exploited by cationic ribonucleases as a means to target cancer cells. Herein, we have used mutant CHO cells to demonstrate a relationship between cell-surface charge and the internalization and toxicity of a mammalian ribonuclease (Fig. 2.2D and 2.3A–C; Tables 2.1 and 2.2). Interestingly, a correlation between cell-surface charge and tumorigenicity is known among these same cell lines. CHO-K1 cells, with the most complete complement of cell-surface carbohydrates and highest μ value, have the highest frequency of tumor formation in nude mice, whereas CHO-677 and CHO-745 do not produce tumors (Table 2.1). Hence, our finding that the μ value of cells correlates directly with the cell-surface binding, internalization, and cytotoxicity of a mammalian ribonuclease is consistent with the therapeutic index arising, at least in part, from the targeting of the anionic cell-surface moieties that are especially abundant on tumor cells.

Unlike with RNase A, no correlation was apparent in the cell-surface binding, internalization, and cytotoxicity of ONC. We find that, for example, ONC does not

distinguish between highly anionic cancerous cells (here, CHO-K1) and noncancerous cells (CHO-745). Evidently, this amphibian ribonuclease, which has clinical utility as an anticancer agent (Lee and Raines, 2008), does not target cancer cells by interacting with abundant anionic cell-surface glycans.

The cellular entry of a mammalian ribonuclease could have important biological implications. For example, Asn88, a key RI-contact site in human pancreatic ribonuclease (Johnson *et al.*, 2007c), is known to be *N*-glycosylated in humans (Ribó *et al.*, 1994). The *N*-glycosylation of ONC increases its toxicity for cancer cells, presumably by enhancing its stability *in cellulo* (Kim *et al.*, 2004). Accordingly, an *N*-glycosylated human ribonuclease could evade RI and provide endogenous anti-tumor activity.

Acknowledgements. This work was supported by grant R01 CA073808 (NIH) and by resources from the Consortium for Functional Glycomics (Core H), which is supported by grant U54 GM062116 (NIH). T.-Y.C. was supported by the Dr. James Chieh-Hsia Mao Wisconsin Distinguished Graduate Fellowship. L.D.L was supported by Biotechnology Training Grant 08349 (NIH) and an ACS Division of Organic Chemistry Fellowship sponsored by Genentech.

Table 2.1 Electrophoretic mobility and tumorigenicity of CHO cells

Cell line	Cell-surface GAG deficiency	μ ((μm/s)/(V/cm))[a]	Tumorigenicity[b]
CHO-K1	none	-1.5 ± 0.1	+++ (19/22)
CHO-677	No heparan sulfate	-1.2 ± 0.1	– (0/7)
CHO-745	No heparan sulfate No chondroitin sulfate	-1.08 ± 0.05	– (0/28)

[a]Calculated with eq 2.2 from the value of ζ measured at pH 7.0.
[b]Based on ref. (Esko *et al.*, 1988). Values indicate the frequency of tumor formation when 10^7 cells were injected subcutaneously into nude mice.

Table 2.2 Values of IC_{50} (μM) for cell proliferation in the presence of ribonucleases

Cell line	ribonuclease		
	DRNG RNase A	KDRNG RNase A	ONC
CHO-K1	18.5 ± 0.1	20.1 ± 0.1	2.2 ± 0.1
CHO-745	27.1 ± 0.1	39.8 ± 0.03	0.6 ± 0.3
Pro 5	4.63 ± 0.09	8.79 ± 0.03	0.4 ± 0.1
Lec 2	6.7 ± 0.1	14.44 ± 0.04	0.6 ± 0.2

[a]Values of IC_{50} (±SE) are for incorporation of [*methyl*^{3}H]thymidine into the DNA of cells treated with a ribonuclease.

Figure 2.1 Binding of ribonucleases immobilized mammalian glycans. RNase A (A) and ONC (B) were detected by using a primary antibody and fluorescent secondary antibody. For glycan structures, see: www.functionalglycomics.org/static/consortium/resources/resourcecoreh8.shtml.

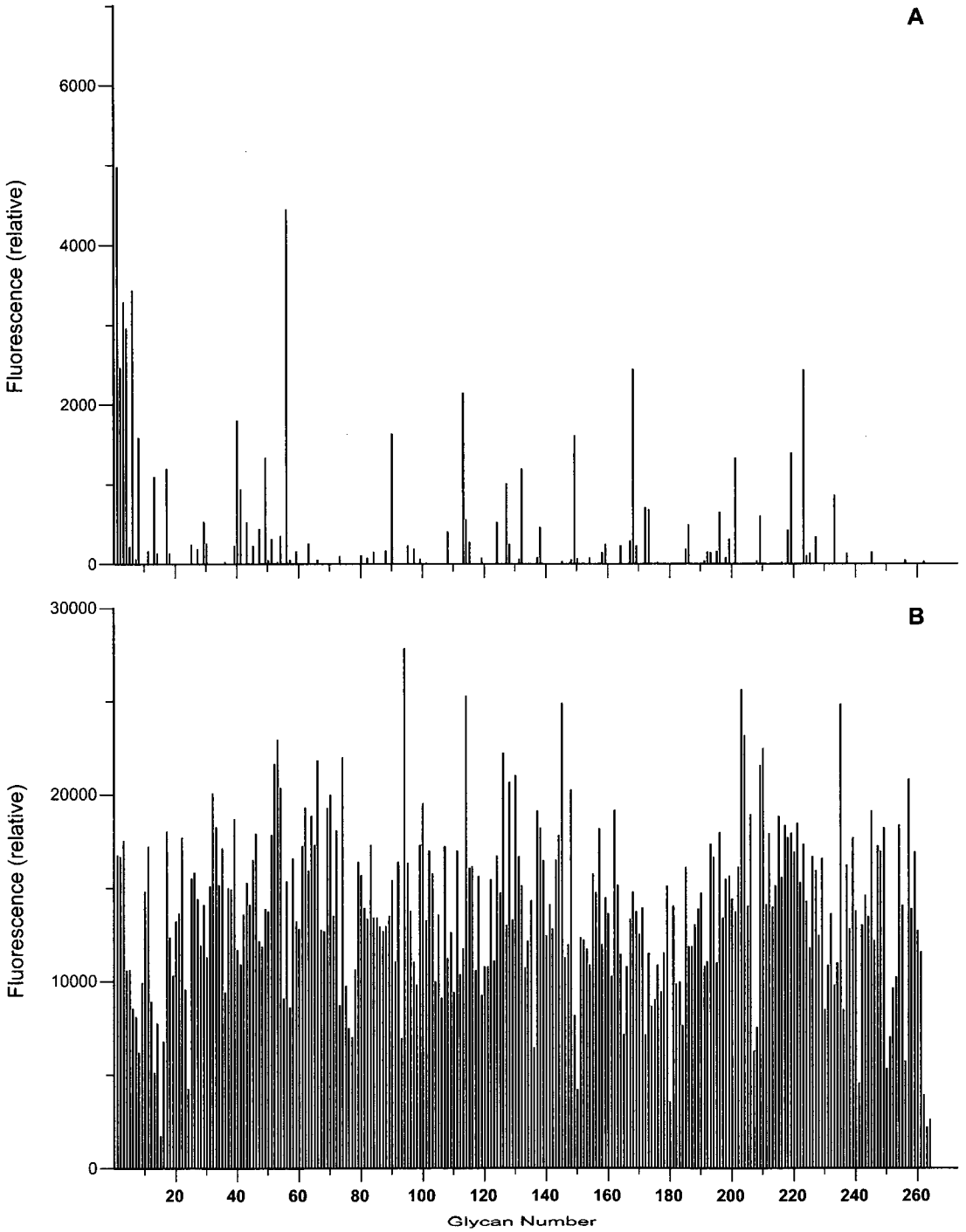
A
6000
4000
2000
0
Fluorescence (relative)
B
30000
20000
10000
0
Fluorescence (relative)
20
40
60
80
100
120
140
160
180
200
220
240
260
Glycan Number

Figure 2.2 Interaction of ribonucleases with GAGs *in vitro* and *in cellulo*. (A) Elution profile of DRNG RNase A and ONC from immobilized heparin. Ribonucleases (1.0 mg each) were loaded onto a column of immobilized heparin in PBS at pH 7.2. Protein elution was monitored by absorbance at 280 nm (black line) during a linear gradient of NaCl (0.00–0.45 M) (conductivity, grey line). ONC did not bind to heparin, eluting during the PBS wash (conductivity 14 mS/cm). DRNG RNase A eluted at a conductivity of 40 mS/cm. (B) Scheme for the labeling of a ribonuclease with latent fluorophore **2.1**. (C) Uptake of labeled RNase A (10 μM; i and ii) and ONC (10 μM; iii and iv) by CHO-K1 (i and iii) and CHO-745 (ii and iv) cells after incubation for 6 h at 37 °C. Nuclear stain Hoechst 33342 (blue) was added for the last 5 min of incubation. Scale bar: 10 μm. (D and E) Kinetics of uptake of labeled DRNG RNase A (10 μM; D) and ONC (10 μM; E) by detached CHO-K1 (•) and CHO-745 (○) cells. Total cellular fluorescence was measured by flow cytometry. Data points are mean values (±SE) for 20,000 cells from ≥6 cell populations. Initial rates of DRNG RNase A uptake were 220 ± 30 and 60 ± 20 RFU h^{-1} for CHO-K1 and CHO-745 cells, respectively. Initial rates of ONC uptake were 4.1 ± 0.2 and 3.2 ± 0.1 RFU h^{-1} for CHO-K1 and CHO-745 cells, respectively.

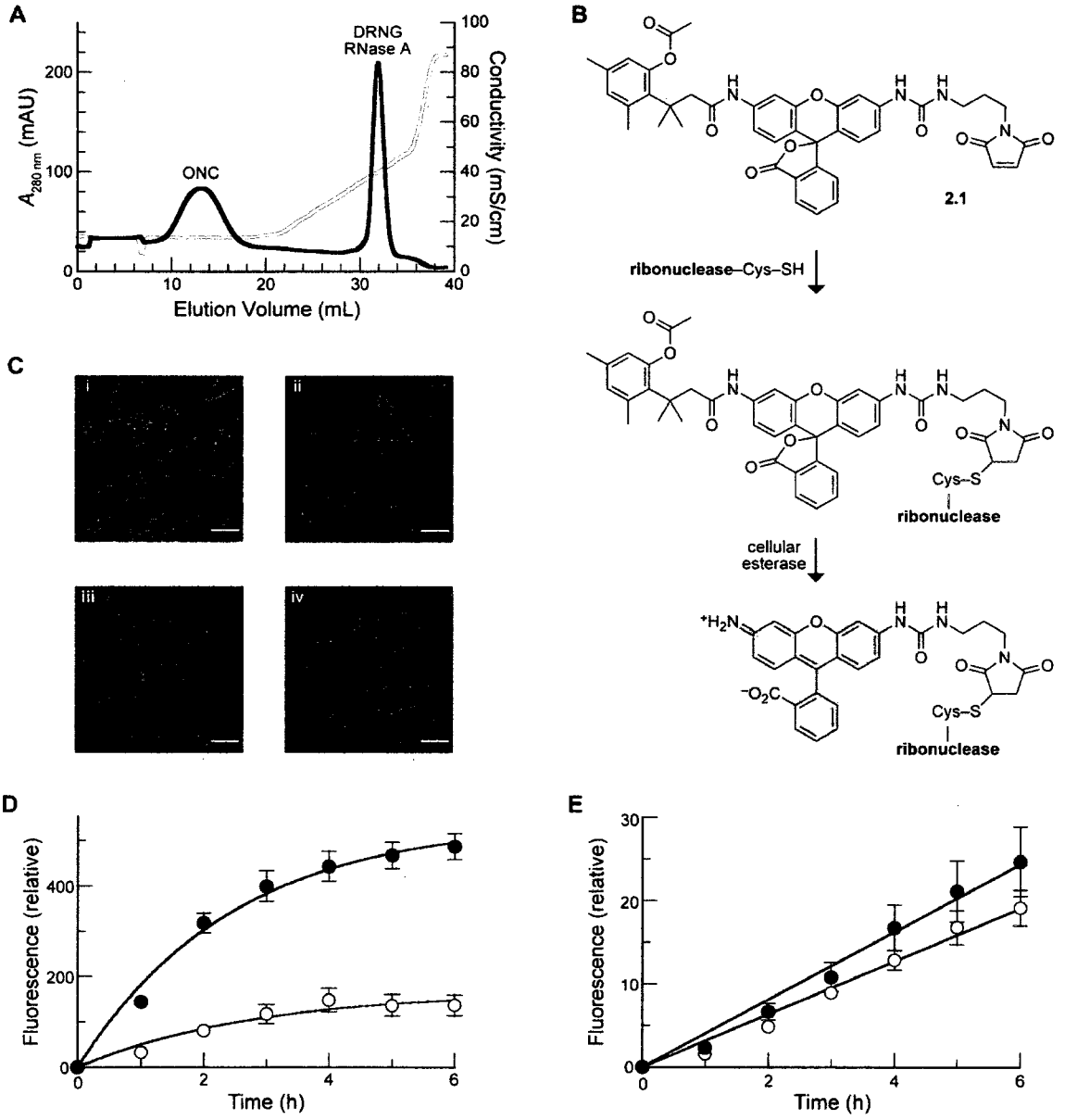
A
DRNG
RNase A
ONC
$A_{280\,nm}$ (mAU)
Conductivity (mS/cm)
Elution Volume (mL)
B
2.1
ribonuclease–Cys–SH
Cys–S
ribonuclease
cellular
esterase
C
i
ii
iii
iv
D
Fluorescence (relative)
Time (h)
E
Fluorescence (relative)
Time (h)

Figure 2.3 Binding of ribonucleases to wild-type and GAG-deficient mammalian cells.

RNase A (A–C) and ONC (D–F) were detected by using a primary antibody and fluorescent secondary antibody. (A) and (D), CHO-K1 cells. (B) and (E), CHO-677 cells. (C) and (F), CHO-745 cells. Scale bar: 10 μm.

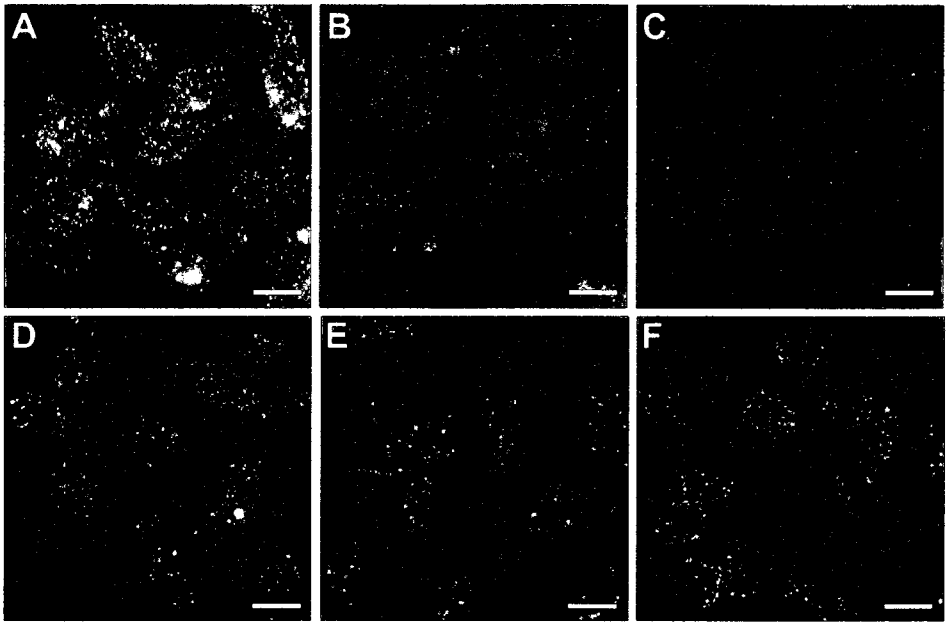
A
B
C
D
E
F

Figure 2.4 Kinetics of ribonuclease uptake by wild-type and sialic acid-deficient mammalian cells.

Labeled DRNG RNase A (10 μM; A) and ONC (10 μM; B) were incubated with detached Pro 5 (◆) and Lec 2 (◇) cells. Total cellular fluorescence was measured by flow cytometry. Data points are mean values (±SE) for 20,000 cells from ≥6 cell populations. Initial rates of DRNG RNase A uptake were 140 ± 20 and 110 ± 30 RFU h^{-1} for Pro 5 and Lec 2 cells, respectively. Initial rates of ONC uptake were 4.5 ± 0.2 and 4.0 ± 0.1 RFU h^{-1} for Pro 5 and Lec 2 cells, respectively.

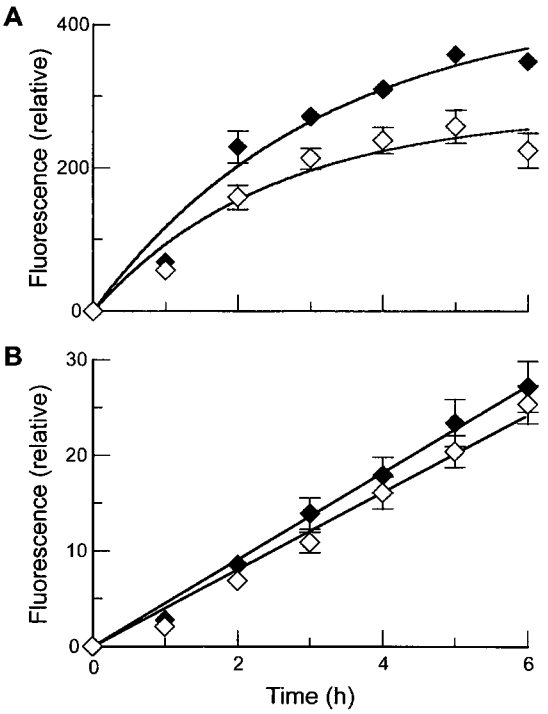
A
400
200
0
Fluorescence (relative)
B
30
20
10
0
Fluorescence (relative)
0
2
4
6
Time (h)

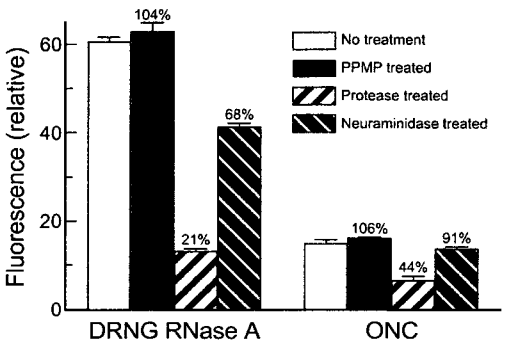

Figure 2.5 Uptake of ribonucleases by chemical- or enzyme-treated mammalian cells. Labeled DRNG RNase A and ONC were incubated for 1 and 3 h, respectively, with CHO-K1 cells that had been treated with D-*threo*-PPMP, trypsin, or neuraminidase. Total cell fluorescence was measured by flow cytometry. Values of fluorescence intensity are the mean (±SE) for 20,000 cells from ≥6 cell populations.

CHAPTER 3

Ribonuclease A as a Cell-Penetrating Protein

Contribution: I performed all of the research described in this chapter, except for the synthesis of a rhodamine$_{110}$-based latent fluorophore (L.D. Lavis).

Prepared for submission as:
Chao, T.-Y. and Raines, R.T. (2010)
Ribonuclease A as a cell-penetrating protein.

3.1 Abstract

Pancreatic-type ribonuclease can exert toxic activity by catalyzing the degradation of cellular RNA. Their ability to enter cells is essential in their cytotoxicity. Here, we show that bovine pancreatic ribonuclease (RNase A) is internalized simultaneously by both clathrin-mediated endocytosis and macropinocytosis. Inhibiting clathrin-dependent endocytosis in HeLa cells by treatment with dynasore or chlorpromazine resulted in a ~70% decrease in RNase A-uptake. Limited colocalization between RNase A and transferrin indicates that RNase A is not routed through recycling endosomes. Instead, vesicular staining of RNase A overlapped substantially with that of nonaarginine and the cationic peptide corresponging to residues 47–57 of the HIV-1 TAT protein. At low concentrations (<5 μM), internalization of RNase A and these cell-penetrating peptides (CPPs) was inhibited by chlorpromazine as well as the macropinocytosis inhibitors cytochalasin D and 5-(*N*-ethyl-*N*-isopropyl)amiloride to a similar extent, indicative of common endocytic mechanism. At high concentrations, the CPPs appear to adopt a non-endocytic mechanism of cell entry that is not shared by RNase A. Collectively, these data suggest that RNase A is internalized via a multi-pathway mechanism that involves both clathrin-coated vesicles and macropinosomes. The parallel between the uptake of RNase A and CPPs validates reference to RNase A as a "cell-penetrating protein".

3.2 Introduction

The pancreatic-type ribonuclease family encompasses a large group of secretory enzymes with diverse biological actions, including angiogenic activity from angiogenin (Riordan, 1997; Fett *et al.*, 1985), bactericidal and antiviral activities demonstrated by the eosinophil cationic protein (ECP) (Ackerman *et al.*, 1983; Domachowske and Rosenberg, 1997), as well as cytotoxic and antitumoral activities exhibited by ECP, bovine-seminal ribonuclease, Onconase® (ONC), and variants of bovine pancreatic ribonuclease (RNase A) (Arnold, 2008; Lee and Raines, 2008). Internalization by the target cell is an indispensible step in mediating a broad range of biological activities (Leich *et al.*, 2007; Benito *et al.*, 2008). In particular, the endocytosis of cytotoxic ribonucleases, along with affinity for the ribonuclease inhibitor protein and conformational stability, are known to be key determinants of ribonuclease-mediated cytotoxicity (Rutkoski and Raines, 2008; Klink and Raines, 2000). Several cytotoxic ribonucleases, including ONC and RNase A variants, demonstrate selective toxicity towards cancer cells and show promise as chemotherapeutic agents (Rutkoski *et al.*, 2005; Leland and Raines, 2001). Yet, little is known about the mechanism of cellular uptake of these ribonucleases.

Mammalian cells have an intricate endocytic system with parallel pathways. One of the best characterized pathways is clathrin-mediated endocytosis, which occurs constitutively in all mammalian cells (Conner and Schmid, 2003). The vesicles created are signified by a coating of clathrin oligomers on the cytosolic side of the membrane. Receptor·ligand complexes destined for clathrin-mediated endocytosis are recruited by

adaptor protein complex AP2 to these clathrin-coated pits (Mukherjee *et al.*, 1997). In the final step of endocytosis, the GTPase dynamin is required for fission of clathrin-coated vesicles (Mukherjee *et al.*, 1997). Transferrin is a widely recognized marker of clathrin-mediated endocytosis (Conner and Schmid, 2003). Another well-characterized endocytic pathway is caveolar-mediated endocytosis. Similar to clathrin-mediated endocytosis, the coat protein caveolin-1 is necessary for the formation of caveolae; dynamin is also implicated in this pathway (Parton and Simons, 2007). Caveolar-dependent uptake has been associated with cholesterol- and sphinogolipid-rich plasma microdomains known as lipid rafts, though the raft domains could also be internalized through non-caveolar pathways, such as macropinocytosis (Lajoie and Nabi, 2007). The formation of macropinosomes often involves membrane ruffling, an actin-dependent process, but does not require dynamin (Cao *et al.*, 2007). Molecules that have been demonstrated to use this route for cell entry include dextran, horseradish peroxidase, and the cell-penetrating peptides (CPPs) polyarginine and residues 47–57 of the HIV-1 trans-activator of transcription (TAT) (Nakase *et al.*, 2004; Cao *et al.*, 2007; Jones, 2007). Finally, there are additional clathrin- and caveolar-independent endocytic pathways that are less characterized and often defined only by specific markers (Doherty and McMahon, 2009).

Utilization of clathrin-mediated pathways is dependent on specific cell-surface receptors. Although colocalization with transferrin strongly suggests a clathrin-dependent mechanism for ONC uptake (Rodriguez *et al.*, 2007), the existence of specific receptors for ONC on mammalian cell surfaces is debatable. Two saturable binding sites with K_d values of 0.062 and 0.25 μM were proposed to exist on 9L glioma cells with ^{125}I-labeled

ONC (Wu *et al.*, 1993). In contrast, the binding of ONC to HeLa cells was shown to be non-saturable at protein concentrations up to 10 μM, indicative of nonspecific binding (Haigis and Raines, 2003). Consistent with this result, cationic residues in pancreatic-type ribonucleases have been proposed to participate in nonspecific Coulombic interactions with anionic cell-surface moieties (Turcotte *et al.*, 2009; Johnson *et al.*, 2007a; Fuchs *et al.*, 2007).

ECP, which is the most cationic pancreatic-type ribonuclease, has been shown to interact with anionic cell-surface heparan sulfate proteoglycans (HSPG) (Fan *et al.*, 2007). A thorough characterization of HSPG-mediated ECP uptake revealed independence of both clathrin and caveolin. Moreover, the requirement for actin, phosphoinositide-3-kinase (PI3K), ADP-ribosylation factor 6, and Ras-related botulinum toxin substrate 1 showed unambiguously that ECP was taken up by raft-dependent macropinocytosis into Beas-2B human bronchial epithelial cells (Fan *et al.*, 2007).

RNase A has also been shown to interact with cell-surface HSPGs, which subsequently mediate its uptake (Chao *et al.*, 2010). Also, the cytotoxicity of a variant of RNase A was unaffected by the overproduction of K44 dynamin, indicative of a dynamin-independent mechanism (Haigis and Raines, 2003). Other aspects of the uptake mechanism are not clear.

Here, we delineate the pathway(s) by which RNase A enters live mammalian cells. To do so, we make extensive use of small-molecule pharmacological agents that inhibit specific endocytic pathways and small-molecule fluorescent tags that enable the detection of cell entry. By comparing the uptake and subsequent cellular distribution of

RNase A with those of nonaarginine (R_9) and TAT, we conclude that RNase A is an exemplary "cell-penetrating protein".

3.3 Experimental Procedures

3.3.1 Reagents and cell lines

Escherichia coli strains BL21 (DE3) and pET22b (+) plasmid were from Novagen (Madison, WI). Specific endocytic inhibitors *Zygosporium mansonil* cytochalasin D (CD), chlorpromazine hydrochloride, 5-(*N*-ethyl-*N*-isopropyl)amiloride (*EIPA*), dynasore, *Penicillium funiculosum* wortmannin, nystatin, and methyl-β-cyclodextrin (MβCD) were from Sigma–Aldrich (St. Louis, MO). The endocytic markers Alexa Fluor 594-transferrin and Alexa Fluor 594-cholera toxin B subunit were from Invitrogen (Carlsbad, CA). Tetramethylrhodamine-labeled dextran (MW 65–76K) was from Sigma–Aldrich (St. Louis, MO). FAM–TAT, TAMRA–TAT, FAM–R_9, and TAMRA–R_9, which are labeled on their N termini, were from Anaspec (Fremont, CA). All other chemicals and reagents were of commercial reagent grade or better, and were used without further purification.

3.3.2 Mammalian cell culture

HeLa cells were from the American Type Culture Collection (Manassas, VA) and grown in minimum essential medium containing fetal bovine serum (10% v/v), penicillin (100 units/mL), and streptomycin (100 μg/mL). Cell culture medium and supplements

were from ATCC. Cells were cultured at 37°C in a humidified incubator containing CO_2 (g) (5% v/v).

3.3.3 Instrumentation

Molecular mass was measured by MALDI–TOF mass spectroscopy using a Voyager-DE-PRO Biospectrometry Workstation (Applied Biosystems, Foster City, CA) with sinapinic acid as a matrix in the campus Biophysics Instrumentation Facility. Flow cytometry data were collected in the University of Wisconsin Paul P. Carbone Comprehensive Cancer Center with a FACSCalibur flow cytometer equipped with a 488-nm argon-ion laser (Becton Dickinson, Franklin Lakes, NJ). Microscopy images were obtained with a Nikon C1 laser scanning confocal microscope with a 60× oil immersion objective with NA 1.4.

3.3.4 Production and purification of ribonucleases

Wild-type RNase A and its A19C variant were produced in *E. coli* BL21(DE3) cells and purified as described previously (Leland *et al.*, 1998). Following purification, protein solutions were dialyzed against PBS and filtered (0.2-μm pore size) prior to use.

3.3.5 Fluorescent labeling of ribonucleases

A19C RNase A contains a free cysteine residue for site-specific conjugation (Haigis and Raines, 2003). During its purification, the free thiol group was protected by reaction with 5,5′-dithio-bis(2-nitrobenzoic acid). Immediately prior to fluorophore

attachment, the protected A19C RNase A was deprotected with a 4-fold excess of dithiothreitol and desalted by chromatography on a PD-10 desalting column (GE Biosciences, Piscataway, NJ). Deprotected ribonucleases were reacted for 6 h at 25°C with a 10-fold molar excess of either fluorescein-5-maleimide (Anaspec, Fremont, CA) or a maleimide-containing rhodamine$_{110}$-based pro-fluorophore (Lavis *et al.*, 2006a). This pro-fluorophore is not fluorescent until activated by cellular esterase, such as those in endosomes. The resulting RNase A conjugates were purified by chromatography using a HiTrap SP HP column (GE Biosciences, Piscataway, NJ). The molecular masses of RNase A, its A19C variant, and its conjugates were confirmed by MALDI–TOF mass spectrometry. Protein concentration was determined by using a bicinchoninic acid assay kit (Pierce, Rockford, IL) with wild-type RNase A as a standard.

3.3.6 Flow cytometry

The internalization of RNase A conjugates was monitored directly in living cells. HeLa cells from near confluent flasks were plated in 6-well plates at 1.2×10^5 cells/mL/well 18–24 h prior to experiments. Fluorescently labeled proteins and peptides were added to each well. Samples were allowed to incubate at 37°C for varying times. To quench internalization, HeLa cells were washed twice with ice-cold PBS, and treated with trypsin/EDTA (0.05% w/v) for several minutes. Complete medium containing fetal bovine serum (10% v/v) was added to each well to inhibit the action of trypsin. Samples remained on ice until analyzed by flow cytometry. For drug sensitivity studies, cells were

pretreated with drugs for 30 min in minimum essential medium (Invitrogen, Carlsbad, CA) followed by incubation with protein or peptide conjugates for 1 h at 37°C.

Fluorescence was detected through a 530/30-nm band-pass filter. Cell viability was determined by staining with propidium iodide, which was detected with a 660-nm long-pass filter. The mean channel fluorescence intensity of 20,000 viable cells was determined for each sample using CellQuest software and used for subsequent analysis.

3.3.7 Microscopy

HeLa cells were plated on Nunc Lab-tek II 8-well chambered coverglass (Fisher Scientific, Pittsburgh, PA) and grown to 70% confluency. Cells were then incubated with fluorescently labeled conjugates for 1 h at 37°C. Cell nuclei were stained by the addition of Hoechst 33342 (2 μg/mL) for the final 5 min of incubation. For pharmacological studies, cells were pretreated with compounds in minimum essential medium for 30 min at 37°C.

Cells were imaged on a Nikon Eclipse TE2000-U laser scanning confocal microscope equipped with a Zeiss AxioCam digital camera. Excitation at 408 nm was provided by a blue-diode laser, and emission light was passed through a filter centered at 450 nm with a 35-nm band-pass. Excitation at 488 nm was provided by an argon-ion laser, and emission light was passed through a filter centered at 515 nm with a 40-nm band-pass. Excitation at 543 nm was provided by a HeNe laser, and emission light was passed through a filter centered at 605 nm with a 75-nm band-pass.

3.4 Results

3.4.1 Effects of endocytic inhibitors on RNase A-uptake

Endocytic pathways can be distinguished by blocking specific molecular components with pharmacological compounds. To determine the mechanism of cellular entry by RNase A, we examined RNase A-uptake in the presence of endocytic inhibitors qualitatively by using confocal microscopy and quantitatively by using flow cytometry. Specifically, dynasore (80 μM) was used to test for dependence on dynamin; chlorpromazine (CPZ; 10 μg/mL) and nystatin (25 μg/mL) were used as inhibitors of clathrin- and caveolar-mediated pathways, respectively; and CD (5 μg/mL) and EIPA (10 μM) served as probes for macropinocytosis. MβCD (5 mM) and wortmannin (50 nM) were used to assess the requirement for cholesterol and PI3K, respectively, during RNase A internalization. The use of each of these inhibitory compounds in mammalian cell lines is well-established (Ivanov, 2008; Macia *et al.*, 2006). Here, pretreatments with a drug for 30 min at 37°C resulted in expected effects on the uptake of endocytic markers transferrin, cholera toxin subunit B (CTB), and dextran (data not shown). Toxicity did not exceed 5% of the cell population during the course of an experiment.

The dominant-negative K44A dynamin variant has been used widely to probe the internalization of various molecules, including RNase A. Still, tetracyclin-induced overexpression of K44A dynamin in HeLa cells has been reported to lead to an increase in endosomal pH by 0.4 to 0.7 units (Rodriguez *et al.*, 2007; Bayer *et al.*, 2001). This change in pH might not affect early endocytic events, but could alter the trafficking of the

internalized molecules. For example, a decrease in the IC_{50} value of ONC upon K44A dynamin expression was suggested to be due to increased translocation as a result of a change in endosomal pH (Rodriguez *et al.*, 2007). As a similar decrease in IC_{50} value was observed for RNase A in K44A dynamin cells, we sought to revisit the dynamin-dependence of RNase A-uptake by using dynasore, a noncompetitive inhibitor of the GTPase activity of dynamin (Macia *et al.*, 2006). Dynasore abolishes dynamin activity within 30 min of incubation, thereby providing temporal control superior to that of tetracycline-induced expression of K44A dynamin. No obfuscating biological effects have been associated with dynasore treatment. Unexpectedly, the endocytosis of RNase A was highly sensitive to dynasore treatment; the level of internalization was reduced by $^2/_3$ (Fig. 3.1B). The cellular distribution of RNase A was sparse and dispersed in dynasore-treated cells (Fig. 3.1Aii). The marked decrease in internalization indicates that RNase A-uptake is dependent on dynamin, at least in part.

Both clathrin- and caveolar-mediated pathways require the action of dynamin in the process of vesicle scission (Conner and Schmid, 2003). To determine which dynamin-dependent pathway is involved in RNase A-uptake, we next treated cells with CPZ and nystatin. CPZ is an amphiphilic cationic drug known to disrupt clathrin-mediated endocytosis (Subtil *et al.*, 1994), as well as a pathway distinct from clathrin-mediated endocytosis that is characterized by the formation of cell-surface nucleation zones and is utilized by cell-penetrating peptides at high concentrations (Duchardt *et al.*, 2007). As shown in Fig. 3.1Aiii and 3.1B, treatment with CPZ reduced RNase A internalization by $^2/_3$ without affecting its localization. In contrast, RNase A-uptake was only slightly

decreased in the presence of nystatin (Fig. 3.1Aiv), which is a selective inhibitor of the lipid raft/caveolae pathway (Ivanov, 2008). Cholesterol extraction with MβCD also had little effect on RNase A-uptake (Fig. 3.1Av). These results indicate that RNase A internalization is mediated by a CPZ-sensitive pathway, possibly involving clathrin, but not by a lipid raft/caveolae-dependent endocytic pathway.

Dynasore treatment did not abolish RNase A-uptake completely. Accordingly, we tested other inhibitors of macropinocytosis, a dynamin-independent pathway (Kirkham and Parton, 2005). CD is an F-actin depolymerizing drug that blocks membrane ruffling and hence macropinocytosis (Dharmawardhane *et al.*, 2000). Although formation of macropinosomes is most sensitive to CD treatment, CD is also believed to affect endocytosis via clathrin-coated pits and caveolae, which depend on actin to a lesser extent (Kaksonen *et al.*, 2006; Ivanov, 2008). Here, we found that RNase A-uptake was reduced by $^{3}/_{4}$ (Fig. 3.1Avi and 3.1B) in CD-treated cells; likewise, transferrin-uptake decreased by $^{1}/_{3}$ (data not shown). The sensitivity to CD treatment suggests that the actin cytoskeleton is required for RNase A-uptake, but does not necessarily imply the involvement of macropinocytosis. Next, we tested the effects of EIPA, a selective inhibitor of the Na^{+}/H^{+} antiporter specific to macropinocytosis (Fretz *et al.*, 2006). As shown in Fig. 3.1Avii, peripheral RNase A staining is much reduced in the presence of EIPA compared with non-treated cells (Fig. 3.1Ai), and a $^{1}/_{3}$ decrease in RNase A-uptake was observed (Fig. 3.1B). These results, together with those from CD treatment, indicate that macropinocytosis is partially responsible for mediating RNase A cellular entry. Furthermore, co-treatment with CD and either dynasore or CPZ resulted in a ~90%

reduction in RNase A-uptake by HeLa cells (Fig. 3.1B), which suggest that RNase A is internalized simultaneously via macropinocytosis and clathrin-mediated pathways.

The fungal metabolite wortmannin inhibits the enzymatic activity of PI3K (Patki *et al.*, 1997). Though it has been used to block constitutive and stimulated macropinocytosis in some cell types, the role of PI3K in macropinocytosis is not well-established (Ivanov, 2008). Wortmannin is also known to inhibit homotypic fusion of early endosomes (Kjeken *et al.*, 2001). Indeed, RNase A staining in wortmannin-treated cells was more dispersed and RNase A positive vesicles were smaller in size (Fig. 3.1Aviii). Yet, the overall level of internalization was unaffected by wortmannin (Fig. 3.1B), suggesting that PI3K activity is not required for RNase A-uptake.

3.4.2 RNase A colocalizes with CTB and the CPPs

To analyze further the cellular entry route availed by RNase A, we examined the colocalization of RNase A with various endocytic markers. RNase A (10 μM) and transferrin (1 μM) were incubated with wild-type HeLa cells for 1 h at 37°C. Transferrin exhibits rapid uptake and labels early sorting endosomes and recycling compartments (Mukherjee *et al.*, 1997). RNase A-uptake is comparatively slower in HeLa cells. As a result, a 1-h incubation was allowed to facilitate visualization of its subcellular distribution. As shown in Fig. 3.2i, limited overlap between transferrin and RNase A was apparent. The majority of transferrin-positive vesicles appear to be smaller in size and distinct from RNase A-containing compartments. The two were found to colocalize in perinuclear compartments, which are likely the rab11-positive recycling endosomes in

which transferrin resides (Ullrich *et al.*, 1996). This finding is consistent with previous reports on RNase A-uptake, which demonstrated that RNase A does not colocalize with transferrin in K-562 cells and in K44A dynamin HeLa cells (Haigis and Raines, 2003). Although sensitivity to CPZ and dynasore treatment is indicative of a clathrin-mediated mechanism for RNase A internalization, its localization suggests that the routing of RNase A is distinct from that of transferrin.

Next, we analyzed colocalization of RNase A and CTB. CTB prefers the caveolar-mediated pathway but can also be internalized by other pathways. In cells with low levels of caveolin-1 expression, such as HeLa cells, roughly 50% of CTB is internalized via clathrin-coated pits (Torgersen *et al.*, 2001). Another pathway implicated in CTB-uptake involves clathrin-independent carriers (Kirkham and Parton, 2005; Doherty and McMahon, 2009). They are typically tubular or ring-shaped endocytic structures whose formation do not require dynamin or coat proteins (Kirkham and Parton, 2005). Surprisingly, there was extensive colocalization between RNase A and CTB (Fig. 3.2ii), both in peripheral endocytic vesicles and perinuclear compartments. As pathways dependent on clathrin or clathrin-independent carriers are the main routes by which CTB is taken up by HeLa cells, a high degree of colocalization is indicative of the involvement of both pathways in RNase A-uptake.

The cell-penetrating peptides constitute a class of short cationic polypeptides that enter cells efficiently. Owing to their small size and ability to deliver various molecules into mammalian cells, the CPPs represent valuable vehicles in drug delivery (Langel, 2007). The internalization of CPPs has been thoroughly studied but data concerning the

mechanisms of uptake are not always consistent for the same peptides. For example, TAT was reported to be taken up by lipid raft-dependent macropinocytosis (Wadia *et al.*, 2004; Nakase *et al.*, 2004) and clathrin-dependent endocytosis (Richard *et al.*, 2005; Zhang *et al.*, 2009) in HeLa cells. Moreover, a recent report showed that both R_9 and TAT utilize all three major endocytic pathways simultaneously in addition to an apparently non-endocytic entry pathway (Duchardt *et al.*, 2007).

To discern if RNase A shares a common endocytic route with the CPPs, we searched for colocalization. When equal molar quantities of the two were added to cells at the same time, RNase A-uptake was reduced greatly, presumably due to competition for cell-surface binding sites (data not shown). Both RNase A and the CPPs bind to anionic cell-surface glycans such as heparan sulfate and chondroitin sulfate (Richard *et al.*, 2005; Chao *et al.*, 2010; Fuchs and Raines, 2004). R_9 has a higher affinity for the cell-surface than does RNase A, as R_9-uptake was unaffected by excess RNase A (data not shown). To visualize RNase A localization in the presence of CPPs, cells were pre-incubated with RNase A for 15 min prior to the addition of R_9 and TAT. As shown in Fig. 3.2iii, RNase A staining overlaps significantly with R_9 positive vesicles, even in cells with prominent cytosolic staining of R_9. Similarly, TAT colocalizes with RNase A both in perinuclear compartments and peripheral endocytic structures (Fig. 3.2iv). To ensure that the strong colocalization is not merely a result of merging endocytic pathways, experiments were repeated with shorter incubation times. Upon co-incubation for 15 min, fewer and smaller vesicles were observed, but the overall degree of colocalization was similar (data not shown).

3.4.3 RNase A-uptake is independent of concentration

R_9 and TAT adopt a novel mode of cell entry above threshold concentrations, involving the formation of nucleation zones at the cell surface and resulting in diffuse cytosolic staining (Duchardt *et al.*, 2007). This pathway is sensitive to heparinase, CPZ, and the protein kinase C inhibitor rottlerin, but not wortmannin (Duchardt *et al.*, 2007). Interestingly, although vesicles are not detected, dynamin is required for this novel cell-penetration process (Duchardt *et al.*, 2007). Because the uptake of RNase A exhibits a similar drug sensitivity pattern as this pathway, we sought to determine if RNase A also utilizes this pathway at higher concentrations by assessing the concentration-dependence of RNase A-uptake and localization. First, RNase A was conjugated to fluorescein for direct comparison with carboxyfluorescein-labeled R_9 and TAT. The conjugates were then incubated with HeLa cells for 30 min at 37°C and washed extensively with serum-free medium prior to imaging. Fluorescein has a pK_a of 6.4 and, as a result, its fluorescence decreases in acidic environments. At 10 μM, fluorescein-labeled RNase A has diminished staining (Fig. 3.3Ai) compared with the rhodamine$_{110}$-labeled RNase A shown in Fig. 3.1 and 3.2, suggesting that the majority of internalized RNase A resides in acidic endosomes at this concentration. The subcellular distribution of RNase A is unchanged at 20 μM (Fig. 3.3Aiv). In contrast, both R_9 and TAT had substantially greater fluorescence, presumably due to strong cytosolic staining (Fig. 3.3Av and 3Avi). Flow cytometry quantitation of RNase A-and CPP-uptake revealed that both TAT and RNase A-uptake increased steadily with increasing concentration, whereas R_9-uptake increased sharply above 20 μM. Moreover, R_9 and TAT-uptake is several fold to nearly

two orders of magnitude greater than that of RNase A. Together, these results suggest that RNase A does not use the novel non-endocytic pathway for cell entry and that RNase A-uptake is concentration independent.

3.4.4 Mechanism of RNase A-uptake is similar to CPPs at low concentrations

The contribution of different endocytic pathways for RNase A and CPP internalization were compared directly by subjecting R_9 and TAT to CD-, CPZ-, and EIPA-treatment under the same conditions as RNase A. First, CPP-uptake was reduced by 10–20% at 1 μM CPP and 30–40% at 10 μM CPP upon treatment with CD (Fig. 3.4A). The molecular basis for the increased sensitivity to the higher concentration of CD is unclear, but could result from actin being required for the non-endocytic mechanism. RNase A-uptake, on the other hand, is more dependent on actin than is CPP internalization. Second, as expected, the sensitivity to CPZ was highly concentration-dependent for the CPPs (Fig. 3.4B). At 1 μM, R_9- and TAT-uptake were highly sensitive to CPZ-treatment; at 10 μM, however, CPP-uptake increased in the presence of CPZ. A similar trend in CPP-uptake was also observed with EIPA treatment (Fig. 3.4C). These results suggest that CPZ-treatment augmented the use of the non-endocytic pathway by the CPPs at high concentrations, whereas RNase A-uptake is still dependent on clathrin-mediated endocytosis and macropinocytosis at the same concentrations. In conclusion, based on sensitivity to these drugs, RNase A-uptake was similar to R_9 and TAT at low concentrations ($\leq$5 μM), suggesting that the mechanisms mediating RNase A-uptake

overlaps significantly with those mediating the cell entry of R_9 and TAT at low concentrations (Table 3.1).

3.5 Discussion

RNase A is a cationic protein that enters cells without the need for any specific receptors (Chao *et al.*, 2010). A thorough understanding of the mechanisms underlying RNase A internalization not only elicits interest from a biological perspective but also has implications for the development of ribonuclease-based chemotherapeutic agents. Here, through a pharmacological approach, we have shown that macropinocytosis and clathrin-mediated endocytosis are both responsible for mediating the cellular entry of RNase A (Fig. 3.5).

The involvement of clathrin-mediated endocytosis in RNase A-uptake was unexpected from previous reports. The cytotoxicity of an RNase A variant was found to increase in the presence of the dominant-negative K44A dynamin variant, suggesting that dynamin does not have a role in RNase A internalization (Haigis and Raines, 2003). This finding can, however, be reconciled with a multi-pathway model for RNase A internalization. For example, RNase A internalized through different pathways is likely to have different endosomal escape efficiencies. A slight upregulation of macropinocytosis in cells that overproduce K44A Dyn could lead to greater delivery of cytotoxic RNase A molecules in the cytosol.

In the present study, RNase A-uptake in dynasore-treated cells was reduced to $^{1}/_{3}$ of that in untreated cells (Fig. 3.1B). Because dynasore-treatment diminishes transferrin internalization by >95% (Macia *et al.*, 2006), this high level of residual RNase A-uptake indicates that RNase A also avails a dynamin-independent mechanism for cell entry. Alternatively, dynasore could reduce unstimulated fluid-phase endocytosis by 50–60% (Macia *et al.*, 2006; Cao *et al.*, 2007); fluid-phase endocytosis in the absence of serum or epidermal growth factor has been shown to be a dynamin-dependent process (Cao *et al.*, 2007). Yet, considering the strong overlap between CTB and RNase A as well as partial colocalization between transferrin and RNase A (Fig. 3.2i and 3.2ii), the dynamin-dependent mechanism involved in RNase A-uptake is likely to be clathrin- or caveolar-dependent endocytosis. Caveolae inhibitors nystatin and MβCD had only a minimal effect on RNase A-uptake (Fig. 3.1B), suggesting that caveolar-dependent endocytosis is not a major mechanism utilized by RNase A in HeLa cells. We note, though, that HeLa cells have relatively low levels of caveolin-1 (Skretting *et al.*, 1999), and the contribution of caveolar-dependent endocytosis to RNase A-uptake could be greater in other types of cells. Finally, $^{2}/_{3}$ of RNase A-uptake was determined to be CPZ-sensitive (Fig. 3.1B), which is consistent with a partial dependence on clathrin.

ONC is an RNase A homologue that is also internalized via clathrin-mediated endocytosis (Rodriguez *et al.*, 2007). Routing through transferrin-associated early recycling endosomes is thought to be an effective pathway for ONC due to better translocation efficiencies at near neutral pH. On the other hand, our data shows that RNase A does not accumulate in early recycling endosomes but colocalizes with

transferrin only at perinuclear late endosomal structures (Fig. 3.2i). Although both ribonucleases utilize clathrin-dependent pathways, differential routing could account for the differential cytotoxicity of ONC and RNase A variants. Specifically, ONC is ≥10-fold more toxic than the most cytotoxic known variants towards A549, MCF-7, NIC/ADR-RES, and CHO cells (Chao *et al.*, 2010; Rutkoski *et al.*, 2005). Traversing in recycling endosomes could be advantageous to ribonuclease-mediated cytotoxicity.

Clathrin-dependent pathways are mediated by receptors. Previous studies have demonstrated that RNase A interacts with cell-surface HSPGs and sialic acid-containing glycoproteins through Coulombic interactions (Chao *et al.*, 2010). Interestingly, HSPGs are receptors for cationic serum proteins such as fibroblast growth factors (FGFs) and vascular endothelial growth factor (VEGF) (Gitaygoren *et al.*, 1992; Rapraeger *et al.*, 1994). By interacting with heparan sulfate, these proteins induce dimerization of the receptors and subsequent internalization via macropinocytosis (FGF2) and clathrin-dependent endocytosis (VEGF) (Lampugnani *et al.*, 2006; Tkachenko *et al.*, 2004). The RNase A–heparan sulfate interaction might trigger endocytosis. Alternatively, RNase A could be internalized passively along with receptor·ligand complexes. Similar to RNase A, the R_9 and TAT both interact with cell-surface HSPGs (Richard *et al.*, 2005; Fuchs and Raines, 2004) (Table 3.1). Coincidently, their cellular uptake has been described as adsorptive rather than receptor-mediated, and all major pathways are implicated in the internalization of the CPPs (Duchardt *et al.*, 2007; Patel *et al.*, 2007). Thus, interaction with cell-surface sulfated glycosaminoglycans seems to invoke a multi-pathway mechanism of endocytosis. Depending on the exact display of proteoglycans on

different cell types, certain pathways may be favored and dominate the internalization of the cationic molecule.

Sensitivity to CD and EIPA unequivocally indicts macropinocytosis in RNase A-uptake (Fig. 3.1B). Macropinocytosis is an F-actin driven process involving membrane ruffling and formation of lamellipodia (Kirkham and Parton, 2005). Although no specific receptor is required for this endocytic pathway, membrane-associated proteoglycans are thought to be important in the induction of F-actin organization and macropinocytosis (Futaki *et al.*, 2007). Indeed, both ECP and the CPPs R_9 and TAT have been shown to interact with cell-surface proteoglycans followed by internalization by macropinocytosis (Fan *et al.*, 2007; Wadia *et al.*, 2004; Nakase *et al.*, 2004). A high content of arginine residues seems to be essential in inducing this pathway, as ECP (which contains 19 arginine and 1 lysine residue), is the only RNase A homologue known to be internalized solely by macropinocysis (Fan *et al.*, 2007). ONC (12 lysine and 3 arginine residues) is internalized via clathrin-mediated endocytosis (Rodriguez *et al.*, 2007); whereas RNase A (10 lysine and 4 arginine residues; Fig. 3.6), is internalized by both pathways (Fig. 3.5). Although all three ribonoucleases are cationic proteins similar in size and structure, the number of lysine and arginine residues and their ratio could play a role in determining the endocytic route. Unlike other cell-penetrating proteins, such as the transcription factor BETA2/NeuroD (Noguchi *et al.*, 2005) and the rattlesnake toxin crotamine (Kerkis *et al.*, 2004), the cationic residues in RNase A are not confined to a short segment in its primary structure but coalesce in its tertiary structure (Fig. 3.6).

No proteins other than RNase A homologues have cell-penetrating ability of demonstrated clinical utility. RNase A is internalized by a multi-pathway endocytic mechanism similar to that of the CPPs (Fig. 3.5). In comparison to well-known determinants of ribonuclease-mediated cytotoxicity (Rutkoski and Raines, 2008; Klink and Raines, 2000; Rutkoski *et al.*, 2005), the uptake of ribonucleases affords an opportunity for marked improvement (Fig. 3.3). Hence, the findings reported herein inform the development of superior ribonuclease-based chemotherapeutic agents, as well as the creation of other useful cell-penetrating proteins (Fuchs and Raines, 2007; Cronican *et al.*, 2010).

Acknowledgements. We are grateful to Dr. Luke D. Lavis (Janelia Farm Research Campus, Howard Hughes Medical Institute) for providing the maleimide-containing rhodamine$_{110}$-based pro-fluorophore, and G. A. Ellis and J. E. Lomax for contributive discussions and critical reading of the manuscript.

Table 3.1 Protein transduction properties of RNase A and CPPs

	RNase A	R_9	TAT
Total residues	124	9	11
Arginine residues	4	9	6
Lysine residues	10	0	2
Net charge	+4	+9	+8
Cell-surface receptors	Heparan sulfate proteoglycans Chondroitin sulfate proteoglycans Sialic acid-containing glycoproteins	Heparan sulfate proteoglycans Chondroitin sulfate proteoglycans	
Cell-types targeted	All cell types	All cell types	
Mechanism of internalization	Clathrin-mediated endocytosis Macropinocytosis	Clathrin-mediated endocytosis Caveolar-mediated endocytosis Macropinocytosis Possible non-endocytic mechanism	

Figure 3.1 Effect of endocytic inhibitors on RNase A-uptake.

HeLa cells at 37°C were pretreated with endocytic inhibitors for 30 min, and then incubated with pro-fluorophore-labeled RNase A for 1 h in the presence of the inhibitors. (A) Confocal microscopy. (i) Untreated cells; (ii) dynasore at 80 μM; (iii) CPZ at 10 μg/mL; (iv) nystatin at 25 μg/mL; (v) MβCD at 5 mM; (vi) CD at 5 μg/mL; (vii) EIPA at 10 μM; (viii) wortmannin at 50 nM. Scale bars: 10 μm. (B) Flow cytometry. Data are mean values (±SE) of total fluorescence for 20,000 washed cells from ≥6 cell populations.

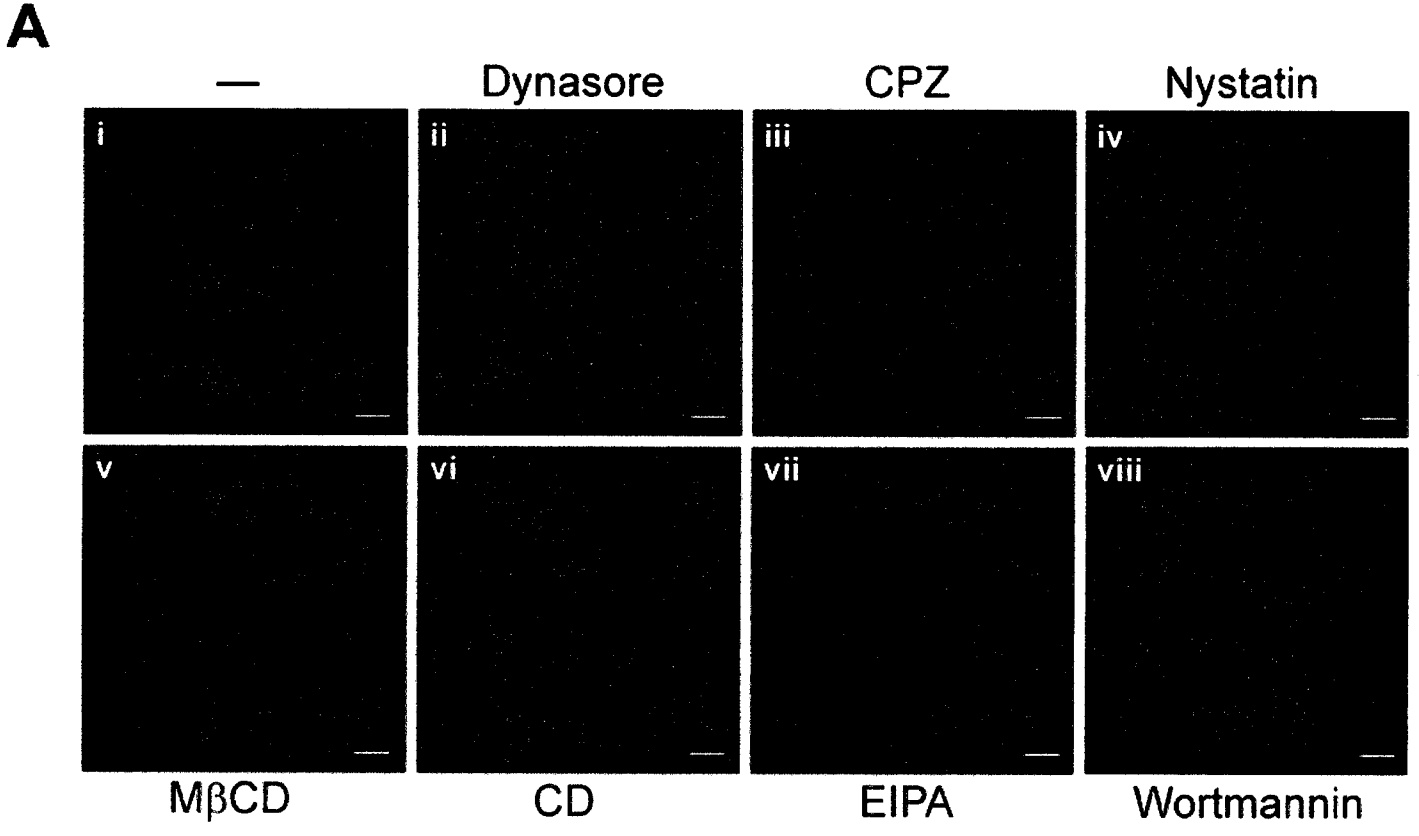
A
—
Dynasore
CPZ
Nystatin
i
ii
iii
iv
v
vi
vii
viii
MβCD
CD
EIPA
Wortmannin

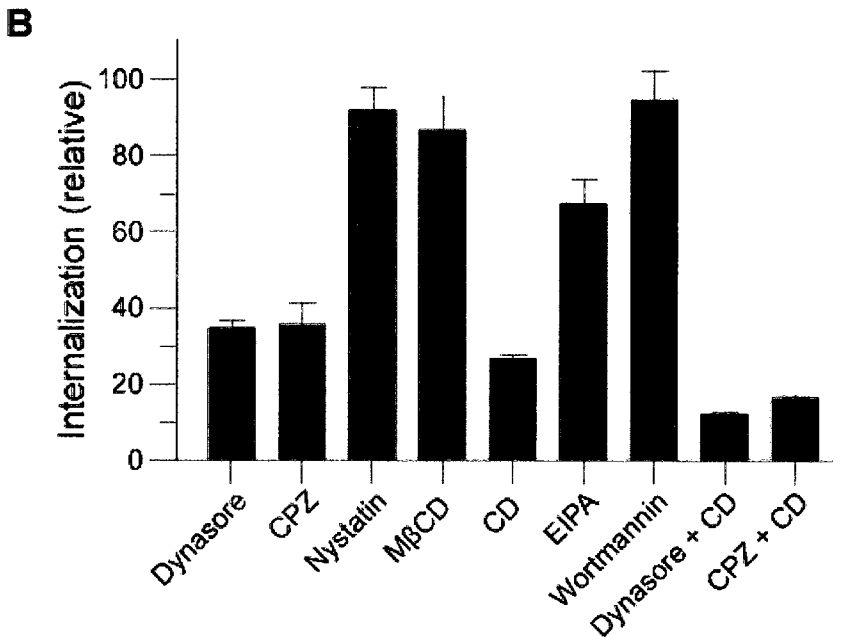
B
Internalization (relative)
100
80
60
40
20
0
Dynasore
CPZ
Nystatin
MβCD
CD
EIPA
Wortmannin
Dynasore + CD
CPZ + CD

Figure 3.2 Colocalization of RNase A with endocytic markers.

Confocal microscopy of HeLa cells incubated with pro-fluorophore-labeled RNase A (Lavis *et al.*, 2006a) (10 μM) and (i) Alexa Flour 594–transferrin (1 μM), (ii) Alexa Flour 594–CTB (1 μg/mL), (iii) 10 μM TAMRA–R_9 (10 μM), or (iv) TAMRA–TAT (10 μM) for 1 h at 37°C, and washed. Incubations with CPPs followed a 15-min pretreatment with RNase A. Scale bars: 10 μm.

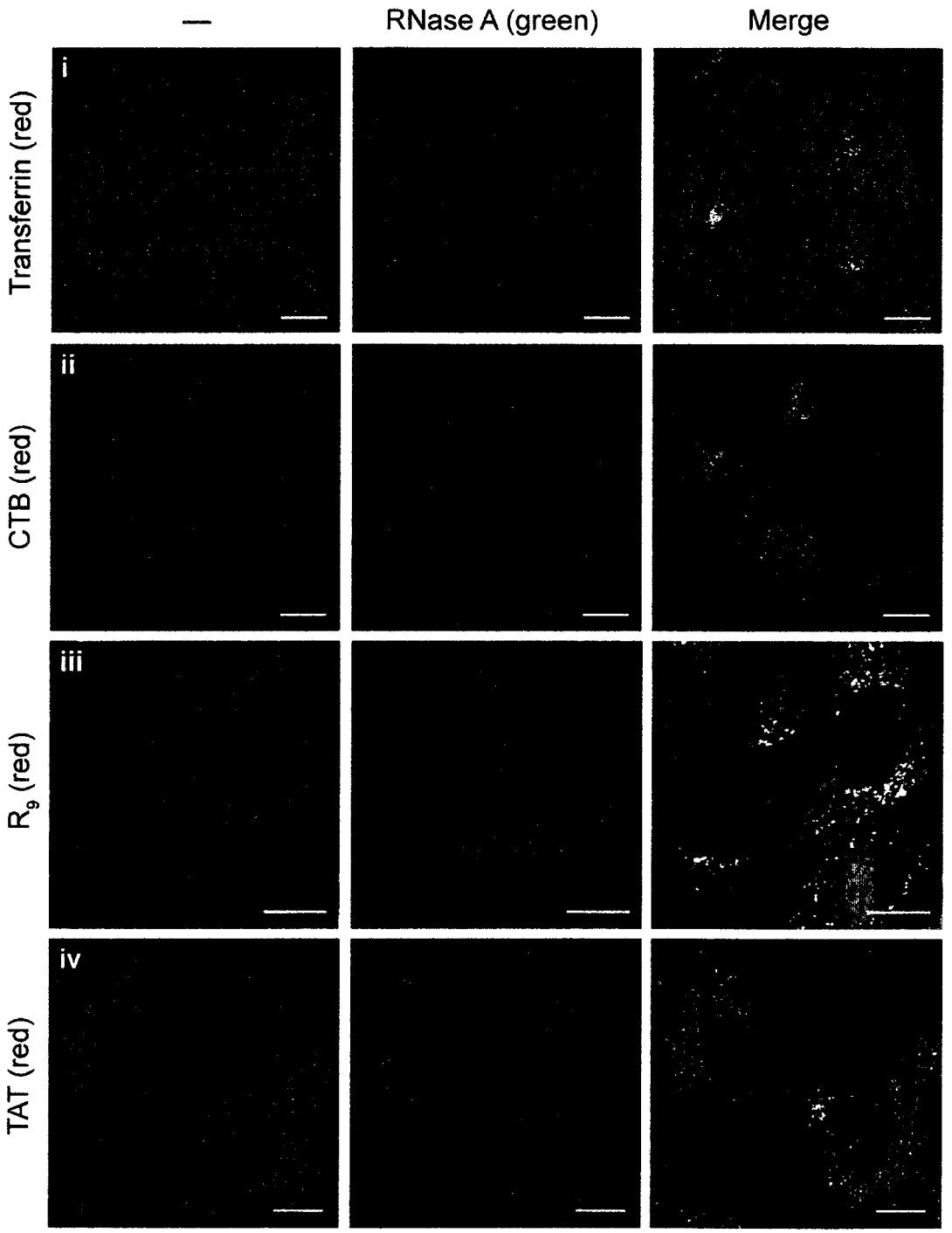
—
RNase A (green)
Merge
i
ii
iii
iv
Transferrin (red)
CTB (red)
R_9 (red)
TAT (red)

Figure 3.3 Concentration-dependence of RNase A- and CPP-uptake. (A) Confocal microscopy. HeLa cells were incubated with fluorescein–RNase A (i and iv), FAM–R_9 (ii and v), and FAM–TAT (iii and vi) for 1 h at 37°C, and washed. Scale bars: 10 μm. (B) Flow cytometry. Data points are mean values (±SE) of total fluorescence for 20,000 washed cells from 3 cell populations.

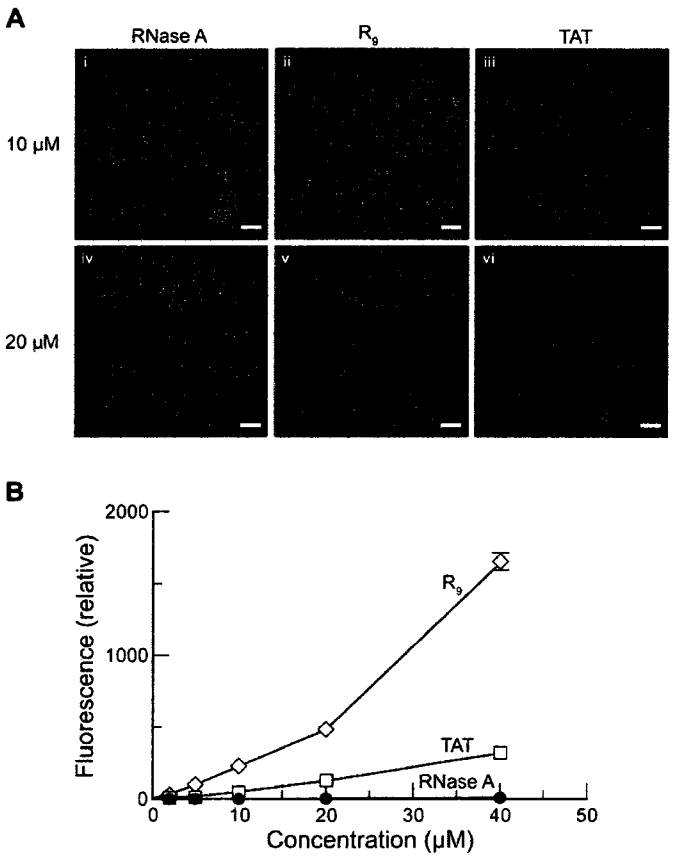
A
RNase A
R9
TAT
i
ii
iii
10 μM
iv
v
vi
20 μM
B
2000
1000
0
Fluorescence (relative)
R9
TAT
RNase A
0
10
20
30
40
50
Concentration (μM)

Figure 3.4 Comparative effect of endocytic inhibitors on RNase A- and CPP-uptake. HeLa cells at 37° were pretreated with CD, CPZ, or EIPA for 30 min, and then incubated with pro-fluorophore-labeled RNase A, FAM–R_9, or FAM–TAT for 1 h in the presence of the endocytic inhibitors. Data are mean values (±SE) of total fluorescence for 20,000 washed cells from ≥6 cell populations.

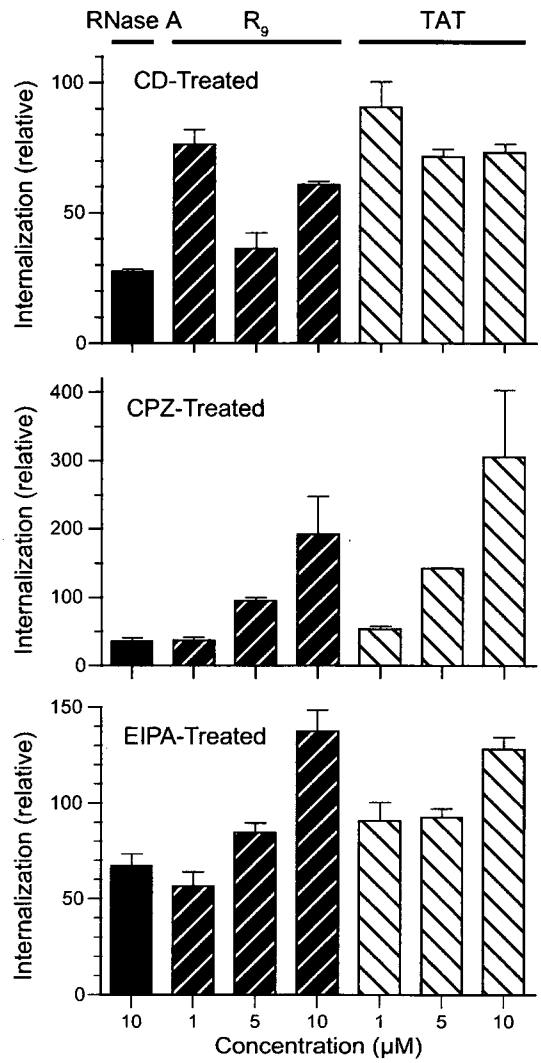
RNase A
R_9
TAT
CD-Treated
CPZ-Treated
EIPA-Treated
Internalization (relative)
100
50
0
400
300
200
150
10
1
5
Concentration (μM)

Figure 3.5 Portals of entry into a mammalian cell.

RNase A and CPPs enter cells in a similar manner as discerned, in part, by the blocking of portals with the indicated drugs. Image was adapted from ref. (Conner and Schmid, 2003).

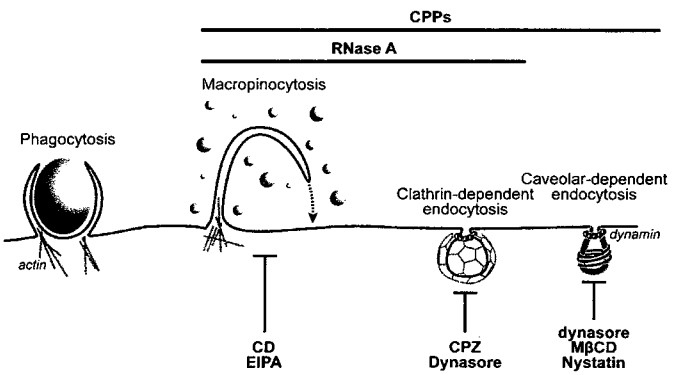
CPPs
RNase A
Macropinocytosis
Phagocytosis
Caveolar-dependent
endocytosis
Clathrin-dependent
endocytosis
dynamin
actin
CD
EIPA
CPZ
Dynasore
dynasore
MβCD
Nystatin

Figure 3.6 Cationic residues of RNase A.

Lysine residues (10) are light blue; arginine residues (4) are dark blue. A large cationic patch consists of Lys1, Lys7, Arg10, Lys37, Arg39, and Lys41. A small cationic patch consists of Lys66, Arg85, Lys98, and Lys104.

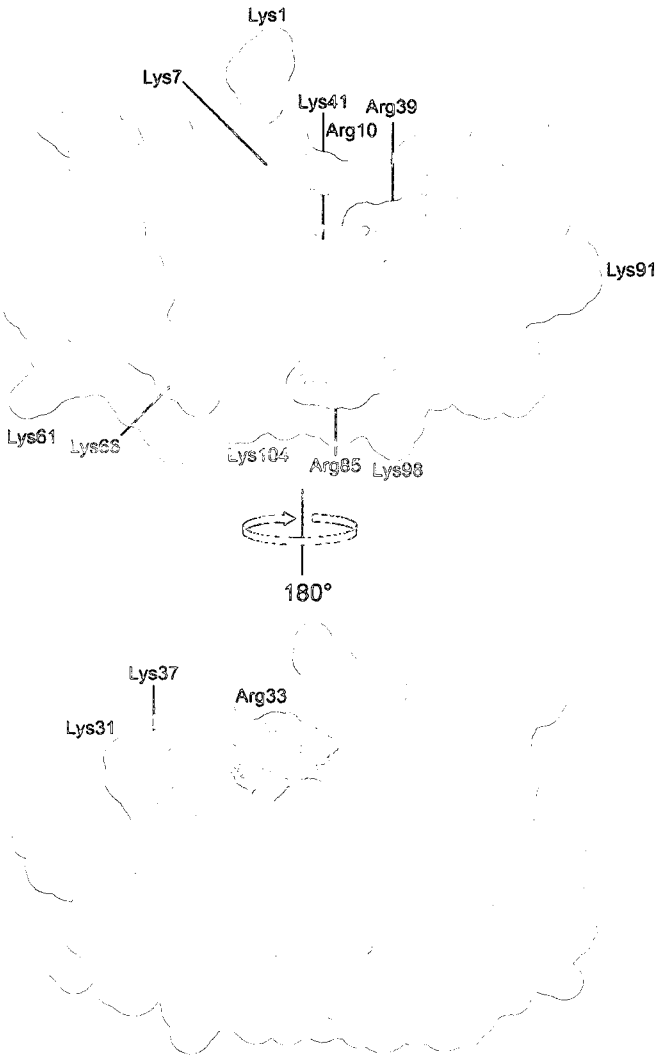
Lys1
Lys7
Lys41
Arg39
Arg10
Lys91
Lys61
Lys68
Lys104
Arg85
Lys98
180°
Lys37
Arg33
Lys31

CHAPTER 4

A Novel Assay for Endosomal Translocation

Contribution: I performed all of the research described in this chapter, except for the synthesis of 5-Carboxamidefluorescein, C_2 Maleimide, Di-β-D-Galactoside for preliminary characterization (L.D. Lavis).

Prepared for submission as:
Chao, T.-Y. and Raines, R.T. (2010)
A novel assay for endosomal translocation.

4.1 Abstract

Monitoring the cytosolic delivery of intracellularly targeted macromolecules is difficult, as the bulk of the internalized molecules are often entrapped in endosomal compartments. Here, we have developed a novel strategy for the direct quantification of endosomal translocation in human cells. To visualize the cytosolic pool exclusively, we employed the fluorogenic label, 5-chloromethylfluorescein di-β-D-galactopyranoside (CMFDG), which remains nonfluorescent until hydrolyzed by the bacterial enzyme β-galactosidase in the cytosol of *lacZ*-transfected cells. We conjugated two homologous ribonucleases, ribonuclease A and onconase, with the label, and used the ensuing fluorescence to quantify endosomal translocation. The fluorescence-based assay described here is amenable to high-throughput analysis of cytosolic delivery of a wide range of macromolecules.

4.2 Introduction

The cytosol of mammalian cells represents an important target site for the action of macromolecular therapeutic compounds, such as polypeptide-based drugs, antisense oligonucleotides, and plasmid DNA (Torchilin, 2006). Successful cytosol delivery of these macromolecules requires the initial endocytosis by target cells, followed by translocation from endosomal compartments into the cytosol. Although the relative delivery efficiency of the macromolecular therapeutics can be inferred indirectly from their biological activities, a direct assessment of cytosol delivery both in a qualitative and a quantitative fashion is essential for drug development.

Despite the development of cytosol-targeting vehicles to facilitate endosomal escape, traversing the phospholipid bilayer is still highly inefficient for hydrophilic macromolecules, often leading to significant accumulation in endosomal compartments (Larson and Lee, 1998). It is therefore challenging to monitor the rare events of endosomal translocation against the overwhelming background from macromolecules saturating the endocytic pathway (Jensen *et al.*, 2003). Few existing methods specifically monitor the cytosol influx of internalized macromolecules (Henriques *et al.*, 2007).

In general, there are two means of distinguishing the cytosol pool from the endo/lysosomal pool of internalized molecules. One is to separate the membrane-bound compartments from the cytosol by subcellular fractionation, which is dependent on cell lysis and thus susceptible to contamination. To study endosomal translocation in live cells, translocated molecules must be modified by an orthogonal biological activity in the

cytosol, such that the cytosol pool is differentiated from the rest of the internalized molecules upon translocation. For example, the endosomal translocation of cell-penetrating peptides (CPP's) has been examined by using fluorescence resonance energy transfer (FRET) between FlAsH-tagged peptides and a tetracysteine-containing FRET receptor installed in the cytosol (Adams and Tsien, 2006). Although the FlAsH fluorophore has a picomolar affinity for tetracysteine moieties, it also binds nonspecifically to endogenous cytoplasmic thiols, giving rise to high background fluorescence. Alternatively, the endosomal translocation of a redox-sensitive CPP-cargo complex has been measured by exploiting the reducing potential of the cytosol to unquench fluorescence of the CPP (Cheung *et al.*, 2009). This approach has limited applicability, as it requires the construction of a quenching FRET pair linked by a disulfide bond, which could be difficult to install on a protein containing a cysteine residue.

Here we report on a novel, fluorescence-based strategy for the quantification of cytosol delivery with low background levels and broad applicability. In our strategy, macromolecules are tagged with a latent fluorogenic label whose fluorescence is specifically and efficiently activated by an orthogonal enzyme stably expressed in the cytoplasm of engineered human cells (Fig. 4.1A). Based on this method, the cytosol entry of two homologous pancreatic ribonucleases into human cells was characterized quantitatively. The powerful combination of a small fluorogenic label with cells possessing an orthogonal enzymatic activity allows live-cell quantitative analysis of the cytosol delivery of a wide range of macromolecules.

4.3 Experimental Procedures

4.3.1 Materials

Escherichia coli strain BL21(DE3) and the pET22b (+) plasmid were from Novagen (Madison, WI). Purified *E. coli* β-galactosidase was from Sigma–Aldrich (St. Louis, MO). *lacZ* gene was cloned into p3313-IRES-mRFP vector, which was a generous gift from the Sugden Group (University of Wisconsin–Madison). The Small hairpin RNA (shRNA #1) construct targeting human *GLB1* mRNA (M34423) was a generous gift from Dr. Daniel DiMaio (Yale University School of Medicine, New Haven, CT). Anti-GLB1 antibody was purchased from Abcam (Cambridge, MA). 5-Chloromethylfluorescein di-β-D-galactopyranoside (CMFDG) was from Invitrogen (Carlsbad, CA). Quantum™ FITC MESF beads were from Bangs Laboratories (Fishers, IN). TAT-HA2 peptide was custom synthesized by GenScript Corporation (Piscatway, NJ) and has the following sequence: RRRQRRKKRGGDIMGEWGNEIFGAIAGFLG. All other chemicals and reagents were of commercial reagent grade or better, and were used without further purification.

4.3.2 Mammalian cell culture

Hela cells were from the American Type Culture Collection (Manassas, VA) and grown in MEM medium containing FBS (10% v/v), penicillin (100 units/mL) and streptomycin (100 μg/mL). *GLB1* knockdown Hela cells were created by transfecting wild-type cells with shRNA #1 construct and continuous selection with 10 μg/mL puromycin (Sigma–Aldrich, St. Louis, MO). Cell culture medium and supplements were

from ATCC. Cells were cultured at 37 °C in a humidified incubator containing CO_2 (g) (5% v/v).

4.3.3 Instrumentation

Molecular mass was measured by MALDI–TOF mass spectroscopy using a Voyager-DE-PRO Biospectrometry Workstation (Applied Biosystems, Foster City, CA) with sinapinic acid as a matrix in the campus Biophysics Instrumentation Facility. Fluorescence spectroscopy was performed with a QuantaMaster1 photon-counting fluorimeter equipped with sample stirring (Photon Technology International, South Brunswick, NJ). Flow cytometry data were collected at the University of Wisconsin Paul P. Carbone Comprehensive Cancer Center with a FACSAria SORP Sorter equipped with UV, 405-nm, 488-nm, 532-nm, and 640-nm solid state laser (Becton Dickinson, Franklin Lakes, NJ). Microscopy images were obtained with a Nikon C1 laser scanning confocal microscope with a 60× oil immersion objective with NA 1.4.

4.3.4 Purification of ribonucleases

Unlabeled variants of RNase A and onconase were produced in *E. coli* BL21(DE3) and purified as described previously (Leland *et al.*, 1998). Following purification, protein solutions were dialyzed against PBS and filtered (0.2-μm pore size) prior to use. Protein concentrations were determined by UV spectroscopy using extinction coefficients of $\varepsilon_{278} = 0.72$ $(mg/mL)^{-1}cm^{-1}$ for RNase A and $\varepsilon_{280} = 0.87$ $(mg/mL)^{-1}cm^{-1}$ for onconase.

4.3.5 Fluorescent labeling of ribonucleases

A19C RNase A and H10A/S61C onconase contain free cysteine residues for site-specific conjugation. During their purification, the free thiol groups were protected by reaction with 5,5′-dithio-bis(2-nitrobenzoic acid) (DTNB). Immediately prior to fluorophore attachment, TNB-protected ribonucleases were deprotected with a four-fold excess of dithiothreitol and desalted by chromatography on a PD-10 desalting column (GE Biosciences, Piscataway, NJ). Deprotected ribonucleases were reacted for 6 h at ambient temperature (25 °C) followed by 18 h at 4 °C with a twofold molar excess of thiol-reactive fluorophore. Conjugates were purified by chromatography using a HiTrap SP HP column (GE Biosciences, Piscataway, NJ). The molecular masses of RNase A and onconase variants and/or conjugates were confirmed by MALDI–TOF mass spectrometry. Protein concentration was determined by using a bicinchoninic acid (BCA) assay kit (Pierce, Rockford, IL) with wild-type RNase A as a standard. The degree of labeling was determined by reacting known concentrations of ribonuclease conjugates with excess purified *E. coli* β-galactosidase (Sigma–Aldrich, St. Louis, MO). The reactions were allowed to proceed to completion and the fluorescence generated was used for quantity determination based on a standard curve of fluorescence versus quantity of fluorophore.

4.3.6 Fluorescence spectroscopy

The fluorescence released from labeled ribonuclease conjugates was monitored with a fluorimeter. All measurements were recorded at ambient temperature (25 °C) at

excitation wavelength 495-nm and emission wavelength 519-nm. For pH-sensitivity studies, ribonuclease conjugates were incubated in 50 mM sodium phosphate buffer (pH 4.0) or PBS (pH 7.2) at 37 °C. At each time point, the fluorescence of ribonuclease conjugates was determined in PBS buffer (pH 7.2). The activities of ribonuclease conjugates as enzyme substrates were measured by incubating 0.5 μM of ribonuclease conjugates with excess *E. coli* β-galactosidase. The fluorescence generated was monitored continuously for up to 8 h.

4.3.7 Flow cytometry

The internalization of RNase A conjugates were monitored directly in living cells. Hela cells from near confluent flasks were plated in 6-well plates at 1.2×10^5 cells/mL/well 18–24 h prior to transfection. The next day, cells were transfected with the *lacZ* construct. 24 h following transfection, fluorescently labeled proteins were added to each well at 5 μM. Samples were then allowed to incubate at 37 °C for varying times. To quench translocation, Hela cells were washed extensively with ice-cold PBS, trypsinized with trypsin/EDTA (0.05% w/v) for several minutes. Complete media containing FBS (10% v/v) was added to each well to inhibit the action of trypsin. Samples remained on ice until analyzed by flow cytometry.

Fluorescence of ribonuclease conjugates was detected through a 525/50-nm band-pass filter. mRFP fluorescence was detected through a 610/20-nm band-pass filter. Cell viability was determined by staining with DAPI, which was detected through a 450/40-

nm band-pass filter. The mean channel fluorescence intensity of 10,000 viable cells was determined for each sample using FlowJo software and used for subsequent analysis.

4.3.8 Microscopy

Hela cells were treated under the same conditions as for flow cytometry analysis. Living cells were imaged on a Nikon Eclipse TE2000-U laser scanning confocal microscope equipped with a Zeiss AxioCam digital camera. Excitation at 408 nm was provided by a blue-diode laser, and emission light was passed through a filter centered at 450 nm with a 35-nm band-pass. Excitation at 488 nm was provided by an argon-ion laser, and emission light was passed through a filter centered at 515 nm with a 40-nm band-pass. Excitation at 543 nm was provided by a HeNe laser, and emission light was passed through a filter centered at 605 nm with a 75-nm band-pass.

4.4 Results

To demonstrate the utility of this fluorescence-based endosomal translocation assay, we employed ribonuclease A (RNase A) as the model protein. RNase A is a small cationic protein with exceptionally well-established biochemical and biophysical attributes (Raines, 1998). Recent reports unraveling the biological properties of RNase A have shown that it is taken up by mammalian cells, and its ability to degrade intracellular RNA contributes to the anti-cancer properties observed with certain RNase A variants (Chao *et al.*, 2010; Haigis and Raines, 2003). Similar to most macromolecules with cell-

penetrating capabilities, the majority of the endocytosed RNase A remains entrapped in endocytic compartments; only a small fraction of internalized RNase A reaches the cytoplasm (Rutkoski and Raines, 2008; Leich *et al.*, 2007).

To quantify the cytosolic entry of RNase A, we site-specifically attached the thiol-reactive latent fluorogenic label, 5-chloromethylfluorescein di-β-D-galactopyranoside (CMFDG), to the free cysteine variant, A19C RNase A. As shown in Fig. 4.1B, at the core of CMFDG is fluorescein di-β-D-galactopyranoside (FDG), which is a highly sensitive β-galactosidase substrate that has been used widely for detecting *lacZ* expression in cells, tissues, and model organisms (Plovins *et al.*, 1994). The fluorescence of fluorescein is masked by the two galactoside moieties and released upon hydrolysis of the glycosidic bonds. To test if CMFDG-RNase A serves as a substrate for β-galactosidase, 10 μg of the conjugate was incubated with excess *E. coli* β-galactosidase while the fluorescence generated was monitored continuously until maximum fluorescence was reached. As shown in Fig. 4.2A, the fluorescence of CMFDG-RNase A increased ~90 fold upon addition of the enzyme, indicating that the conjugate is indeed a substrate for bacterial β-galactosidase. As CMFDG-RNase A is expected to enter acidic endosomal compartments, the stability of the conjugate in acidic environment was tested by monitoring the release of fluorescence. As demonstrated in Fig. 4.2B, the fluorescence of CMFDG-RNase A remains quenched for at least 12 h at 37°C, pH 4, and is comparable to that at pH 7.

Following *in vitro* analyses, the stability of CMFDG-RNase A was examined further in wild-type Hela cells (*lacZ*$^-$). Surprisingly, extended incubation (24 h) did result

in low levels of background fluorescence, suggesting that an endogenous β-galactosidase is accessible to CMFDG-RNase A and able to manifest its fluorescence. The human β-galactosidase, GLB1, is a 76-kDa lysosomal enzyme that does not resemble the bacterial β-galactosidase. To reduce background fluorescence, we created Hela cell clones that stably express a short hairpin RNA (shRNA) knockdown construct targeting *GLB1*. Three clones with decreased *GLB1* expression (lanes 1-3, 1-9, and 1-10, Fig. 4.3A) were incubated with CMFDG-RNase A and the fluorescence generated was measured by flow cytometry. As shown in Fig. 4.3B, *GLB1* knockdown cell lines lost 50–65% of the background fluorescence, indicating that GLB1 activity is partially responsible for activating CMFDG. The residual fluorescence observed for clone 1-3 could be due to autofluorescence or activity from other glycosidases.

Next, we transfected clone 1-3 cells with a plasmid containing the *lacZ*-IRES-*mRFP* construct, in which the internal ribosomal entry site (IRES) permits correlation between the expression of the monomeric red fluorescent protein (mRFP) and of the *lacZ* gene, thereby allowing $lacZ^+$ cells to be identified definitively by mRFP fluorescence. The cytosolic entry of RNase A was then determined by incubating CMFDG-RNase A with $lacZ^+$ cells. As a control, the same amount of ribonuclease conjugate was incubated with cells transfected with the empty vector containing IRES-*mRFP* but not *lacZ*. As shown in Fig. 4.4A, the cytosolic influx of RNase A was detected after only 6 h of incubation, and it exhibits a rapid increase in fluorescence during the first 12 h of incubation, followed by a gradual increase thereafter. By contrast, levels of background fluorescence, as measured with $lacZ^-$ cells, remain relatively constant for 24 h and

account for ~20% of the fluorescence of *lacZ*$^+$ cells. To confirm that fluorescent CMFDG-RNase A is only detected in the cytoplasm, subcellular localization of labeled RNase A was visualized by live-cell microscopy. As expected, diffused RNase A staining was observed in cells with high levels of bacterial β-galactosidase, while little or no fluorescence was detected in *lacZ*$^-$ cells (Fig. 4.4B). Finally, the total internalization of RNase A, which was measured with fluorescein-labeled RNase A, is several fold greater than the levels of RNase A in the cytoplasm (Fig. 4.4A). Together, these results illustrate that the rate of RNase A cytosolic entry can be determined by using the fluorogenic substrate CMFDG with *lacZ*$^+$ cells.

The cytosolic content of RNase A can be quantified precisely in terms of molecules by using standardizing beads that correlate relative fluorescence to the number of fluorescein molecules. As shown in Fig. 4.5, approximately 3×10^4 molecules of RNase A were found to reach the cytoplasm at 24 h of incubation when 5 μM CMFDG-RNase A was added to *lacZ*$^+$ cells. In addition, endosomal translocation of RNase A was slightly enhanced in the presence of a known fusogenic peptide, TAT-HA2, which has been shown to augment cytosolic delivery (Wadia *et al.*, 2004). Interestingly, the effect of TAT-HA2 was more prominent when used *in trans* with onconase, a homologue of RNase A that is currently in Phase IIIb clinical trials for treating malignant mesothelioma (Lee and Raines, 2008). The cytosolic entry of onconase is increased by ~twofold in the presence of 10 μM TAT-HA2 (Fig. 4.5), suggesting that the efficacy of these cytotoxins can be improved by increasing cytosolic delivery without changing the overall level of internalization (data not shown).

4.5 Discussion

Monitoring the cytosolic delivery of macromolecules with traditional tools has been challenging mainly due to the obfuscating background from endo- and lysosomal compartments. Although recent strategies have overcome the difficulty in excluding signals from endocytic compartments, those methods suffer from high background and limited application (Adams and Tsien, 2006; Cheung *et al.*, 2009). Here, we have demonstrated the utility of a common reporter gene, *lacZ*, in a novel strategy for the quantification of cytosolic entry, in which macromolecules are tagged with a latent fluorogenic label that is activated by β-galactosidase upon translocation. Unexpectedly, our studies showed that human endogenous β-galactosidase in lysosomes contributes to low levels of background fluorescence. siRNA knockdown of *GLB1* reduced background by nearly 70%, and yet, fluorescence in *lacZ*$^-$ cells is ~1/5 of the cytosol signal in *lacZ*$^+$ cells. The use of a more orthogonal enzyme-latent fluorogenic substrate pair could lower background even further.

Cytotoxic ribonucleases are promising chemotherapeutic agents (Arnold and Ulbrich-Hofmann, 2006; Lee and Raines, 2008); however, the cytosolic entry of these toxins have never been characterized. Here, by incubating CMFDG labeled RNase A and onconase with *lacZ*$^+$ Hela cells at 5 μM, we revealed that approximately 3×10^4 molecules of both ribonucleases were able to reach the cytoplasm after 24 h of incubation, which corresponds to <10% of total internalized proteins. Prior studies have shown that the dosage of cytotoxic ribonuclease variants required for inhibiting

mammalian cell line proliferation (IC_{50}) ranges from 0.031–4.8 μM, with most IC_{50} values in the sub-micromolar range (Rutkoski *et al.*, 2005). Thus, a few thousand molecules of ribonuclease could mediate cancer cell toxicity. As endosomal translocation is evidently a highly inefficient process for ribonucleases, as well as for other macromolecular chemotherapeutics alike, the translocation assay we describe here would be a powerful tool in the development of drugs with enhanced cytosolic delivery.

Acknowledgements. We are grateful to Dr. Luke D. Lavis (Janelia Farm Research Campus, Howard Hughes Medical Institute) for synthesis of 5-carboxamidefluorescein, C2-maleimide, bis-β-galactoside for initial characterizations. We thank Dr. Bill Sugden and Dr. Daniel DiMaio for the generous gifts of p3313-IRES-mRFP and pSIREN-shRNA #1 constructs.

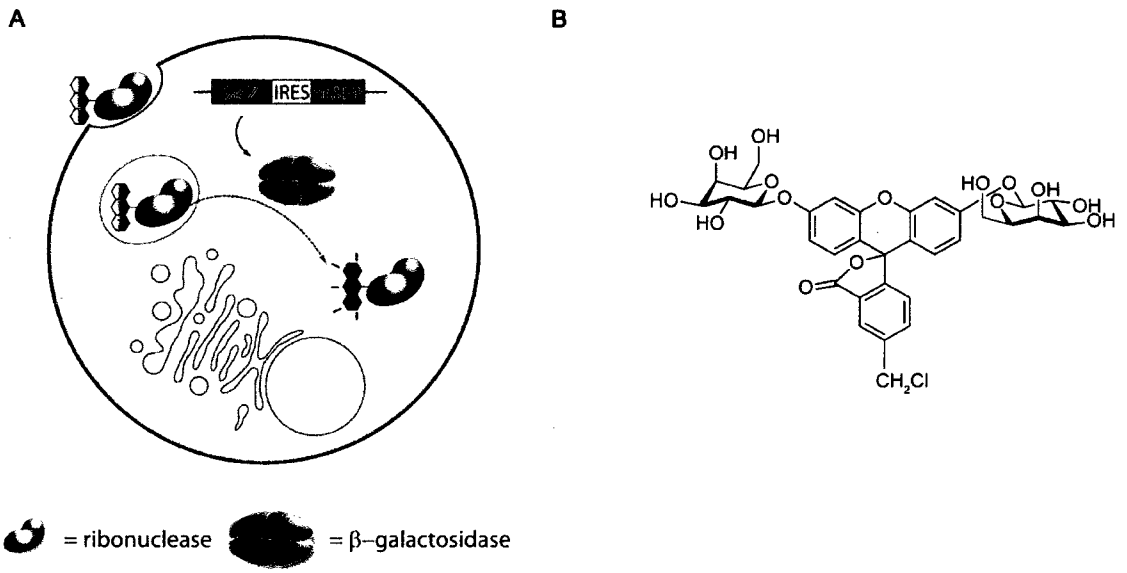

Figure 4.1 Schematic diagram illustrating the β-galactosidase-based endosomal translocation assay.

(A) Ribonucleases, which are shown in blue, are labeled with 5-chloromethylfluorescein di-β-D-galactopyranoside (CMFDG; B), a latent fluorogenic substrate for β-galactosidase. Labeled conjugates remain nonfluorescent in their cellular entry pathway until catalyzed by β-galactosidase in the cytoplasm of *lacZ*$^+$ cells. Expression of monomeric RFP aids the identification of *lacZ*$^+$ cells.

Figure 4.2 CMFDG-RNase A conjugate as a stable substrate for β-galactosidase. (A) CMFDG-RNase A was incubated with excess purified β-galactosidase at 0.5 μM, and the fluorescence released was monitored continuously by fluorescence spectrometry. (B) pH stability of CMFDG-RNase A was determined by extended incubated in 50mM sodium phosphate buffer (pH 4.0) and PBS buffer (pH 7.2) at 37°C. At each time point, the fluorescence of ribonuclease conjugates was determined in PBS buffer (pH 7.2).

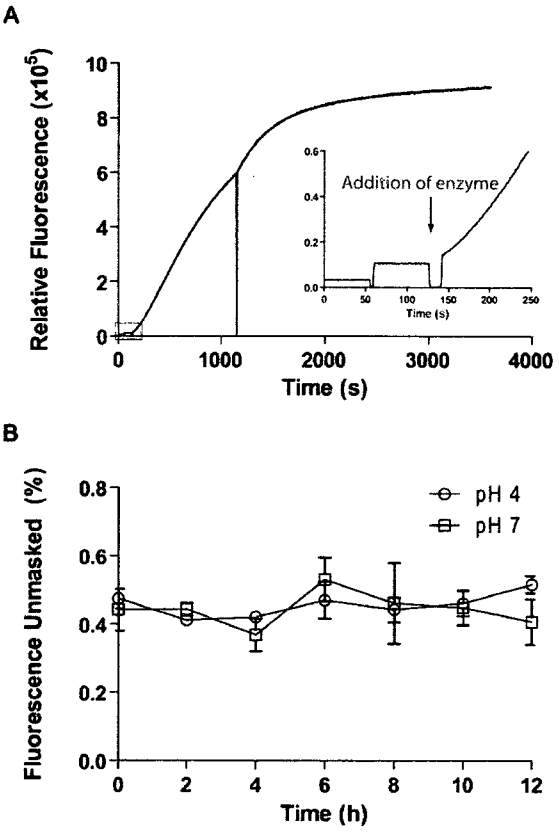
A
Relative Fluorescence (x10^5)
10
8
6
4
2
0
0
1000
2000
3000
4000
Time (s)
Addition of enzyme
0.6
0.4
0.2
0.0
0
50
100
150
200
250
Time (s)
B
Fluorescence Unmasked (%)
0.8
0.6
0.4
0.2
0.0
0
2
4
6
8
10
12
Time (h)
pH 4
pH 7

Figure 4.3 Stable Hela *GLB1* knockdown clones with reduced background fluorescence.

(A) Cell lysates from wild-type Hela cells as well as cells stably transfected with *GLB1*-targeting shRNA were analyzed by western blot with anti- *GLB1* antibodies. (B) CMFDG-RNase A was incubated with wild-type Hela cells and *GLB1* knockdown clones for 24 h at 37°C. The resulting total cellular fluorescence was measured by flow cytometry. Data points are mean values (±SE) for 20,000 live cells from ≥3 cell populations.

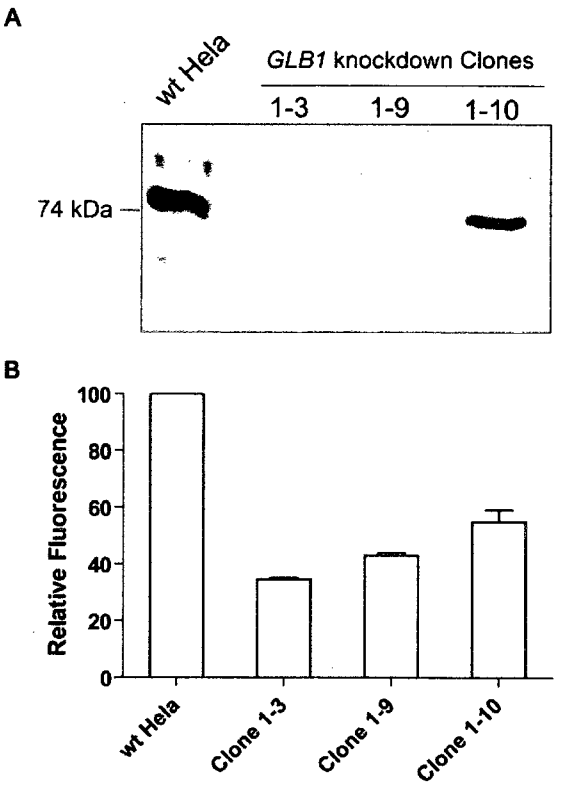
A
wt Hela
GLB1 knockdown Clones
1-3
1-9
1-10
74 kDa
B
Relative Fluorescence
100
80
60
40
20
0
wt Hela
Clone 1-3
Clone 1-9
Clone 1-10

Figure 4.4 Kinetic profile of RNase A uptake and cytosolic entry.

(A) Total RNase A cellular uptake was measured with fluorescein labeled proteins (○), while CMFDG-RNase A was added to *lacZ*$^+$ (■) and *lacZ*$^-$ (□) Hela cells. All proteins were used at 5 μM. The resulting total cellular fluorescence was measured by flow cytometry. Data points are mean values (±SE) for ~10,000 live, mRFP$^+$ cells from ≥6 cell populations. (B) Hela cells transfected with the *lacZ*-IRES-mRFP (*lacZ*$^+$) construct were incubated with 5 μM CMFDG-RNase A for 24 h at 37°C. To avoid potential physiological changes induced by transfection, control cells were transfected with the empty vector containing IRES-mRFP (*lacZ*$^-$). Scale bars indicate 10 μm.

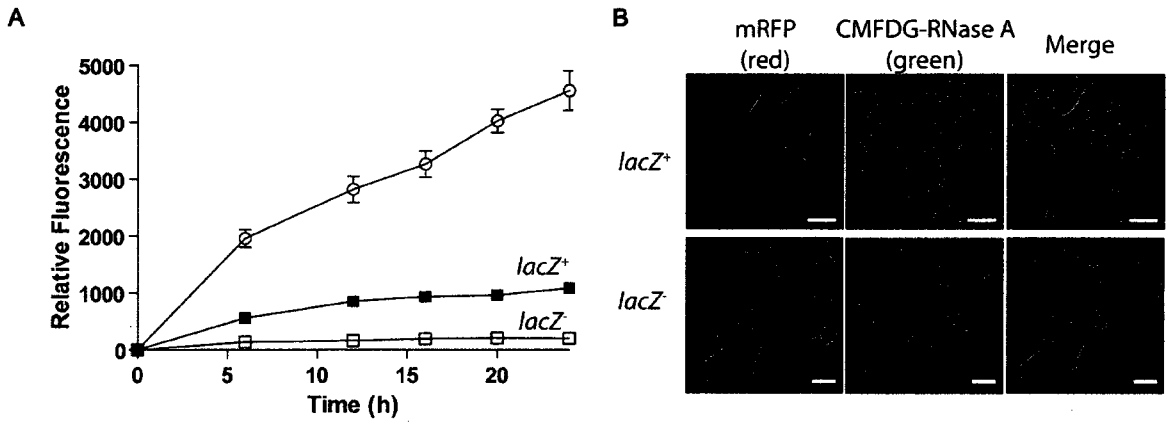
A
Relative Fluorescence
5000
4000
3000
2000
1000
0
0
5
10
15
20
Time (h)
lacZ+
lacZ-
B
mRFP
(red)
CMFDG-RNase A
(green)
Merge
lacZ+
lacZ-

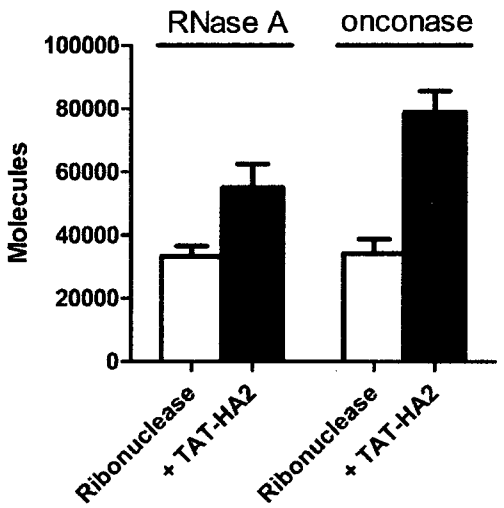

Figure 4.5 Quantification of RNase A and onconase translocation.

The cytosolic fluorescence of Hela cells incubated with 5 μM RNase A and onconase (24 h) was converted to molecules of equivalent soluble fluorophores (MESF) using standardizing beads. The fusogenic peptide TAT-HA2 was added in *trans* at 10 μM. Data points are mean values (±SE) calculated from 3 independent flow cytometry experiments measuring the total cellular fluorescence of ~10,000 live, $mRFP^+$ cells from 9 cell populations.

CHAPTER 5

Cytotoxic Ribonucleases:

The Dichotomy of Coulombic Forces

Contribution: Flow cytometry. All other experiments were performed by R.J. Johnson. Design and synthesis of profluorophore was performed by L.D. Lavis.

This chapter was published as:
Johnson, R.J., Chao, T.-Y., Lavis, L.D., and Raines, R.T. (2007) Cytotoxic Ribonuclease: The Dichotomy of Coulombic Forces. *Biochemistry* **46**, 10308–10316.

5.1 Abstract

Cells tightly regulate their contents. Still, nonspecific Coulombic interactions between cationic molecules and anionic membrane components can lead to adventitious endocytosis. Here, we characterize this process in a natural system. To do so, we create variants of human pancreatic ribonuclease (RNase 1) that differ in net molecular charge. By conjugating a small-molecule latent fluorophore to these variants and using flow cytometry, we are able to determine the kinetic mechanism for RNase 1 internalization into live human cells. We find that internalization increases with solution concentration and is not saturable. Internalization also increases with time to a steady-state level, which varies linearly with molecular charge. In contrast, the rate constant for internalization ($t_{1/2}$ = 2 h) is independent of charge. We conclude that internalization involves an extracellular equilibrium complex between the cationic proteins and abundant anionic cell-surface molecules, followed by rate-limiting internalization. The enhanced internalization of more cationic variants of RNase 1 is, however, countered by their increased affinity for the cytosolic ribonuclease inhibitor protein, which is anionic. Thus, Coulombic forces mediate extracellular and intracellular equilibria in a dichotomous manner that both endangers cells and defends them from the potentially lethal enzymatic activity of ribonucleases.

5.2 Introduction

Cells control their intracellular environment through careful gating of the influx of extracellular material (Conner and Schmid, 2003; Polo and Di Fiore, 2006). To distinguish between molecules to be internalized from those to be excluded, cells use specific interactions with cell-surface proteins, lipids, and carbohydrates. Nonspecific interactions mediated by Coulombic forces can also lead to internalization, often in an unregulated manner (Conner and Schmid, 2003; Cho and Stahelin, 2005; Mulgrew-Nesbitt *et al.*, 2006; Murray and Honig, 2002; Polo and Di Fiore, 2006). Such nonspecific interactions can be modulated by increasing, decreasing, or masking the cationic charge on the biomolecule (Mulgrew-Nesbitt *et al.*, 2006; Murray and Honig, 2002).

Two classes of molecules that exploit high cationicity to effect nonspecific adsorption to the cell surface and internalization are cell-penetrating peptides (CPPs) and ribonucleases (Fotin-Mleczek *et al.*, 2005; Fuchs and Raines, 2006; Kaplan *et al.*, 2005; Notomista *et al.*, 2006). CPPs have received considerable attention due to their ability to transport otherwise membrane-impermeable cargo into cells (Zorko and Langel, 2005; Fuchs and Raines, 2006; Chauhan *et al.*, 2006). The detailed mechanism of CPP internalization is unclear, but is known to involve multiple steps. Those steps include binding to anionic cell-surface molecules, internalization in an ATP- and temperature-dependent manner, and ultimately translocation from endosomes into the cytoplasm (Fuchs and Raines, 2004; Richard *et al.*, 2005; Drin *et al.*, 2003; Fuchs and Raines, 2006). Similar to cationic peptides, the endocytosis of pancreatic-type ribonucleases is

facilitated by their cationic nature (Haigis and Raines, 2003; Notomista *et al.*, 2006). Ribonucleases bind to the cell surface through Coulombic interactions between positively charged residues and negatively charged cell-surface molecules (Notomista *et al.*, 2006), and are endocytosed by a dynamin-independent pathway without the necessity for a specific receptor (Haigis and Raines, 2003).

Pancreatic-type ribonucleases have diverse biological activities, including selective toxicity to cancerous cells (Arnold and Ulbrich-Hofmann, 2006; Benito *et al.*, 2005; D'Alessio and Riordan, 1997; Leland and Raines, 2001; Makarov and Ilinskaya, 2003; Matoušek, 2001). The archetype of a cytotoxic ribonuclease is Onconase® (ONC), a ribonuclease isolated from the oocytes of *Rana pipiens* that is currently in confirmatory phase IIIb clinical trials for the treatment of malignant mesothelioma (Pavlakis and Vogelzang, 2006). The specific toxicity of ONC and engineered ribonucleases toward tumor cells relies on multiple biochemical attributes, such as evasion of the cytosolic ribonuclease inhibitor protein (RI) (Dickson *et al.*, 2005), high ribonucleolytic activity, and resistance to proteolysis (Bretscher *et al.*, 2000; Dickson *et al.*, 2003; Klink and Raines, 2000).

Cationic charge is also important for ribonuclease cytotoxicity. For example, the cytotoxicity of bovine pancreatic ribonuclease (RNase A, EC 3.1.27.5) (Raines, 1998) and microbial ribonucleases can be increased through mutagenic or chemical cationization (Ilinskaya *et al.*, 2002; Ilinskaya *et al.*, 2004; Futami *et al.*, 2001; Futami *et al.*, 2002; Fuchs *et al.*, 2007). Traditional studies on the relationship between the cationicity and cytotoxicity of ribonucleases have used cell death as the read-out (Ogawa

et al., 2002; Notomista *et al.*, 2006; Ilinskaya *et al.*, 2002; Ilinskaya *et al.*, 2004; Futami *et al.*, 2001; Futami *et al.*, 2002; Fuchs *et al.*, 2007). This phenotype is manifested, however, only after a complex, multi-step process (Arnold and Ulbrich-Hofmann, 2006; Benito *et al.*, 2005; D'Alessio and Riordan, 1997; Leland and Raines, 2001; Makarov and Ilinskaya, 2003; Matoušek, 2001). Hence, a direct measurement of ribonuclease internalization is necessary to dissect the effect of cationicity on internalization.

Here, we isolate internalization from cell death by using a novel fluorogenic label with fluorescence that remains quiescent until an encounter with an intracellular esterase (Lavis *et al.*, 2006a; Chandran *et al.*, 2005). By using this latent fluorophore along with flow cytometry, we directly quantitate the internalization of variants of human pancreatic ribonuclease (RNase 1; Fig. 5.1A). We then characterize the effect of charge on two equilibria that mediate ribonuclease cytotoxicity. Our findings reveal new information about the role of Coulombic forces in protein–cell and protein–protein interactions.

5.3 Experimental Procedures

5.3.1 Materials

Escherichia coli strain BL21(DE3) was from Novagen (Madison, WI). 6-FAM–dArU$(dA)_2$–6-TAMRA, a fluorogenic ribonuclease substrate, was from Integrated DNA Technologies (Coralville, IA). Enzymes were from Promega (Madison, WI). K-562 cells, which are an erythroleukemia cell line derived for a chronic myeloid leukemia patient, were from the American Type Culture Collection (Manassas, VA). Cell culture medium

and supplements were from Invitrogen (Carlsbad, CA). [*methyl*-^{3}H]Thymidine (6.7 Ci/mmol) was from Perkin–Elmer (Boston, MA). Protein purification columns were from GE Biosciences (Piscataway, NJ). MES buffer (Sigma–Aldrich, St. Louis, MO) was purified by anion-exchange chromatography to remove trace amounts of oligomeric vinylsuflonic acid (Smith *et al.*, 2003). Phosphate-buffered saline (PBS) contained (in 1.00 L) NaCl (8.0 g), KCl (2.0 g), $Na_2HPO_4 \cdot 7H_2O$ (1.15 g), KH_2PO_4 (2.0 g), and NaN_3 (0.10 g) and had a pH of 7.4. All other chemicals were of commercial grade or better, and were used without further purification.

5.3.2 Instrumentation

Fluorescence spectroscopy was performed with a QuantaMaster1 photon-counting fluorimeter equipped with sample stirring (Photon Technology International, South Brunswick, NJ). Thermal denaturation data were collected using a Cary 3 double-beam spectrophotometer equipped with a Cary temperature-controller (Varian, Palo Alto, CA). [*methyl*-^{3}H]Thymidine incorporation into genomic DNA was quantitated by liquid scintillation counting using a Microbeta TriLux liquid scintillation and luminescence counter (Perkin–Elmer, Wellesley, MA). The mass of RNase 1 and its variants was confirmed by matrix-assisted laser desorption/ionization time-of-flight (MALDI–TOF) mass spectrometry with a Voyager-DE-PRO Biospectrometry Workstation (Applied Biosystems, Foster City, CA) at the campus Biophysics Instrumentation Facility. Flow cytometry data were collected by using a FACSCalibur flow cytometer equipped with a 488-nm argon-ion laser (Becton Dickinson, Franklin Lakes, NJ). Microscopy images

were obtained with a Nikon Eclipse TE2000-U confocal microscope equipped with a Zeiss AxioCam digital camera.

5.3.3 Protein purification and labeling

DNA encoding variants of RNase 1 were made by using plasmid pHP-RNase (Leland *et al.*, 2001) and the Quikchange site-directed mutagenesis or Quikchange Multi site-directed mutagenesis kit (Stratagene, La Jolla, CA). RNase 1 variants were produced in *E. coli* and purified by using methods described previously for wild-type RNase 1 (Leland *et al.*, 2001). D38R/R39D/N67R/G88R RNase A, which is a highly cytotoxic variant (Rutkoski *et al.*, 2005), was a gift from T. J. Rutkoski. Human RI was produced in *E. coli* and purified as described previously (Johnson *et al.*, 2007d).

Variants with a free cysteine at position 19 were protected by reaction with 5,5′-dithio-bis(2-nitrobenzoic acid) (DTNB) (Lavis *et al.*, 2006a; Riddles *et al.*, 1983). Immediately prior to latent-fluorophore attachment, TNB-protected ribonucleases were deprotected with a three-fold molar excess of dithiothreitol (DTT) and desalted by chromatography on a PD-10 desalting column (GE Biosciences, Piscataway, NJ). The maleimide-containing latent fluorophore was synthesized as described previously (Lavis *et al.*, 2006a). Deprotected ribonucleases were reacted for 4–6 h at 25 °C with a ten-fold molar excess of thiol-reactive latent fluorophore (Lavis *et al.*, 2006a). Conjugates were purified by chromatography using a HiTrap SP FF column. The molecular masses of RNase 1, its variants, and conjugates were confirmed by MALDI–TOF mass

spectrometry. Protein concentration was determined by using a bicinchoninic acid assay kit from Pierce (Rockford, IL) with bovine serum albumin as a standard.

5.3.4 Conformational stability measurements

The conformational stability of RNase 1 and its variants was determined by following the change in UV absorbance at 287 nm with increasing temperature (Klink and Raines, 2000). The temperature of PBS containing an RNase 1 variant (0.1–0.2 mg/mL) was heated from 20 to 80 °C at 0.15 °C/min. The A_{287} was followed at 1-°C intervals, and the absorbance change was fitted to a two-state model of denaturation, wherein the temperature at the midpoint of the transition curve corresponds to the value of T_m.

5.3.5 Ribonucleolytic activity assays

The ribonucleolytic activity of RNase 1 and its variants was determined by quantitating its ability to cleave 6-FAM–dArU(dA)$_2$–6-TAMRA (Kelemen *et al.*, 1999). Assays were carried out at 23 (±2) °C in 2.0 mL of 0.10 M MES–NaOH buffer (pH 6.0) containing NaCl (0.10 M). Fluorescence data were fitted to eq 5.1, in which $\Delta I/\Delta t$ is the initial reaction velocity, I_0 is the fluorescence intensity before addition of a ribonuclease, I_f is the fluorescence intensity after complete substrate hydrolysis, and [E] is the total ribonuclease concentration.

$$k_{cat}/K_M = \frac{(\Delta I/\Delta t)}{(I_f - I_0)[E]} \quad (5.1)$$

5.3.6 *RI-binding assays*

The affinity of RNase 1 variants for human RI was determined by using a fluorescent competition assay reported previously (Abel *et al.*, 2002). Briefly, PBS (2.0 mL) containing DTT (5 mM), fluorescein-labeled G88R RNase A (50 nM), and various concentrations of an unlabeled RNase 1 variant was incubated at 23 (±2) °C for 20 min. The initial fluorescence intensity of the unbound fluorescein-labeled G88R RNase A was monitored for 3 min (excitation: 491 nm, emission: 511 nm). RI (50 nM) was then added, and the final fluorescence intensity was measured. The value of K_d for RI·RNase 1 complexes as defined in eq 5.2 was obtained by nonlinear least squares analysis of the binding isotherm using GraphPad Prism 4.02 (GraphPad Software, San Diego, CA). The K_d value for the complex between RI and fluorescein-labeled G88R RNase A was taken to be 1.4 nM (Rutkoski *et al.*, 2005).

$$\text{RI·RNase 1} \overset{K_d}{\rightleftharpoons} \text{RI + RNase 1} \quad (5.2)$$

5.3.7 *Cytotoxicity assays*

The effect of RNase 1 and its variants on the proliferation of K-562 cells was assayed as described previously (Rutkoski *et al.*, 2005; Leland *et al.*, 2001; Haigis *et al.*,

2002). After a 44-h incubation with ribonuclease, K-562 cells were treated with [*methyl*-^{3}H]thymidine for 4 h, and the incorporation of radioactive thymidine into cellular DNA was quantitated by liquid scintillation counting. Results are shown as the percentage of [*methyl*-^{3}H]thymidine incorporated relative to control cells. Data are the average of three measurements for each concentration, and the entire experiment was repeated in triplicate. Values for IC_{50} were calculated by fitting the curves by nonlinear regression with eq 5.3 (Rutkoski *et al.*, 2005), in which y is the total DNA synthesis following the [*methyl*-^{3}H]thymidine pulse and h is the slope of the curve.

$$y = \frac{100\%}{1+10^{(\log(IC_{50})-\log[\text{ribonuclease}])h}} \tag{5.3}$$

5.3.8 Flow cytometry assays

The internalization of ribonuclease variants with latent fluorophore attached (Fig. 5.1B) was followed by monitoring the unmasking of fluorescence by intracellular esterases. K-562 cells from near confluent flasks were collected by centrifugation and resuspended at a density of 1×10^6 cells/mL in fresh RPMI 1640. Labeled ribonuclease (10 μM) or unlabeled RNase 1 (10 μM) was added to 250 μL of RPMI containing 1×10^6 cells/mL of K-562 cells. K-562 cells were allowed to incubate at 37 °C for varying times with the ribonucleases. To quench internalization, K-562 cells were collected by centrifugation at 750*g* for 3 min at 4 °C, and cell pellets were resuspended gently in ice-cold PBS (250 μL). Samples remained on ice until analyzed by flow cytometry.

Latent fluorophore fluorescence was detected through a 530/30-nm band-pass filter. Cell viability was determined by staining with propidium iodide, which was detected through a 660-nm long-pass filter. The mean channel fluorescence intensity of 20,000 viable cells was determined for each sample using CellQuest software and used for subsequent analysis. To determine the steady-state rate constant for ribonuclease internalization, fluorescence intensity data were fitted to eq 5.4, in which F_{max} is the fluorescence intensity upon reaching the steady-state and k_I is the rate constant for ribonuclease internalization into K-562 cells.

$$F = F_{max}(1 - e^{-k_I t}) \tag{5.4}$$

5.3.9 Microscopy

Confocal microscopy was used to observe ribonuclease localization. K-562 cells were prepared as described for flow cytometry. Latent fluorophore-labeled RNase 1 variant (10 μM) or fluorescein-labeled RNase 1 variant (10 μM) were added to 250 μL of RPMI 1640 containing K-562 cells (1×10^6 cells/mL) and incubated at 37 °C for 30 min. Cell nuclei were stained by the addition of Hoechst 33342 (2 μg/mL) for the final 5 min of incubation. Excitation at 408 nm was provided by a blue-diode laser, and emission light was passed through a filter centered at 450 nm with a 35-nm band-pass. Excitation at 488 nm was provided by an argon-ion laser, and emission light was passed through a filter centered at 515 nm with a 40-nm band-pass. Excitation at 543 nm was provided by

a HeNe laser, and emission light was passed through a filter centered at 605 nm with a 75-nm band-pass.

5.4 Results

5.4.1 Design of RNase 1 variants

Recently, we reported on variants of RNase 1 that evade the inhibitory action of RI (Johnson *et al.*, 2007d). In these variants, positions 39, 67, 88, 89, and 91 of RNase 1 were determined to be important contact residues between human RI and RNase 1 (Fig. 5.1A). By engendering Coulombic repulsion at these positions, a variant of RNase 1 ($DDADD^3$) was endowed with 5×10^9-fold lower affinity for RI. This variant was, however, only moderately toxic to human chronic myeloid leukemia cells *in vitro* (IC_{50} = 13.3 μM) (Johnson *et al.*, 2007d).

The lowered cytotoxicity of this RNase 1 variant when compared to other ribonucleases with similar biochemical characteristics was proposed to result from its net neutral charge, which could diminish its cellular internalization (Johnson *et al.*, 2007d). To investigate the effect of both positively and negatively charged amino acid substitutions at these same positions in RNase 1 on ribonuclease internalization and RI evasion, a series of RNase 1 variants were constructed (Table 5.1). To maintain a basal level of RI evasion and cytotoxicity, these RNase 1 variants maintained an aspartate or leucine substitution at positions 39 and 91, as these residues contributed most to the evasion of RI (Johnson *et al.*, 2007d). Then, the net charge of the RNase 1 variant was

varied by incorporating positively or negatively charged residues at positions 67, 88, or 89, which are known to contribute less to the stability of the RI·RNase 1 complex (Johnson *et al.*, 2007d). These substitutions neither create nor destroy a canonical nuclear localization signal, which could contribute to cytotoxicity (Bosch *et al.*, 2004). The resulting RNase 1 variants had a net charge (Z) ranging from 0 to +6.

5.4.2 Biochemical properties of RNase 1 variants

The cytotoxicity of a ribonuclease is governed by the biochemical parameters listed in Table 5.1 (Bretscher *et al.*, 2000; Dickson *et al.*, 2003; Klink and Raines, 2000): conformational stability, ribonucleolytic activity, RI affinity, and molecular charge of the RNase 1 variants. The conformational stability of a ribonuclease, which provides a measure of its vulnerability to proteolysis, correlates with its cytotoxic activity (Klink and Raines, 2000). Conformational stability could not, however, have had a significant effect on the cytotoxicity of the RNase 1 variants, as each T_m value is within 8 °C of that of wild-type RNase 1 and significantly above physiological temperature (37 °C). Like conformational stability, ribonucleolytic activity correlates with cytotoxicity (Kim *et al.*, 1995a; Bretscher *et al.*, 2000). Here, however, each of the RNase 1 variants cleaved an RNA substrate with a k_{cat}/K_M value that was within 3-fold of that of the wild-type enzyme (Kelemen *et al.*, 1999).

The biochemical attribute that varied most dramatically between the different RNase 1 variants was the affinity for RI (Table 5.1), which is known to be an important factor in cytotoxicity (Leland *et al.*, 1998; Bretscher *et al.*, 2000; Haigis *et al.*, 2002;

Rutkoski *et al.*, 2005). Consequently, the 1500-fold range of affinities for RI, between the most RI-evasive variant (DDADD RNase 1; K_d = 1.7 μM) and the least RI-evasive variant (LRRRD RNase 1; K_d = 1.1 nM), foreshadows a large range of cytotoxic activity.

5.4.3 Ribonuclease cytotoxicity

Surprisingly, the RNase 1 variants varied little in their cytotoxic activity (Fig. 5.2; Table 5.1). None of the RNase 1 variants was as cytotoxic as D38R/R39D/N67R/G88R RNase A. This variant of the bovine enzyme is both highly evasive of RI (K_d = 510 nM) and highly cationic, having a net molecular charge (*i.e.*, Arg + Lys – Asp – Glu) of Z = +6 (Rutkoski *et al.*, 2005).

5.4.4 Ribonuclease internalization

To determine whether the molecular charge of an RNase 1 variant affects its cellular internalization, we employed a synthetic latent fluorophore (Fig. 5.1B) (Lavis *et al.*, 2006a; Chandran *et al.*, 2005). This latent fluorophore is not fluorescent until activated by an intracellular esterase, allowing for the direct and continuous visualization of protein internalization (Fig. 5.1C,D). RNase 1, like RNase A, has eight cysteine residues that form four disulfide bonds in the native enzyme. To enable the attachment of the latent fluorophore, we replaced Pro19 of each RNase 1 variant with a cysteine residue. Position 19 was chosen because it is remote from the regions of interest (Fig. 5.1A), and attachment of fluorescent groups at this position is not known to have a detectable effect on the ribonucleolytic activity, RI-affinity, or cell-surface binding of

ribonuclease variants (Haigis and Raines, 2003; Abel *et al.*, 2002). The latent fluorophore was attached to Cys19 of each ribonuclease by a standard maleimide coupling reaction (Lavis *et al.*, 2006a).

The internalization of latent fluorophore-conjugated ribonuclease variants was observed by fluorescence microscopy and quantitated by flow cytometry. Initial experiments revealed that the amount of ribonuclease internalized into live human cells increased linearly during the first 2 h (Fig. 5.3A) and accumulated in endocytic vesicles (Fig. 5.3B). Bright-field images indicated that the cells were alive and appeared to have normal physiology during the time course of the experiments (Fig. 5.1D).

Detailed experiments were then performed to quantify the internalization of a ribonuclease as a function of time (Fig. 5.4A), its net charge (Fig. 5.4B), and its concentration (Fig. 5.4C). Using eq 5.4 and the data in Fig. 5.4A, the values of $t_{1/2}$ (= $\ln 2/k_I$) for the internalization of the RNase 1 variants were calculated to be (110 ± 17) min for RNase 1, (131 ± 16) min for DRRDD RNase 1, and (129 ± 26) min for DDADD RNase 1. These $t_{1/2}$ values are indistinguishable, suggesting that each variant is endocytosed by the same mechanism.

The amount of ribonuclease internalized into K-562 cells in 30 min was related linearly to the net charge of the ribonuclease (Fig. 5.4B). The relative amount of ribonuclease internalized at 30 min also increased by greater than 4-fold between the RNase 1 variants with the lowest and highest net charge (DDADD ($Z = 0$) and LRRRD ($Z = +6$), respectively). Two variants of RNase 1 (DRRRD and LRRRD, with the G89R

substitution underlined) were internalized to a somewhat greater extent than expected based on their net charge. These two variants are the only ones with a G89R substitution.

The amount of ribonuclease internalized into K-562 cells in 30 min increased with the solution concentration of the ribonuclease, at least up to 10 μM (Fig. 5.4C). These data suggest that the binding of RNase 1 to the cell surface is not saturable (Haigis and Raines, 2003), consistent with internalization being mediated by a non-specific interaction with an abundant cell-surface molecule rather than by a specific interaction with a receptor. Again, internalization correlated with net charge, as more wild-type RNase 1 ($Z = +6$) than its DRRDD ($Z = +3$) or DDADD ($Z = 0$) variant was internalized at each concentration.

5.5 Discussion

Coulombic forces can lead to the unregulated internalization of cationic peptides and proteins into cells (Conner and Schmid, 2003; Cho and Stahelin, 2005; Mulgrew-Nesbitt *et al.*, 2006; Murray and Honig, 2002; Polo and Di Fiore, 2006). To assess the biological consequences of increasing the charge of a ribonuclease, we created RNase 1 variants with a range of net charges (Table 5.1). We then quantitated their cellular internalization by using a latent fluorophore (Fig. 5.1B) and flow cytometry. This combination obviated any signal from ribonucleases bound to the cell membrane (Fig. 5.1C) without the need for protease treatment or washing steps (Richard *et al.*,

2005; Lavis *et al.*, 2006a), permitting more timely and precise measurements than are accessible with any other method.

The net charge of a ribonuclease has a positive linear relationship with its internalization (Fig. 5.4B). The two variants with the highest internalization based on their net charge have an arginine residue at position 89 (DRRRD and LRRRD). Installing arginine in the analogous site of RNase A yielded G88R RNase A, which was the first monomeric mammalian ribonuclease endowed with cytotoxicity (Leland *et al.*, 1998). This cytotoxicity was attributed to a 10^4-fold decrease in affinity for RI (Leland *et al.*, 1998). Our analyses of the G89R variants of RNase 1 suggest, however, that this substitution in RNase A could instill the added benefit of increasing cellular internalization. Our data also indicate that a positive net charge is *not* essential for ribonuclease internalization, as a neutral RNase 1 variant (DDADD) is internalized significantly and is cytotoxic (Fig. 5.2 and 5.4; Table 5.1). Instead, the disposition of charge could govern the internalization of ribonucleases (Notomista *et al.*, 2006) and other proteins (Fuchs and Raines, 2007).

The opposite trend is observed between charge and the affinity for RI, which is highly anionic ($Z = -22$). In Fig. 5.4D, the net charge of RNase 1 variants substituted at positions 39, 67, 88, 89, and 91 is plotted *versus* the K_d value for their complex with RI. An inverse relationship between the net charge of an RNase 1 variant and its affinity for RI is observed, reinforcing the unusual nature of the RI–RNase 1 interaction and the importance of Coulombic forces to RI·RNase 1 complex formation (Johnson *et al.*, 2007d).

Hence, two competing equilibria involving ribonuclease charge seem to imperil and protect cells from the cytotoxic activity of rogue ribonucleases (Haigis and Raines, 2003). In these equilibria, increasing the positive charge of a ribonuclease increases its internalization but also increases its RI affinity (Fig. 5.4), yielding RNase 1 variants with similar cytotoxic activity (Fig. 5.2; Table 5.1). These competing equilibria make net charge a difficult variable to optimize in the design of cytotoxic ribonucleases.

The internalization of a ribonuclease seems to limit its cytotoxicity, as microinjected ribonucleases are cytotoxic at picomolar concentrations (Saxena *et al.*, 1991). Thus, fully understanding the factors involved in ribonuclease internalization could lead to more effective ribonuclease chemotherapeutics (Haigis and Raines, 2003). The cationicity of RI-evasive ribonucleases correlates with their cytotoxicity (Ilinskaya *et al.*, 2002; Ilinskaya *et al.*, 2004; Futami *et al.*, 2001; Futami *et al.*, 2002) and destabilization of anionic membranes (Notomista *et al.*, 2006). The endocytic mechanism is dynamin-independent (Haigis and Raines, 2003), but the remaining steps in the pathway are unknown.

Further insight into the mechanism of ribonuclease internalization can be gathered by comparing its kinetic mechanism to that of CPPs. CPP internalization reaches a steady-state level, like that of ribonucleases (Fig. 5.4A) (Hallbrink *et al.*, 2001; Drin *et al.*, 2003). The half-time for the internalization of a CPP ($t_{1/2} \leq 60$ min (Zorko and Langel, 2005; Drin *et al.*, 2003)) is, however, less than that for the internalization of an RNase 1 variant ($t_{1/2} = 2$ h, Fig. 5.4A). This difference in rate constant likely arises from the difference in molecular mass, as CPPs carrying large cargo internalize more slowly

(Zorko and Langel, 2005). As with ribonucleases (Fig. 5.4C), CPP internalization is dose-dependent (Drin *et al.*, 2003). These similarities are consistent with ribonucleases and CPPs having similar internalization mechanisms.

The steady-state kinetics of CPP internalization have been interpreted in terms of an equilibrium formed between CPP free in solution and CPP bound to anionic cell-surface molecules, concomitant with the degradation of the CPP (Zorko and Langel, 2005; Drin *et al.*, 2003; Hallbrink *et al.*, 2001). Based on the similarities between CPPs and ribonucleases, the same explanation seems to be applicable for ribonucleases: an extracellular pre-equilibrium is formed between ribonuclease free in solution and bound to the cell surface. Further evidence for the existence of such a prior equilibrium is provided by the charge dependence of internalization. All three ribonucleases tested had a similar half-time for internalization (2 h), indicative of the same mechanism of internalization. Yet, their steady-state level of internalization varied by up to 4-fold based on their net charge (Fig. 5.4A). Thus, ribonucleases that are more cationic have higher affinities for anionic cell-surface molecules, shifting the extracellular distribution toward the cell-surface bound state. This shift in distribution leads to more ribonucleases being internalized in the rate-limiting step (k_I), but without affecting the internalization rate of any individual molecule.

Based on these data, we propose a model for the effect of ribonuclease charge on internalization and cytotoxicity (Fig. 5.5). First, ribonucleases form an extracellular equilibrium with an anionic cell-surface molecule that is mediated by the cationicity of the ribonuclease. A candidate for this cell-surface molecule is heparan sulfate, which is

an abundant glycosaminoglycan necessary for the efficient internalization of ribonucleases (Soncin *et al.*, 1997) and CPPs (Fuchs and Raines, 2004), as well as a cationic variant of the green fluorescent protein (Fuchs and Raines, 2007). Second, an intracellular equilibrium based on ribonuclease charge is formed upon ribonuclease translocation to the cytosol (Fig. 5.5). This second equilibrium between ribonucleases bound by RI and those that evade RI is apparent by the opposing trends depicted in Fig. 5.4B,D. In these figures, ribonucleases that are internalized at a higher rate (Fig. 5.4B) are not necessarily more cytotoxic (Fig. 5.4) because they are also bound more tightly by RI (Fig. 5.4D).

Finally, the Coulombic interactions characterized herein could have clinical significance. Cells derived from cancerous tissue tend to be more anionic than cells derived from similar normal tissue (Slivinsky *et al.*, 1997; Orntoft and Vestergaard, 1999). In contrast, RI levels are constant in cells with a cancerous and noncancerous origin (Haigis *et al.*, 2003). Accordingly, variation in the position of the extracellular equilibrium (Fig. 5.5) could contribute to the therapeutic index of ONC and other ribonucleases.

Understanding how cationic proteins enter human cells and exerting control over this process portends the development of better chemotherapeutics. Toward this end, we developed a method to quantitate the effect of the net charge of a ribonuclease on its cellular internalization. We found ribonuclease internalization to be related linearly to net charge and to reach a steady-state level of internalization based on that net charge. These two characteristics suggest that ribonuclease internalization is controlled by an

extracellular equilibrium formed between ribonuclease molecules free in solution and those bound to anionic moieties on the cell surface. This extracellular equilibrium is then counteracted by an intracellular equilibrium in which more cationic ribonucleases bind more tightly to RI. Thus, these two equilibria cause cells to entice and then entrap ribonucleases.

Acknowledgements. We are grateful to W.W. Cleland, T.J. Rutkoski, S.M. Fuchs, and R.F. Turcotte for contributive discussions.

Table 5.1 Properties of wild-type RNase 1 and its variants

RNase 1 [2]	T_m (°C)[a]	k_{cat}/K_M[b] (10^6 $M^{-1}s^{-1}$)	K_d (nM)[c]	IC_{50} (μM)[d]	Z
wild type[e]	57	21 ± 2	29×10^{-8} [e]	>25	+6
DDADD[e]	58	6.3 ± 0.5	$(1.7 \pm 0.5) \times 10^3$	13.3 ± 1.7	0
LLALL[e]	65	30 ± 3	30 ± 1	>25	+4
DRRDD	53	14 ± 3	28 ± 4	5.69 ± 0.37	+3
DRRRD	49	6.7 ± 0.6	1.3 ± 0.2	10.8 ± 0.93	+5
LRRDD	54	19 ± 2	1.8 ± 0.1	16.2 ± 1.3	+4
LRRRD	53	9.1 ± 2	1.1 ± 0.2	>25	+6

[a] Values of T_m (±2 °C) were determined in PBS by UV spectroscopy.

[b] Values of k_{cat}/K_M (±SE) were determined for catalysis of 6-FAM–dArU$(dA)_2$–6- TAMRA cleavage at 25 °C in 0.10 M MES–NaOH buffer (OVS-free), pH 6.0, containing 0.10 M NaCl and were calculated with eq 5.1.

[c] Values of K_d (±SE) were determined for the complex with human RI (eq 5.2) at 25 °C.

[d] Values of IC_{50} (±SE) are for incorporation of [*methyl*-^{3}H]thymidine into the DNA of K-562 cells treated with the ribonuclease, and were calculated with eq 5.3.

[e] From ref. (Johnson *et al.*, 2007d)

Figure 5.1 Design of ribonuclease variants and latent fluorophore. (A) Ribbon diagram of RNase 1 (PDB entry 1Z7X, chain Z (Johnson *et al.*, 2007d)). Residues substituted herein are depicted in red. The image was created with the program PyMOL (DeLano Scientific, South San Francisco, CA). (B) Structure of latent fluorophore before and after activation by cellular esterases. (C,D) Confocal microscopy images of unwashed K-562 cells incubated at 37 °C for 30 min with fluorescein-labeled RNase 1 (10 μM; C) or latent fluorophore-labeled RNase 1 (10 μM; D). Nuclei were stained by adding Hoechst 33342 (2 μg/mL) during the final 5 min of incubation. Insets: bright-field images. Scale bar: 10 μm.

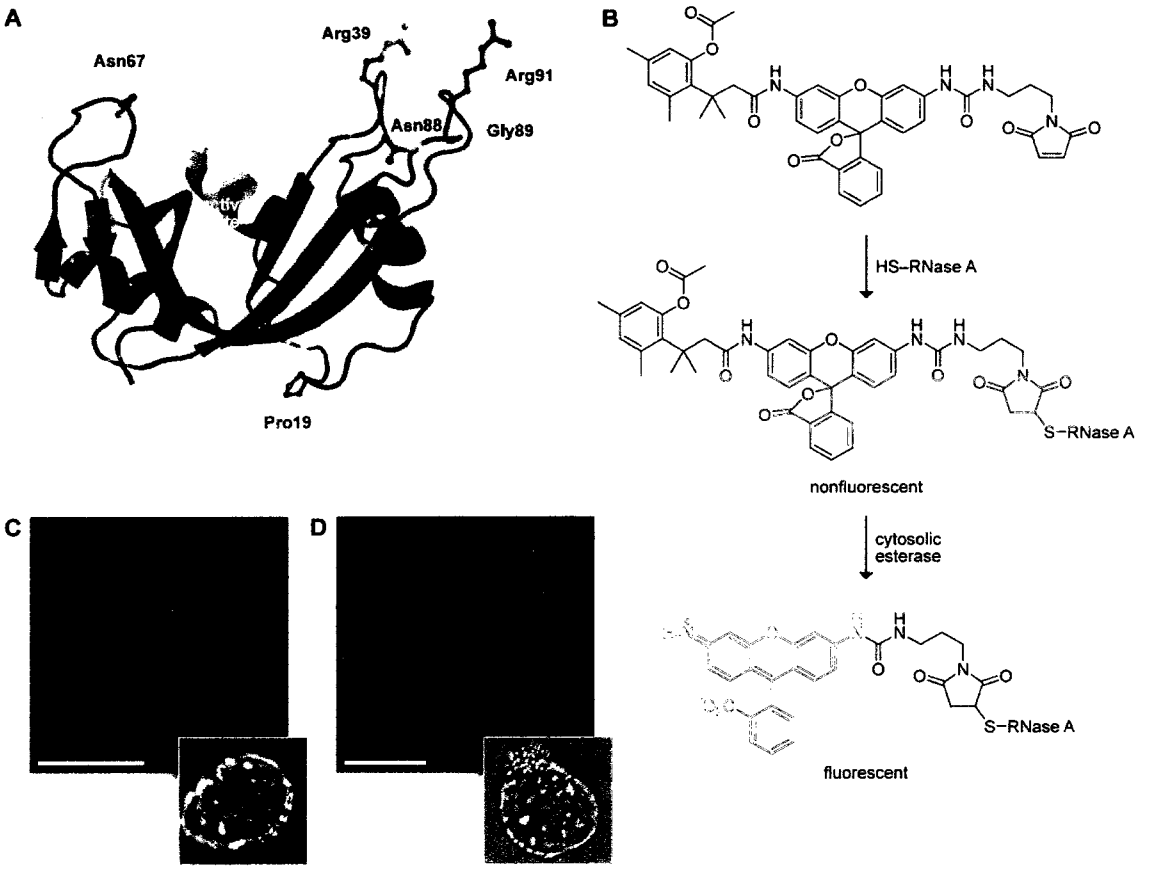
A
Asn67
Arg39
Arg91
Asn88
Gly89
Pro19
B
HS–RNase A
S–RNase A
nonfluorescent
cytosolic
esterase
S–RNase A
fluorescent
C
D

Figure 5.2 Cytotoxicity of ribonuclease variants.

Effect of ribonucleases on the proliferation of K-562 cells was determined by monitoring the incorporation of [*methyl*-^{3}H]thymidine into cellular DNA in the presence of ribonucleases. Data points are mean values (±SE) from ≥3 experiments, each carried out in triplicate, and were fitted to eq 5.3. Variants in order of increasing cytotoxicity: D38R/R39D/N67R/G88R RNase A (◇); DRRDD RNase 1 (♦); DRRRD RNase 1 (▼); DDADD RNase 1 (●); LRRDD RNase 1 (▲); LRRRD RNase 1 (■); and wild-type RNase 1 (○).

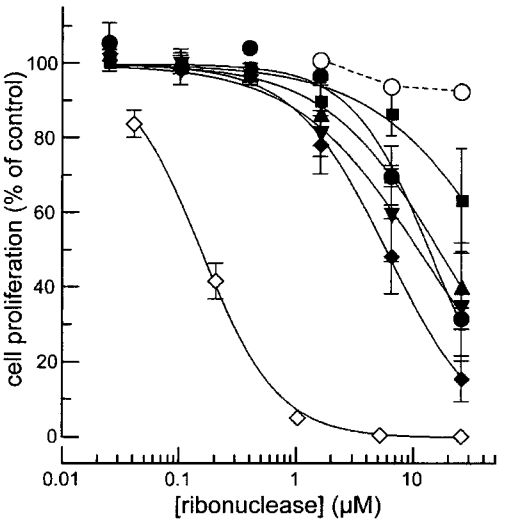
cell proliferation (% of control)
100
80
60
40
20
0
0.01
0.1
1
10
[ribonuclease] (μM)

Figure 5.3 Kinetics of ribonuclease internalization.

(A) Initial velocity of cellular internalization versus time (≤2 h). Internalization was determined by incubating latent fluorophore-labeled RNase 1 (○) with K-562 cells at 37 °C. Incubations were quenched at known times by immersing the K-562 cells in ice-cold PBS and storing them on ice before quantitation by flow cytometry. Data points are mean values (±SE) from ≥3 cell populations. (B) Confocal microscopy images of unwashed K-562 cells incubated at 37 °C for varying time periods (0–6 h) with latent fluorophore-labeled RNase 1 (10 μM). Nuclei were stained by adding Hoechst 33342 (2 μg/mL) during the final 5 min of incubation. Scale bar: 10 μm.

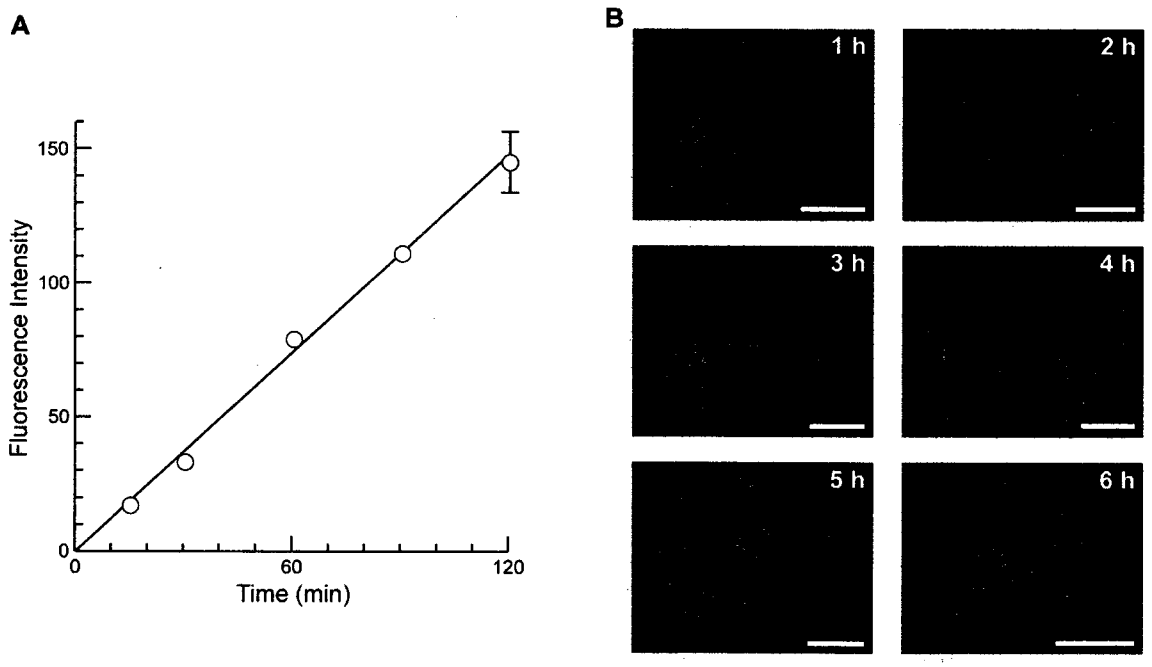
A
Fluorescence Intensity
150
100
50
0
0
60
120
Time (min)
B
1 h
2 h
3 h
4 h
5 h
6 h

Figure 5.4 Properties of RNase 1, its variants, and RNase A. Wild-type RNase 1 (○), DDADD RNase 1 (●), DRRDD RNase 1 (♦), LRRDD RNase 1 (▲), LLALL RNase 1 (□), DRRRD RNase 1 (▼), LRRRD RNase 1 (■), and wild-type RNase A (◇). (A) Plot of internalization of a ribonuclease into K-562 cells *versus* time. Internalization was measured by using flow cytometry and following the fluorescence manifested by activation of a latent fluorophore attached to the ribonuclease (10 μM) after incubation for the specified times points. Data points are mean values (±SE) for 20,000 cells from ≥3 cell populations, and were fitted to eq 5.4. (B) Plot of internalization of a ribonuclease into K-562 cells *versus* its net charge. Internalization was monitored as in panel A, except that all incubations were for 30 min at 37 °C. (C) Plot of internalization of a ribonuclease into K-562 cells *versus* its concentration. Internalization was followed as in panel A, except for the variable concentration of ribonuclease (0.1, 1.0, or 10 μM). (D) Semilog plot of affinity of a ribonuclease for RI *versus* its net charge. Data points are mean values (±SE). Variants of RNase 1 from ref (Johnson *et al.*, 2007d) are indicated by their amino acids at positions 39, 67, 88, 89, and 91, with "–" indicating the wild-type residue.

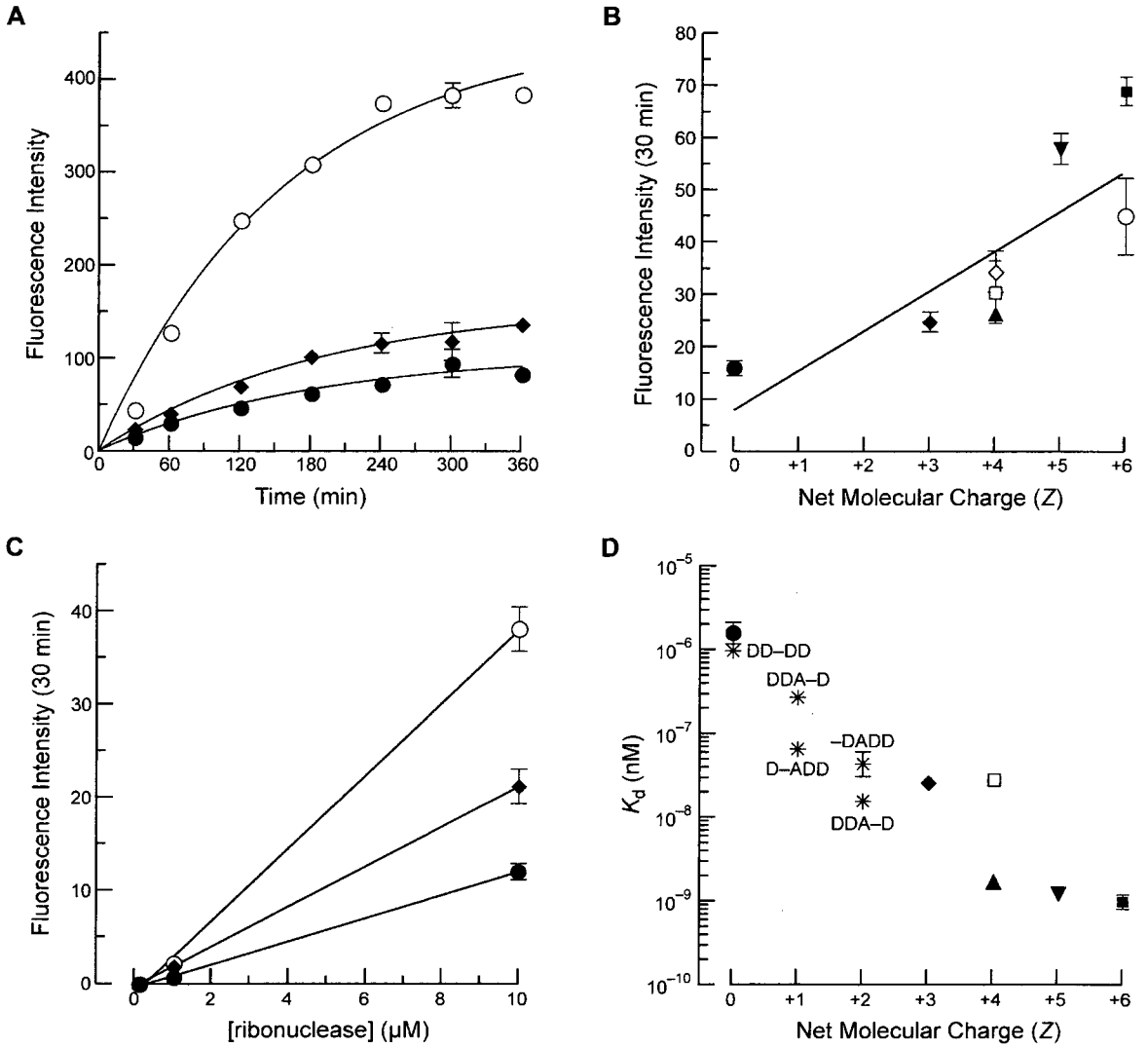
A
Fluorescence Intensity
Time (min)
B
Fluorescence Intensity (30 min)
Net Molecular Charge (Z)
C
Fluorescence Intensity (30 min)
[ribonuclease] (μM)
D
K_d (nM)
DD–DD
DDA–D
D–ADD
–DADD
DDA–D
Net Molecular Charge (Z)

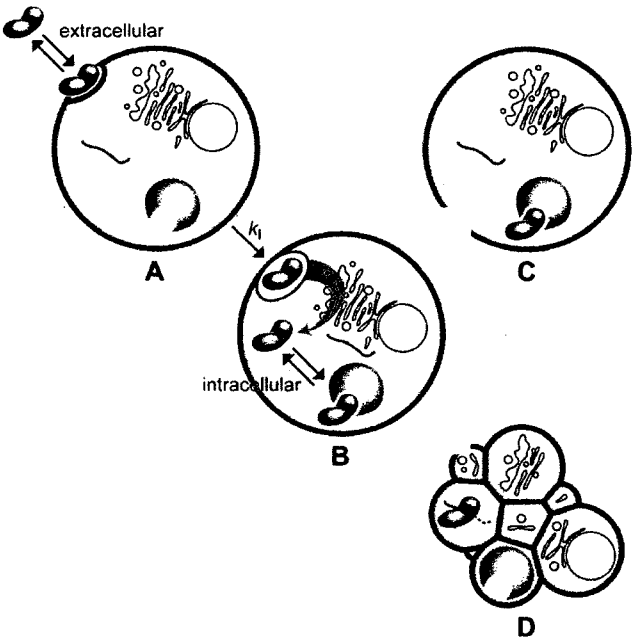

Figure 5.5 Coulombic effects on ribonuclease-mediated cytotoxicity.

Coulombic effects on ribonuclease-mediated cytotoxicity. Cationic and anionic molecules are depicted in blue and red, respectively. (A) Ribonucleases form an extracellular equilibrium complex with abundant anionic cell-surface molecules, such as heparan sulfate. Bound ribonucleases are internalized into endosomes with rate constant k_I. (B) Internalized ribonucleases translocate to the cytosol by an unknown mechanism. (C) In the cytosol, ribonucleases form an intracellular equilibrium complex with RI. (D) Ribonucleases that evade RI degrade cellular RNA, leading to apoptosis.

CHAPTER 6

Fluorogenic Label for Biomolecular Imaging

Contribution: Cellular studies and imaging. All other experiments were performed by L.D. Lavis.

This chapter was published as:
Lavis, L.D., Chao, T.-Y., and Raines, R.T. (2006) Fluorogenic label for biomolecular imaging. *ACS Chem. Biol.* **1**, 252–260.

6.1 Abstract

Traditional small-molecule fluorophores are always fluorescent. That attribute can obscure valuable information in biological experiments. Here, we report on a versatile "latent" fluorophore that overcomes this limitation. At the core of the latent fluorophore is a derivative of rhodamine in which one nitrogen is modified as a urea. That modification enables rhodamine to retain half of its fluorescence while facilitating conjugation to a target molecule. The other nitrogen of rhodamine is modified with a "trimethyl lock", which enables fluorescence to be unmasked fully by a single user-designated chemical reaction. An esterase-reactive latent fluorophore was synthesized in high yield and attached covalently to a cationic protein. The resulting conjugate was not fluorescent in the absence of esterases. The enzymatic activity of esterases in endocytic vesicles and the cytosol educed fluorescence, enabling the time-lapse imaging of endocytosis into live human cells and thus providing unprecedented spatiotemporal resolution of this process. The modular design of this "fluorogenic label" enables the facile synthesis of an ensemble of small-molecule probes for the illumination of numerous biochemical and cell biological processes.

6.2 Introduction

Fluorescent molecules are critical tools in the study of biochemical and cell biological processes (Haugland *et al.*, 2005). In many studies, however, only few of the fluorescent molecules experience a phenomenon of interest. Because traditional fluorophores, such as rhodamine and fluorescein, are always fluorescent, bulk fluorescence can obscure valuable information. To overcome this limitation, molecules can be designed such that a chemical reaction elicits a change in their fluorescence. Such "latent" fluorophores are at the core of common methods, including the enzyme linked immunosorbent assay (ELISA), high-throughput screening of enzyme inhibitors, detection of reporter genes, and evaluation of cell viability (Haugland *et al.*, 2005). We reasoned that the use of a latent fluorophore as a "fluorogenic label" could overcome limitations of traditional fluorescent labels and thereby improve the spatial and temporal resolution of bioimaging.

Recently, our laboratory reported on a new class of latent fluorophores based on the "trimethyl lock" (Chandran *et al.*, 2005; Lavis *et al.*, 2006b). The rapid lactonization (Milstein and Cohen, 1972; Borchardt and Cohen, 1972) of the trimethyl lock had been exploited previously to prepare stable pro-drugs that were unmasked by an enzyme-catalyzed reaction (Shan *et al.*, 1997; Testa and Mayer, 2003). We first used the trimethyl lock to shroud the fluorescence of a xanthene dye, rhodamine 110 (Rh_{110}) (Chandran *et al.*, 2005), and then an oxazine dye, cresyl violet (Lavis *et al.*, 2006b). This approach

afforded highly stable bis(trimethyl lock) "pro-fluorophores" that were labile to esterase catalysis *in vitro* and *in cellulo*.

Our bis(trimethyl lock) pro-fluorophores had two problematic attributes. First, two chemical reactions were necessary to unveil the vast majority of their fluorescence, decreasing the rate of fluorescence manifestation and limiting the linear range of assays (Fiering *et al.*, 1991; Urano *et al.*, 2005). Analogous fluorogenic protease substrates based on a rhodamine diamide display complex hydrolysis kinetics (Leytus *et al.*, 1983a; Leytus *et al.*, 1983b; Liu *et al.*, 1999), as we observed with our bis(trimethyl lock) pro-fluorophores (Chandran *et al.*, 2005; Lavis *et al.*, 2006b). The second problematic attribute was the absence of a handle for target-molecule conjugation. Such a handle is available in derivatives, such as 5- or 6-carboxyrhodamine, that are accessible only from low-yielding synthetic routes.

We suspected that we could solve both problems by capping one of the amino groups of Rh_{110}. The capping of rhodamine dyes with an amide (Zhang *et al.*, 2003; Guzikowski *et al.*, 2000; Lorey *et al.*, 2002), carbamate (Cai *et al.*, 2001), or urea (Wang *et al.*, 2005) can preserve much of their fluorescence. We were especially intrigued by the attributes of urea–rhodamine, which according to recent reports in the scientific (Wang *et al.*, 2005) and patent (Diwu *et al.*, 2003; Zhang *et al.*, 2000) literature appears to retain significant fluorescence intensity relative to Rh_{110}.

Here, we report on a versatile fluorogenic label for biomolecular imaging. First, we describe the synthesis of a complete set of ureated and amidated derivatives of Rh_{110}, as well as a characterization of their fluorescent properties. Then, we show that imposing

our trimethyl lock strategy upon a urea–rhodamine yields a stable latent fluorophore with a high rate of enzymatic hydrolysis. Finally, we demonstrate the power of our modular approach by using the urea moiety as a handle for protein conjugation and subsequent continuous imaging of endocytosis by live human cells.

6.3 Experimental Procedures

6.3.1 General spectroscopic methods

HEPES (2[4-(2-hydroxyethyl)-1-piperazinyl]ethanesulfonic acid) was from Research Products International. Fluorescein (reference standard grade) was from Molecular Probes. Other reagents were from Sigma–Aldrich or Fisher Scientific. Phosphate-buffered saline, pH 7.4 (PBS) contained (in 1.00 liter) KCl (0.20 g), KH_2PO_4 (0.20 g), NaCl (8.0 g), and $Na_2HPO_4 \cdot 7H_2O$ (2.16 g). All measurements were recorded at ambient temperature (23 ± 2 °C) and buffers were not degassed prior to measurements. Compounds were prepared as stock solutions in DMSO and diluted such that the DMSO concentration did not exceed 1% v/v. Porcine liver esterase (PLE, MW = 163 kDa (Horgan *et al.*, 1969)) was obtained from Sigma Chemical (product number E2884) as a suspension in 3.2 M $(NH_4)_2SO_4$, and was diluted to appropriate concentrations in PBS before use. In pH-dependency studies, the pH of PBS was adjusted by additions of 1.0 M HCl or 1.0 M NaOH and measured using a Beckmann glass electrode that was calibrated prior to each use. Graphs were manipulated and parameters were calculated with Microsoft Excel 2003 and GraphPad Prism 4.

6.3.2 *Ultraviolet–visible and fluorescence spectroscopy*

Absorption spectra were recorded in 1-cm path length cuvettes having a volume of 1.0 or 3.5 mL on a Cary Model 50 spectrometer from Varian. The extinction coefficients were measured in 10 mM HEPES–NaOH buffer, pH 7.5. Fluorometric measurements were made using fluorescence grade quartz or glass cuvettes from Starna Cells and a QuantaMaster1 photon-counting spectrofluorometer from Photon Technology International equipped with sample stirring. The quantum yields of Rh_{110} and compounds **6.1–6.5** were measured with dilute samples ($A \leq 0.1$) in 10 mM HEPES–NaOH buffer, pH 7.5. These values were obtained by the comparison of the integrated area of the emission spectrum of the samples with that of fluorescein in 0.1 M NaOH, which has a quantum efficiency of 0.95 (Lakowicz, 1999). The concentration of the fluorescein reference was adjusted to match the absorbance of the test sample at the excitation wavelength. Under these conditions, quantum yields were calculated by using eq 1.

$$\Phi_{sample} = \Phi_{standard}(\int F_{em,sample} / \int F_{em,standard}) \quad (6.1)$$

6.3.3 *Protein purification and labeling*

The TNB-protected A19C variant of RNase A and the Oregon Green-labeled RNase A conjugate were prepared as described previously (Haigis and Raines, 2003). The TNB-protected protein was deprotected with a three-fold molar excess of dithiothreitol (DTT) and desalted by chromatography using a HiTrap Desalting column (Amersham). The protein conjugate then was prepared by reaction with ten-fold molar

excess of thiol-reactive maleimide **6.13** for 16 h at 4 °C. Purification by chromatography using a HiTrap HP SP column (Amersham) afforded the desired conjugate (MS (MALDI): *m/z* 14,468 (expected: 14,475)). Protein concentration was determined by using a bicinchoninic acid (BCA) assay kit from Pierce with wild-type RNase A as a standard.

6.3.4 Cell preparation

HeLa cells were plated on Nunc Lab-Tek II 8-well Chamber Coverglass (Fisher Scientific) and grown to 70–80% confluence at 37 °C in DMEM (Invitrogen) containing FBS (10% v/v). For static imaging, cells were first washed with Dulbecco's phosphate-buffered saline (DPBS, Invitrogen). Cells were then incubated with pro-fluorophore **6.8** (10 μM), RNase A conjugated to maleimide **6.13** (10 μM), or Oregon Green-labeled RNase A (10 μM) for 1 h at 37 °C prior to imaging. Nuclear staining was accomplished by addition of Hoechst 33342 (2 μg/mL) for the final 5 min of incubation. Lysosomal staining involved washing the cells with DPBS followed by incubation with 100 nM LysoTracker Red (Molecular Probes) in DPBS for 1 min at ambient temperature. For dynamic imaging, cells were incubated with Hoechst 33342 (2 μg/mL) for 5 min at 37 °C, and then washed twice with DPBS. Pro-fluorophore **6.13**–RNase A conjugate (10 μM) was added to the cells at ambient temperature (23 ± 2 °C). Imaging of endocytosis started within 1 min after the addition of the conjugate.

6.3.5 Cell imaging

Cells were imaged on a Nikon Eclipse TE2000-U confocal microscope equipped with a Zeiss AxioCam digital camera, unless indicated otherwise. Excitation at 408 nm was provided by a blue-diode laser, and emission light was passed though a filter centered at 450 nm with a 35-nm band-pass. Excitation at 488 nm was provided by an argon-ion laser and emission light was passed through a filter centered at 515 nm with a 40-nm band-pass. Excitation at 543 nm was provided by a HeNe laser, and emission light was passed through a filter centered at 605 nm with a 75-nm band-pass. For time-lapse imaging, 1 image/min was recorded during the first 30 min of incubation, 2 images/min were recorded during the next 10 min, and 5 images/min were recorded during the last 50 min. The resulting movie condenses these 300 images recorded over 90 min into 40 s. Brightfield images indicated that the cells were alive and appeared to have normal physiology, both before and after the time-lapse imaging.

6.4 Results and Discussion

6.4.1 Synthesis of model compounds

To gain a comprehensive understanding of the urea and amide derivatives of rhodamine, we undertook the synthesis of compounds **6.1–6.5** (Table 6.1). Rhodamine itself and these five derivatives encompass the ensemble of possible ureated and amidated derivatives. We were especially interested in those properties of **6.1–6.5** with biological implications, such as the extinction coefficient and quantum yield in aqueous solution.

Previous reports (Ioffe and Otten, 1965a; Wang *et al.*, 2005; Diwu *et al.*, 2003; Zhang *et al.*, 2000; Leytus *et al.*, 1983b; Leytus *et al.*, 1983a) of similar derivatives did not provide a complete listing of relevant fluorescent characteristics.

Installation of the urea moiety to produce urea **6.1** proved to be surprisingly difficult. In our hands, the reported conditions (Wang *et al.*, 2005) involving the reaction of Rh_{110} with a carbamoyl chloride using Hünig's base gave an intractable mixture of products. In contrast, we found that Rh_{110} was deprotonated effectively with NaH, and that the resulting anion reacted with dimethylcarbamyl chloride to yield the desired urea **6.1**. This deprotonation strategy also proved useful for the synthesis of amide **6.2** and diurea **6.3**. The additional acetamide group in urea–amide **6.4** and diamide **6.5** were installed by reaction with acetyl chloride in the presence of a base.

6.4.2 Fluorescence properties

The absorbance and fluorescence spectra of Rh_{110} and each derivative are shown in Fig. 6.1. The corresponding values of λ_{max}, extinction coefficient at λ_{max} (ε), λ_{em}, and quantum yield (Φ) are listed in Table 6.1. We determined the relative fluorescence intensity of these compounds by calculating the product of extinction coefficient and quantum yield and then normalizing these values to those of Rh_{110}. In our measurement, urea **6.1** retained 35% of the fluorescence intensity of Rh_{110} with a quantum yield value of 0.49. Amide **6.2** is only 12% as fluorescent as Rh_{110}, which is consistent with earlier reports (Leytus *et al.*, 1983a; Leytus *et al.*, 1983b). The fluorescence of the bis-substituted dyes was largely quenched in aqueous solution. Diurea **6.3** did, however,

possess significant absorbance and fluorescence compared to the urea–amide **6.4** or diamide **6.5**. These latter two rhodamine derivatives are essentially nonfluorescent.

We also determined the pH-dependence of the fluorescence of urea **6.1** and amide **6.2**. The fluorescence of Rh_{110} is relatively insensitive to pH values between 4 and 10 (Haugland *et al.*, 2005). This property is beneficial in biological assays, where unknown variations in pH can hamper quantitative measurements. Like Rh_{110}, urea **6.1** and amide **6.2** show no significant spectral change between pH values of 4 and 10.

Substituent effects on the fluorescent properties of rhodamine dyes are challenging to predict or interpret due to the complexity of the rhodamine system (López Arbeloa *et al.*, 1991). In solution, rhodamine derivatives exist in equilibrium between a zwitterion that absorbs visible light and is fluorescent and a lactone that is colorless and nonfluorescent. Substitution on nitrogen can affect both this open–closed equilibrium and the spectral characteristics of the fluorescent zwitterions (Ioffe and Otten, 1965b; López Arbeloa *et al.*, 1989). We suspected that the differences in optical properties seen in compounds **6.1–6.5** could be rationalized, in part, through examination of the electron-donation capability of the different nitrogen substituents. According to this reasoning, weakly donating substituents would favor the colorless lactone as well as decrease the intrinsic absorptivity of the zwitterions and, hence, the extinction coefficient. Weakly donating substituents could also reduce the quantum yield by decreasing the C–N bond-order and thereby enhancing nonradiative decay of the excited state through vibrational relaxation processes (López Arbeloa *et al.*, 1992; Vogel *et al.*, 1988).

We explored the relationship between the values of extinction coefficient and quantum yield and the Hammett σ_p substituent constants (Hansch *et al.*, 1991). An unprotonated amino group is a good electron donor ($\sigma_p = -0.66$), whereas an amide group is a relatively poor donor ($\sigma_p = 0.00$), due to amidic resonance. A urea group is peculiar—its carbonyl group is cross-conjugated and both of its nitrogens participate in amidic resonance. This cross-conjugation attenuates its electron-donating ability, as reflected in an intermediate Hammett constant ($\sigma_p = -0.26$). A plot of both extinction coefficient and quantum yield versus σ_p substituent constant for Rh_{110} and monosubstituted rhodamines **6.1** and **6.2** are shown in Fig. 6.2. The correlation indicates that both spectral properties are affected by electron donation from the nitrogens. A similar trend in quantum yields has been observed in substituted phenoxazinone dyes (Descalzo *et al.*, 2005).

The moderate electron-donating character of the urea moiety provides an explanation for the advantageous properties of urea **6.1**. Substitution with the cross-conjugated urea suppresses the fluorescence intensity of urea **6.1** relative to Rh_{110}. This decrease is not, however, as severe as seen in amide **6.2**, due to the greater electron-donating properties of the urea moiety. Still, the attenuated electron-donation allows complete suppression of fluorescence upon amidation of the remaining nitrogen in urea–amide **6.4**. Finally, the effect of electron-rich substituents on the rhodamine system are apparent again in the fluorescence of diurea **6.3** being greater than that of diamide **6.5**.

6.4.3 Synthesis of urea–rhodamine trimethyl lock

Having affirmed the desirable properties of urea–rhodamine, we next sought to apply our trimethyl lock strategy to this dye. The synthetic route to the fluorogenic substrate, which employs rhodamine morpholino-urea **6.6** (Wang *et al.*, 2005), is shown in Scheme 1. Again, we found that the use of Hünig's base in the synthesis afforded a mixture of products. Deprotonation of Rh_{110} with NaH followed by dropwise addition of 4-morpholinecarbonyl chloride furnished rhodamine morpholino-urea **6.6**. This compound exhibited similar fluorescent characteristics to urea **6.1** (Table 6.1), having an extinction coefficient of 51,700 $M^{-1}cm^{-1}$ and quantum yield of 0.44. Carbodiimide coupling of rhodamine morpholino-urea **6.6** with acid **6.7** (Amsberry *et al.*, 1991) afforded the desired pro-fluorophore **6.8**.

6.4.4 Chemical stability

Pro-fluorophore **6.8** must be stable in aqueous solution to be useful in biological assays. Such stability can be problematic for hydrolase substrates, as spontaneous hydrolysis can compete effectively with enzymatic activity and raise background levels. As shown in Fig. 6.3, pro-fluorophore **6.8** showed remarkable stability in both phosphate-buffered saline (PBS) and Dulbecco's modified Eagle's medium (DMEM) supplemented with 10% v/v fetal bovine serum (FBS). In contrast, fluorescein diacetate, which is a widely used esterase substrate (Rotman and Papermaster, 1966), suffered relatively rapid hydrolysis in both solutions. This dramatic increase in stability arises from the large difference in pK_a values between the conjugate acids of the two leaving groups.

Specifically, fluorescein (pK_a 6.32 (Goldberg and Baldwin, 1998)) is a much better leaving group than is the electron-rich trimethyl-lock phenol (*o*-methylphenol has pK_a 10.28 (Fickling *et al.*, 1959)).

6.4.5 Enzymatic reactivity

An objective in the design of pro-fluorophore **6.8** was to improve its reactivity as an esterase substrate relative to the original bis(trimethyl lock) rhodamine substrate. The appearance of fluorescence upon reaction of porcine liver esterase (PLE) with pro-fluorophore **6.8** was indicative of single-hit kinetics (Fig. 6.4). The kinetic constants were calculated to be $k_{cat}/K_M = 8.2 \times 10^5$ $M^{-1}s^{-1}$ and $K_M = 0.10$ μM. Comparison with the apparent kinetic constants from the original bis(trimethyl lock) rhodamine substrate (Chandran *et al.*, 2005) ($k_{cat}/K_M = 1.9 \times 10^3$ $M^{-1}s^{-1}$ and $K_M = 0.47$ μM) shows a 430-fold increase in k_{cat}/K_M value. A more appropriate comparison takes into account the expected 65% decrease in fluorescence of urea **6.8** (Table 6.1), which is the hydrolysis product of pro-fluorophore **6.8**, relative to Rh_{110}. After this adjustment, latent fluorophore performance is still enhanced by 150-fold.

The substantial increase in catalytic efficiency is likely due to the change from the double-hit kinetics observed for the bis-substituted substrate to the single-hit kinetics of pro-fluorophore **6.8**. Hydrolysis of the bis-substituted fluorogenic substrate progresses from diamide to free Rh_{110} via a monoamide intermediate, with the unmasking of the second amino group producing the majority (~90%) of the fluorescence (Leytus *et al.*,

1983b; Leytus *et al.*, 1983a). In contrast, the urea–rhodamine substrate requires only a single cleavage event for the complete manifestation of fluorescence.

6.4.6 Cellular imaging

Having established the high chemical stability and enzymatic reactivity of pro-fluorophore **6.8**, we next evaluated the behavior of this compound in live human cells. Pro-fluorophore **6.8** was incubated with HeLa cells and imaged using confocal fluorescence microscopy. As shown in Fig. 6.5A, the substrate was activated *in cellulo* by endogenous esterases to produce diffuse green cytosolic staining. Importantly, the high chemical stability of the fluorogenic probe allowed for its imaging in the cytosol without an intermediate washing step. Counter-staining with LysoTracker Red showed significant but incomplete colocalization, suggesting that after hydrolysis, a portion of the free urea–rhodamine localized in acidic vesicles (yellow color in Fig. 6.5B). To ensure that the fluorescence increase was due to trimethyl lock activation and not hydrolysis of the urea moiety, we incubated HeLa cells with the relatively non-fluorescent diurea-rhodamine **6.5**. In these experiments we observed virtually no intracellular fluorescence (Fig. 6.6).

6.4.7 Fluorogenic label

The high chemical stability and rapid *in cellulo* unmasking of pro-fluorophore **6.8** prompted us to develop a derivative for bioconjugation. We reasoned that such a fluorogenic label would be stable enough to survive conjugation and purification protocols while still providing a strong signal for continuous biological experiments. It is

noteworthy that simple fluorescein diesters have found only limited use as fluorogenic labels (Laurent *et al.*, 1997; Bergsdorf *et al.*, 2003; Drobni *et al.*, 2003; Kamal *et al.*, 2004), as fluorescein diesters suffer from low chemical stability in aqueous solution (Fig. 6.3).

Developing pro-fluorophore **6.8** into a fluorogenic label requires the installation of a functional group with selective reactivity. We chose to install the maleimide functionality (Ji, 1983; Aslam and Dent, 1998), which react rapidly with thiol groups (Bednar, 1990). The resulting conjugates are stable (Yoshitake *et al.*, 1979), even after the slow hydrolysis of the nascent sulfosuccinimidyl ring (Ishii and Lehrer, 1986).

Traditionally, reactive groups are attached to the pendant carboxyphenyl ring of rhodamine and fluorescein dyes (Haugland *et al.*, 2005). Synthesis of these compounds requires difficult chromatographic steps to obtain isomerically pure compounds (Jiao *et al.*, 2003). We envisioned a facile and economical alternative involving the attachment of a maleimide derivative via the desirable urea functionality. Although uncommon, bioconjugation via the amino groups of rhodamines has been used previously (Corrie *et al.*, 1998; Meunier and Wilkinson, 2002; Lorey *et al.*, 2002). This strategy allows for the use of commercially available (and relatively inexpensive) Rh_{110} as the starting material for the synthesis of maleimidourea–rhodamine trimethyl lock **6.13**, as shown in Scheme 2. Desymmetrization of Rh_{110} was accomplished by its deprotonation with NaH and reaction with Boc_2O to give *t*-Boc–rhodamine **6.9**. An isocyanate was generated *in situ* from maleimide **6.10** by a Curtius rearrangement (Curtius, 1894; Curtius, 1890), and that isocyanate was reacted with *t*-Boc–rhodamine **6.9** to generate a urea (Scriven and

Turnbull, 1988; Bräse *et al.*, 2005). Deprotection of maleimidourea–rhodamine–*t*-Boc **6.11** with TFA afforded fluorescent urea–rhodamine **6.12**. Condensation with **6.7** using EDC gave thiol-reactive fluorogenic label **6.13**.

6.4.8 Bioconjugation

To test the utility of fluorogenic label **6.13** in a biological experiment, we attached it to a thiol-containing variant of bovine pancreatic ribonuclease (RNase A) (Raines, 1998). RNase A is a cationic protein that is internalized by mammalian cells via endocytosis (Haigis and Raines, 2003). This internalization is critical to the action of cytotoxic RNase A variants and homologs (Haigis *et al.*, 2003). Fluorogenic label **6.13** reacted cleanly with the A19C variant of RNase A to give a mono-substituted conjugate as determined by MALDI mass spectrometry. This protein conjugate was stable to purification by cation-exchange chromatography at pH 5.0 and showed a 1200-fold increase in fluorescence upon incubation with PLE (data not shown).

At physiological pH, the protein conjugate was less stable than unconjugated pro-fluorophore **6.8**. Spontaneous hydrolysis of the acetate ester was slow but significant in PBS, presumably because conjugation to the protein places the probe in close proximity to nucleophilic functional groups of the protein. Storage at pH 5.0 did, however, extend the stability of the conjugate, allowing multiple experiments to be performed with one preparation.

6.4.9 Cellular imaging with a bioconjugate

Fluorescently labeled biomolecules have been used to image endocytotic events (Watson *et al.*, 2005). We sought to determine the efficacy of our fluorogenic label approach by comparing endocytosis of HeLa cells incubated with Oregon Green-labeled RNase A (Haigis and Raines, 2003) to that of cells incubated with the protein conjugated with fluorogenic label **6.13**. As shown in Fig. 6.7A, the Oregon Green conjugate showed intense extracellular background signal that obscures the fluorescence from endocytosed material. This background could be eliminated only with many vigorous washing steps (Fig. 6.7B). In contrast, the pro-fluorophore conjugate allowed imaging without intermediate washing steps. As shown in Fig. 6.7C, unwashed HeLa cells incubated with the RNase A conjugate have bright, punctate staining, indicative of the conjugate being localized in small vesicles. Counterstaining with LysoTracker Red shows a large degree of colocalization (Fig. 6.7D), suggesting that the latent conjugate is internalized via endocytosis and activated by endosomal or lysosomal esterases (Leinweber, 1987; Runquist and Havel, 1991; Hornick *et al.*, 1992). Images with the protein conjugate (Fig. 6.7C) are less diffuse and more punctate that are images with free pro-fluorophore **6.8** (Fig. 6.5), which has much more ready access to the cytosol. To ensure that the signal in Fig. 6.7C is due to unmasked fluorophore attached to RNase A, we fixed cells incubated with our latent conjugate and counterstained them with a primary antibody to RNase A and a secondary antibody labeled with AlexaFluor 594. In a fluorescence microscopy image, we observed a significant overlap of the green and red fluorescent signals to

produce a yellow signal, indicating that the unmasked RNase A conjugate is largely intact (Fig. 6.8).

The high chemical stability and low background fluorescence of the fluorogenic label conjugate allowed for the time-lapse imaging of its endocytosis. Cells were incubated with the fluorogenic label **6.13**–RNase A conjugate at room temperature, and images were recorded without washing during the next 90 min. The compilation of these images into a movie revealed that internalization of the conjugate occurred continuously and that vesicular fluorescence increased monotonically

6.4.10 Envoi

We have demonstrated how a common fluorophore, Rh_{110}, can be elaborated into a powerful new tool for biochemistry and cell biology. The use of a trimethyl lock provides a latent fluorophore with high chemical stability while maintaining enzymatic reactivity (Chandran *et al.*, 2005; Lavis *et al.*, 2006b). The use of a urea group (rather than a second trimethyl lock) improves enzymatic reactivity markedly while preserving desirable fluorescence properties, as in pro-fluorophore **6.8**. The elaboration of the urea to include an electrophile outfits the latent fluorophore for conjugation, as in fluorogenic label 13. Conjugation of this fluorogenic label to a target molecule enables, for example, the continuous imaging of the endocytosis of a target molecule by live human cells.

We note that the urea–rhodamine–trimethyl lock probe can be tailored to suit a variety of applications (Scheme 3). For example, modification of the enzyme-reactive group on the trimethyl lock could be used to detect the entry of a conjugate into a

particular compartment within a cell. Alteration of the bioconjugative group on the urea moiety could be used to change conjugation chemistry, enhance cellular internalization, or target a conjugate to a specific subcellular location. In addition, the fluorogenic label strategy could transcend cultured cells and allow continuous imaging in tissues or *in vivo*. These goals are facilitated by inventories of the enzymes in various organs and organelles (Kislinger *et al.*, 2006; Foster *et al.*, 2006). This versatility will enable the development of specific probes for biological experiments of ever-increasing sophistication.

Acknowledgments. We are grateful to K. A. Dickson for preliminary bioimaging experiments and S. S. Chandran, Z. Diwu, and M. B. Soellner for contributive discussions. L.D.L was supported by Biotechnology Training grant 08349 (NIH). This work was supported by Grant CA73808 (NIH). The University of Wisconsin–Madison Biophysics Instrumentation Facility was established with grants BIR-9512577 (NSF) and RR13790 (NIH). NMRFAM was supported by grant P41RR02301 (NIH).

Table 6.1 Spectroscopic properties of Rh_{110} and its derivatives

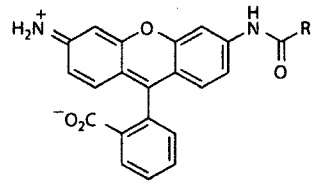

6.1: R = $N(CH_3)_2$
6.2: R = CH_3

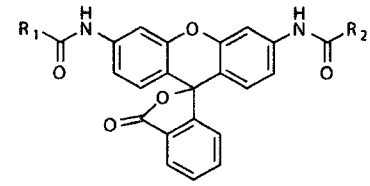

6.3: $R_1,R_2 = N(CH_3)_2$
6.4: $R_1 = CH_3, R_2 = N(CH_3)_2$
6.5: $R_1,R_2 = CH_3$

Dye	λ_{max} (nm)	ε ($M^{-1}cm^{-1}$)	λ_{em} (nm)	Φ	$\varepsilon \times \Phi$ (rel)
Rh_{110}	496	74,000	517	0.92	100%
6.1	492	48,600	518	0.49	35%
6.2	489	30,200	522	0.28	12%
6.3	482	3300	517	0.01	0.05%
6.4	475	400	—	—	—
6.5	~469	≤200	—	—	—

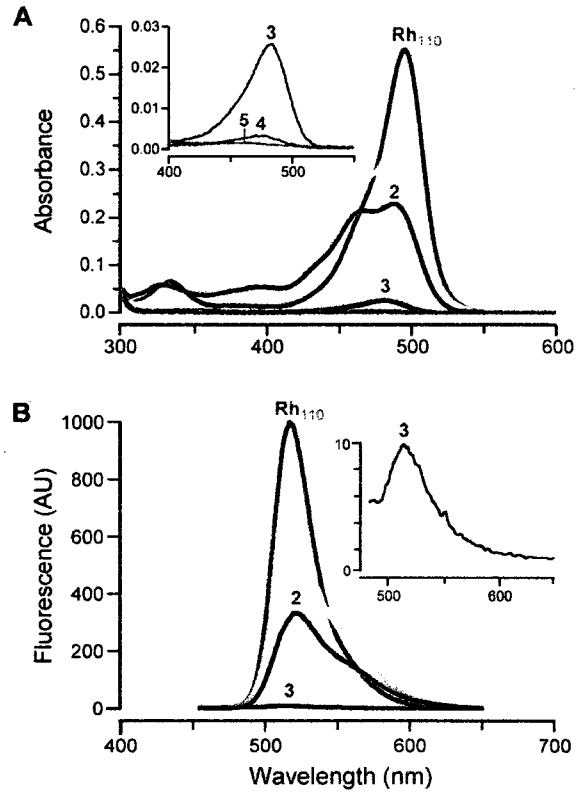

Figure 6.1 Spectra of Rh_{110} and its derivatives.

(A) Absorption spectra of Rh_{110} and derivatives **6.1–6.5** (7.5 μM). (B) Fluorescent emission spectra of Rh_{110} and **6.1–6.3** (λ_{ex} = 450 nm, not to scale).

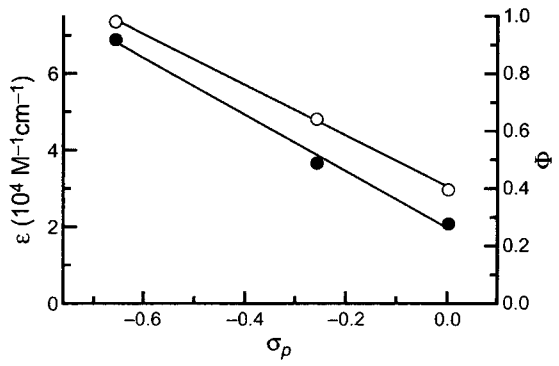

Figure 6.2 Hammett plots for Rh_{110}, urea **6.1**, and amide **6.2**.

Hammett plot of extinction coefficient (○) and quantum yield (●) versus σ_p for Rh_{110}, urea **6.1**, and amide **6.2**.

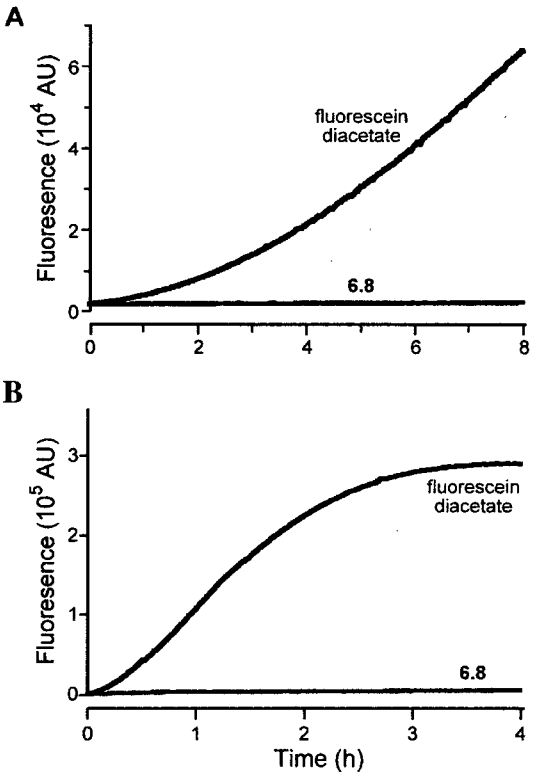

Figure 6.3 Stability of pro-fluorophore **6.8** and fluorescein diacetate in aqueous solution.

(A) Time course for the generation of fluorescence (λ_{ex} 496 nm, λ_{em} 520 nm) of pro-fluorophore **6.8** (25 nM) and fluorescein diacetate (25 nM) in PBS. (B) Time course of the generation of fluorescence (λ_{ex} 496 nm, λ_{em} 520 nm) of pro-fluorophore **6.8** (25 nM) and fluorescein diacetate (25 nM) in DMEM containing FBS (10% v/v).

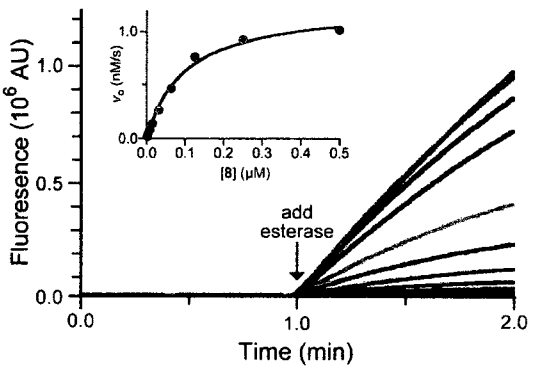

Figure 6.4 Kinetic characterization of pro-fluorophore **6.8**.

Kinetic traces (λ_{ex} 496 nm, λ_{em} 520 nm) and Michaelis–Menten plot (inset) of a serial dilution of pro-fluorophore **6.8** (0.5 μM → 2 nM) with PLE (2.5 μg/mL).

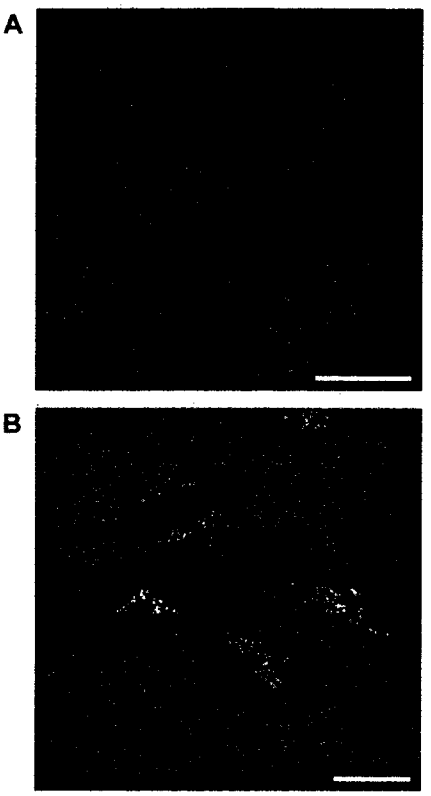

Figure 6.5 Unmasking of pro-fluorophore **6.8** in live human cells.

(A) Unwashed HeLa cells incubated for 1 h with pro-fluorophore **6.8** (10 μM) at 37 °C in DMEM and counter-stained with Hoechst 33342.

(B) Washed HeLa cells incubated for 1 h with pro-fluorophore **6.8** (10 μM) at 37 °C in DMEM and counter-stained with Hoechst 33342 and LysoTracker Red (5% v/v CO_2(g), 100% humidity). Scale bar: 20 μm.

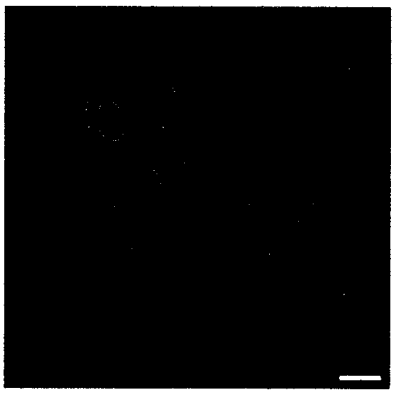

Figure 6.6 Stability of diurea-rhodamine **6.5** in live Hela cells.

Unwashed HeLa cells incubated for 1 h with diurea-rhodamine (10 μM) at 37 °C in DMEM (5% v/v CO_2(g), 100% humidity) and counter-stained with Hoechst 33342. Scale bar: 20 μm.

Figure 6.7 Live-cell imaging experiments with protein conjugates. (A) Unwashed HeLa cells incubated for 1 h with Oregon Green–RNase A conjugate (10 μM) at 37 °C in DPBS and counter-stained with Hoechst 33342. (B) Washed HeLa cells incubated for 1 h with Oregon Green–RNase A conjugate (10 μM) at 37 °C in DPBS and counter-stained with Hoechst 33342. (C) Unwashed HeLa cells incubated for 1 h with fluorogenic label **6.13**–RNase A conjugate (10 μM) at 37 °C in DPBS and counter-stained with Hoechst 33342. d) Washed HeLa cells incubated for 1 h with fluorogenic label **6.13**–RNase A conjugate (10 μM) at 37 °C in DPBS and counter-stained with Hoechst 33342 and LysoTracker Red (5% v/v CO_2(g), 100% humidity). Scale bar: 20 μm.

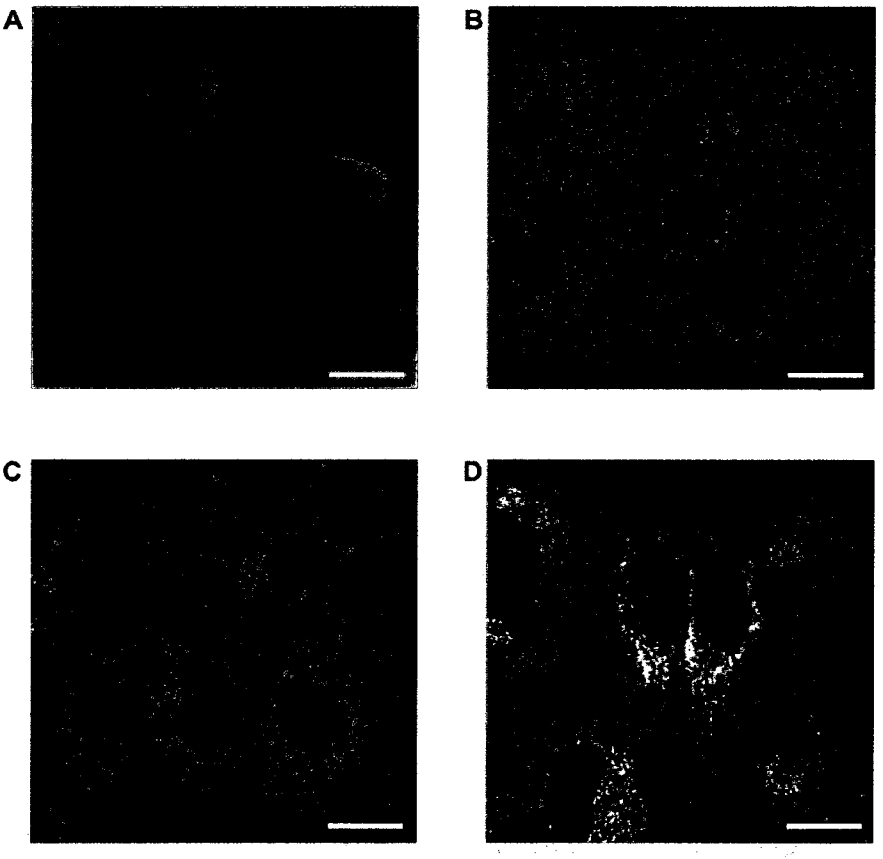
A
B
C
D

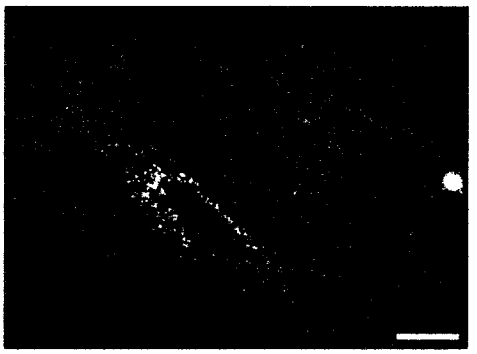

Figure 6.8 Colocalization between anti-RNase A antibody and fluorogenic label **6.13**–RNase A conjugate.

HeLa cells incubated for 1 h with the fluorogenic label **6.13**–RNase A conjugate (10 μM) at 37 °C in DMEM (5% v/v CO_2(g), 100% humidity). Cells were fixed with 4% paraformaldehyde, washed extensively, and counter-stained with a primary antibody to RNase A and secondary antibody labeled with AlexaFluor 594. Scale bar: 20 μm.

Scheme 6.1 Synthetic route to pro-fluorophore **6.8**.

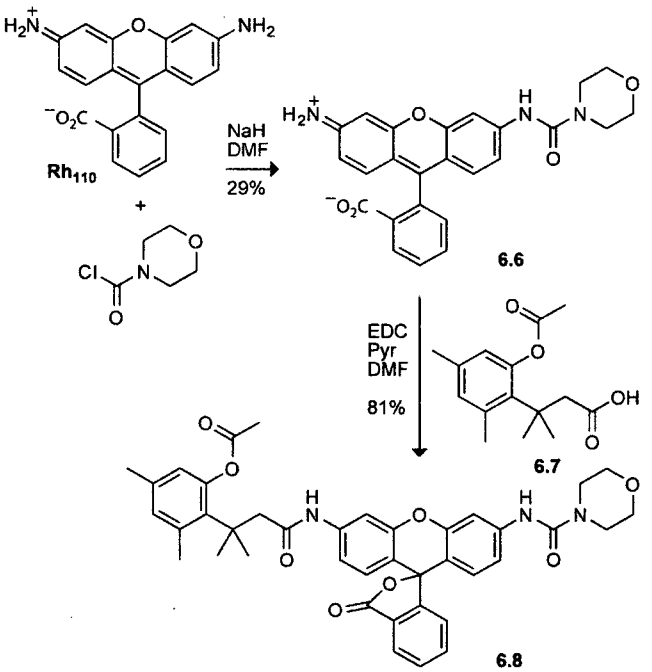

Scheme 6.2 Synthetic route to fluorogenic label **6.13**.

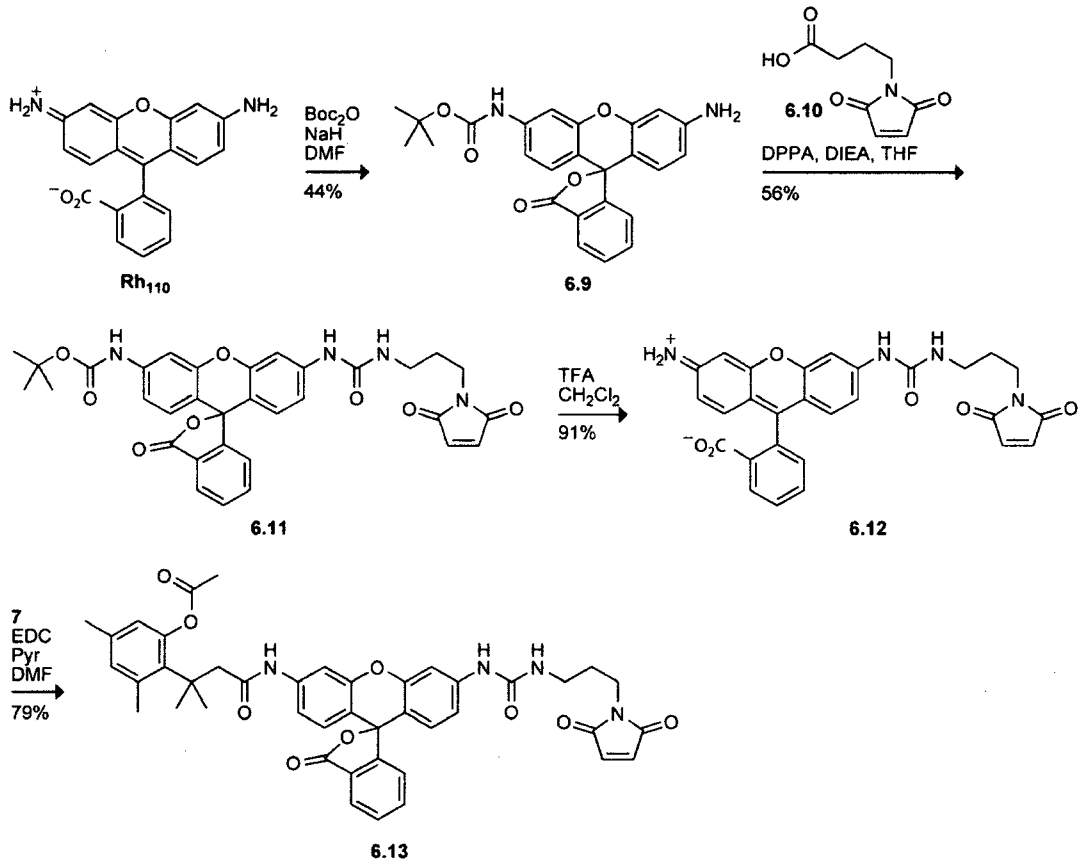

Scheme 6.3 Modules in fluorogenic label **6.13**.

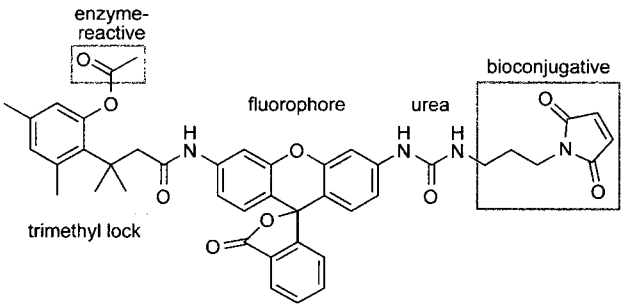

CHAPTER 7

Latent Blue and Red Fluorophores

Based on the Trimethyl Lock

Contribution: Cellular studies and imaging. All other experiments were performed by L.D. Lavis.

This chapter was published as:
Lavis, L.D., Chao, T.-Y., and Raines, R.T. (2006) Latent blue and red fluorophores based on the trimethyl lock. *ChemBioChem* **7**, 1151–1154.

7.1 Introduction

Fluorescent molecules are indispensable tools in modern biochemical and biological research, being used as labels for biomolecules, indicators for ions, stains for organelles, and substrates for enzymes.(Haugland *et al.*, 2005) The major targets of this last class are hydrolases that catalyze the removal of a masking moiety, thereby modulating fluorescence.(Johnson, 1998) A critical property of fluorogenic hydrolase substrates is their chemical stability in aqueous solution, as spontaneous hydrolysis can compete deleteriously with enzymatic activity. New substrate classes that exhibit increased stability while maintaining enzymatic reactivity would be highly desirable.

Our laboratory recently reported on the use of the "trimethyl lock" strategy in the design of a latent fluorophore.(Chandran *et al.*, 2005) This latent fluorophore consists of a trimethyl lock component inserted between a dye and enzyme-reactive group. The trimethyl lock is an *o*-hydroxycinnamic acid derivative in which unfavorable steric interactions between three methyl groups encourage rapid lactonization to form a hydrocoumarin and release a leaving group.(Borchardt and Cohen, 1972; Milstein and Cohen, 1972) Our initial latent fluorophore exhibited remarkable stability in aqueous solution, but released a xanthene dye (rhodamine 110) upon hydrolytic cleavage by an esterase. Here, we explore the modularity of our design, probing its applicability to unrelated dyes that absorb at short (blue) and long (red) wavelengths.

7.2 Experimental Procedures

7.2.1 Materials

AMC (*i.e.*, Coumarin 440) and CV·$HClO_4$ (*i.e.*, Cresyl Violet 670 Perchlorate) were from Exciton (Dayton, OH). Dimethylformamide was drawn from a Baker CYCLE-TAINER™ solvent delivery system. All other reagents were from Aldrich Chemical (Milwaukee, WI) or Fisher Scientific (Hanover Park, IL) and used without further purification.

7.2.2 Thin-layer chromatography

Thin-layer chromatography was performed using aluminum-backed plates coated with silica gel containing F_{254} phosphor and visualized by UV illumination or developed with I_2, ceric ammonium molybdate, or phosphomolybdic acid stain. Flash chromatography was performed on open columns with silica gel-60 (230–400 mesh), or on a FlashMaster Solo system (Argonaut, Redwood City, CA) with Isolute® Flash Si II columns (International Sorbent Technology, Hengoed, Mid Glamorgan, UK).

7.2.3 NMR

NMR spectra were obtained with a Bruker DMX-400 Avance spectrometer at the National Magnetic Resonance Facility at Madison (NMRFAM). Mass spectrometry was performed with a Micromass LCT (electrospray ionization, ESI) mass spectrometer in the Mass Spectrometry Facility in the Department of Chemistry.

7.2.4 Fluoresence spectroscopy

Fluorometric measurements were made with a QuantaMaster1 photon-counting spectrofluorometer from Photon Technology International (South Brunswick, NJ) equipped with sample stirring, and fluorescence grade quartz or glass cuvettes from Starna Cells (Atascadero, CA). All measurements were recorded at ambient temperature (23 ± 2 °C). Compounds were prepared as stock solutions in DMSO and diluted such that the DMSO concentration did not exceed 1% v/v. PLE (MW = 163 kDa) (Horgan *et al.*, 1969) was from Sigma Chemical (St. Louis, MO; product number E2884) as a suspension in 3.2 M $(NH_4)_2SO_4$, and was diluted to appropriate concentrations in PBS before use. Kinetic parameters were calculated with Microsoft Excel 2003 and GraphPad Prism 4.

7.2.5 Cell preparation and imaging

CHO K1 or HeLa cells were plated on Nunc Lab-Tek II 8-well Chamber Coverglass (Fisher Scientific, Hanover Park, IL) and grown to 70% confluence at 37 °C in Dulbecco's modified Eagle's medium (Invitrogen, Carlsbad, CA) containing FBS (10% v/v). Cells were then incubated with pro-fluorophore **7.4** (10 μM) for 15 min at 37 °C and imaged immediately. Nuclear staining was accomplished by addition of Hoechst 33342 (2 μg/mL) for the final 5 min of incubation.

Cells were imaged with a Nikon Eclipse TE2000-U confocal microscope equipped with a Zeiss AxioCam digital camera. Excitation at 408 nm was provided by a blue-diode laser, and emission light was passed though a filter centered at 450 nm with a

35-nm band-pass. Excitation at 543 nm was provided by a HeNe laser, and emission light was passed through a filter centered at 605 nm with a 75-nm band-pass.

7.3 Results and Discussion

7.3.1 Coumarin-based latent fluorophore

Coumarin-based compounds comprise an important class of blue dyes possessing UV or near-UV excitation wavelengths.(Valeur, 2002) Acyl esters and acyloxymethyl ethers of 7-hydroxycoumarin (*i.e.*, umbelliferone) can be substrates for esterases.(Leroy *et al.*, 2003; Babiak and Reymond, 2005; Hyatt *et al.*, 2005) 7-Amino-4-methylcoumarin (AMC) is used widely as the basis for protease substrates.(Zimmerman *et al.*, 1977; Morita *et al.*, 1977; Zimmerman *et al.*, 1976) Upon amidation, the excitation and emission wavelengths of AMC are shifted to shorter wavelengths with concomitant reduction in quantum yield.(Zimmerman *et al.*, 1976)

We reasoned that AMC could be subjected to our latent fluorophore strategy. Accordingly, we condensed AMC with acetylated trimethyl lock **1**(Amsberry *et al.*, 1991) to give pro-fluorophore **7.2** (Scheme 7.1), which displayed the expected hypsochromic shift of excitation and emission spectra relative to free AMC (Fig. 7.1). The hydrolysis of pro-fluorophore **7.2** was catalyzed by porcine liver esterase (PLE) with $k_{cat}/K_M = 2.5 \times 10^5\ M^{-1}s^{-1}$ and $K_M = 8.2\ \mu M$ (Fig. 7.2A). This k_{cat}/K_M value is 10^2-fold greater than the apparent k_{cat}/K_M value for the latent fluorophore based on rhodamine 110.(Chandran *et al.*, 2005) (We use the term "apparent" because full fluorescence

manifestation requires the lactonization of two trimethyl lock moieties.(Chandran *et al.*, 2005))

To evaluate the relative stability of pro-fluorophore **7.2**, we monitored the accretion of fluorescence in phosphate-buffered saline (PBS) containing bovine serum albumin (BSA; 1.0 mg/mL) and either pro-fluorophore **7.2** or 4-methylumbelliferyl acetate (**7.3**, which is a common esterase substrate (Hyatt *et al.*, 2005)). Pro-fluorophore **7.2** proved to be highly stable compared to 4-methylumbelliferyl acetate (Fig. 7.3). An additional advantage of pro-fluorophore **7.2** is that the product of its hydrolysis, AMC, shows little change in fluorescence at pH $\geq$ 5.(Haugland *et al.*, 2005) In contrast, the fluorescence of 4-methylumbelliferone is highly variable due to its pK_a = 7.40(Graber *et al.*, 1986) being near the physiological pH.

7.3.2 Cresyl violet-based latent fluorophore

To access longer wavelengths, we turned to the oxazine class of red dyes. One such dye, cresyl violet (CV) has been used for decades to stain tissues(Banny and Clark, 1950; Culling *et al.*, 1985) and as a laser dye.(Gacoin and Flamant, 1972) Although CV has a maximal absorbance at 586 nm, its fused benzo ring broadens its absorption spectrum(Drexhage, 1977) and thereby allows excitation with a variety of light sources. Diamide derivatives of CV are virtually nonfluorescent and thus useful in the production of fluorogenic protease substrates.(Van Noorden *et al.*, 1997; Boonacker *et al.*, 2003; Lee *et al.*, 2003)

The attributes of CV make this dye an attractive candidate for our latent fluorophore strategy. Accordingly, we condensed CV with acetylated trimethyl lock **7.1** (Amsberry *et al.*, 1991) to give pro-fluorophore **7.4** (Scheme 7.2). Although pro-fluorophore **7.4** was stable in PBS containing BSA (data not shown), its hydrolysis was catalyzed by PLE with apparent kinetic parameters of $k_{cat}/K_M = 1.2 \times 10^5$ $M^{-1}s^{-1}$ and $K_M = 0.14$ μM (Fig. 7.2B). The k_{cat}/K_M value for the hydrolysis of pro-fluorophore **7.4** is similar to that of pro-fluorophore **7.2**; the K_M value is, however, 10-fold lower than that of pro-fluorophore **7.2**.

Pro-fluorophore **7.4** serves as a probe for esterase activity in live mammalian cells. The broad excitation peak allowed confocal microscopy experiments using excitation at 543 nm and emission at 605 nm. Pro-fluorophore **7.4** was hydrolyzed by esterases endogenous in the cells of a rodent (Fig. 7.4A) or human (Fig. 7.4B) to give a red-stained cytosol within minutes. The somewhat enhanced fluorescence observed in the human cells could be indicative of more efficient internalization or hydrolysis of the latent fluorophore. After longer incubation, the liberated CV became further localized in subcellular compartments (data not shown), which is consistent with previous reports.(Lee *et al.*, 2003) To date, there have been few reports of long-wavelength esterase substrates that are useful in cell biology.(Haugland *et al.*, 2005) Its evident stability, optical properties, and fast intracellular eduction make pro-fluorophore **7.4** useful in a wide variety of biological applications, especially in assays involving fluorophores of different wavelengths.

In conclusion, we have established that one component of our latent fluorophores—the dye—is modular (Fig. 7.5). Specifically, we have now prepared useful latent fluorophores from three dyes (blue, green,(Chandran *et al.*, 2005) and red), all linked by a trimethyl lock moiety to an esterase-reactive group. In future work, we shall explore the modularity of the other component—the enzyme-reactive group. We anticipate that the end result will be a broad spectrum of stable latent fluorophores with numerous applications in biochemical and biological research.

Acknowledgements. We are grateful to S.S. Chandran and Z. Diwu for contributive discussions. L.D.L. was supported by biotechnology training grant 08349 (NIH). This research was supported by grant CA73808 (NIH). NMRFAM was supported by grant P41RR02301 (NIH).

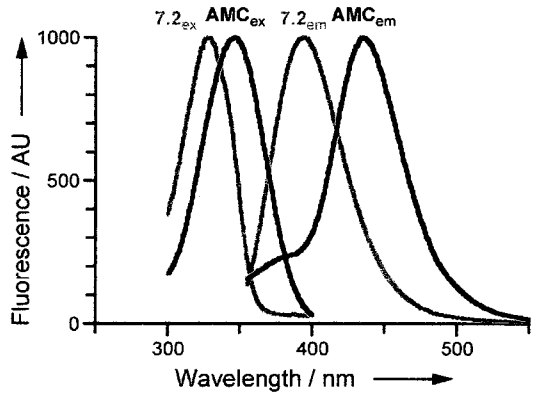

Figure 7.1 Normalized fluorescent excitation–emission spectra of pro-fluorophore **7.2** and AMC.

Figure 7.2 Kinetic characterization of pro-fluorophores **7.2** and **7.4**. (A) Kinetic traces (l_{ex} 365 nm, l_{em} 460 nm) and Michaelis–Menten plot (inset) for the hydrolysis of pro-fluorophore **7.2** (20 μM→9.8 nM) by PLE (2.5 μg/mL); $k_{cat}/K_M = 2.5 \times 10^5$ $M^{-1}s^{-1}$ and $K_M = 8.2$ μM. (B) Kinetic traces (l_{ex} 586 nm, l_{em} 620 nm) and Michaelis–Menten plot (inset) for the hydrolysis of pro-fluorophore **7.4** (2.5 μM→4.9 nM) by PLE (2.5 μg/mL); apparent $k_{cat}/K_M = 1.2 \times 10^5$ $M^{-1}s^{-1}$ and apparent $K_M = 0.14$ μM.

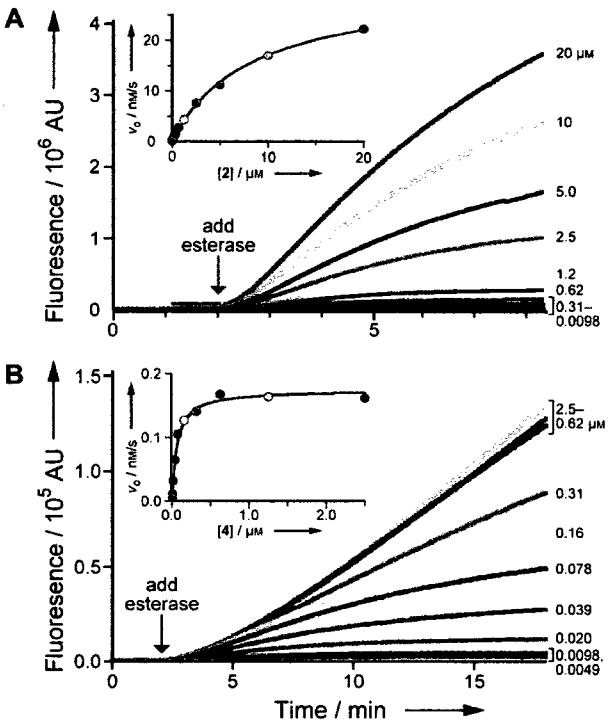
A
Fluoresence / 10^6 AU
4
3
2
1
0
0
5
add
esterase
20 μM
10
5.0
2.5
1.2
0.62
0.31–
0.0098
v0 / nM/s
20
10
0
0
10
20
[2] / μM
B
Fluoresence / 10^5 AU
1.5
1.0
0.5
0.0
0
5
10
15
Time / min
add
esterase
2.5–
0.62 μM
0.31
0.16
0.078
0.039
0.020
0.0098,
0.0049
v0 / nM/s
0.2
0.1
0.0
0.0
1.0
2.0
[4] / μM

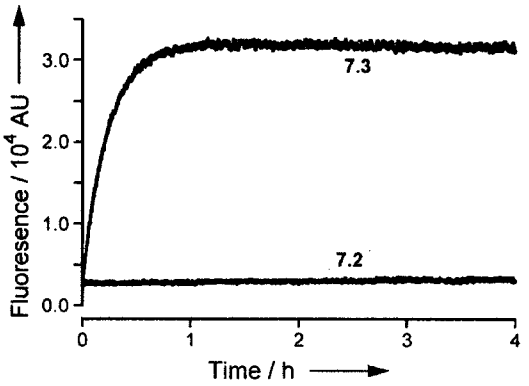

Figure 7.3 Stability of pro-fluorophores **7.2** and **7.3**.

Time course of the generation of fluorescence (l_{ex} 365 nm, l_{em} 460 nm) from pro-fluorophore **7.2** (50 nM) or methylumbelliferyl acetate **7.3** (50 nM) in PBS containing BSA (1 mg/mL).

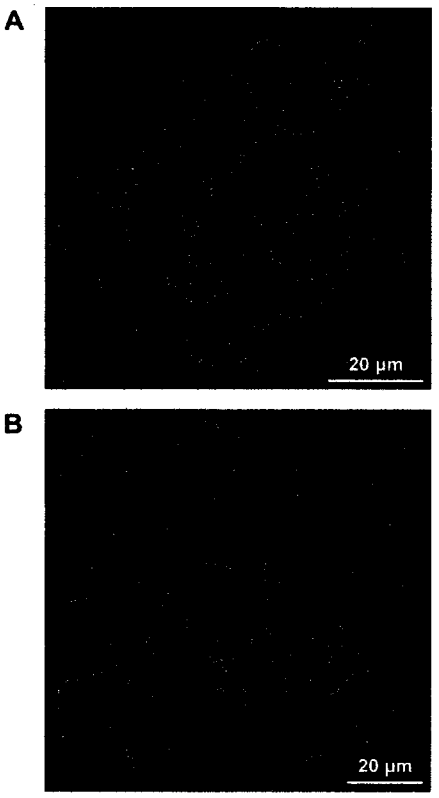

Figure 7.4 Unmasking of pro-fluorophore **7.4** in live cells.

Unwashed mammalian cells incubated for 15 min with pro-fluorophore **7.4** (10 μM) at 37 °C in DMEM and counter-stained with Hoechst 33342 (5% v/v CO_2(g), 100% humidity). (A) CHO K1 cells. (B) HeLa cells.

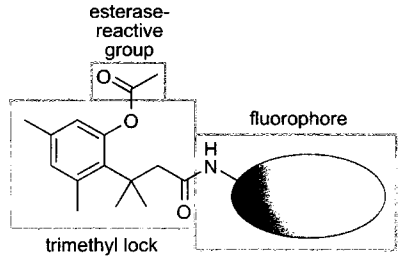

Figure 7.5 Modules in the latent fluorophores described in this work.

Scheme 7.1 Route for the synthesis of pro-fluorophore **7.2,** and the chemical structure of 4-methylumbelliferyl acetate (**7.3**).

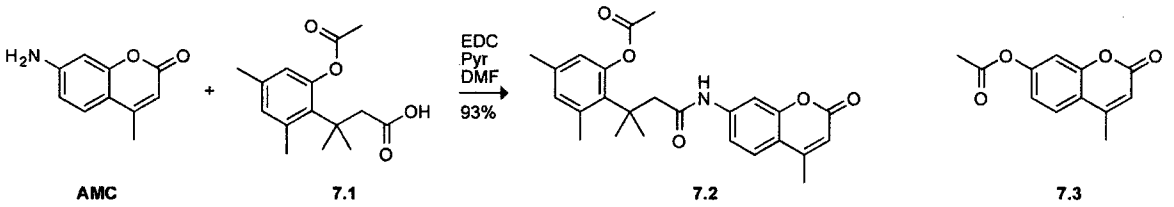

AMC 7.1 7.2 7.3

Scheme 7.2 Route for the synthesis of pro-fluorophore **7.4**.

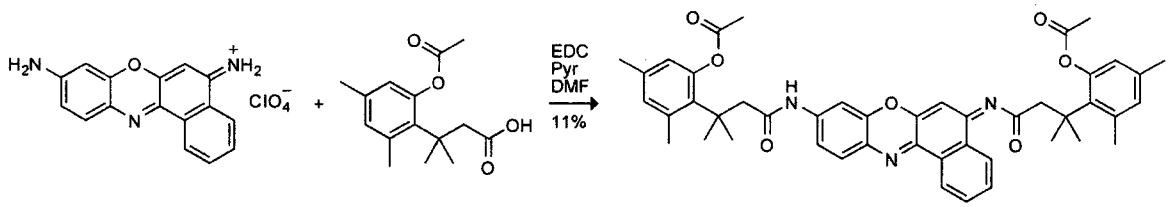

CV 7.1 7.4

CHAPTER 8

Synthesis and Utility of Fluorogenic Acetoxymethyl Ethers

Contribution: Cellular studies and imaging. All other experiments were performed by L.D. Lavis.

Prepared for submission as:
Lavis, L.D., Chao, T.-Y. and Raines, R.T. (2010)
Synthesis and utility of fluorogenic acetoxymethyl ethers.

8.1 Abstract

The acetoxymethyl (AM) group is an esterase-sensitive motif that can mask polar functionalities in small molecules. Here, we report on the synthesis of AM ethers of derivatives of fluorescein and resorufin. These pro-fluorophores have a desirable combination of low background fluorescence, excellent chemical stability, and high enzymatic reactivity *in vitro* and *in cellulo*. The structures are themselves useful for biological experiments, and can be incorporated into even more elaborate small-molecule fluorophores for bioresearch.

8.2 Introduction

The utility of small-molecule fluorescent probes is well established in biology.(Lavis and Raines, 2008) In particular, fluorogenic esterase substrates are vital tools for examining biological and biochemical processes. Such compounds can be used to assess cell viability,(Haugland *et al.*, 2005) to measure enzymatic activity,(Goddard and Reymond, 2004) as fluorogenic labels for biomolecular imaging,(Lavis *et al.*, 2006a) or as part of a delivery strategy for fluorescent ion indicators.(Tsien, 1981; Kao *et al.*, 1989) Chemical "masking" of polar functionalities with ester groups can stifle fluorescence and facilitate efficient diffusion across lipid bilayers.(Testa and Mayer, 2003; Rotman and Papermaster, 1966) Esterases endogenous in eukaryotic cells are able to catalyze the hydrolysis of some synthetic ester bonds,(Lavis, 2008) thereby releasing the fluorescent molecule.

The archetype of fluorogenic esterase substrates is based on the antique fluorophore fluorescein (**8.1a**; Scheme 8.1).[(Baeyer, 1871)] Functionalization of the phenolic oxygens found in fluorescein with a suitable acylating agent (*e.g.*, acetic anhydride) gives fluorescein diacetate (FDA; **8.2a**). This acyl substitution secures the molecule in a colorless, nonfluorescent lactone form. Rotman and Papermaster demonstrated that the lipophilic FDA can cross cell membranes and be activated by cellular esterases.(Rotman and Papermaster, 1966) This diester strategy has been used to mask numerous fluorescein derivatives for intracellular delivery.(Haugland *et al.*, 2005)

Despite the extensive use of FDA and its derivatives in biological experiments, fluorescein diesters suffer from two juxtaposed problems. Fluorescein displays a relatively low phenolic pK_a value of 6.4, causing instability of the ester bonds in aqueous solution.(Lavis *et al.*, 2006a) These low pK_a values are, however, necessary for utility because the conjugate base of the fluorophore is much more fluorescent than the protonated form.(Lavis *et al.*, 2007) Substitution on the fluorescein xanthene ring system can affect this pK_a. For example, 2′,7′-difluorofluorescein (**8.1b**; Scheme 8.1) exhibits a phenolic pK_a of 4.7 and is thus less sensitive to biologically-relevant pH fluctuations.(Sun *et al.*, 1997) This fluorine substitution, however, leads to even lower chemical stability for 2′,7′-difluorofluorescein diacetate (DFFDA; **8.2b**) in aqueous solution (*vide infra*).

High chemical stability of fluorogenic probes is vital, as spontaneous hydrolysis compromises the ability to assess enzymatic activity, raises background fluorescence levels, and diminishes membrane permeance of the masked dye. One strategy to improve the stability of fluorogenic substrates involves insertion of a self-immolative chemical

functionality between the fluorophore and the enzyme-reactive moiety.(Ho *et al.*, 2007) Enzymatic catalysis yields an intermediate that undergoes rapid decomposition to release the free fluorophore. We have employed this strategy, using the "trimethyl lock" motif to mask amine-containing fluorophores.(Watkins *et al.*, 2009; Chandran *et al.*, 2005; Lavis *et al.*, 2006b; Lavis *et al.*, 2006a; Yatzeck *et al.*, 2008) These "pro-fluorophores" possess high chemical stability, and are unmasked by esterases efficiently both *in vitro* and *in cellulo*.

The trimethyl lock motif cannot offer significant advantages to phenolic fluorophores, such as fluorescein. We reasoned, however, that insertion of a simple oxygen–methylene group into a fluorophore acetate ester substrate to give an acetoxymethyl (AM) ether could endow the compound with increased stability. Hydrolysis of the enzyme-labile moiety in these AM-containing substrates results in a hemiacetal that decomposes spontaneously to liberate the free oxygen substituent. This modification alters significantly the leaving group pK_a (formaldehyde hydrate has a pK_a of 12.78, ref (Taylor, 1995)), thereby increasing chemical stability. The modification should also insulate the labile ester group from the dye, allowing flexibility in dye type.

The acetoxymethyl strategy has been used in other contexts. AM esters were first used to increase the cell-permeability of certain antibiotics(Jansen and Russell, 1965) and is now a well-known prodrug strategy.(Testa and Mayer, 2003) Tsien, Schultz, and their coworkers established AM esters as an effective and innocuous means to deliver carboxylate-containing ion chelators and even phosphorylated molecules into cells.(Schultz, 2003; Schultz *et al.*, 1993; Tsien, 1981)

AM ethers of phenols have also been used in prodrug strategies,(Bodor *et al.*, 1983; Ouyang *et al.*, 2002; Thomas and Sloan, 2007; Thomas and Sloan, 2008) to mask the fluorophoric portions of cell-permeable fluorescent ion indicators,(Goddard and Reymond, 2004; Kao *et al.*, 1989) and to create fluorogenic enzyme substrates. Reymond and coworkers showed that acyloxymethyl ethers of 4-methylumbelliferone could be useful pro-fluorophores with significantly improved chemical stability.(Leroy *et al.*, 2003)

Fluorescein is one of the brightest dyes in common use by chemical biologists.(Lavis and Raines, 2008) Curiously, the synthesis of monoacyloxymethyl ethers of fluorescein has been reported,(Bensel *et al.*, 2001; Yang *et al.*, 2006) but to our knowledge no report of a fully masked, diacyloxymethyl ether of fluorescein exists. Moreover, the acetoxymethyl strategy has not been used to shield modified fluoresceins or fluorophores with longer excitation and emission wavelengths, nor have fluorogenic AM ethers been used to examine esterase activity in a cellular context. Finally, fluorogenic esterase substrates exhibiting excitation wavelengths >500 nm remain noticeably sparse.(Lavis *et al.*, 2006b; Haugland *et al.*, 2005)

Here, we use the AM ether system to prepare substrates based on fluorescein, 2′,7′-difluorofluorescein ("Oregon Green"), the "Tokyo Green" fluorophore,(Urano *et al.*, 2005) and derivatives of resorufin. We first determine experimental conditions that enable the efficient synthesis of such compounds from accessible chemical reagents in a single step. We then assess their hydrolytic stability, enzymatic turnover, and utility in live human cells. Our results show the AM ether pro-fluorophores possess much greater

chemical stability than simple fluorophore esters, and can be unmasked efficiently by esterases both *in vitro* and *in cellulo*.

8.3 Experimental Procedures

8.3.1 Materials

Dulbecco's phosphate-buffered saline (DPBS), Dulbecco's modified Eagle's medium (DMEM) and fetal bovine serum (FBS) were from Invitrogen. 2′,7′-Difluorofluorescein diacetate (**8.2b**) was synthesized as described previously.(Sun *et al.*, 1997) All other reagents were from Sigma–Aldrich or Fisher Scientific. HEPES buffer at pH 7.3 was prepared from a 1 M stock solution from Fisher.

8.3.2 Fluorometry

Fluorometric measurements were made with a QuantaMaster1 photon-counting spectrofluorometer from Photon Technology International or an Eclipse spectrofluorometer from Varian, both equipped with sample stirring. Sample solutions were in fluorescence-grade quartz or glass cuvettes from Starna Cells, or fluorescence-grade polystyrene cuvettes from Perfector Scientific. All measurements were recorded at ambient temperature (23 ± 2 °C), and buffers were not degassed prior to measurements.

8.3.3 Chemical stability and reactivity

Long-term stability studies (>12 h) were performed in black, clear-bottom, 96-well polystyrene microplates from Corning (product number 3651) sealed with SealPlate Film from PGC Scientifics. Plates were read from the bottom on a FlexStation 3 from Molecular Devices. Values of $t_{½}$ (= ln 2/k) were determined by fitting the data to a single exponential decay with equation 8.1:

$$F = (F_0 - F_{max})e^{-kt} + F_{max} \tag{8.1}$$

where F is fluorescence intensity, F_0 and F_{max} are the initial and maximal fluorescence, respectively, t is time, and k is the unimolecular rate constant. Some pro-fluorophores started to hydrolyze prior to initial monitoring; their $t_{½}$ values were estimated by setting F_0 equal to background fluorescence of the buffer.

Non-specific chemical reactivity was assessed by incubating pro-fluorophore (100 μM) with Ac-Arg–Phe–Met–Trp–Met–Lys-NH_2 (1.0 mg/mL; Bachem; product number H-1994) in 10 mM HEPES buffer, pH 7.3, for 2 h at ambient temperature. The reaction mixture was analyzed on an Agilent 1200 HPLC system equipped with a G1315B diode array detector and a 6130 mass spectrometry detector using an 4.6 × 150 mm Eclipse XDB-C18 column with a gradient of 10→95% v/v CH_3CN in H_2O containing 0.1% v/v formic acid over 20 min.

8.3.4 Enzyme kinetics

Compounds were prepared as stock solutions in anhydrous DMSO and diluted such that the DMSO concentration did not exceed 1.5% v/v. Porcine liver esterase (PLE, MW = 163 kDa, ref (Horgan *et al.*, 1969)) was obtained from Sigma–Aldrich (product number E2884; lot 129K7010) as a suspension in 3.2 M $(NH_4)_2SO_4$, and was diluted to appropriate concentrations in HEPES buffer, pH 7.4, before use in Protein LoBind tubes from Eppendorf. Kinetic parameters were calculated by fitting the data to the Michaelis–Menten equation with GraphPad Prism software.

8.3.5 Cell preparation and imaging

HeLa cells were plated on Nunc Lab-Tek II 8-well Chamber Coverglass (Fisher Scientific) and grown to 70–80% confluence at 37 °C in DMEM containing FBS (10% v/v). Cells were then washed with Dulbecco's phosphate-buffered saline, and incubated with substrates **8.2a**, **8.2b**, **8.4a**, **8.4b**, **8.6**, **8.9**, or **8.12** (2 or 10 μM) for 20 min at 37 °C. Nuclei were stained by the addition of Hoechst 33342 (2 μg/mL) during the final 5 min of incubation. Cells were imaged on a Nikon Eclipse TE2000-U confocal microscope equipped with a Zeiss AxioCam digital camera or a Zeiss 510-Meta confocal microscope. Excitation at 408 nm was provided by a blue-diode laser, and the ensuing emission light was passed though a filter centered at 450 nm with a 35-nm band-pass. Excitation at 488 nm was provided by an argon-ion laser, and the ensuing emission light was passed through a filter centered at 515 nm with a 40-nm band-pass. Excitation at 543 nm was

provided by a HeNe laser, and the ensuing emission light was passed through a filter centered at 605 nm with a 75-nm band-pass.

8.4 Results and Discussion

8.4.1 Chemical stability and reactivity of fluorescein diacetate derivatives

The chemical stability of both fluorescein diacetate (**8.2a**) and 2′,7′-difluorofluorescein diacetate (**8.2b**) was assessed by incubating these compounds in aqueous solution and monitoring the accretion of fluorescence over time. Both compounds exhibited low initial fluorescence signals in Dulbecco's phosphate-buffered saline (DPBS) but underwent slow, spontaneous hydrolysis (Fig. 8.1A). As expected from the leaving group pK_a values, the hydrolysis of fluorinated acetate ester **8.2b** is faster than that of **8.2a**. The two compounds exhibit poor stability in Dulbecco's modified Eagle's medium containing fetal bovine serum (DMEM–FBS; Fig. 8.2B). Here, DFFDA (**8.2b**) exhibited an apparent half-life of 6 min and FDA (**8.2a**) was hydrolyzed completely in hours ($t_{1/2}$ = 1.5 h).

We suspected this instability is likely due in part to the non-specific reactivity of the acyl groups with the ample nucleophiles in the tissue culture milieu. To test this hypothesis, we incubated acetate esters **8.2a** and **8.2b** with Ac-Arg–Phe–Met–Trp–Met–Lys-NH_2. This hexapeptide contains a single Lys residue along with charged and chromophoric residues that allow facile separation and detection by tandem liquid chromatography–mass spectrometry (LC–MS). Analysis of this reaction mixture showed

significant acylation of the peptide, with fluorinated **8.2b** being more reactive than **8.2a** These data reveal a critical limitation of acetate ester dyes in the accurate monitoring of esterase activity, providing additional incentive to us.

8.4.2 Synthesis of fluorescein AM ethers

The synthesis of diacetoxymethyl ethers of fluorescein derivatives was complicated by several factors. In previous reports of AM-ether derivatives of fluorophores, syntheses involved deprotonation of the fluorophore phenolic moiety with NaH followed by addition of a halomethyl ester such as bromomethyl acetate.(Bensel *et al.*, 2001; Leroy *et al.*, 2003; Yang *et al.*, 2006) Halomethyl esters possess two electrophilic centers: the halide-bearing carbon and the carbonyl carbon. Thus, strong base-mediated installation of a single AM ether leads to a mixture of ester and ether products, resulting in low conversion to the desired compound.(Ouyang *et al.*, 2002; Yang *et al.*, 2006) Based on the poor reported yield (~10%) of monosubstituted acetoxymethyl fluorescein with this strategy,(Yang *et al.*, 2006) we suspected the preparation of disubstituted AM ether pro-fluorophores would require different reaction conditions.

An additional caveat involves the complexity of the fluorescein molecule. In solution, xanthene dyes such as fluorescein exist as an equilibrium mixture of quinoid and lactone forms, their distribution depending on the environment.(Ioffe and Otten, 1965b; Zanker and Peter, 1958; Watkins *et al.*, 2009) Treatment of fluorescein with an alkylating agent typically gives an ether–ester as the major product.(Miller, 1983;

Sparano *et al.*, 2004; Mugherli *et al.*, 2006) Thus, despite the apparent simplicity of the desired molecules, the bifurcated reactivity of the halomethyl acetate in tandem with the fluorescein equilibrium issue leads to several reaction products.

Similar nucleophilic substitution reactions between oxygen nucleophiles and halomethyl esters have used a variety of conditions: amine bases in DMF,(Tsien, 1981) carbonate salts in polar aprotic solvents,(Bodor *et al.*, 1983; Ouyang *et al.*, 2002) or phase-transfer conditions.(Thomas and Sloan, 2007) Alkylation of fluoresceins sometimes involves the use of Ag(I) salts to enable diether formation.(Krafft *et al.*, 1988; Mitchison, 1989; Haugland *et al.*, 1990; Mitchison *et al.*, 1998) Acetonitrile has been used as the solvent in the synthesis of fluorescein glycosides from α-halo sugar derivatives.(Kasai *et al.*, 1993) We screened several conditions to find optimal conditions for the synthesis of the desired AM ether products **8.4a** and **8.4b** from dyes **8.1a** and **8.1b** with commercially available bromomethyl acetate (**8.3**). As shown in Scheme 8.1, we found the use of Ag_2O in acetonitrile with molecular sieves to be effective for the synthesis of both fluorescein derivatives **8.4a** and **8.4b** in moderate isolated yield. The superior yield observed of compound **8.4b** relative to **8.4a** can be explained, in part, by the lower nucleophilicity of the relevant phenolic oxygen leading to a tighter S_N2 transition state and subsequent increase in alkylation over acylation.(Sloan and Koch, 1983) We note that DMF/toluene mixtures with Ag_2O gave low yields of 5% and 15% for **8.4a** and **8.4b**, respectively. We also observed success in the synthesis of the fluorescein diacetoxymethyl ether (**8.4a**) by using a phase-transfer reaction protocol,(Thomas and

Sloan, 2007) which gave the desired molecule in 31% isolated yield. The phase-transfer recipe gave only a poor yield (6%) of **8.4b**. We conclude that our reaction conditions constitute a marked improvement in the route to fluorophore AM ethers compared to existing methods that employ strong bases such as NaH.(Leroy *et al.*, 2003; Yang *et al.*, 2006)

8.4.3 Chemical stability and reactivity of AM ethers

As with fluorescein diacetate (**8.2a**) and 2′,7′-difluorofluorescein diacetate (**8.2b**), the chemical stability of both fluorescein diacetoxymethyl ether (**8.4a**) and 2′,7′-difluorofluorescein diacetoxymethyl ether (**8.4b**) pro-fluorophores was assessed in aqueous solution. These two compounds showed low initial fluorescence signals in Dulbecco's phosphate-buffered saline (DPBS; Fig. 8.1A), indicating that both acylation and alkylation of the phenolic groups in fluorescein lock the molecule into the colorless, nonfluorescent lactone form. The AM ether pro-fluorophores (**8.4a** and **8.4b**) suffered spontaneous hydrolysis slower than did their acetate ester congeners (**8.2a** and **8.2b**) in either DPBS (Fig. 8.1A) or DMEM–FBS (Fig. 8.1B). Longer incubation in a microplate format revealed the apparent half-life for both **8.4a** and **8.4b** to be 32 h in DMEM–FBS. We also incubated these pro-fluorophores with the lysine-containing hexapeptide. In contrast to the acetate esters **8.2a** and **8.2b**, we observed no measurable acylation of **8.4a** and **8.4b** by the hexapeptide. The similarity in the chemical stability of the AM ether dyes support our hypothesis that the acetoxymethyl group insulates the ester bond, and thereby abolishes the effect of the fluoro groups on the chemical stability of the substrate. Pro-

fluorophore **8.4b** and its derivatives could prove to be especially valuable to chemical biologists as a fluorogenic esterase substrate exhibiting higher chemical stability than fluorescein diacetate (**8.2a**), but releasing difluorofluorescein, a pH-insensitive dye with high photostability (Sun *et al.*, 1997).

8.4.4 Enzyme kinetics

Having established the enhanced chemical stability of pro-fluorophores **8.4a** and **8.4b**, we sought to assess the enzymatic reactivity of these potential enzyme substrates *in vitro*, comparing them to the parent diacetate dyes. Incubation of each of these four compounds with porcine liver esterase (PLE) elicited a rapid increase in fluorescence intensity. Fluorescein diacetate (**8.2a**) proved to be the best substrate, with $k_{cat}/K_M = 1.4 \times 10^6\ M^{-1}s^{-1}$ and $K_M = 11\ \mu M$. These data are in gratifying agreement with values reported previously.(Hofmann and Sernetz, 1983) Surprisingly, difluorofluorescein diacetate (**8.2b**) exhibited slower turnover, giving apparent kinetic constants of $k_{cat}/K_M = 2.9 \times 10^5\ M^{-1}s^{-1}$ and $K_M = 5.3\ \mu M$. The two AM ether substrates behaved similarly, with $k_{cat}/K_M = 6.8 \times 10^5\ M^{-1}s^{-1}$ and $K_M = 3.2\ \mu M$ for **8.4a**, and $k_{cat}/K_M = 3.8 \times 10^5\ M^{-1}s^{-1}$ and $K_M = 4.9\ \mu M$ for **8.4b**. We conclude the AM ether modification does not greatly diminish the performance of these substrates *in vitro*.

8.4.5 Cellular imaging

Then, we assessed the utility of the AM ether-masked dyes in human cells. To determine whether these compounds could be unmasked by endogenous esterase activity,

we obtained confocal fluorescence microscopy images of live, unwashed HeLa cells incubated with fluorescein diacetate (**8.2a**; Fig. 8.2A), fluorescein diacetoxymethyl ether (**8.4a**; Fig. 8.2B), 2′,7′-difluorofluorescein diacetate (**8.2b**; Fig. 8.2C), or 2′,7′-difluorofluorescein diacetoxymethyl ether (**8.4b**; Fig. 8.2D). All four experiments produced bright cellular staining after 20 min, suggesting that each molecule is internalized and unmasked by cellular esterases. The overall brightness of the cells follows the *in vitro* enzymatic data—higher laser powers are required for AM ethers **8.4a** and **8.4b** to obtain comparable images. An exception to this trend is difluorofluorescein diacetate (**8.2b**) where the cellular fluorescence is similar to that of **8.2a**, which is a better esterase substrate. The poor chemical stability and high reactivity of **8.2b** could be the cause for this discrepancy. Under more intense illumination, cells incubated with the AM ethers **8.4a** and **8.4b** exhibit lower extracellular background fluorescence relative to cells with acetate esters **8.2a** and **8.2b** (data not shown). Accordingly, pro-fluorophores **8.4a** and **8.4b** could be useful in biological experiments where extracellular washing is either undesirable (*e.g.*, high-throughput screening) or impossible (*e.g.*, tissue and *in vivo* imaging).

8.4.6 Tokyo green acetoxymethyl ether

Based on the promising results from the fluorescein-based AM ether pro-fluorophores, we applied our strategy to other dyes, as shown in Schemes 8.2 and 8.3. Reaction of Tokyo Green (**8.5**) (Urano *et al.*, 2005) with bromomethyl acetate (**8.3**) in the presence of Hünig's base gave the desired AM ether **8.6** in good yield (Scheme 8.2). The

Tokyo Green acetate **8.7** was also prepared in 84% yield via microwave-assisted synthesis in neat acetic anhydride. Unlike fluorescein, the Tokyo Green molecule does not bear an *ortho* carboxyl group on its pendant phenyl ring, thus circumventing the complex lactone–quinoid equilibria. Instead, this electron-rich aromatic substituent facilitates photoinduced electron transfer (PeT) that quenches fluorescence when the xanthenyl moiety is protonated or alkylated.(Kobayashi *et al.*, 2007; Urano *et al.*, 2005) We reasoned that the acetoxymethyl ether strategy could suppress the fluorescence of this dye, providing a stable substrate that would be unmasked in a single step.

Evaluation of the stability of the Tokyo green-based pro-fluorophores was performed as with the other fluorescein-based pro-fluorophores. As expected, AM ether **8.6** proved to be more resistant to hydrolysis than acetate ester **8.7** in both DPBS (Fig. 8.3A) and DMEM–FBS (Fig. 8.3B). Tokyo Green derivative **8.6** underwent spontaneous hydrolysis somewhat faster than did the classic fluorescein derivatives **8.4a** and **8.4b**. Data from a longer incubation revealed AM ether **8.6** to have a half-life of 5 h in DMEM–FBS. Acetate ester **8.7** showed little chemical stability in this solution, having $t_{1/2} < 2$ min. Acetate ester **8.7** also acylated the hexapeptide readily, whereas AM ether **8.6** did not exhibit any appreciable reaction.

The Tokyo Green derivatives proved to be excellent substrates for PLE, giving kinetic constants of $k_{cat}/K_M = 3.2 \times 10^6\ M^{-1}s^{-1}$ and $K_M = 12\ \mu M$ for acetate ester **8.7**, and $k_{cat}/K_M = 4.2 \times 10^6\ M^{-1}s^{-1}$ and $K_M = 13\ \mu M$ for AM ether **8.6**. Pro-fluorophore **8.6** was also a substrate for esterases within living cells. We observed extensive unmasking of these probes by endogenous cellular esterases, resulting in the cellular fluorescence in

Fig. 8.3C. The overall brightness of the fluorescence in cells with pro-fluorophore **8.6** appears to be more localized and the overall staining less intense relative to the fluorescein derivatives. These distinctions could be due to a greater pH-sensitivity and increased lipophilicity of the released dye. Tokyo Green could partition into membranes and exist there in its protonated, less fluorescent form.

8.4.7 Resorufin acetoxymethyl ethers

Resorufin (**8.8**) exhibits excitation and emission wavelengths that are red-shifted relative to fluorescein (λ_{ex} = 572 nm, λ_{em} = 585 nm).(Bueno *et al.*, 2002) Substitution on the phenolic group of resorufin elicits a hypsochromic shift and a dramatic decrease in quantum yield. Alkylated and glycosylated variants of resorufin are used extensively as enzyme substrates.(Hofmann and Sernetz, 1984; Burke *et al.*, 1994) Based on this precedence, resorufin seemed to be a good candidate for the acetoxymethyl ether strategy.

We prepared pro-fluorophore **8.9** through both Ag_2O-mediated alkylation and phase-transfer conditions. We note the poor solubility of resorufin in organic solvents—a pernicious problem with this fluorophore—resulted in a low yield of 33% for the Ag(I)-mediated reaction. Phase-transfer conditions gave a significantly better yield of 73% (Scheme 8.3). The extra carboxyl group of 4-carboxyresorufin (**8.11**) alters the partitioning of the dye *in cellulo*.(Klein *et al.*, 1990) We subjected this dye to the AM ether strategy, using phase-transfer conditions to prepare the isomeric substrates **8.12** and **8.13** in 37 and 35% yield, respectively.

We examined the stability of AM ether **8.9** and commercial resorufin acetate (**8.10**). Pro-fluorophore **8.10** has long been recognized as an effective esterase substrate,(Kramer and Guilbault, 1964) but the utility of this compound is limited by its poor stability in aqueous solution.(Kitson, 1996) The chemical stability of resorufin derivatives **8.9** and **8.10** was similar to that of the Tokyo Green-based substrates, as expected from their similar structures. As with the other substrates, AM ether **8.9** exhibits higher stability than does acetate **8.10** in DPBS (Fig. 8.4A). In DMEM–FBS, the observed half-lives were 3 min and 2 h for substrates **8.10** and **8.9**, respectively (Fig. 8.4B). Following the trend of the previous substrates, compound **8.10** serves as an acyl donor for the lysine-containing peptide, whereas AM ether dyes **8.9** and **8.12** did not modify the peptide. Compounds **8.9** and **8.10** were substrates for an PLE *in vitro*. The kinetic constants were $k_{cat}/K_M = 3.1 \times 10^6\ M^{-1}s^{-1}$ and $K_M = 16\ \mu M$ for pro-fluorophore **8.10**, and $k_{cat}/K_M = 3.6 \times 10^6\ M^{-1}s^{-1}$ and $K_M = 21\ \mu M$ for pro-fluorophore **8.9**. These kinetic constants are similar to the other monosubstituted pro-fluorophores, **8.6** and **8.7**.

We exposed live human cells to pro-fluorophores **8.9** and **8.12**. The diminished autofluorescence at this longer excitation wavelength allowed lower substrate concentrations (2 μM) to be used relative to the green pro-fluorophores. Fluorescence microscopy imaging experiments with AM ether **8.9** showed only minor cellular fluorescence with substantial extracellular background (Fig. 8.4C). We suspect this background and low fluorescence *in cellulo* is due partly to the poor retention and chemical reduction(O'Brien *et al.*, 2000) of resorufin (**8.8**) within the cell. In contrast,

incubation with the same concentration of the carboxyresorufin derivative **8.12** resulted in bright red cellular staining with minimal background fluorescence (Fig. 8.4D), showcasing the effect of a single carboxylate moiety on the cellular retention and stability of this dye.

8.4.8 Conclusions

The insertion of simple oxygen–methylene group into a fluorophore ester endows molecules with high chemical stability, while maintaining enzymatic reactivity *in vitro* and *in cellulo*. We have discovered reaction conditions, such as the use of Ag(I) salts in acetonitrile or phase-transfer conditions, that enable the synthesis of problematic compounds such as fluorescein and resorufin derivatives in moderate yields. Importantly, we have shown this modification insulates the ester moiety from the fluorophore structure, allowing the stable masking of disparate dyes to create a portfolio of substrates with different chemical and spectroscopic properties.

Numerous applications are possible. For example, the distribution of esterases between the secretory pathway and cytosol is unknown,(Testa and Mayer, 2003) and these stable fluorogenic substrates could be used to map esterase activity within cells as well as tissues.(Boonacker *et al.*, 2004) Bioconjugation with derivatives of these compounds could facilitate biomolecular imaging experiments(Lavis *et al.*, 2006a) and substitution of the acetyl functionality with other acyl groups(Yang *et al.*, 2006) or even phosphoryl moieties(Golik *et al.*, 1996) could allow the construction of substrates for

disparate enzymes. Overall, this strategy could supplement or supplant fluorophore acetate esters, allowing sophisticated, facile assays for illuminating biological systems.

Acknowledgments. We are grateful to Z. J. Diwu, J. B. Binder, R. J. Johnson, and K. J. Kolonko for contributive discussions, and Alma Arnold for assistance with microscopy. L.D.L was supported by Biotechnology Training Grant 08349 (NIH) and an ACS Division of Organic Chemistry Fellowship sponsored by Genentech. T.-Y.C. was supported by the Dr. James Chieh-Hsia Mao Wisconsin Distinguished Graduate Fellowship. This work was supported by grant R01 CA073808 (NIH) and the Howard Hughes Medical Institute. NMRFAM was supported by grant P41 RR02301 (NIH).

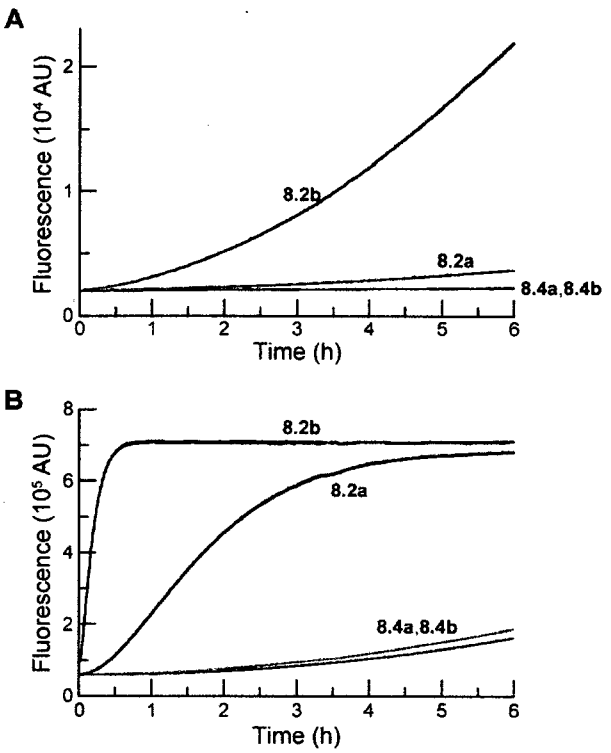

Figure 8.1 Stability of pro-fluorophores **8.2** and **8.4**.

Time course for the spontaneous generation of fluorescence (λ_{ex} 496 nm, λ_{em} 520 nm) from acetate esters **8.2a** and **8.2b** (25 nM), and AM ethers **8.4a** and **8.4b** (25 nM). (A) In DPBS. (B) In DMEM containing 10% v/v FBS.

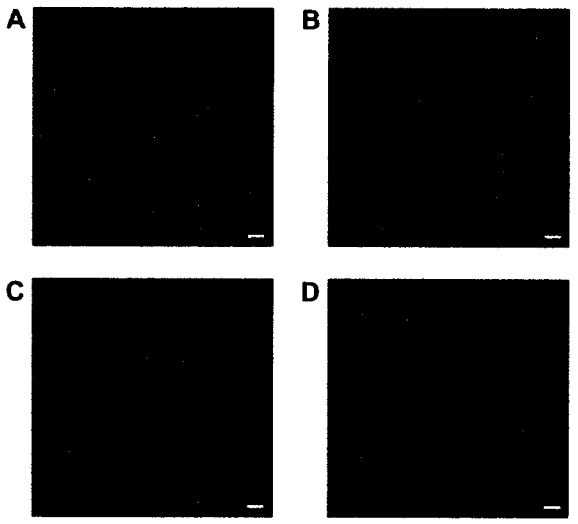

Figure 8.2 Unmasking of pro-fluorophores **8.2** and **8.4** in live human cells. Live, unwashed HeLa cells incubated with acetate esters **8.2a** and **8.2b**, AM ethers **8.4a** and **8.4b** (10 μM) in DMEM–FBS for 20 min and counterstained with Hoechst 33342 (5% v/v CO_2(g), 100% humidity). (A) Acetate ester **8.2a** (FDA); 1× laser power. (B) AM ether **8.4a**; 2× laser power. (C) Acetate ester **8.2b** (DFFDA); 1× laser power. (D) AM ether **8.4b**; 4× laser power. Scale bars: 10 μm.

Figure 8.3 Properties of Tokyo green-based pro-fluorophores.

Time course for the spontaneous generation of fluorescence (λ_{ex} 496 nm, λ_{em} 520 nm) from acetate ester **8.7** and AM ether **8.6** (25 nM). (A) In DPBS. (B) In DMEM containing 10% v/v FBS. (C) Live-cell imaging experiments with AM ether **8.6** (10 μM) incubated for 20 min in DMEM–FBS and counterstained with Hoechst 33342 (5% v/v CO_2(g), 100% humidity). Scale bar: 10 μm.

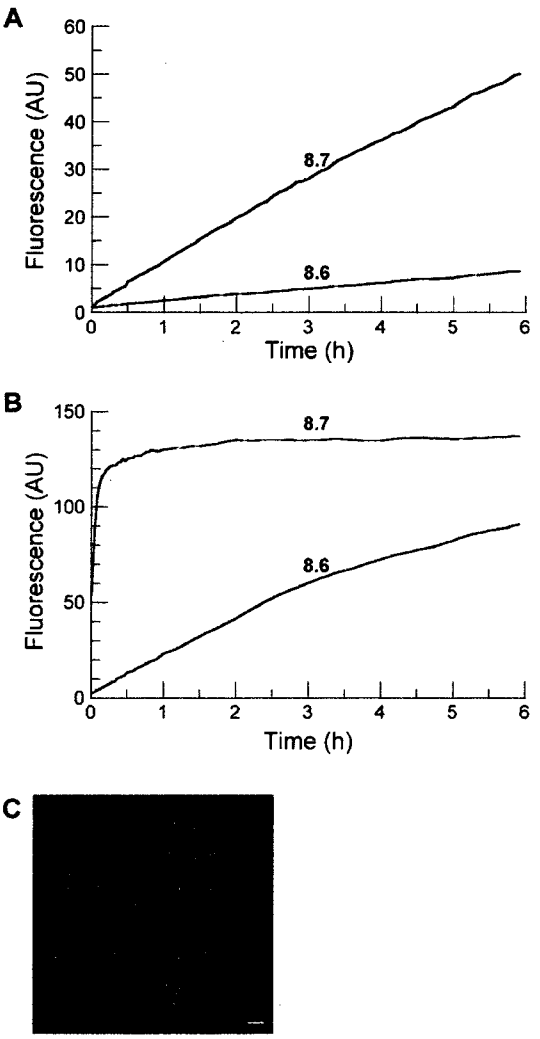
A
Fluorescence (AU)
60
50
40
30
20
10
0
8.7
8.6
0
1
2
3
4
5
6
Time (h)
B
Fluorescence (AU)
150
100
50
0
8.7
8.6
0
1
2
3
4
5
6
Time (h)
C

Figure 8.4 Properties of resorufin-based pro-fluorophores.

Time course for the spontaneous generation of fluorescence (λ_{ex} 572 nm, λ_{em} 585 nm) for acetate ester **8.10** and AM ether **8.9** (25 nM) in (A) DPBS and (B) DMEM containing 10% v/v FBS. (C) Live-cell imaging experiments with AM ether **8.9** (2 μM) incubated for 20 min and counterstained with Hoechst 33342 (5% v/v CO_2(g), 100% humidity). (D) Live-cell imaging experiments with AM ether **8.12** (2 μM) incubated for 20 min and counterstained with Hoechst 33342 (5% v/v CO_2(g), 100% humidity). Scale bars: 10 μm.

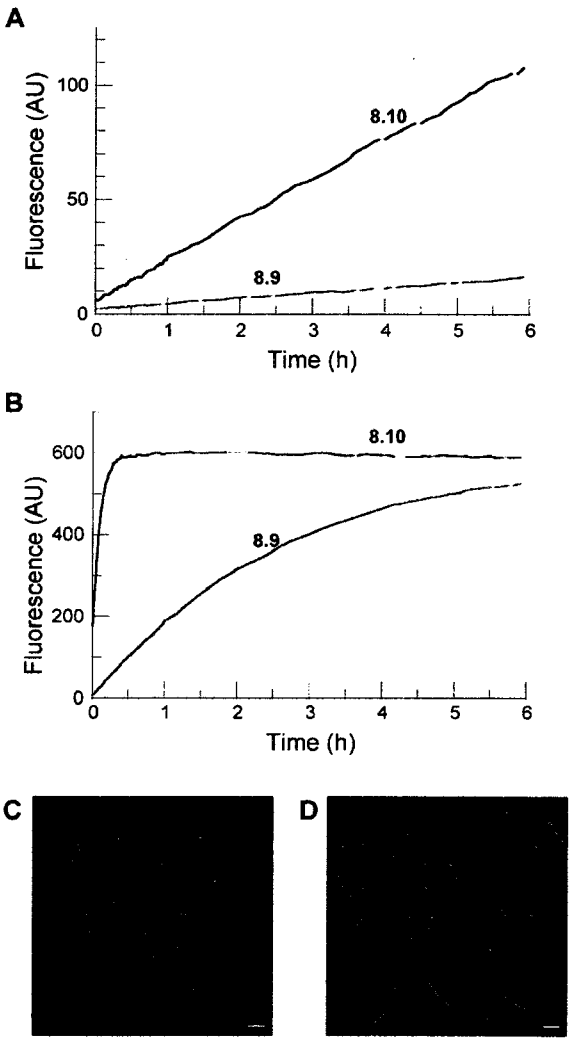
A
Fluorescence (AU)
100
50
0
8.10
8.9
0
1
2
3
4
5
6
Time (h)
B
Fluorescence (AU)
600
400
200
0
8.10
8.9
0
1
2
3
4
5
6
Time (h)
C
D

Scheme 8.1 Fluorescein-based pro-fluorophores.

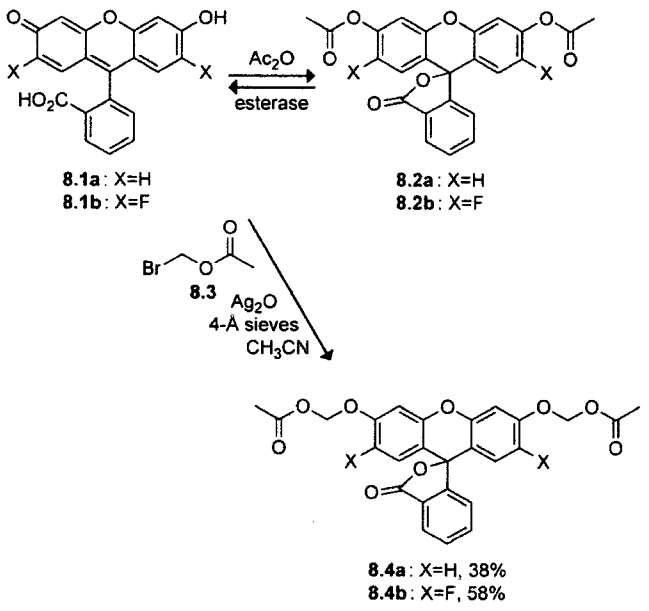

Scheme 8.2 Tokyo Green-based pro-fluorophores.

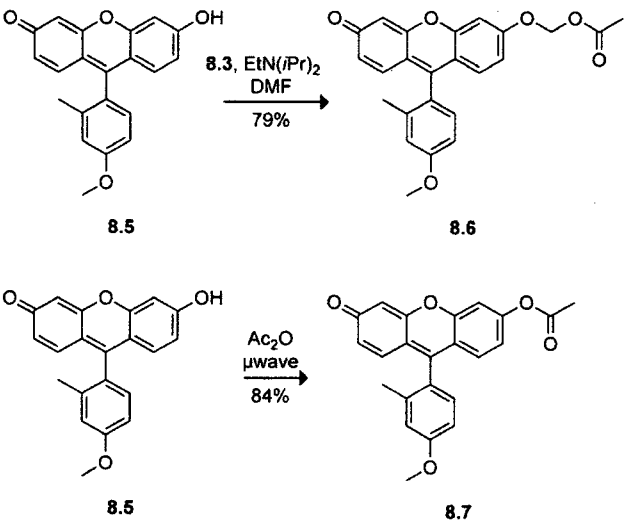

Scheme 8.3 Resorufin-based pro-fluorophores.

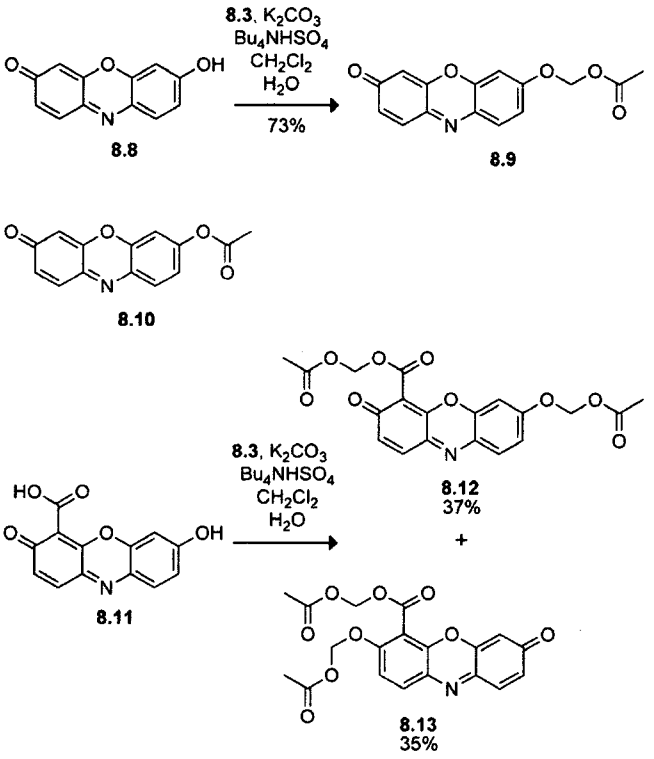

CHAPTER 9

A Highly Sensitive Fluorogenic Probe for Cytochrome P450 Activity in Live Cells

Contribution: Cellular studies and imaging. All other experiments were performed by M.M. Yatzeck.

This chapter was published as:
Yatzeck, M.M., Lavis, L.D., Chao, T.-Y., Chandran, S.S., and Raines, R.T. (2006) A highly sensitive fluorogenic probe for cytochrome P450 activity in live cells. *Bioorg. Med. Chem. Lett.* **7**, 5864–5866.

9.1 Abstract

A derivative of rhodamine 110 has been designed and assessed as a probe for cytochrome P450 activity. This probe is the first to utilize a "trimethyl lock" that is triggered by cleavage of an ether bond. *In vitro*, fluorescence was manifested by the CYP1A1 isozyme with $k_{cat}/K_M = 8.8 \times 10^3\ M^{-1}s^{-1}$ and $K_M = 0.09\ \mu M$. *In cellulo*, the probe revealed the induction of cytochrome P450 activity by the carcinogen 2,3,7,8-tetrachlorodibenzo-*p*-dioxin, and its repression by the chemoprotectant resveratrol.

9.2 Introduction

The cytochrome P450 (P450) family of enzymes is responsible for the oxidative metabolism of a wide variety of compounds, including chemotherapeutic agents and environmental toxins.(Ortiz de Montellano, 2005; Johnson, 2008; Gungerich, 2008) The catalytic activity of P450 enzymes controls the rate of xenobiotic metabolism, and can produce undesirable byproducts.(Nebert and Dalton, 2006) Originally, this activity had been assessed by using HPLC or other methods to separate and quantify metabolites. In the 1970's, 7-ethoxycoumarin and 7-ethoxyresorufin were introduced as the first fluorogenic substrates for assays of P450 activity.(Lavis and Raines, 2008; Burke and Mayer, 1974; Ullrich and Weber, 1972) Although these and other fluorogenic substrates have been used to assay P450 activity *in vitro* and enable assays *in cellulo*,(Burke *et al.*, 1983; White, 1988; Mayer *et al.*, 1990; Buters *et al.*, 1993; Ghosal *et al.*, 2003; Mayer *et*

al., 2007) they suffer from background fluorescence.(Wright and Cravatt, 2007) For example, alkoxycoumarins exhibit moderate fluorescence and are used frequently as fluorophores in peptidase substrates based on Forster resonance energy transfer (FRET).(Lesner *et al.*, 2008) In addition, both 7-ethoxyresorufin and resorufin fluoresce brightly.(Ghosal *et al.*, 2003) This problem arises because *O*-alkylation of the hydroxyl group of fluorophores such as coumarin and resorufin does little to deter the oxygen electrons from participating in the resonance that gives rise to fluorescence.

Here, we report on a superior small-molecule probe for assessing P450 activity. Our probe employs the trimethyl lock.(Levine *et al.*, 2008; Chandran *et al.*, 2005; Lavis *et al.*, 2006a; Lavis *et al.*, 2006b; Huang and Lin, 2006; Mangold *et al.*, 2008; Johnson *et al.*, 2007a) The trimethyl lock is an *o*-hydroxycinnamic acid derivative in which severe crowding of three methyl groups induces rapid lactonization to form a hydrocoumarin.(Milstein and Cohen, 1972; Borchardt and Cohen, 1972) In this strategy, the phenolic oxygen of the *o*-hydroxycinnamic acid is modified to create a functional group that is a substrate for a designated enzyme, and the carboxyl group is condensed with the amino group of a dye. Unmasking of the phenolic oxygen leads to rapid lactonization with concomitant release of the dye. An important attribute of this strategy is that the fluorescence/absorbance of the dye is masked completely by amidic resonance and the resulting lactonization within the rhodamine moiety.(Levine *et al.*, 2008; Chandran *et al.*, 2005; Lavis *et al.*, 2006a; Lavis *et al.*, 2006b; Huang and Lin, 2006)

9.3 Experimental Procedures

9.3.1 Instrumentation

NMR spectra were obtained with a Bruker DMX-400 Avance spectrometer (^{1}H, 400 MHz; ^{13}C, 100.6 MHz; ^{31}P, 161 MHz) at the National Magnetic Resonance Facility at Madison (NMRFAM). Carbon-13 spectra were proton-decoupled. Mass spectrometry was performed with a Micromass LCT (electrospray ionization, ESI) mass spectrometer in the Mass Spectrometry Facility in the Department of Chemistry. Fluorometric measurements were recorded with fluorescence grade quartz or glass cuvettes (Starna Cells) and a QuantaMaster1 photon-counting spectrofluorometer equipped for sample stirring (Photon Technology International). Cells were imaged with a Nikon Eclipse TE2000-U confocal microscope equipped with a Zeiss AxioCam digital camera.

9.3.2 Kinetics assays with purified enzyme

Kinetic parameters were determined by using microsomes that contained recombinant human cytochrome P450 CYP1A1 isozyme and human NADPH–P450 reductase (Sigma Chemical; product number C3735) as a suspension in 100 mM potassium phosphate buffer, pH 7.4. The enzyme was diluted in phosphate-buffered saline (PBS) before use. PBS (pH 7.4) contained (in 1.00 L) NaCl (8.0 g), KCl (2.0 g), $Na_2HPO_4 \cdot 7H_2O$ (1.15 g), KH_2PO_4 (2.0 g), and NaN_3 (0.10 g).

Kinetic assays were conducted at 37 °C by fluorometric detection of morpholinourea–Rh_{110} (**9.6**) using excitation and emission wavelengths of 496 and 520 nm, respectively. The reaction mixture (2.00 mL) contained 10 μL of a 0.5 pmol/mL

solution of enzyme, 10 μL of 0.8 M $MgCl_2$, 10 μL of 0.8 M NADPH, and 10 μL of a solution of morpholinourea–Rh_{110} trimethyl lock (**9.1**) (final concentration: 0.0624–1.00 mM) in PBS. The reaction was initiated by the addition of substrate, and the reaction rate was quantified by comparison to the fluorescence of solutions containing known concentrations of morpholinourea–Rh_{110} (**9.6**). Values of k_{cat}/K_M and K_M were calculated by standard methods.

9.3.3 Cell culture and imaging

Human lung adenocarcinoma cell line A549 was obtained from the American Type Culture Collection (Rockville, MD). Cells were cultured at 37 °C in medium supplemented with fetal bovine serum (10% v/v) and antibiotics, and in the presence of CO_2(g) (5% v/v). Nearly confluent cells were seeded in 8-well chambers and allowed to grow for 24 h. Cells were then incubated for 1 h after the addition of morpholinourea–Rh_{110} trimethyl lock (**9.1**) (to 10 μM), TCDD (to 10 nM), and resveratrol (to 50 μM). Hoechst 33342 nuclear stain was added 5 min prior to the end of the incubation time and before imaging. In pilot experiments, a range of TCDD, resveratrol, and morpholinourea–Rh_{110} trimethyl lock (**9.1**) concentrations were tested. The concentrations chosen for the actual studies were the ones causing substantial induction or inhibition without detectable cytotoxicity.

9.4 Results and Discussion

We suspected that the trimethyl lock could provide the basis for a useful probe for CYP1A1 activity. As a dye, we chose a morpholino urea derivative of rhodamine 110 (Rh_{110}) that is bright ($\varepsilon \times \Phi = 2.38 \times 10^4\ M^{-1}cm^{-1}$) but has no measurable fluorescence after *N*-acylation.(Lavis *et al.*, 2006a) We installed an ethyl group on the phenolic oxygen of the trimethyl lock because ethyl ethers are especially effective substrates for CYP1A1.(Liu *et al.*, 2003) The synthetic route to fluorogenic probe **9.1** is shown in Fig. 9.1. Briefly, known intermediate **9.2** (Nicolaou *et al.*, 1996) was alkylated with diethyl sulfate to give ethyl ether **9.3**. Removal of the silyl group followed by Jones oxidation afforded carboxylic acid **9.5**. Condensation with urea–rhodamine **9.6** gave fluorogenic probe **9.1** in 5% overall yield.

Fluorogenic probe **9.1** was first assayed as a substrate for human CYP1A1 *in vitro*. Fluorogenesis was rapid, with $k_{cat}/K_M = 8.8 \times 10^3\ M^{-1}s^{-1}$ and $K_M = 0.09\ \mu M$ (Fig. 9.2A). These values are comparable to the highest values obtained with other fluorogenic substrates.(Ortiz de Montellano, 2005; Johnson, 2008; Gungerich, 2008) These data are the first to demonstrate that the trimethyl lock can be activated by the cleavage of an ether bond.

Next, fluorogenic probe **9.1** was assayed as a substrate for CYP1A1 in live human cells. These experiments employed human lung adenocarcinoma cell line A549, which is especially well suited for studying the expression of the pulmonary CYP

system.(Hukkanen *et al.*, 2000; Urani *et al.*, 1998) A low but observable level of CYP1A1 was apparent after a 1-h incubation with fluorogenic probe **9.1** (Fig. 9.2B).

Then, fluorogenic probe **9.1** was evaluated as a means to detect an increase in CYP1A1 levels. To do so, A549 cells were incubated with 2,3,7,8-tetrachlorodibenzo-*p*-dioxin (TCDD; 10 nM), which is the notorious contaminant in the herbicide Agent Orange and the most potent known inducer of CYP1A1.(Whitlock, 1999) The effect of TCDD on fluorogenesis within A549 cells was dramatic (Fig. 9.2C).

Finally, fluorogenic probe **9.1** was used to reveal a more complex modulation of P450 activity. Levels of P450 are highly variable in individuals, and there are many known P450 polymorphisms.(Murray and Petrovic, 2006; Ingelman-Sundberg *et al.*, 2007) Inhibitors of P450 activity have potential as chemotherapeutic agents.(Schuster and Bernhardt, 2007) For example, resveratrol (3,5,4′-trihydroxystilbene), which is a natural phytoalexin present in grapes and other foods, has been proposed to have a chemoprotective effect against lung cancer by virtue of its ability to decrease CYP1A1 activity.(Mollerup *et al.*, 2001; Chen *et al.*, 2004; Ciolino *et al.*, 1998) To test this hypothesis with fluorogenic probe **9.1**, live A549 cells were treated with both TCDD and resveratrol, along the probe. After a 1-h incubation, cells exhibited a dramatic decrease in fluorescence compared with cells treated with TCDD (Fig. 9.2D). The levels appeared to be even lower than those in untreated cells. These and other data(Mollerup *et al.*, 2001; Chen *et al.*, 2004; Ciolino *et al.*, 1998) provide direct and conclusive evidence that resveratrol decreases CYP1A1 activity *in cellulo*.

In conclusion, fluorogenic probe **9.1** is the first to utilize a "trimethyl lock" that is triggered by cleavage of an ether bond. This probe has numerous desirable attributes. Its chemical and photophysical properties allow for real-time imaging of P450 levels *in cellulo*. The modularity of this probe enables its extension to enzymes throughout the P450 family, and its success indicates that the trimethyl lock strategy can be applied to P450-activated prodrugs. Finally, appending the urea group with a trichloromethyl ketone or other weak electrophile would allow the probe to react with an intracellular thiol and enable its retention within a cell, providing additional utility.(Haugland *et al.*, 2005)

Acknowledgements. This paper is dedicated to Professor Benjamin F. Cravatt on the occasion of his winning the 2008 Tetrahedron Young Investigator Award. This work was supported by grant CA073808 (NIH). NMRFAM was supported by grant P41 RR02301 (NIH). M.M.Y. was a Pfizer Undergraduate Summer Fellow in Chemistry and a Hilldale Undergraduate/Faculty Research Fellow. L.D.L was supported by Biotechnology Training Grant 08349 (NIH) and an ACS Division of Organic Chemistry Graduate Fellowship sponsored by the Genentech Foundation. T.-Y.C. was supported by the Dr. James Chieh-Hsia Mao Wisconsin Distinguished Graduate Fellowship.

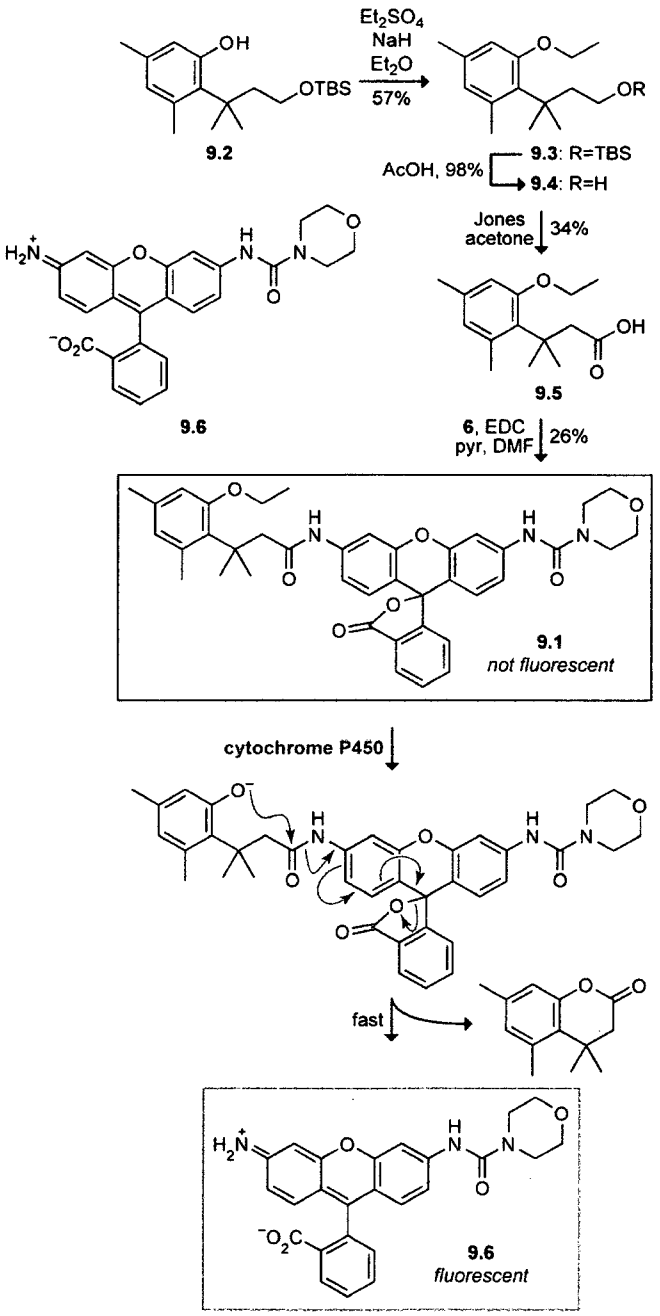

Figure 9.1 Scheme for the synthesis and use of fluorogenic probe **9.1**.

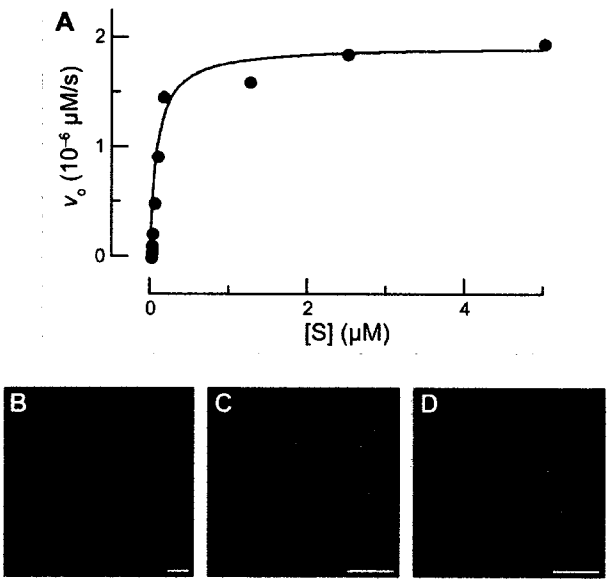

Figure 9.2 Fluorogenesis from fluorogenic probe **9.1** *in vitro* and *in cellulo*. (A) Data for the *in vitro* cleavage of fluorogenic probe **1** by human CYP1A1 (5.0 pM) in PBS containing NADPH (8 mM) and $MgCl_2$ (8 mM). (B–D) Images of the *in cellulo* cleavage of fluorogenic probe **1**. A549 cells were incubated with fluorogenic probe **9.1** (10 μM) and an additive for 1 h and counterstained with Hoechst 33342. (B) No additive. (C) TCDD (10 nM). (D) TCDD (10 nM) and resveratrol (50 μM). Scale bars: 10 μm.

CHAPTER 10

Future Directions

10.1 Cytotoxic mechanism of ONC

ONC is a promising chemotherapeutic agent for the treatment of malignant mesothelioma, an aggressive cancer with no known cure (Lee and Raines, 2008; Lee, 2008). Being granted fast-track status and orphan drug designation after undergoing several Phase III clinical trials (Rutkoski and Raines, 2008), ONC is the most advanced ribonuclease-based therapeutic currently in clinical development. Despite the proven anticancer properties of ONC (Lee *et al.*, 2000), the fundamental mechanisms underlying its cytotoxic actions have not been fully delineated.

ONC-mediated RNA degradation appears to result in the activation of a multitude of signaling cascades. In addition to activating the p53-independent apoptotic pathway involving caspase-9, -3, and -7 (Iordanov *et al.*, 2000a), ONC treatment has been associated with the phosphorylation and activation of JUK1, JUK2, p38MAP, and PI3K/Akt (Iordanov *et al.*, 2000b; Ramos-Nino *et al.*, 2005). Induction of caspase-independent apoptosis through activating autophagic pathways has also been demonstrated in neuroblastoma cells (Lee, 2008). Furthermore, ONC-induced changes in gene expression profile were recently examined in human mesothelioma cells, and MAPK signaling, cytokine-cytokine receptor interactions, and Jak-STAT signaling were shown to be up-regulated (Altomare *et al.*, 2010). Although the activation of these signal transduction pathways furthers our understanding of cellular responses to ONC treatment, the molecular interactions leading to these responses need to be further explored to fully understand the cytotoxic action of ONC.

In a study comparing the cytotoxicity of ONC and RNase A variants towards a variety of human cancer cell lines, ONC was found to be 2–30-fold more toxic than DRNG RNase A, the most toxic RNase A variant (Rutkoski *et al.*, 2005). As discussed in CHAPTER 2, the exceptional toxicity displayed by ONC cannot be explained by its internalization properties. Translocation efficiency of ONC, as demonstrated in CHAPTER 4, was not significantly different from that of RNase A. These results rule out the possibility of ONC adopting a more effective cellular entry route in comparison to RNase A. It is therefore likely that the ability to induce certain signaling pathways provides an advantage in ribonuclease-mediated cytotoxicity and differentiates ONC from RNase A variants. Screening cellular factors essential in ribonuclease-mediated cytotoxicity is key to the understanding of the mechanism of cytotoxic ribonucleases.

10.2 Basis for cancer cell selectivity

Several cytotoxic ribonucleases demonstrate selective toxicity towards cancer cells in *vitro* and *in vivo* (Youle and D'Alessio, 1997). Differences between cancer and noncancer cells, including replication rate, display of cell-surface anionic glycans, and membrane composition, have been proposed to be factors leading to disparate susceptibilities to ribonuclease attack.

To determine the basis for cancer cell specificity, the cytotoxic actions of ribonucleases have been examined in matching cancerous and noncancerous cells. For example, differential intracellular routing in immortalized and transformed mouse

fibroblasts have been observed for BS-RNase (Bracale *et al.*, 2002). Also, ONC was reported to activate a proapoptotic pathway specific to primary cells that had been immortalized with human papilloma virus (HPV 16) gene products E6 and E7 (Iordanov *et al.*, 2000b). Indeed, cellular trafficking and specific signal transduction pathways in cancer cells could be targets of cytotoxic ribonucleases. Nevertheless, no experimental evidence suggests these factors directly lead to selective toxicity mediated by ribonucleases.

Cytotoxic ribonucleases have been proposed to target cancer cells at the cell surface—by forming more favorable Coulombic interaction with cancer cell surfaces, which are more anionic than those of noncancer cells (Benito *et al.*, 2005). The relationship between cell-surface anionicity and ribonuclease cell-surface binding, internalization, and toxicity was determined and described in CHAPTER 2. Consistent with this hypothesis, RNase A was found to have higher affinity towards more anionic cancer cells. However, differential internalization rates of cancer and noncancer cells, which was less than 10-fold different between wild-type and mutant CHO cells, does not fully account for the therapeutic index observed for RNase A in other studies (~100–500 fold difference in cytotoxicity) (Rutkoski *et al.*, 2005). In addition to cell-surface anionicity, the contribution of other factors such as substrate specificity and membrane composition must be further explored. In particular, the translocation efficiency of cytotoxic ribonucleases could be compared between cancer and noncancer cells using the translocation assay described in CHAPTER 4.

10.3 Further improvement and application of the fluorescence-based translocation assay

Endosomal escape is a prerequisite for many intracellularly targeted peptide-, protein-, oligonucleotide-, and polymer-based macromolecular therapeutic agents. Hence, the ability to monitor endosomal translocation *in cellulo* is highly valuable to pharmaceutical development. As outlined in CHAPTER 4, we have devised a β-galactosidase-based fluorescence assay for measuring endosomal translocation in live human cells, in which molecules tagged with latent fluorogenic substrates of β-galactosidase are only visualized in the cytoplasm of *lacZ*$^+$ cells. The utility of this translocation assay was demonstrated by the quantification of the cytosolic delivery of ribonucleases, which are representatives of protein-based drugs. Furthermore, the applicability of this assay is not limited to peptides or proteins—fluorescein di-β-D-galactopyranoside (FDG) can be modified with other functional groups such as an azide or an N-hydroxysuccimide for conjugation with oligonucleotides and polymers. In addition to ONC and RNase A, the translocation efficiency of other monomeric and oligomeric cytotoxic ribonucleases can be compared in the same cell line to establish determinants essential in ribonuclease translocation, as well as in matched cancer and noncancer cell lines to determine if differential translocation contributes to therapeutic index. Moreover, chemicals and peptides can be screened for their ability to enhance translocation in a high-throughput fashion.

The β-galactosidase-based translocation assay could be further optimized with respect to background fluorescence levels in several ways. Although the short hairpin antisense RNA construct reduced the expression of human β-galactosidase (*GLB1*) in lysosomes, a low level of background was still observed, indicating that the latent fluorophore was activated by β-galactosidase activity prior to entering the cytoplasm. The source of β-galactosidase activity could be residual endogenous β-galactosidase expression, in which case the use of a *GLB1*$^-$ cell line or a more orthogonal enzyme–substrate pair will further lower background fluorescence. Alternatively, because potent transfection reagents such as Lipofectamine 2000 are moderately toxic to cells and could result in cell death through lysis and apoptosis, the media could contain β-galactosidases there were from compromised cells, which could activat latent fluorophore conjugates even before they enter cells. Creating cell lines stably transfected with all constructs through a viral transfection protocol is expected to greatly reduce premature latent fluorophore activation in conditioned culture media.

10.4 Interaction between mammalian ribonucleases and RI *in cellulo*

The use of latent fluorescence technology can be expanded to examine complex-formation between mammalian ribonucleases and RI in live cells. This could be achieved by biomolecular fluorescence complementation, which involves the reconstitution of fluorescence upon association of fragments of a fluorescent protein (Hu *et al.*, 2002). For example, complementary fragments of the enhanced yellow fluorescent protein could be attached to a ribonuclease and RI such that fluorescence is reconstituted upon formation

of the complex. As the complex dissociation rate is extremely slow (Johnson *et al.*, 2007d), such an approach allows long-term monitoring of the fate of the complexes including potential colocalization with other cellular factors. Alternatively, fluorescence resonance energy transfer could be utilized to visualize or quantify complex-formation *in cellulo*. Since the role(s) of RI in several ribonucleases-mediated processes, such as angiogenesis, have not been fully elucidated, a sensitive method for detecting ribonuclease–RI complexes could shed light on the biological roles of RI and mammalian ribonucleases.

REFERENCES

Abel, R. L., Haigis, M. C., Park, C. and Raines, R. T. (2002). Fluorescence assay for the binding of ribonuclease A to the ribonuclease inhibitor protein. *Anal. Biochem.* **306**, 100–107.

Ackerman, S. J., Loegering, D. A., Venge, P., Olsson, I., Harley, J. B., Fauci, A. S. and Gleich, G. J. (1983). Distinctive cationic proteins of the human eosinophil granule: Major basic protein, eosinophil cationic protein, and eosinophil-derived neurotoxin. *J. Immunol.* **131**, 2977–2982.

Adams, S. R. and Tsien, R. Y. (2006). Imaging the influx of cell-penetrating peptides into the cytosol of individual live cells. Handbook of Cell-Penetrating Peptides *(2nd edition)*, (ed. U. Langel), pp. 505–512.

Agarraberes, F. A. and Dice, J. F. (2001). Protein translocation across membranes. *Biochim. Biophys. Acta, Biomembr.* **1513**, 1–24.

Altomare, D. A., Rybak, S. M., Pei, J. M., Maizel, J. V., Cheung, M., Testa, J. R. and Shogen, K. (2010). Onconase responsive genes in human mesothelioma cells: implications for an RNA damaging therapeutic agent. *BMC Cancer* **10**:34.

Alvarez-Salas, L. M. (2008). Nucleic acids as therapeutic agents. *Curr. Top. Med. Chem.* **8**, 1379–1404.

Amsberry, K. L., Gerstenberger, A. E. and Borchardt, R. T. (1991). Amine prodrugs which utilize hydroxy amide lactonization. II. A potential esterase-sensitive amide prodrug. *Pharm. Res.* **8**, 455–461.

Arnold, U. (2008). Aspects of the cytotoxic action of ribonucleases. *Curr. Pharm. Biotechnol.* **9**, 1615–1622.

Arnold, U. and Ulbrich-Hofmann, R. (2006). Natural and engineered ribonucleases as potential cancer therapeutics. *Biotechnol. Lett.* **28**, 1615–1622.

Aslam, M. and Dent, A. (1998). Bioconjugation: Protein Coupling Techniques for the Biomedical Sciences. London: Macmillan Reference.

Babiak, P. and Reymond, J.-L. (2005). A high-throughput, low-volume enzyme assay on solid support. *Anal. Chem.* **77**, 373–377.

Badet, J., Soncin, F., Guitton, J. D., Lamare, O., Cartwright, T. and Barritault, D. (1989). Specific binding of angiogenin to calf pulmonary-artery endothelial-cells. *Proc. Natl. Acad. Sci. U. S. A.* **86**, 8427–8431.

Baeyer, A. (1871). Ueber eine neue Klasse von Farbstoffen. *Ber. Dtsch. Chem. Ges.* **4**, 555–558.

Banny, T. M. and Clark, G. (1950). The new domestic cresyl echt violet. *Stain Technol.* **25**, 195–196.

Bayer, N., Schober, D., Huttinger, M., Blaas, D. and Fuchs, R. (2001). Inhibition of clathrin-dependent endocytosis has multiple effects on human rhinovirus serotype 2 cell entry. *J. Biol. Chem.* **276**, 3952–3962.

Bednar, R. A. (1990). Reactivity and pH dependence of thiol conjugation to *N*-ethylmaleimide: Detection of a conformational change in chalcone isomerase. *Biochemistry* **29**, 3684–3690.

Beintema, J. J., Schüller, C., Irie, M. and Carsana, A. (1988). Molecular evolution of the ribonuclease superfamily. *Prog. Biophys. Molec. Biol.* **51**, 165–192.

Benito, A., Ribó, M. and Vilanova, M. (2005). On the track of antitumor ribonucleases. *Mol. Biosyst.* **1**, 294–302.

Benito, A., Vilanova, M. and Ribo, M. (2008). Intracellular routing of cytotoxic pancreatic-type ribonucleases. *Curr. Pharm. Biotechnol.* **9**, 169–179.

Bensel, N., Reymond, M. T. and Reymond, J.-L. (2001). Pivalase catalytic antibodies: Towards abzymatic activation of prodrugs. *Chem. Eur. J.* **7**, 4604–4612.

Bergsdorf, C., Beyer, C., Umansky, V., Werr, M. and Sapp, M. (2003). Highly efficient transport of carboxyfluorescein diacetate succinimidyl ester into COS7 cells using human papillomavirus-like particles. *FEBS Lett.* **536**, 120–124.

Blixt, O., Head, S., Mondala, T., Scanlan, C., Huflejt, M. E., Alvarez, R., Bryan, M. C., Fazio, F., Calarese, D., Stevens, J. et al. (2004). Printed covalent glycan array for ligand profiling of diverse glycan binding proteins. *Proc. Natl. Acad. Sci. U. S. A.* **101**, 17033–17038.

Blow, N. (2009). Small RNAs: biology's brave new world. *Nat. Methods* **6**, 231–234.

Bodor, N., Sloan, K. B., Kaminski, J. J., Shih, C. and Pogany, S. (1983). A convenient synthesis of (acyloxy)alkyl a-ethers of phenols. *J. Org. Chem.* **48**, 5280–5284.

Boonacker, E., Elferink, S., Bardai, A., Fleischer, B. and Van Noorden, C. J. F. (2003). Fluorogenic substrate [Ala-Pro]2-cresyl violet but not ala-pro-rhodamine 110 is cleaved specifically by DPPIV activity: A study in living Jurkat cells and CD26/DPPIV-transfected Jurkat cells. *J. Histochem. Cytochem.* **51**, 959–968.

Boonacker, E., Stap, J., Koehler, A. and Van Noorden, C. J. F. (2004). The need for metabolic mapping in living cells and tissues. *Acta Histochem.* **106**, 89–96.

Borchardt, R. T. and Cohen, L. A. (1972). Stereopopulation control. II. Rate enhancement of intramolecular nucleophilic displacement. *J. Am. Chem. Soc.* **94**, 9166–9174.

Bosch, M., Benito, A., Ribó, M., Puig, T., Beaumelle, B. and Vilanova, M. (2004). A nuclear localization sequence endows human pancreatic ribonuclease with cytotoxic activity. *Biochemistry* **43**, 2167–2177.

Bräse, S., Gil, C., Knepper, K. and Zimmermann, V. (2005). Organic azides: An exploding diversity of a unique class of compounds. *Angew. Chem. Int. Ed. Engl.* **44**, 5188–5240.

Bracale, A., Spalletti-Cernia, D., Mastronicola, M., Castaldi, F., Mannucci, R., Nitsch, L. and D'Alessio, G. (2002). Essential stations in the intracellular pathway of cytotoxic bovine seminal ribonuclease. *Biochem. J.* **362**, 553–560.

Bretscher, L. E., Abel, R. L. and Raines, R. T. (2000). A ribonuclease A variant with low catalytic activity but high cytotoxicity. *J. Biol. Chem.* **275**, 9893–9896.

Brooks, H., Lebleu, B. and Vives, E. (2005). Tat peptide-mediated cellular delivery: back to basics. *Adv. Drug Deliv. Rev.* **57**, 559–577.

Bueno, C., Villegas, M. L., Bertolotti, S. G., Previtali, C. M., Neumann, M. G. and Encinas, M. V. (2002). The excited-state interaction of resazurin and resorufin with amines in aqueous solutions. Photophysics and photochemical reaction. *Photochem Photobiol* **76**, 385–390.

Burke, M. D. and Mayer, R. T. (1974). Ethoxyresorufin—direct fluorimetric assay of a microsomal *O*-dealkylation which is preferentially inducible by 3-methylcholanthrene. *Drug Metab. Dispos.* **2**, 583–588.

Burke, M. D., Murray, G. I. and Lees, G. M. (1983). Fluorescence-microscopic measurement of intracellular cytochrome P-450 enzyme activity (ethoxyresorufin *O*-de-ethylation) in unfixed liver section. *Biochem. J.* **212**, 15–24.

Burke, M. D., Thompson, S., Weaver, R. J., Wolf, C. R. and Mayer, R. T. (1994). Cytochrome P450 specificities of alkoxyresorufin *O*-dealkylation in human and rat liver. *Biochem. Pharmacol.* **48**, 923–936.

Buters, J. T., Schiller, C. D. and Chou, R. C. (1993). Direct fluorescence monitoring of the deethylation of 7-ethoxy-4-trifluoromethylcoumarin. *Biochem. Pharmacol.* **46**, 1577–1584.

Cai, S. X., Zhang, H.-Z., Guastella, J., Drewe, J., Yang, W. and Weber, E. (2001). Design and synthesis of rhodamine 110 derivative and caspase-3 substrate for enzyme and cell-based fluorescent assay. *Bioorg. Med. Chem. Lett.* **11**, 39–42.

Calnan, B. J., Tidor, B., Biancalana, S., Hudson, D. and Frankel, A. D. (1991). Arginine-mediated RNA recognition—the arginine fork. *Science* **252**, 1167–1171.

Cao, H., Chen, J., Awoniyi, M., Henley, J. R. and McNiven, M. A. (2007). Dynamin 2 mediates fluid-phase micropinocytosis in epithelial cells. *J. Cell Sci.* **120**, 4167–4177.

Carreras, E., Boix, E., Rosenberg, H. F., Cuchillo, C. M. and Nogues, M. V. (2003). Both aromatic and cationic residues contribute to the membrane-lytic and bactericidal activity of eosinophil cationic protein. *Biochemistry* **42**, 6636–6644.

Chandran, S. S., Dickson, K. A. and Raines, R. T. (2005). Latent fluorophore based on the trimethyl lock. *J. Am. Chem. Soc.* **127**, 1652–1653.

Chao, T.-Y., Lavis, L. D. and Raines, R. T. (2010). Contribution of anionic glycans to the cellular uptake of ribonucleases. *(Submitted).*

Charlwood, J., Birrell, H., Tolson, D. and Camilleri, P. (1998). Two-dimensional chromatography in the analysis of complex glycans from transferrin. *Anal. Chem.* **70**, 2530–2535.

Chauhan, A., Tikoo, A., Kapur, A. K. and Singh, M. (2006). The taming of the cell penetrating domain of the HIV TAT: Myths and realities. *J. Controlled Release* **117**, 148–162.

Chen, X. and Varki, A. (2010). Advances in the biology and chemistry of sialic acids. *ACS Chem. Biol.* **5**, 163–176.

Chen, Z.-H., Hurh, Y.-J., Na, H.-K., Kim, J.-H., Chun, Y.-J., Kim, D.-H., Kang, K.-S., Cho, M.-H. and Surh, Y.-J. (2004). Resveratrol inhibits TCDD-induced expression of CYP1A1 and CYP1B1 and catechol estrogen-mediated oxidative DNA damage in cultured human mammary epithelial cells. *Carcinogenesis* **25**, 2005–2013.

Cheung, J. C., Chiaw, P. K., Deber, C. M. and Bear, C. E. (2009). A novel method for monitoring the cytosolic delivery of peptide cargo. *J. Controlled Release* **137**, 2–7.

Cho, W. and Stahelin, R. V. (2005). Membrane-protein interactions in cell signaling and membrane trafficking. *Annu. Rev. Biophys. Biomol. Struct.* **34**, 119–151.

Ciolino, H. P., Daschner, P. J. and Yeh, G. C. (1998). Resveratrol inhibits transcription of CYP1A1 in vitro by preventing activation of the aryl hydrocarbon receptor. *Cancer Res.* **58**, 5707–5712.

Conner, S. D. and Schmid, S. L. (2003). Regulated portals of entry into the cell. *Nature* **422**, 37–44.

Corrie, J. E. T., Craik, J. S. and Munasinghe, V. R. N. (1998). A homobifunctional rhodamine for labeling proteins with defined orientations of a fluorophore. *Bioconjugate Chem.* **9**, 160–167.

Costanzi, J., Sidransky, D., Navon, A. and Goldsweig, H. (2005). Ribonucleases as a novel pro-apoptotic anticancer strategy: Review of the preclinical and clinical data for ranpirnase. *Cancer Invest.* **23**, 643–650.

Crespo, P. M., Zurita, A. R., Giraudo, C. G., Maccioni, H. J. and Daniotti, J. L. (2004). Ganglioside glycosyltransferases and newly synthesized gangliosides are excluded from detergent-insoluble complexes of Golgi membranes. *Biochem. J.* **377**, 561–568.

Cronican, J. J., Thompson, D. B., Beier, K. T., McNaughton, B. R., Cepko, C. L. and Liu, D. R. (2010). Potent delivery of functional proteins into mammalian cells in vitro and in vivo using a supercharged protein. *ACS Chem. Biol.* **5**, xxx–xxx.

Culling, C. F. A., Allison, R. T., Barr, W. T. and Culling, C. F. A. (1985). Cellular Pathology Technique. Boston: Butterworths.

Curtius, T. (1890). Ueber Stickstoffwasserstoffsäure (Azoimid) N_3H. *Ber. Dtsch. Chem. Ges.* **23**, 3023–3033.

Curtius, T. (1894). Hydrazide und Azide organischer Säuren. *J. Prakt. Chem.* **50**, 275–294.

D'Alessio, G. and Riordan, J. F. (1997). Ribonucleases: Structures and Functions. New York: Academic Press.

Damke, H., Baba, T., Vanderbliek, A. M. and Schmid, S. L. (1995). Clathrin-independent pinocytosis induced in cells overexpressing a temperature-sensitive mutant of dynamin. *J. Cell Biol.* **131**, 69–80.

Dan, S., Tsunoda, T., Kitahara, O., Yanagawa, R., Zembutsu, H., Katagiri, T., Yamazaki, K., Nakamura, Y. and Yamori, T. (2002). An integrated database of chemosensitivity to 55 anticancer drugs and gene expression profiles of 39 human cancer cell lines. *Cancer Res.* **62**, 1139–1147.

Darzynkiewicz, Z., Carter, S. P., Mikulski, S. M., Ardelt, W. J. and Shogen, K. (1988). Cytostatic and cytotoxic effect of Pannon (P-30 Protein), a novel anticancer agent. *Cell Tissue Kinet.* **21**, 169–182.

Descalzo, A. B., Rurack, K., Weisshoff, H., Martinex-Manez, R., Marcos, M. D., Amoros, P., Hoffmann, K. and Soto, J. (2005). Rational design of a chromo- and fluorogenic hybrid chemosensor material for the detection of long-chain carboxylates. *J. Am. Chem. Soc.* **127**, 184–200.

Deutscher, M. P. (1988). The metabolic role of RNases. *Trends in Biochem. Sci.* **13**, 136–139.

Deutscher, M. P. and Li, Z. W. (2001). Exoribonucleases and their multiple roles in RNA metabolism. *Prog. Nucleic Acid Res. Mol. Biol.* **66**, pp. 67–105.

Deutscher, S. L., Nuwayhid, N., Stanley, P., Briles, E. I. B. and Hirschberg, C. B. (1984). Translocation across Golgi vesicle membranes: A CHO glycosylation mutant deficient in CMP-sialic acid transport. *Cell* **39**, 295–299.

Dharmawardhane, S., Schurmann, A., Sells, M. A., Chernoff, J., Schmid, S. L. and Bokoch, G. M. (2000). Regulation of macropinocytosis by p21-activated kinase-1. *Mol. Biol. Cell* **11**, 3341–3352.

Dickson, K. A., Dahlberg, C. L. and Raines, R. T. (2003). Compensating effects on the cytotoxicity of ribonuclease A variants. *Arch. Biochem. Biophys.* **415**, 172–177.

Dickson, K. A., Haigis, M. C. and Raines, R. T. (2005). Ribonuclease inhibitor: structure and function. *Prog. Nucleic Acid Res. Mol. Biol.* **80**, 349–374.

Diwu, Z., Liao, J. and Wang, Z. (2003). Preparation of rhodamine peptide derivatives as luminogenic protease substrates, pp. 64. WO Patent Application: (Molecular Devices Corporation, USA).

Doherty, G. J. and McMahon, H. T. (2009). Mechanisms of Endocytosis. *Annu. Rev. Biochem.* **78**, 857–902.

Domachowske, J. B. and Rosenberg, H. F. (1997). Eosinophils inhibit retroviral transduction of human target cells by a ribonuclease-dependent mechanism. *J. Leukoc. Biol.* **62**, 363–368.

Drexhage, K. H. (1977). Structure and Properites of Laser Dyes. Dye Lasers, (ed. F. P. Schäfer), pp. 144–193. Berlin ; New York: Springer-Verlag.

Drickamer, K. and Taylor, M. E. (2002). Glycan arrays for functional glycomics. *Genome Biol.* **3**, 1031–1034.

Drin, G., Cottin, S., Blanc, E., Rees, A. R. and Temsamani, J. (2003). Studies on the internalization mechanism of cationic cell-penetrating peptides. *J. Biol. Chem.* **278**, 31192–31201.

Drobni, P., Mistry, N., McMillan, N. and Evander, M. (2003). Carboxy-fluorescein diacetate, succinimidyl ester labeled papillomavirus virus-like particles fluoresce after internalization and interact with heparan sulfate for binding and entry. *Virology* **310**, 163–172.

Dube, D. H. and Bertozzi, C. R. (2005a). Glycans in cancer and inflammation—potential for therapeutics and diagnostics. *Nat. Rev. Drug Discov.* **4**, 477–488.

Duchardt, F., Fotin-Mleczek, M., Schwarz, H., Fischer, R. and Brock, R. (2007). A comprehensive model for the cellular uptake of cationic cell-penetrating peptides. *Traffic* **8**, 849–866.

Endo, M., Suzuki, K., Schmid, K., Fournet, B., Karamanos, Y., Montreuil, J., Dorland, L., Vanhalbeek, H. and Vliegenthart, J. F. G. (1982). The structures and microheterogeneity of the carbohydrate chains of human plasma ceruloplasmin. A study employing 500-MHz ^{1}H-NMR spectroscopy. *J. Biol. Chem.* **257**, 8755–8760.

Esko, J. D., Rostand, K. S. and Weinke, J. L. (1988). Tumor formation dependent on proteoglycan biosynthesis. *Science* **241**, 1092–1096.

Esko, J. D., Stewart, T. E. and Taylor, W. H. (1985). Animal cell mutants defective in glycosaminoglycan biosynthesis. *Proc. Natl. Acad. Sci. U. S. A.* **82**, 3197–3201.

Fan, T. C., Chang, H. T., Chen, I. W., Wang, H. Y. and Chang, M. D. T. (2007). A heparan sulfate-facilitated and raft-dependent macropinocytosis of eosinophil cationic protein. *Traffic* **8**, 1778–1795.

Fett, J. W., Strydom, D. J., Lobb, R. R., Alderman, E. M., Bethune, J. L., Riordan, J. F. and Vallee, B. L. (1985). Isolation and characterization of angiogenin, an angiogenic protein from human carcinoma cells. *Biochemistry* **24**, 5480–5486.

Fickling, M. M., Fischer, A., Mann, B. R., Packer, J. and Vaughan, J. (1959). Hammett substituent constants for electron-withdrawing substituents: Dissociation of phenols, anilinium ions and dimethylanilinium ions. *J. Am. Chem. Soc.* **81**, 4226–4230.

Fiering, S. N., Roederer, M., Nolan, G. P., Micklem, D. R., Parks, D. R. and Herzenberg, L. A. (1991). Improved FACS-Gal: Flow cytometric analysis and sorting of viable eukaryotic cells expressing reporter gene constructs. *Cytometry* **12**, 291–301.

Fisher, B. M., Schultz, L. W. and Raines, R. T. (1998). Coulombic effects of remote subsites on the active site of ribonuclease A. *Biochemistry* **37**, 17386–17401.

Foster, L. J., de Hoog, C. L., Zhang, Y., Zhang, Y., Xie, X., Mootha, V. K. and Mann, M. (2006). A mammalian organelle map by protein correlation profiling. *Cell* **125**, 187–199.

Fotin-Mleczek, M., Fischer, R. and Brock, R. (2005). Endocytosis and cationic cell-penetrating peptides—a merger of concepts and methods. *Curr. Pharm. Des.* **11**, 3613–3628.

Frankel, A. D. and Pabo, C. O. (1988). Cellular Uptake of the TAT protein from human immunodeficiency virus. *Cell* **55**, 1189–1193.

Fretz, M., Jin, J., Conibere, R., Penning, N. A., Al-Taei, S., Storm, G., Futaki, S., Takeuchi, T., Nakase, I. and Jones, A. T. (2006). Effects of Na^+/H^+ exchanger inhibitors on subcellular localisation of endocytic organelles and intracellular dynamics of protein transduction domains HIV-TAT peptide and octaarginine. *J. Controlled Release* **116**, 247–254.

Fuchs, S. M. and Raines, R. T. (2004). Pathway for polyarginine entry into mammalian cells. *Biochemistry* **43**, 2438–2444.

Fuchs, S. M. and Raines, R. T. (2006). Internalization of cationic peptides: The road less (or more?) traveled. *Cell. Mol. Life Sci.* **63**, 1819–1822.

Fuchs, S. M. and Raines, R. T. (2007). Arginine grafting to endow cell permeability. *ACS Chem. Biol.* **2**, 167–170.

Fuchs, S. M., Rutkoski, T. J., Kung, V. M., Groeschl, R. T. and Raines, R. T. (2007). Increasing the potency of a cytotoxin with an arginine graft. *Protein Eng. Des. Select.* **20**, 505–509.

Futaki, S., Nakase, I., Taclokoro, A., Takeuchi, T. and Jones, A. T. (2007). Arginine-rich peptides and their internalization mechanisms. *Biochem. Soc. Trans.* **35**, 784–787.

Futami, J., Kitazoe, M., Maeda, T., Nukui, E., Sakaguchi, M., Kosaka, J., Miyazaki, M., Kosaka, M., Tada, H., Seno, M. et al. (2005). Intracellular delivery of proteins into mammalian living cells by polyethylenimine-cationization. *J. Biosci. Bioeng.* **99**, 95–103.

Futami, J., Maeda, T., Kitazoe, M., Nukui, E., Tada, H., Seno, M., Kosaka, M. and Yamada, H. (2001). Preparation of potent cytotoxic ribonucleases by cationization: Enhanced cellular uptake and decreased interaction with ribonuclease inhibitor by chemical modification of carboxyl groups. *Biochemistry* **26**, 7518–7524.

Futami, J., Nukui, K., Maeda, T., Kosaka, M., Tada, H., Seno, M. and Yamada, H. (2002). Optimum modification for the highest cytotoxicity of cationized ribonuclease. *J. Biochem. (Tokyo)* **132**, 223–228.

Futami, J. and Yamada, H. (2008). Design of cytotoxic ribonucleases by cationization to enhance intracellular protein delivery. *Curr. Pharm. Biotechnol.* **9**, 180–184.

Gacoin, P. and Flamant, P. (1972). High efficiency cresyl violet laser. *Optics Commun.* **5**, 351–353.

Garcia-Mayoral, M. F., Moussaoui, M., de la Torre, B. G., Andreu, D., Boix, E., Nogues, M. V., Rico, M., Laurents, D. V. and Bruix, M. (2010). NMR Structural Determinants of Eosinophil Cationic Protein Binding to Membrane and Heparin Mimetics. *Biophys. J.* **98**, 2702–2711.

Ghosal, A., Hapangama, N., Yuan, Y., Lu, X., Horne, D., Patrick, J. E. and Zbaida, S. (2003). Rapid determination of enzyme activities of recombinant human cytochromes P450, human liver microsomes and hepatocytes. *Biopharm. Drug Dispos.* **24**, 375–384.

Gitaygoren, H., Soker, S., Vlodavsky, I. and Neufeld, G. (1992). The binding of vascular endothelial growth-factor to its receptors is dependent on cell surfac-associated heparin-like molecules. *J. Biol. Chem.* **267**, 6093–6098.

Goddard, J.-P. and Reymond, J.-L. (2004). Enzyme assays for high-throughput screening. *Curr. Opin. Biotechnol.* **15**, 314.

Goldberg, J. M. and Baldwin, R. L. (1998). Kinetic mechanism of a partial folding reaction. 1. Properties of the reaction and effects of denaturants. *Biochemistry* **37**, 2546–2555.

Golik, J., Wong, H. S. L., Chen, S. H., Doyle, T. W., Wright, J. J. K., Knipe, J., Rose, W. C., Casazza, A. M. and Vyas, D. M. (1996). Synthesis and antitumor evaluation of paclitaxel phosphonooxymethyl ethers: A novel class of water soluble paclitaxel pro-drugs. *Bioorg. Med. Chem. Lett.* **6**, 1837–1842.

Graber, M. L., Dilillo, D. C., Friedman, B. L. and Pastorizamunoz, E. (1986). Characteristics of fluoroprobes for measuring intracellular Ph. *Anal. Biochem.* **156**, 202–212.

Gruenberg, J. and van der Goot, F. G. (2006). Mechanisms of pathogen entry through the endosomal compartments. *Nat. Rev. Mol. Cell Biol.* **7**, 495–504.

Gungerich, F. P. (2008). Cytochrome P450 and chemical toxicology. *Chem. Res. Toxicol.* **21**, 70–83.

Guzikowski, A. P., Naleway, J. J., Shipp, C. T. and Schutte, R. C. (2000). Synthesis of a macrocyclic rhodamine 110 enzyme substrate as an intracellular probe for caspase 3 activity. *Tetrahedron Lett.* **41**, 4733–4735.

Haigis, M. C., Kurten, E. L., Abel, R. L. and Raines, R. T. (2002). KFERQ sequence in ribonuclease A-mediated cytotoxicity. *J. Biol. Chem.* **277**, 11576–11581.

Haigis, M. C., Kurten, E. L. and Raines, R. T. (2003). Ribonuclease inhibitor as an intracellular sentry. *Nucleic Acids Res.* **31**, 1024–1032.

Haigis, M. C. and Raines, R. T. (2003). Secretory ribonucleases are internalized by a dynamin-independent endocytic pathway. *J. Cell Sci.* **116**, 313–324.

Hallbrink, M., Floren, A., Elmquist, A., Pooga, M., Bartfai, T. and Langel, U. (2001). Cargo delivery kinetics of cell-penetrating peptides. *Biochim. Biophys. Acta* **1515**, 101–109.

Hansch, C., Leo, A. and Taft, R. W. (1991). A survey of Hammett substituent constants and resonance and field parameters. *Chem. Rev.* **91**, 165–195.

Haugland, R. P., Naleway, J. J. and Zhang, Y.-Z. (1990). Lipophilic fluorescent glycosidase substrates.

Haugland, R. P., Spence, M. T. Z., Johnson, I. D. and Basey, A. (2005). The Handbook: A Guide to Fluorescent Probes and Labeling Technologies, 10th ed. Eugene, OR: Molecular Probes.

Henriques, S. T., Melo, M. N. and Castanho, M. (2007). How to address CPP and AMP translocation? Methods to detect and quantify peptide internalization in vitro and in vivo (Review). *Mol. Membr. Biol.* **24**, 173–U172.

Herce, H. D. and Garcia, A. E. (2007). Cell penetrating peptides: How do they do it? *J. Biol. Phys.* **33**, 345–356.

Herce, H. D., Garcia, A. E., Litt, J., Kane, R. S., Martin, P., Enrique, N., Rebolledo, A. and Milesi, V. (2009). Arginine-rich peptides destabilize the plasma membrane, consistent with a pore formation translocation mechanism of cell-penetrating peptides. *Biophs. J.* **97**, 1917–1925.

Ho, N. H., Weissleder, R. and Tung, C. H. (2007). A self-immolative reporter for b-galactosidase sensing. *ChemBiochem* **8**, 560–566.

Hofmann, J. and Sernetz, M. (1983). A kinetic study on the enzymatic hydrolysis of fluoresceindiacetate and fluorescein-di-b-D-galactopyranoside. *Anal. Biochem.* **131**, 180–186.

Hofmann, J. and Sernetz, M. (1984). Immobilized enzyme kinetics analyzed by flow-through microfluorimetry : Resorufin-β-galactopyranoside as a new fluorogenic substrate for β-galactosidase. *Anal. Chim. Acta* **163**, 67–72.

Horgan, D. J., Dunstone, J. R., Stoops, J. K., Webb, E. C. and Zerner, B. (1969). Carboxylesterases (EC 3.1.1). The molecular weight and equivalent weight of pig liver carboxylesterase. *Biochemistry* **8**, 2006–2013.

Hornick, C. A., Thouron, C., Delamatre, J. G. and Huang, J. (1992). Triacylglycerol hydrolysis in isolated hepatic endosomes. *J. Biol. Chem.* **267**, 3396–3401.

Hu, C. D., Chinenov, Y. and Kerppola, T. K. (2002). Visualization of interactions among bZip and Rel family proteins in living cells using bimolecular fluorescence complementation. *Mol. Cell* **9**, 789–798.

Hu, G.-F., Chang, S.-I., Riordan, J. F. and Vallee, B. L. (1991). An angiogenin-binding protein from endothelial cells. *Proc. Natl. Acad. Sci. U. S. A.* **88**, 2227–2231.

Hu, G.-F., Strydom, D. J., Fett, J. W., Riordan, J. F. and Vallee, B. L. (1993). Actin is a binding protein for angiogenin. *Proc. Natl. Acad. Sci. U. S. A.* **90**, 1217–1221.

Hu, G. F., Riordan, J. F. and Vallee, B. L. (1994). Angiogenin promotes invasiveness of cultured endothelial-cells by stimulation of cell-assocaited proteolytic activities. *Proc. Natl. Acad. Sci. U. S. A.* **91**, 12096–12100.

Hu, G. F., Riordan, J. F. and Vallee, B. L. (1997). A putative angiogenin receptor in angiogenin-responsive human endothelial cells. *Proc. Natl. Acad. Sci. U. S. A.* **94**, 2204–2209.

Huang, S.-T. and Lin, Y.-L. (2006). New latent fluorophore for DT diaphorase. *Org. Lett.* **8**, 265–268.

Hukkanen, J., Lassila, A., Paivarinta, K., Valanne, S., Sarpo, S., Hakkola, J., Pelkonen, O. and Raunio, H. (2000). Induction and regulation of xenobiotic-metabolizing cytochrome P450s in the human A549 lung adenocarcinoma cell line. *Am. J. Respir. Cell. Mol. Biol.* **22**, 360–366.

Hyatt, J. L., Stacy, V., Wadkins, R. M., Yoon, K. J. P., Wierdl, M., Edwards, C. C., Zeller, M., Hunter, A. D., Danks, M. K., Crundwell, G. et al. (2005). Inhibition of carboxylesterases by benzil (diphenylethane-1,2-dione) and heterocyclic analogues is dependent upon the aromaticity of the ring and the flexibility of the dione moiety. *J. Med. Chem.* **48**, 5543–5550.

Ilinskaya, O. N., Dreyer, F., Mitkevich, V. A., Shaw, K. L., Pace, C. N. and Makarov, A. A. (2002). Changing the net charge from negative to positive makes ribonuclease Sa cytotoxic. *Protein Sci.* **11**, 2522–2525.

Ilinskaya, O. N., Koschinski, A., Mitkevich, V. A., Repp, H., Dreyer, F., Pace, C. N. and Makarov, A. A. (2004). Cytotoxicity of RNases is increased by cationization and counteracted by K(Ca) channels. *Biochem. Biophys. Res. Commun.* **314**, 550–554.

Ingelman-Sundberg, M., Sim, S. C., Gomez, A. and Rodriguez-Antona, C. (2007). Influence of cytochrome P450 polymorphisms on drug therapies: Pharmacogenetic, pharmacoepigenetic and clinical aspects. *Pharmacol. Ther.* **116**, 496–526.

Ioffe, I. S. and Otten, V. F. (1965a). Rhodamine dyes and related compounds. XII. Diacetyl derivatives of rhodamine and rhodol; structure of colorless forms of fluoran dyes. *Zh. Obshch. Khim.* **1**, 336–339.

Ioffe, I. S. and Otten, V. F. (1965b). Rhodamine dyes and related compounds. XIV. Mutual conversions of colorless and colored forms of rhodamine and rhodol. *Zh. Obshch. Khim.* **1**, 343–346.

Iordanov, M. S., Ryabinina, O. P., Wong, J., Dinh, T. H., Newton, D. L., Rybak, S. M. and Magun, B. E. (2000a). Molecular determinants of apoptosis induced by the cytotoxic ribonuclease onconase: Evidence for cytotoxic mechanisms different from inhibition of protein synthesis. *Cancer Res.* **60**, 1983–1994.

Iordanov, M. S., Wong, J., Newton, D. L., Rybak, S. M., Bright, R. K., Flavell, R. A., Davis, R. J. and Magun, B. E. (2000b). Differential requirement for the stress-activated protein kinase/c-Jun NH(2)-terminal kinase in RNAdamage-induced apoptosis in primary and in immortalized fibroblasts. *Mol. Cell Biol. Res. Commun.* **4**, 122–128.

Irie, M., Nitta, K. and Nonaka, T. (1998). Biochemistry of frog ribonucleases. *Cell. Mol. Life Sci.* **54**, 775–784.

Ishii, Y. and Lehrer, S. S. (1986). Effects of the state of succinimido-ring on the fluorescence and structural properties of pyrene maleimide-labeled alpha-alpha-tropomyosin. *Biophys. J.* **50**, 75–80.

Ivanov, A. I. (2008). Pharmacological inhibition of endocytic pathways: is it specific enough to be useful? *Methods Mol. Biol.* **440**, 15–33.

Jansen, A. B. and Russell, T. J. (1965). Some novel penicillin derivatives. *J. Chem. Soc.* **65**, 2127–2132.

Jensen, K. D., Nori, A., Tijerina, M., Kopeckova, P. and Kopecek, J. (2003). Cytoplasmic delivery and nuclear targeting of synthetic macromolecules. *J. Controlled Release* **87**, 89–105.

Ji, T. H. (1983). Bifunctional reagents. *Methods Enzymol.* **91**, 580–609.

Jiao, G. S., Han, J. W. and Burgess, K. (2003). Syntheses of regioisomerically pure 5- and 6-halogenated fluoresceins. *J. Org. Chem.* **68**, 8264–8267.

Johnson, I. (1998). Fluorescent probes for living cells. *Histochem. J.* **30**, 123–140.

Johnson, R. J., Chao, T.-Y., Lavis, L. D. and Raines, R. T. (2007a). Cytotoxic ribonucleases: The dichotomy of Coulombic forces. *Biochemistry* **46**, 10308–10316.

Johnson, R. J., Lavis, L. D. and Raines, R. T. (2007b). Intraspecies regulation of ribonucleolytic activity. *Biochemistry* **46**, 13131–13140.

Johnson, R. J., Lin, S. R. and Raines, R. T. (2007c). Genetic selection reveals the role of a buried, conserved polar residue. *Protein Sci.* **16**, 1609–1616.

Johnson, R. J., McCoy, J. G., Bingman, C. A., Phillips, G. N., Jr. and Raines, R. T. (2007d). Inhibition of human pancreatic ribonuclease by the human ribonuclease inhibitor protein. *J. Mol. Biol.* **367**, 434–449.

Johnson, W. W. (2008). Cytochrome P450 inactivation by pharmaceuticals and phytochemicals: Therapeutic relevance. *Drug Metab. Rev.* **40**, 101–147.

Jones, A. T. (2007). Macropinocytosis: searching for an endocytic identity and role in the uptake of cell penetrating peptides. *J. Cell. Mol. Med.* **11**, 670–684.

Jones, S. W., Christison, R., Bundell, K., Voyce, C. J., Brockbank, S. M. V., Newham, P. and Lindsay, M. A. (2005). Characterization of cell-penetrating peptide-mediated peptide delivery. *Br. J. Pharmacol.* **145**, 1093–1102.

Kaksonen, M., Toret, C. P. and Drubin, D. G. (2006). Harnessing actin dynamics for clathrin-mediated endocytosis. *Nat. Rev. Mol. Cell Biol.* **7**, 404–414.

Kamal, A., Ramulu, P., Srinivas, O., Ramesh, G. and Kumar, P. P. (2004). Synthesis of C8-linked pyrrolo[2,1-*c*][1,4]benzodiazepine–benzimidazole conjugates with remarkable DNA-binding affinity. *Bioorg. Med. Chem. Lett.* **14**, 4791–4794.

Kannagi, R., Cochran, N. A., Ishigami, F., Hakomori, S.-i., Andrews, P. W., Knowles, B. B. and Solter, D. (1983). Stage-specific embryonic antigens (SSEA-3 and -4) are epitopes of a unique globo-series ganglioside isolated from human teratocarcinoma cells. *EMBO J.* **2**, 2355–2361.

Kannemeier, C., Shibamiya, A., Nakazawa, F., Trusheim, H., Ruppert, C., Markart, P., Song, Y. T., Tzima, E., Kennerknecht, E., Niepmann, M. et al. (2007). Extracellular RNA constitutes a natural procoagulant cofactor in blood coagulation. *Proc. Natl. Acad. Sci. U. S. A.* **104**, 6388–6393.

Kao, J., Harootunian, A. and Tsien, R. (1989). Photochemically generated cytosolic calcium pulses and their detection by fluo-3. *J. Biol. Chem.* **264**, 8179–8184.

Kaplan, I. M., Wadia, J. S. and Dowdy, S. F. (2005). Cationic TAT peptide transduction domain enters cells by macropinocytosis. *J. Controlled Release* **102**, 247–253.

Kasai, K., Uchida, R. and Yamaji, N. (1993). Glycosides having chromophores as substrates for sensitive enzyme analysis. IV. Synthesis of N-acetyl-β-D-glucosaminides of fluorescein derivatives and their application to the rate-assay of N-acetyl- β-D -glucosaminidase. *Chem. Pharm. Bull.* **41**, 314–318.

Kawauchi, H., Sakakibara, F. and Watanabe, K. (1975). Agglutinins of frog eggs—new class of proteins causing perferential agglutination of tumor-cells. *Experientia* **31**, 364–365.

Kelemen, B. R., Klink, T. A., Behlke, M. A., Eubanks, S. R., Leland, P. A. and Raines, R. T. (1999). Hypersensitive substrate for ribonucleases. *Nucleic Acids Res.* **27**, 3696–3701.

Kerkis, A., Kerkis, I., Radis-Baptista, G., Oliveira, E. B., Vianna-Morgante, A. M., Pereira, L. V. and Yamane, T. (2004). Crotamine is a novel cell-penetrating protein from the venom of rattlesnake *Crotalus durissus terrificus*. *FASEB J.* **18**, 1407–409.

Khramtsov, Y. V., Rokitskaya, T. I., Rosenkranz, A. A., Trusov, G. A., Gnuchev, N. V., Antonenko, Y. N. and Sobolev, A. S. (2008). Modular drug transporters with diphtheria toxin translocation domain form edged holes in lipid membranes. *J. Controlled Release* **128**, 241–247.

Kim, B.-M., Kim, H., Raines, R. T. and Lee, Y. (2004). Glycosylation of onconase increases it conformational stability and toxicity for cancer cells. *Biochem. Biophys. Res. Commun.* **315**, 976–983.

Kim, H. M., Kang, D. K., Kim, H. Y., Kang, S. S. and Chang, S. K. (2007). Angiogenin-induced protein kinase B/Akt activation is necessary for angiogenesis but is independent of nuclear translocation of angiogenin in HUVE cells. *Biochem. Biophys. Res. Commun.* **352**, 509–513.

Kim, J.-S., Souček, J., Matoušek, J. and Raines, R. T. (1995a). Catalytic activity of bovine seminal ribonuclease is essential for its immunosuppressive and other biological activities. *Biochem. J.* **308**, 547–550.

Kim, J.-S., Souček, J., Matoušek, J. and Raines, R. T. (1995b). Mechanism of ribonuclease cytotoxicity. *J. Biol. Chem.* **270**, 31097–31102.

Kim, W. C. and Lee, C. H. (2009). The role of mammalian ribonucleases (RNases) in cancer. *Biochim. Biophys. Acta, Rev. Cancer* **1796**, 99–113.

Kirkham, M. and Parton, R. G. (2005). Clathrin-independent endocytosis: New insights into caveolae and non-caveolar lipid raft carriers. *Biochim. Biophys. Acta Mol. Cell Res.* **1745**, 273–286.

Kislinger, T., Cox, B., Kannan, A., Chung, C., Hu, P., Ignatchenko, A., Scott, M. S., Gramolini, A. O., Morris, Q., Hallett, M. T. et al. (2006). Global survey of organ and organelle protein expression in mouse: Combined proteomic and transcriptomic profiling. *Cell* **125**, 173–186.

Kitson, T. M. (1996). Comparison of resorufin acetate and *p*-nitrophenyl acetate as substrates for chymotrypsin. *Bioorg. Chem.* **24**, 331–339.

Kjeken, R., Mousavi, S. A., Brech, A., Griffiths, G. and Berg, T. (2001). Wortmanin-sensitive trafficking steps in the endocytic pathway in rat liver endothelial cells. *Biochem. J.* **357**, 497–503.

Klein, C., Batz, H.-G. and Herrmann, R. (1990). Resorufin derivatives, pp. 34 pp: (Molecular Devices Corporation, USA).

Klink, T. A. and Raines, R. T. (2000). Conformational stability is a determinant of ribonuclease A cytotoxicity. *J. Biol. Chem.* **275**, 17463–17467.

Kobayashi, T., Urano, Y., Kamiya, M., Ueno, T., Kojima, H. and Nagano, T. (2007). Highly activatable and rapidly releasable caged fluorescein derivatives. *J. Am. Chem. Soc.* **129**, 6696–6697.

Kosuge, M., Takeuchi, T., Nakase, I., Jones, A. T. and Futaki, S. (2008). Cellular internalization and distribution of arginine-rich peptides as a function of extracellular peptide concentration, serum, and plasma membrane associated proteoglycans. *Bioconjugate Chem.* **19**, 656–664.

Krafft, G. A., Sutton, W. R. and Cummings, R. T. (1988). Photoactivable fluorophores. 3. Synthesis and photoactivation of fluorogenic difunctionalized fluoresceins. *J. Am. Chem. Soc.* **110**, 301–303.

Kramer, D. N. and Guilbault, G. G. (1964). Resorufin acetate as a substrate for determination of hydrolytic enzymes at low enzyme and substrate concentrations. *Anal. Chem.* **36**, 1662–1663.

López Arbeloa, F., López Arbeloa, T., Tapia Estevez, M. J. and López Arbeloa, I. (1991). Photophysics of rhodamines: Molecular structure and solvent effects. *J. Phys. Chem.* **95**, 2203–2208.

López Arbeloa, F., Urrecha Aguirresacona, I. and López Arbeloa, I. (1989). Influence of the molecular structure and the nature of the solvent on the absorption and fluorescence characteristics of rhodamines. *Chem. Phys.* **130**, 371–378.

López Arbeloa, T., López Arbeloa, F., Hernández Bartolomé, P. and López Arbeloa, I. (1992). On the mechanism of radiationless deactivation of rhodamines. *Chem. Phys.* **160**, 123–130.

Laccetti, P., Portella, G., Mastronicola, M. R., Russo, A., Piccoli, R., Dalessio, G. and Vecchio, G. (1992). In vivo and In vitro growth-inhibitory effects of bovine seminal ribonuclease on a system of rat-thyroid epithelial transformed-cells and tumors. *Cancer Res.* **52**, 4582–4586

Lajoie, P. and Nabi, I. R. (2007). Regulation of raft-dependent endocytosis. *J. Cell. Mol. Med.* **11**, 644–653.

Lakowicz, J. R. (1999). Principles of Fluorescence Spectroscopy. New York: Kluwer Academic/Plenum.

Lamaziere, A., Burlina, F., Wolf, C., Chassaing, G., Trugnan, G. and Ayala-Sanmartin, J. (2007). Non-metabolic membrane tubulation and permeability induced by bioactive peptides. *Plos One* **2**.

Lampugnani, M. G., Orsenigo, F., Gagliani, M. C., Tacchetti, C. and Dejana, E. (2006). Vascular endothelial cadherin controls VEGFR-2 internalization and signaling from intracellular compartments. *J. Cell Biol.* **174**, 593–604.

Langel, Ü. (2007). Handbook of Cell-Penetrating Peptides, 2nd ed. Boca Raton, FL: CRC Press.

Laremore, T. N., Zhang, F., Dordick, J. S., Liu, J. and Linhardt, R. J. (2009). Recent progress and applications in glycosaminoglycan and heparin research. *Curr. Opin. Chem. Biol.* **13**, 633–640.

Larson, G. M. and Lee, K. D. (1998). Macromolecular cytosolic delivery: Cell membranes as the primary obstacle. *Arch. Pharmacal. Res.* **21**, 621–628.

Laurent, A., Debart, F., Lamb, N. and Rayner, B. (1997). Esterase-triggered fluorescence of fluorogenic oligonucleotides. *Bioconjugate Chem.* **8**, 856–861.

Lavis, L. D. (2008). Ester bonds in prodrugs. *ACS Chem. Biol.* **3**, 203–206.

Lavis, L. D., Chao, T.-Y. and Raines, R. T. (2006a). Fluorogenic label for biomolecular imaging. *ACS Chem. Biol.* **1**, 252–260.

Lavis, L. D., Chao, T. Y. and Raines, R. T. (2006b). Latent blue and red fluorophores based on the trimethyl lock. *ChemBiochem* **7**, 1151–1154.

Lavis, L. D. and Raines, R. T. (2008). Bright ideas for chemical biology. *ACS Chem. Biol.* **3**, 142–155.

Lavis, L. D., Rutkoski, T. J. and Raines, R. T. (2007). Tuning the pK_a of fluorescein to optimize binding assays. *Anal. Chem.* **79**, 6775–6782.

Lee, B. W., Johnson, G. L., Hed, S. A., Darzynkiewicz, Z., Talhouk, J. W. and Mehrotra, S. (2003). DEVDase detection in intact apoptotic cells using the cell permeant fluorogenic substrate, (z-DEVD)2-cresyl violet. *BioTechniques* **35**, 1080–1085.

Lee, I. (2008). Ranpirnase (Onconase (R)), a cytotoxic amphibian ribonuclease, manipulates tumour physiological parameters as a selective killer and a potential enhancer for chemotherapy and radiation in cancer therapy. *Expert Opin. Biol. Ther.* **8**, 813–827.

Lee, I., Lee, Y. H., Mikulski, S. M., Lee, J., Covone, K. and Shogen, K. (2000). Tumoricidal effects of onconase on various tumors. *J. Sur. Oncol.* **73**, 164–171.

Lee, J. E. and Raines, R. T. (2003). Contribution of active-site residues to the function of onconase, a ribonuclease with antitumoral activity. *Biochemistry* **42**, 11443–11450.

Lee, J. E. and Raines, R. T. (2008). Ribonucleases as novel chemotherapeutics: The ranpirnase example. *BioDrugs* **22**, 53–58.

Leich, F., Stohr, N., Rietz, A., Ulbrich-Hofmann, R. and Arnold, U. (2007). Endocytotic internalization as a crucial factor for the cytotoxicity of ribonucleases. *J. Biol. Chem.* **282**, 27640–27646.

Leinweber, F.-J. (1987). Possible physiological roles of carboxylic ester hydrolases. *Drug Metab. Rev.* **18**, 379–439.

Leland, P. A. and Raines, R. T. (2001). Cancer chemotherapy—ribonucleases to the rescue. *Chem. Biol.* **8**, 405–413.

Leland, P. A., Schultz, L. W., Kim, B.-M. and Raines, R. T. (1998). Ribonuclease A variants with potent cytotoxic activity. *Proc. Natl. Acad. Sci. U. S. A.* **98**, 10407–10412.

Leland, P. A., Staniszewski, K. E., Kim, B.-M. and Raines, R. T. (2001). Endowing human pancreatic ribonuclease with toxicity for cancer cells. *J. Biol. Chem.* **276**, 43095--43102.

Leroy, E., Bensel, N. and Reymond, J.-L. (2003). A low background high-throughput screening (HTS) fluorescence assay for lipases and esterases using acyloxymethylethers of umbelliferone. *Bioorg. Med. Chem. Lett.* **13**, 2105–2108.

Lesner, A., Wysocka, M., Guzow, K., Wiczk, W., Legowska, A. and Rolka, K. (2008). Development of sensitive cathepsin G fluorgenic substrate using combinatorial chemistry methods. *Anal. Biochem.* **15**, 306–312.

Levine, M. N., Lavis, L. D. and Raines, R. T. (2008). Trimethyl lock: A stable chromogenic substrate for esterases. *Molecules* **13**, 204–211.

Leytus, S. P., Melhado, L. L. and Mangel, W. F. (1983a). Rhodamine-based compounds as fluorogenic substrates for serine proteinases. *Biochem. J.* **209**, 299–307.

Leytus, S. P., Patterson, W. L. and Mangel, W. F. (1983b). New class of sensitive and selective fluorogenic substrates for serine proteinases. Amino acid and dipeptide derivatives of rhodamine. *Biochem. J.* **215**, 253–260.

Li, R. X., Manela, J., Kong, Y. and Ladisch, S. (2000). Cellular gangliosides promote growth factor-induced proliferation of fibroblasts. *J. Biol. Chem.* **275**, 34213–34223.

Lidholt, K., Weinke, J. L., Kiser, C. S., Lugemwa, F. N., Bame, K. J., Cheifetz, S., Massague, J., Lindahl, U. and Esko, J. D. (1992). A single mutation affects both *N*-acetylglucosaminyltransferase and glucuronosyltransferase activities in a Chinese hamster ovary cell mutant defective in heparan sulfate biosynthesis. *Proc. Natl. Acad. Sci. U. S. A.* **89**, 2267–2271.

Liu, J., Bhalgat, M., Zhang, C., Diwu, Z., Hoyland, B. and Klaubert, D. H. (1999). Fluorescent molecular probes V: A sensitive caspase-3 substrate for fluorometric assays. *Bioorg. Med. Chem. Lett.* **9**, 3231–3236.

Liu, J., Ericksen, S. S., Besspiata, D., Fisher, C. W. and Szklarz, G. D. (2003). Characterization of substrate binding to cytochrome P450 1A1 using molecular modeling and kinetic analyses: Case of residue 382. *Drug Metab. Dispos.* **31**, 412–420.

Liu, S. M., Yu, D. H., Xu, Z. P., Riordan, J. F. and Hu, G. F. (2001). Angiogenin activates Erk1/2 in human umbilical vein endothelial cells. *Biochem. Biophys. Res. Commun.* **287**, 305–310.

Lorey, S., Faust, J., Mrestani-Klaus, C., Kaehne, T., Ansorge, S., Neubert, K. and Buehling, F. (2002). Transcellular proteolysis demonstrated by novel cell surface-associated substrates of dipeptidyl peptidase IV (CD26). *J. Biol. Chem.* **277**, 33170–33177.

Macia, E., Ehrlich, M., Massol, R., Boucrot, E., Brunner, C. and Kirchhausen, T. (2006). Dynasore, a cell-permeable inhibitor of dynamin. *Dev. Cell* **10**, 839–850.

Magzoub, M., Pramanik, A. and Graslund, A. (2005). Modeling the endosomal escape of cell-penetrating peptides: Transmembrane pH gradient driven translocation across phospholipid bilayers. *Biochemistry* **44**, 14890–14897.

Maiolo, J. R., Ferrer, M. and Ottinger, E. A. (2005). Effects of cargo molecules on the cellular uptake of arginine-rich cell-penetrating epeptides. *Biochim. Biophys. Acta, Biomembr.* **1712**, 161–172.

Makarov, A. A. and Ilinskaya, O. N. (2003). Cytotoxic ribonucleases: Molecular weapons and their targets. *FEBS Lett.* **540**, 15–20.

Mangold, S. L., Carpenter, R. T. and Kiessling, L. L. (2008). Synthesis of fluorogenic polymers for visualizing cellular internalization. *Org. Lett.* **10**, 2997–3000.

Mastronicola, M. R., Piccoli, R. and Dalessio, G. (1995). Key Extracellular and intracellular steps in the antitumor action of seminal ribonucleases. *Eur. J. Biochem.* **230**, 242–249.

Matoušek, J. (2001). Ribonucleases and their antitumor activity. *Comp. Biochem. Physiol.* **129C**, 175–191.

Mayer, R. T., Dolence, E. K. and Mayer, G. E. (2007). A real-time fluorescence assay for measuring *N*-dealkylation. *Drug Metab. Dispos.* **35**, 103–109.

Mayer, R. T., Netter, K. J., Heubel, F., Hanhemann, B., Buchheister, A., Mayer, G. K. and Burke, M. D. (1990). 7-Alkoxyquinolines: New fluorescent substrates for cytochrome P450 monoxygenases. *Biochem. Pharmacol.* **40**, 1645–1655.

Mayor, S. and Pagano, R. E. (2007). Pathways of clathrin-independent endocytosis. *Nat. Rev. Mol. Cell Biol.* **8**, 603–612.

Mehrishi, J. N. (1972). Molecular aspects of the mammalian cell surface. *Prog. Biophys. Mol. Biol.* **25**, 1–70.

Mei, Y., Yong, J., Liu, H., Shi, Y., Meinkoth, J., Dreyfuss, G. and Yang, X. (2010). tRNA bind to cytochrome *c* and inhibits caspase activation. *Mol. Cell* **37**, 668–678.

Melikov, K. and Chernomordik, L. (2005). Arginine-rich cell penetrating peptides: from endosomal uptake to nuclear delivery. *Cell. Mol. Life Sci.* **62**, 2739–2749.

Meunier, F. and Wilkinson, K. J. (2002). Nonperturbing fluorescent labeling of polysaccharides. *Biomacromolecules* **3**, 857–864.

Mikulski, S. M., Ardelt, W., Shogen, K., Bernstein, E. H. and Menduke, H. (1990). Striking increase of survival of mice bearing M109 Madison carcinoma treated with a novel protein from amphibian embryos. *J. Natl. Cancer Inst.* **82**, 151–153.

Miller, A. G. (1983). Ethylated fluoresceins: Assay of cytochrome P-450 activity and application to measurements in single cells by flow cytometry. *Anal. Biochem.* **133**, 46–57.

Milstein, S. and Cohen, L. A. (1972). Stereopopulation control. I. Rate enhancement in the lactonizations of *o*-hydroxyhydrocinnamic acids. *J. Am. Chem. Soc.* **94**, 9158–9165.

Mitchison, T. J. (1989). Polewards microtubule flux in the mitotic spindle: Evidence from photoactivation of fluorescence. *J. Cell Biol.* **109**, 637–652.

Mitchison, T. J., Sawin, K. E., Theriot, J. A., Gee, K., Mallavarapu, A. and Marriott, G. (1998). Caged fluorescent probes. *Methods Enzymol.* **291**, 63–78.

Mollerup, S., Ovrebo, S. and Haugen, A. (2001). Lung carcinogenesis: Resveratrol modulates the expression of genes involved in the metabolism of PAH in human bronchial epithelial cells. *Int. J. Cancer* **92**, 18–25.

Morita, T., Kato, H., Iwanaga, S., Takada, K. and Kimura, T. (1977). New fluorogenic substrates for alpha-thrombin, factor Xa, kallikreins, and urokinase. *J. Biochem.* **82**, 1495–1498.

Mudhakir, D. and Harashima, H. (2009). Learning from the viral journey: How to enter cells and how to overcome intracellular barriers to reach the nucleus. *AAPS J.* **11**, 65–77.

Mugherli, L., Burchak, O., Chatelain, F. and Balakirev, M. (2006). Fluorogenic ester substrates to assess proteolytic activity. *Bioorg. Med. Chem. Lett.* **16**, 4488–4491.

Mukherjee, S., Ghosh, R. N. and Maxfield, F. R. (1997). Endocytosis. *Physiol. Rev.* **77**, 759–803.

Mulgrew-Nesbitt, A., Diraviyam, K., Wang, J., Singh, S., Murray, P., Li, Z., Rogers, L., Mirkovic, N. and Murray, D. (2006). The role of electrostatics in protein-membrane interactions. *Biochim. Biophys. Acta* **1761**, 812–826.

Murray, D. and Honig, B. (2002). Electrostatic control of the membrane targeting of C2 domains. *Mol. Cell* **9**, 145–154.

Murray, M. and Petrovic, N. (2006). Cytochromes P450: Decision-making tools for personalized therapeutics. *Curr. Opin. Mol. Ther.* **8**, 480–486.

Nakano, M., Kakehi, K., Tsai, M.-H. and Lee, Y. C. (2004). Detailed structural features of glycan chains derived from α1-acid glycoproteins of several different animals: The presence of hypersialylated, *O*-acetylated sialic acids but not disialyl residues. *Glycobiology* **14**, 431–441.

Nakase, I., Niwa, M., Takeuchi, T., Sonomura, K., Kawabata, N., Koike, Y., Takehashi, M., Tanaka, S., Ueda, K., Simpson, J. C. et al. (2004). Cellular uptake of arginine-rich peptides: Roles for macropinocytosis and actin rearrangement. *Mol. Ther.* **10**, 1011–1022.

Nakase, I., Tadokoro, A., Kawabata, N., Takeuchi, T., Katoh, H., Hiramoto, K., Negishi, M., Nomizu, M., Sugiura, Y. and Futaki, S. (2007). Interaction of arginine-rich peptides with membrane-associated proteoglycans is crucial for induction of actin organization and macropinocytosis. *Biochemistry* **46**, 492–501.

Nebert, D. W. and Dalton, T. P. (2006). The role of cytochrome P450 enzymes in endogenous signalling pathways and environmental carcinogenesis. *Nat. Rev. Cancer* **6**, 947–960.

Nicolaou, M. G., Yuan, C.-S. and Borchardt, R. T. (1996). Phosphate prodrugs for amines utilizing a fast intramolecular hydroxy amide lactonization. *J. Org. Chem.* **61**, 8636–8641.

Nitta, K., Ozaki, K., Ishikawa, M., Furusawa, S., Hosono, M., Kawauchi, H., Sasaki, K., Takayanagi, Y., Tsuiki, S. and Hakomori, S. (1994a). Inhibition of cell proliferation by *Rana catesbeiana* and *Rana japonica* lectins belonging to the ribonuclease superfamily. *Cancer Res.* **54**, 920–927.

Nitta, K., Ozaki, Z. K., Tsukamoto, Y., Furusawa, S., Ohkubo, Y., Takimoto, H., Murata, R., Hosono, M., Hikichi, N., Sasaki, K. et al. (1994b). Characterization of *Rana catesbeiana* lectin-resistant mutant of leukemia P388 cells. *Cancer Res.* **54**, 928-934.

Nitta, K., Takayanagi, G., Kawauchi, H. and Hakomori, S. (1987). Isolation and characterization of *Rana catesbeiana* lectin and demonstration of the lectin-binding glycoprotein of rodent and human-tumor cell-membranes. *Cancer Res.* **47**, 4877-4883.

Noguchi, H., Bonner-Weir, S., Wei, F. Y., Matsushita, M. and Matsumoto, S. (2005). BETA2/NeuroD protein can be transduced into cells due to an arginine- and lysine-rich sequence. *Diabetes* **54**, 2859–2866.

Noguchi, H. and Matsumoto, S. (2006). Protein transduction technology: A novel therapeutic perspective. *Acta Medica Okayama* **60**, 1–11.

Norgard-Sumnicht, K., Bai, X. M., Esko, J. D., Varki, A. and Manzi, A. E. (2000). Exploring the outcome of genetic modifications of glycosylation in cultured cell lines by concurrent isolation of the major classes of vertebrate glycans. *Glycobiology* **10**, 691–700.

Notomista, E., Mancheño, J. M., Crescenzi, O., Di Donato, A., Gavilanes, J. and D'Alessio, G. (2006). The role of electrostatic interactions in the antitumor activity of dimeric RNases. *FEBS J.* **273**, 3687–3697.

O'Brien, J., Wilson, I., Orton, T. and Pognan, F. (2000). Investigation of the Alamar Blue (resazurin) fluorescent dye for the assessment of mammalian cell cytotoxicity. *Eur. J. Biochem.* **267**, 5421–5426.

Ogawa, Y., Iwama, M., Ohgi, K., Tsuji, T., Irie, M., Itagaki, T., Kobayashi, H. and Inokuchi, N. (2002). Effect of replacing the aspartic acid/glutamic acid residues of bullfrog sialic acid binding lectin with asparagine/glutamine and arginine on the inhibition of cell proliferation in murine leukemia P388 cells. *Biol. Pharm. Bull.* **25**, 722–727.

Onyango, P. (2004). The role of emerging genomics and proteomics technologies in cancer drug target discovery. *Curr. Cancer Drug Targets* **4**, 111–124.

Orntoft, T. F. and Vestergaard, E. M. (1999). Clinical aspects of altered glycosylation of glycoproteins in cancer. *Electrophoresis* **20**, 362–371.

Ortiz de Montellano, P. R. (2005). Cytochrome P450: Structure, Mechanism, and Biochemistry, pp. 378–398. New York: Kluwer Academic/Plenum Publishers.

Ouyang, H., Borchardt, R. T. and Siahaan, T. J. (2002). Steric hindrance is a key factor in the coupling reaction of (acyloxy) alkyl-a-halides with phenols to make a new promoiety for prodrugs. *Tetrahedron Lett.* **43**, 577–579.

Panchuk-Voloshina, N., Haugland, R. P., Bishop-Stewart, J., Bhalgat, M. K., Millard, P. J., Mao, F., Leung, W.-Y. and Haugland, R. P. (1999). Alexa dyes, a series of new fluorescent dyes that yield exceptionally bright, photostable conjugates. *J. Histochem. Cytochem.* **47**, 1179–1188.

Park, C. and Raines, R. T. (2003). Catalysis by ribonuclease A is limited by the rate of substrate association. *Biochemistry* **42**, 3509–3518.

Parton, R. G. and Simons, K. (2007). The multiple faces of caveolae. *Nat. Rev. Mol. Cell Biol.* **8**, 185–194.

Patel, L. N., Zaro, J. L. and Shen, W. C. (2007). Cell penetrating peptides: Intracellular pathways and pharmaceutical perspectives. *Pharm. Res.* **24**, 1977–1992.

Patki, V., Virbasius, J., Lane, W. S., Toh, B. H., Shpetner, H. S. and Corvera, S. (1997). Identification of an early endosomal protein regulated by phosphatidylinositol 3-kinase. *Proc. Natl. Acad. Sci. U. S. A.* **94**, 7326–7330.

Pavlakis, N. and Vogelzang, N. J. (2006). Ranpirnase—an antitumour ribonuclease: Its potential role in malignant mesothelioma. *Expert Opin. Biol. Ther.* **6**, 391–399.

Piccoli, R., Di Gaetano, S., De Lorenzo, C., Grauso, M., Monaco, C., Spalletti-Cernia, D., Laccetti, P., Cinatl, J., Matousek, J. and D'Alessio, G. (1999). A dimeric mutant of human pancreatic ribonuclease with selective cytotoxicity toward malignant cells. *Proc. Natl. Acad. Sci. U. S. A.* **96**, 7768–7773.

Plovins, A., Alvarez, A. M., Ibanez, M., Molina, M. and Nombela, C. (1994). Use of fluorescein-di-beta-D-galactopyranoside (FDG) and C12-FDG as substrates for beta-galactosidase detection by flow cytometry in animal, bacterial, and yeast cells. *Appl. Environ. Microbiol.* **60**, 4638–4641.

Polo, S. and Di Fiore, P. P. (2006). Endocytosis conducts the cell signaling orchestra. *Cell* **124**, 897–900.

Raines, R. T. (1998). Ribonuclease A. *Chem. Rev.* **98**, 1045–1065.

Ramos-Nino, M. E., Vianale, G., Sabo-Attwood, T., Mutti, L., Porta, C., Heintz, N. and Mossman, B. T. (2005). Human mesothelioma cells exhibit tumor cell-specific differences in phosphatidylinositol 3-kinase/AKT activity that predict the efficacy of Onconase. *Mol. Cancer Ther.* **4**, 835–842.

Ran, S., Downes, A. and Thorpe, P. E. (2002). Increased exposure of anionic phospholipids on the surface of tumor blood vessels. *Cancer Res.* **62**, 6132–6140.

Rapraeger, A. C., Guimond, S., Krufka, A. and Olwin, B. B. (1994). Regulation by heparan-sulfate in fibroblast growth-factor signaling, Extracellular Matrix Components, vol. 245, pp. 219–240. San Diego: Academic Press Inc.

Ribó, M., Beintema, J. J., Osset, M., Fernández, E., Bravo, J., de Llorens, R. and Cuchillo, C. M. (1994). Heterogeneity in the glycosylation pattern of human pancreatic ribonuclease. *Biol. Chem. Hoppe-Seyler* **375**, 357–363.

Richard, J. P., Melikov, K., Brooks, H., Prevot, P., Lebleu, B. and Chernomordik, L. V. (2005). Cellular uptake of unconjugated TAT peptide involves clathrin-dependent endocytosis and heparan sulfate receptors. *J. Biol. Chem.* **280**, 15300–15306.

Riddles, P. W., Blakeley, R. L. and Zerner, B. (1983). Reassessment of Ellman's reagent. *Methods Enzymol.* **91**, 49–60.

Riordan, J. F. (1997). Structure and function of angiogenin, Ribonucleases: Structures and Functions, (eds G. D'Alessio and J. F. Riordan), pp. 445–489. New York: Academic Press.

Rodriguez, M., Torrent, G., Bosch, M., Rayne, F., Dubremetz, J.-F., Ribó, M., Benito, A., Vilanova, M. and Beaumelle, B. (2007). Intracellular pathway of onconase that enables its delivery to the cytosol. *J. Cell Sci.* **120**, 1405–1411.

Rosenberg, H. F. (2008). RNase A ribonucleases and host defense: an evolving story. *J. Leukoc. Biol.* **83**, 1079–1087.

Rotman, B. and Papermaster, B. W. (1966). Membrane properties of living mammalian cells as studied by enzymatic hydrolysis of fluorogenic esters. *Proc. Natl. Acad. Sci U. S. A.* **55**, 134–141.

Runquist, E. A. and Havel, R. J. (1991). Acid hydrolases in early and late endosome fractions from rat liver. *J. Biol. Chem.* **266**, 22557–22563.

Rutkoski, T. J., Kink, J. A., Strong, L. E., Schilling, C. I. and Raines, R. T. (2010). Antitumor activity of ribonuclease multimers created by site-specific covalent tethering. . *Bioconjugate Chem.*, (In press).

Rutkoski, T. J., Kurten, E. L., Mitchell, J. C. and Raines, R. T. (2005). Disruption of shape-complementarity markers to create cytotoxic variants of ribonuclease A. *J. Mol. Biol.* **354**, 41–54.

Rutkoski, T. J. and Raines, R. T. (2008). Evasion of ribonuclease inhibitor as a determinant of ribonuclease cytotoxicity. *Curr. Pharm. Biotechnol.* **9**, 185–199.

Rybak, S. M. (2008). Antibody-onconase conjugates: Cytotoxicity and intracellular routing. *Curr. Pharm. Biotechnol.* **9**, 226–230.

Rybak, S. M., Saxena, S. K., Ackerman, E. J. and Youle, R. J. (1991). Cytotoxic potential of ribonuclease and ribonuclease hybrid proteins. *J. Biol. Chem.* **266**, 21202–21207.

Sakakibara, F., Kawauchi, H., Takayanagi, G. and Ise, H. (1979). Egg lectin of *Rana japonica* and its receptor glycoprotein of Ehrlich tumor-cells. *Cancer Res.* **39**, 1347–1352.

Saxena, S. K., Rybak, S. M., Winkler, G., Meade, H. M., McGray, P., Youle, R. J. and Ackerman, E. J. (1991). Comparison of RNases and toxins upon injection into *Xenopus* oocytes. *J. Biol. Chem.* **266**, 21208–21214.

Saxena, S. K., Sirdeshmukh, R., Ardelt, W., Mikulski, S. M., Shogen, K. and Youle, R. J. (2002). Entry into cells and selective degradation of tRNAs by a cytotoxic member of the RNase A family. *J. Biol. Chem.* **277**, 15142–15146.

Schmidt, N., Mishra, A., Lai, G. H. and Wong, G. C. L. (2010). Arginine-rich cell-penetrating peptides. *FEBS Lett.* **584**, 1806–1813.

Schultz, C. (2003). Prodrugs of biologically active phosphate esters. *Bioorg. Med. Chem.* **11**, 885–898.

Schultz, C., Vajanaphanich, M., Harootunian, A. T., Sammak, P. J., Barrett, K. E. and Tsien, R. Y. (1993). Acetoxymethyl esters of phosphates, enhancement of the permeability and potency of cAMP. *J. Biol. Chem.* **268**, 6316–6322.

Schuster, I. and Bernhardt, R. (2007). Inhibition of cytochromes P450: Esixting and new promising therapeutic targets. *Drug Metab. Rev.* **39**, 481–499.

Scriven, E. F. V. and Turnbull, K. (1988). Azides: Their preparation and synthetic uses. *Chem. Rev.* **88**, 297–368.

Shan, D., Nicolaou, M. G., Borchardt, R. T. and Wang, B. (1997). Prodrug strategies based on intramolecular cyclization reactions. *J. Pharm. Sci.* **86**, 765–767.

Simon, M. J., Gao, S., Kang, W. H., Banta, S. and Morrison, B. (2009). TAT-mediated intracellular protein delivery to primary brain cells is dependent on glycosaminoglycan expression. *Biotechnol. and Bioeng.* **104**, 10–19.

Skretting, G., Torgersen, M. L., van Deurs, B. and Sandvig, K. (1999). Endocytic mechanisms responsible for uptake of GPI-linked diphtheria toxin receptor. *J. Cell Sci.* **112**, 3899–3909.

Slivinsky, G. G., Hymer, W. C., Bauer, J. and Morrison, D. R. (1997). Cellular electrophoretic mobility data: A first approach to a database. *Electrophoresis* **18**, 1109–1119.

Sloan, K. B. and Koch, S. A. M. (1983). Reaction of (acyloxy)alkyl a-halides with phenols: Effect of nucleofugicity and nucleophilicity on product distribution. *J. Org. Chem.* **48**, 3777–3783.

Smith, B. D., Soellner, M. B. and Raines, R. T. (2003). Potent inhibition of ribonuclease A by oligo(vinylsulfonic acid). *J. Biol. Chem.* **278**, 20934–20938.

Smith, M. R., Newton, D. L., Mikulski, S. M. and Rybak, S. M. (1999). Cell cycle-related differences in susceptibility of NIH/3T3 cells to ribonucleases. *Exp. Cell Res.* **247**, 220–232.

Soncin, F., Shapiro, R. and Fett, J. W. (1994). A cell-surface proteoglycan mediates human adenocarcinoma HT-29 cell adhesion to human angiogenin. *J. Biol. Chem.* **269**, 899–9005.

Soncin, F., Strydom, D. J. and Shapiro, R. (1997). Interaction of heparin with human angiogenin. *J. Biol. Chem.* **272**, 9818–9824.

Sparano, B. A., Shahi, S. P. and Koide, K. (2004). Effect of binding and conformation on fluorescence quenching in new 2',7'-dichlorofluorescein derivatives. *Org. Lett.* **6**, 1947–1949.

Stanley, P., Sudo, T. and Carver, J. P. (1980). Differential involvement of cell surface sialic acid residues in wheat germ agglutinin binding to parental and wheat germ agglutinin-resistant Chinese hamster ovary cells. *J. Cell Biol.* **85**, 60–69.

Subtil, A., Hemar, A. and Dautryvarsat, A. (1994). Rapid endocytosis of interleukin-2 receptors when clathrin-coated pit endocytosis is inhibited *J. Cell Sci.* **107**, 3461–3468.

Sun, W.-C., Gee, K. R., Klaubert, D. H. and Haugland, R. P. (1997). Synthesis of fluorinated fluoresceins. *J. Org. Chem.* **62**, 6469–6475.

Suzuki, M., Saxena, S. K., Boix, E., Prill, R. J., Vasandani, V. M., Ladner, J. E., Sung, C. and Youle, R. J. (1999). Engineering receptor-mediated cytotoxicity into human ribonucleases by steric blockage of inhibitor interaction. *Nat. Biotechnol.* **17**, 265–270.

Tafech, A., Bassett, T., Sparanese, D. and Lee, C. H. (2006). Destroying RNA as a therapeutic approach. *Curr. Med. Chem.* **13**, 863–881.

Taylor, P. D. (1995). Potentiometric determination of aminal stability constants. *Talanta* **42**, 243–248.

Terrone, D., Sang, S. L. W., Roudaia, L. and Silvius, J. R. (2003). Penetratin and related cell-penetrating cationic peptides can translocate across lipid bilayers in the presence of a transbilayer potential. *Biochemistry* **42**, 13787–13799.

Testa, B. and Mayer, J. M. (2003). Hydrolysis in Drug and Prodrug Metabolism: Chemistry, Biochemistry, and Enzymology. Zürich, Switzerland: Verlag Helvetica Chimica Acta.

Thomas, J. and Sloan, K. (2008). In vitro evaluation of alkylcarbonyloxymethyl (ACOM) ethers as novel prodrugs of phenols for topical delivery: ACOM prodrugs of acetaminophen. *Int. J. Pharm.* **346**, 80–88.

Thomas, J. D. and Sloan, K. B. (2007). Overcoming steric effects in the coupling reaction of alkyloxycarbonyloxymethyl (AOCOM) halides with phenols: An efficient synthesis of AOCOM phenolic prodrugs. *Tetrahedron Lett.* **48**, 109–112.

Tkachenko, E., Lutgens, E., Stan, R. V. and Simons, M. (2004). Fibroblast growth factor 2 endocytosis in endothelial cells proceed via syndecan-4-dependent activation of Rac1 and a Cdc42-dependent macropinocytic pathway. *J. Cell Sci.* **117**, 3189–3199.

Torchilin, V. P. (2006). Recent approaches to intracellular delivery of drugs and DNA and organelle targeting. *Annu. Rev. Biophys. Biomol. Eng.* **8**, 343–375.

Torgersen, M. L., Skretting, G., van Deurs, B. and Sandvig, K. (2001). Internalization of cholera toxin by different endocytic mechanisms. *J. Cell Sci.* **114**, 3737–3747.

Tsien, R. Y. (1981). A non-disruptive technique for loading calcium buffers and indicators into cells. *Nature* **290**, 527–528.

Tubert, P., Rodriguez, M., Ribo, M., Benito, A. and Vilanova, M. (2010). The nuclear transport capacity of a human-pancreatic ribonuclease variant is critical for its cytotoxicity. *Invest New Drugs*.

Tunnemann, G., Martin, R. M., Haupt, S., Patsch, C., Edenhofer, F. and Cardoso, M. C. (2006). Cargo-dependent mode of uptake and bioavailability of TAT-containing proteins and peptides in living cells. *FASEB J.* **20**, 1775–1784.

Turcotte, R. F., Lavis, L. and Raines, R. T. (2009). Onconase cytotoxicity relies on the ditribution of its positive charge. *FEBS J.* **276**, 3846–3857.

Turcotte, R. F. and Raines, R. T. (2008). Interaction of onconase with the human ribonuclease inhibitor protein. *Biochem. Biophys. Res. Commun.* **377**, 512–514.

Ullrich, O., Reinsch, S., Urbe, S., Zerial, M. and Parton, R. G. (1996). Rab11 regulates recycling through the pericentriolar recycling endosome. *J. Cell Biol.* **135**, 913–924.

Ullrich, V. and Weber, P. (1972). *O*-Dealkylation of 7-ethoxycoumarin by liver-microsomes—direct fluorometric test. *Hoppe-Seyler's X. Physiol. Chem.* **353**, 1171–1177.

Urani, C., Doldi, M., Crippa, S. and Camatini, M. (1998). Human-derived cell lines to study xenobiotic metabolism. *Chemosphere* **37**, 2785–2795.

Urano, Y., Kamiya, M., Kanda, K., Ueno, T., Hirose, K. and Nagano, T. (2005). Evolution of fluorescein as a platform for finely tunable fluorescence probes. *J. Am. Chem. Soc.* **127**, 4888–4894.

Valeur, B. (2002). Molecular Fluorescence : Principles and Applications. Weinheim ; New York: Wiley-VCH.

Van Noorden, C. J., Boonacker, E., Bissell, E. R., Meijer, A. J., van Marle, J. and Smith, R. E. (1997). Ala-Pro-cresyl violet, a synthetic fluorogenic substrate for the analysis of kinetic parameters of dipeptidyl peptidase IV (CD26) in individual living rat hepatocytes. *Anal. Biochem.* **252**, 71–77.

Varki, A., Cummings, R. D., Esko, J. D., Freeze, H. H., Stanley, P., Hart, G. and Etzler, M. E. (2008). Essentials of Glycobiology, 2nd Ed. Cold Spring Harbor, NY: Cold Spring Harbor Laboratory Press.

Vasandani, V. M., Wu, Y.-N., Mikulski, S. M., Youle, R. J. and Sung, C. (1996). Molecular determinants in the plasma clearance and tissue distribution of ribonucleases of the ribonuclease A superfamily. *Cancer Res.* **56**, 4180–4186.

Venable, A., Mitalipova, M., Lyons, I., Jones, K., Shin, S. J., Pierce, M. and Stice, S. (2005). Lectin binding profiles of SSEA-4 enriched, pluripotent human embryonic stem cell surfaces. *BMC Dev. Biol.* **5**, 15.

Vicentini, A. M., Kieffer, B., Mathies, R., Meyhack, B., Hemmings, B. A., Stone, S. R. and Hofsteenge, J. (1990). Protein chemical and kinetic characterization of recombinant porcine ribonuclease inhibitor expressed in *S. cerevisiae*. *Biochem.* **29**, 8827–8834.

Vives, E., Brodin, P. and Lebleu, B. (1997). A truncated HIV-1 Tat protein basic domain rapidly translocates through the plasma membrane and accumulates in the cell nucleus. *J. Biol. Chem.* **272**, 16010–16017.

Vogel, M., Rettig, W., Sens, R. and Drexhage, K. H. (1988). Structural relaxation of rhodamine dyes with different N-substitution patterns—A study of fluorescence decay times and quantum yields. *Chem. Phys. Lett.* **147**, 452–460.

Wadia, J. S. and Dowdy, S. F. (2005). Transmembrane delivery of protein and peptide drugs by TAT-mediated transduction in the treatment of cancer. *Adv. Drug Deliv. Rev.* **57**, 579–596.

Wadia, J. S., Stan, R. V. and Dowdy, S. F. (2004). Transducible TAT-HA fusogenic peptide enhances escape of TAT-fusion proteins after lipid raft macropinocytosis. *Nat. Med.* **10**, 310–315.

Wang, J. and London, E. (2009). The membrane topography of the Diphtheria toxin T domain linked to the A chain reveals a transient transmembrane hairpin and potential translocation mechanisms. *Biochemistry* **48**, 10446–10456.

Wang, Z.-Q., Liao, J. and Diwu, Z. (2005). N-DEVD-N′-morpholinecarbonyl-rhodamine 110: Novel caspase-3 fluorogenic substrates for cell-based apoptosis assay. *Bioorg. Med. Chem. Lett.* **15**, 2335–2338.

Warren, J. D., Geng, X. and Danishefsky, S. J. (2007). Synthetic glycopeptide-based vaccines. *Top. Curr. Chem.* **267**, 109–141.

Watkins, R. W., Lavis, L. D., Kung, V. M., Los, G. V. and Raines, R. T. (2009). Fluorogenic affinity label for the facile, rapid imaging of proteins in live cells. *Org. Biomol. Chem.* **7**, 3969–3975.

Watson, P., Jones, A. T. and Stephens, D. J. (2005). Intracellular trafficking pathways and drug delivery: Fluorescence imaging of living and fixed cells. *Adv. Drug Deliv. Rev.* **57**, 1024–1032.

White, I. N. (1988). A continuous fluorometric assay for cytochrome P-450-dependent mixed function oxidases using 3-cyano-7-ethoxycoumarin. *Anal. Biochem.* **172**, 304–310.

White, J. M. (1990). Viral and cellular membrane-fusion proteins. *Annu. Rev. Physiol.* **52**, 675–697.

Whitlock, J. P., Jr. (1999). Induction of cytochrome P4501A1. *Annu. Rev. Pharmacol. Toxicol.* **39**, 103–125.

Wright, A. T. and Cravatt, B. F. (2007). Chemical proteomic probes for profiling cytochrome P450 activities and drug interactions in vivo. *Chem. Biol.* **14**, 1043–1051.

Wu, Y., Mikulski, S. M., Ardelt, W., Rybak, S. M. and Youle, R. J. (1993). A cytotoxic ribonuclease. *J. Biol. Chem.* **268**, 10686–10693.

Wu, Y., Saxena, S. K., Ardelt, W., Gadina, M., Mikulski, S. M., De Lorenzo, V., D'Alessio, G. and Youle, R. J. (1995). A study of the intracellular routing of cytotoxic ribonucleases. *J. Biol. Chem.* **270**, 17476–17481.

Yang, Y. Z., Babiak, P. and Reymond, J. L. (2006). New monofunctionalized fluorescein derivatives for the efficient high-throughput screening of lipases and esterases in aqueous media. *Helv. Chim. Acta* **89**, 404–415.

Yatzeck, M. M., Lavis, L. D., Chao, T. Y., Chandran, S. S. and Raines, R. T. (2008).A highly sensitive fluorogenic probe for cytochrome P450 activity in live cells. *Bioorg. Med. Chem. Lett.* **18**, 5864–5866.

Yoshitake, S., Yamada, Y., Ishikawa, E. and Masseyeff, R. (1979). Conjugation of glucose-oxidase from *Aspergillus niger* and rabbit antibodies using N-hydroxysuccinimide ester of N-(4-carboxycyclohexylmethyl)-maleimide. *Eur. J. Biochem.* **101**, 395–399.

Youle, R. J. and D'Alessio, G. (1997). Antitumor RNases, Ribonucleases: Structures and Functions, (eds G. D'Alessio and J. F. Riordan), pp. 491–514. New York: Academic Press.

Zanker, V. and Peter, W. (1958). Die prototropen Formen des Fluoresceins. *Ber. Dtsch. Chem. Ges.* **91**, 572–580.

Zhang, H.-Z., Cai, S. X., Drewe, J. A. and Yang, W. (2000). Novel fluorescence dyes and their applications for whole cell fluorescence screening assays for caspases, peptidases, proteases and other enzymes and the use thereof, pp. 174.

Zhang, H. Z., Kasibhatla, S., Guastella, J., Tseng, B., Drewe, J. and Cai, S. X. (2003). N-Ac-DEVD-N′-(polyfluorobenzoyl)-R110: Novel cell-permeable fluorogenic caspase substrates for the detection of caspase activity and apoptosis. *Bioconjugate Chem.* **14**, 458–463.

Zhang, X. P., Jin, Y. J., Pllummer, M. R., Pooyan, S., Gunaseelan, S. and Sinko, P. J. (2009). Endocytosis and membrane potential are required for HeLa cell uptake of RI-CKTat9, a retro-inverso Tat cell penetrating peptide. *Mol. Pharmaceutics* **6**, 836–848.

Zhao, H., Ardelt, B., Ardelt, W., Shogen, K. and Darzynkiewicz, Z. (2008). The cytotoxic ribonuclease onconase targets RNA interference (siRNA). *Cell Cycle* **7**, 3258–3261.

Zimmerman, M., Ashe, B., Yurewicz, E. C. and Patel, G. (1977). Sensitive assays for trypsin, elastase, and chymotrypsin using new fluorogenic substrates. *Anal. Biochem.* **78**, 47.

Zimmerman, M., Yurewicz, E. and Patel, G. (1976). A new fluorogenic substrate for chymotrypsin. *Anal. Biochem.* **70**, 258.

Zorko, M. and Langel, U. (2005). Cell-penetrating peptides: mechanism and kinetics of cargo delivery. *Adv. Drug Deliv. Rev.* **57**, 529–545.

Zurita, A. R., Maccioni, H. J. F. and Daniotti, J. L. (2001). Modulation of epidermal growth factor receptor phosphorylation by endogenously expressed gangliosides. *Biochem. J.* **355**, 465–472.